NUFFIELD DEPARTMENT
OF OPHTHALMOLOGY

Investigating Treatment Options For

Battlefield Retinal Laser Injury

Thesis submitted for the degree of Doctor of Philosophy

Sher Aslam

MERTON COLLEGE

TRINITY TERM 2013

Supervisor: Professor Robert E. MacLaren

Abstract

Battlefield retinal laser injury is an infrequent but potentially devastating cause of irreversible blindness. Resultant laser-induced photoreceptor death may occur by necrosis or apoptosis, the latter which is a form of programmed cell death that may be physiological or pathological. Though necrosis cannot be prevented, apoptosis may be inhibited under certain conditions. Therefore, following retinal laser injury, specific treatment aims to target apoptotic photoreceptors and may take the form of neuroprotection or cell replacement.

The primary aim of this thesis was to construct an *in vivo* model in which to observe the effects of retinal laser exposure on cone photoreceptor apoptosis. Current methodology to determine the effects involves histological techniques and is therefore limited to being cross-sectional. An *in vivo* model would permit longitudinal study to observe the cone response to injury using clinically relevant applications, including fundus autofluorescence imaging. Such a construct would enable more sensitive evaluation of new therapies which would be of direct translational relevance. The secondary aim was to investigate potential therapeutic options for retinal laser injury by pharmacological means in the form of CNTF or cell transplantation. To identify the possible molecular signals involved in neurotrophic factor-induced photoreceptor cell survival, apoptotic gene expression was investigated focusing on those genes modulated by the CNTF pathway.

Acknowledgments

First and foremost, I thank my supervisor, Professor Robert E. MacLaren for his encouragement and support throughout this research period. I am hard pushed to think of any more inspirational a teacher throughout my education, from school days to present.

I too thank my colleagues at the Nuffield Laboratory of Ophthalmology for their guidance, in particular Alun Barnard, Mandeep Singh, Peter Charbel Issa, Sumarthi Sekaran, and Wayne Davies.

Also, I am extremely grateful to Wg Cdr Robert A.H. Scott for his having paved the way for this thesis project and I thank the various parties within the Ministry of Defence, including Dr Amarjit Samra, for their assistance in acquiring funding.

I sincerely thank my father for having instilled a love of learning. Lastly, and most importantly, I thank my dear wife, for being there as a shoulder to lean on, for her patience, and for her wonderful nature. Lovingly yours.

ABBREVIATIONS

AAV: adeno-associated virus

AF: autofluorescence

AMD: age-related macular degeneration

CMZ: ciliary marginal zone

CNTF: ciliary neurotrophic factor

cSLO: confocal scanning laser ophthalmoscope

ECT: Encapsulated Cell-based Technology

EGFP: enhanced green fluorescent protein

ERG: electroretinography

ES: embryonic stem

FACS: Fluorescence activated cell sorting

GFAP: Glial fibrillary acidic protein

GFP: green fluorescent protein

GS: Glutamine synthetase

IGF: insulin-like growth factor

IPSC: induced pluripotent stem cell

IR: infrared

IS: inner segments

LM: long-medium

MACS: Magnetic-activated cell sorting

MAPK: mitogen-activated protein kinase

MVL: minimum visible lesion

MSC: mesenchymal stem cell

NSC: neural stem cells

OPL: outer plexiform layer

OS: outer segments

PNA: peanut agglutinin

RGC: retinal ganglion cell

RPE: retinal pigment epithelium

TUNEL: Terminal dUTP Nick End-Labeling

TABLE OF CONTENTS

LIST OF FIGURES

LIST OF TABLES

CHAPTER 1

GENERAL INTRODUCTION

1.1 Introduction

Retinal laser injuries represent an infrequent but potentially devastating cause of irreversible blindness. Since its inception, the application of laser technology has become widespread in a number of fields, including within the military and industry. As such, there are several reports of significant ocular injuries related to its use. These comprise anterior segment injuries or retinal burns, the latter which may cause permanent visual loss and for which there is currently no satisfactory treatment.

Laser energy is primarily absorbed by the retinal pigment epithelium (RPE). However, it is damage to the photoreceptor cells that is responsible for the visual loss incurred following exposure. Potential therapy would therefore target these cells specifically and may take the form of neuroprotection or neural replacement. Neuroprotection aims to minimise cell loss and therefore limit the extent of damage. A number of compounds have been found to have neuroprotective properties. Neural replacement would aim to restore a functioning photoreceptor population by means such as transplantation.

1.2 Retinal anatomy

1.2.1 Morphological subdivision

The retina is a light sensitive tissue that comprises neuronal cells in addition to glia. Following light absorption and activation of the visual cycle in the region of the outer retina, downstream signalling continues via the inner retina before exiting the eye

via the optic nerve. The human retina is further subdivided into a central and peripheral retina. The central retina comprises the macula lutea, which contains yellow pigment to filter out short wavelength light defocused due to chromatic aberration. Together with increased photoreceptor density, this makes it an area of greater spatial resolving power than the peripheral retina. This is further subdivided into an area of maximal cone density, the fovea centralis.

The retina consists of ten layers, as shown in Figure 1.1, that extend from the outer retina adjacent to the RPE to the inner retina consisting of the ganglion cell layer.

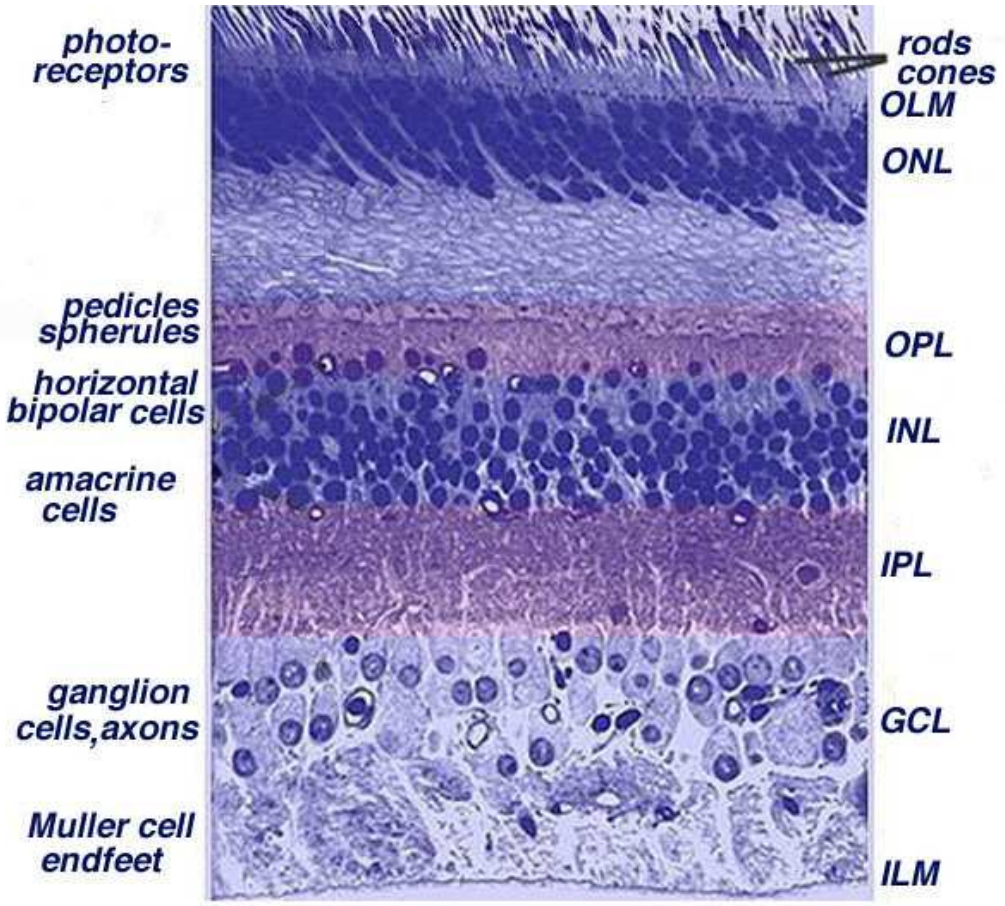

Figure 1.1. The layers of the retina.*

* Taken from Webvision, http://webvision.med.utah.edu/

1.2.1.1 Neuronal cells

Photoreceptors

The outer retina comprises the light-sensitive rod and cone photoreceptors. The human retina contains 120 million rods and 6 million cones. Both types of cell contain outer segments (OS) that interact with the RPE layer. The OS contain discs that are composed of visual pigments (opsins) and are continually shed and processed by the RPE. Each OS is connected via a cilium to an inner segment (IS) that contains a high density of mitochondria. The photoreceptor cell bodies are located in the outer nuclear layer (ONL). Processes extending from the ONL form synapses at the outer plexiform layer (OPL).[1]

Bipolar cells

Bipolar cells are second order neurons that form synapses with either rods or cones in the ONL and ganglion cells in the inner nuclear layer. They may also synapse with horizontal cells, the latter introducing the function of lateral inhibition. There are two types of bipolar cells, ON and OFF, which differ in function. Under scotopic conditions, release of the neurotransmitter, glutamate, from photoreceptors, causes hyperpolarisation of ON bipolar cells and depolarisation of OFF bipolar cells. This situation reverses under photopic conditions.[2]

Rather than forming direct synaptic connections with ganglion cells, rod bipolar cells synapse on to AII amacrine cells. This causes subsequent depolarisation of cone ON bipolar cells and hyperpolarisation of cone OFF bipolar cells, the latter mediated via

inhibitory glycine synapses.[3]

Horizontal, amacrine and interplexiform cells

Horizontal cells, of which there are three types (HI, HII and HIII), are the laterally interconnecting neurons of the OPL. HI cells have been shown to connect to all three cone subtypes (S, M and L cones) whereas HII cells connect to both rods and cones. HIII cells form connections to S cones only. Together with ON- and OFF-bipolar cells, horizontal cells have a role in lateral inhibition, which they achieve via GABAergic mediated mechanisms.[4]

Amacrine cells are located in the OPL, where they act as interneurons between bipolar cells and ganglion cells. Of the approximately 40 subtypes of amacrine cells, one particular subtype, AII cells, connect rod bipolar with cone bipolar cells, and subsequently to their respective ganglion cells.[3]

The function of interplexiform cells is to communicate information between the two plexiform layers of the retina using either GABA or dopamine as a neurotransmitter.[5]

Retinal ganglion cells

Located at the inner retina, retinal ganglion cells (RGCs) receive input from the photoreceptors via bipolar and amacrine cells. RGC axons form the optic nerve which transmits to the brain, forming synapses in the thalamus, hypothalamus and midbrain.[3]

1.2.1.2 Glial cells

Müller cells

Müller cells are glial cells arranged in a scaffold network that protects the underlying retinal architecture. In studies of the zebrafish retina following injury, Müller cells have been shown to undergo transdifferentiation, including into photoreceptors.[6] Müller cells terminate at the inner limiting membrane in an expansion of "footplates" whilst the opposite ends terminate at the outer limiting membrane comprising tight junctions between these cells and photoreceptor inner segments.

Aside from their role in providing anatomical support and in retinal histiogenesis, Müller cells are also responsible for maintaining water and pH homeostasis, production of vitreal collagens, stimulating glycogenolysis, and in the removal of extracellular K^+ to the vitreous.[7]

Astrocytes

Astrocytes comprise the other type of retinal microglia and are so-named due to their characteristic star shape. Predominantly found in the nerve fibre layer, astrocytes provide nutritional and metabolic support to the retinal ganglion cells.[8] As they are intimately associated with retinal blood vessels, astrocytes are thought to have a role in maintaining the blood-retinal barrier.[9]

Microglia

Microglia are small glial cells distributed throughout the retina from the nerve fiber

layer to the OPL. Possessing phagocytic activity, activation of microglia under physiological or pathological conditions can result in their release of a number of growth factors, including brain-derived nerve factor, nerve growth factor, neurotrophin 3, in addition to the cytokines, TNF-α and interleukin (IL)-6.[10]

1.2.1.3 Retinal pigment epithelium

Located in the posterior part of the eye, the RPE comprises a monolayer of polarised epithelial cells situated between the photoreceptors and the choroidal blood supply. The RPE has a major role in the phototransduction cascade[11] and in the phagocytosis and renewal of photoreceptor outer segments.[12] The RPE selectively transports ions, fluid, nutrients, and metabolic waste products between the retina and the choriocapillaris.[13] By this action, it maintains the integrity of the outer retina by regulating the composition of the extracellular spaces that face the RPE apical and basolateral membranes.[14,15]

1.3 Retinal laser injury

1.3.1 Biology of optical tissue-light interaction

Light energy spans the electromagnetic spectrum between the ultraviolet [UV (100 to 400 nm)], visible [VIS (400 to 700 nm)] and infrared [IR (700 to 10000+ nm)] bands. UV radiation is further classified as UVC (100 to 260 nm), UVB (260 to 315 nm) and UVA (315 to 400 nm) light whilst IR is subdivided into an IRA (700 to 1400 nm), IRB (1400 to 3000 nm) and IRC (3000 to 10000+ nm) range.[16] These classifications are useful for defining safety margins as individual bands possess similar properties of tissue penetration and resultant bioeffects. The VIS band can be

classified into short (blue), medium (green) and long (red) wavelength as each point reflects the peak spectral absorption of the three cone photoreceptor subtypes. The biological response to laser exposure is critically dependent on a number of factors: the wavelength of incident light, duration of exposure, total energy delivered and size of the optical zone. Much of the human data regarding laser safety levels has been derived from primate research. The threshold levels for injury are related to the ED50 values, which are produced by plotting lesion detection against retinal irradiance as determined by ophthalmoscopy, fluorescein angiography and electron microscopy.[17] The ED50 value reflects the 50% probability of producing damage detectable by each of these techniques. Determinants for safe viewing as given by the maximum permissible exposure (MPE) are related to the ED50 values. As the MPE levels have been established from monkeys which have double the amount of melanin within their RPE compared to the average Caucasian human, there is an inherent safety margin when these values are applied to humans.[18]

The optical zone is defined as the volume of tissue which absorbs incident light. Absorption is itself dependent on propagation of light through tissue versus scatter. The eye is most vulnerable to laser injury owing to its refractive properties and the presence of its clear media. These factors allow for delivery of a highly focused point of energy per unit area. Indeed, the energy density of a focused spot on the retina is 10^5-fold higher than the incident point at the cornea.[19] As a result of this refractive property, light, and by extension, laser exposure, may have no effect on a structure such as skin but may be significantly injurious to the eye.

Light propagation by the eye is limited by the absorption characteristics of individual tissues. The anterior and intermediate structures of the eye act to attenuate UV and IR radiation to different degrees, thereby protecting the retina from photodamage. UV light is absorbed by nucleotide bases and proteins and does not penetrate beyond the cornea (UVC and UVB specific) and lens (UVB and UVA specific). IR radiation beyond 1400 nm is absorbed by water and also does not penetrate beyond the cornea.[20] Therefore, retinal injury may only arise from visible or near-IR light as only these radiation bands penetrate the clear media of the eye. As described in the following section, the pathophysiology of retinal laser injury owes itself to the mechanism of photothermal, photomechanical or photochemical damage.

1.3.2 Principles and uses of laser technology

Initially developed in 1960,[21] laser technology has since been used in a wide range of fields with military, medical and industrial applications. 'Laser' is an acronym for 'Light Amplification by the Stimulated Emission of Radiation'. The principle behind laser energy involves the amplification of light of a specific wavelength by a gain medium. Energising the gain medium via an electrical current or by light at a different wavelength enables this amplification process. At the atomic level, this results in the excitation of an electron to a higher energy level. On return to its resting state, this results in the release of energy in the form of a photon of light.

The first lasers produced light in pulses with milliseconds duration in the far-red spectrum (694nm). This was followed by the development of continuous wave (CW) lasers which emitted a continuous beam of light of which the earliest also emitted in the red spectrum (632nm).[22] Since then, lasers have been developed which operate

in all regions of the visible spectrum and in both the UV and IR spectral domains.

Within the military, lasers are used for range finding, target acquisition, guiding "smart" weapons, and destroying electro-optical sensors. Increasingly, laser dazzlers are being used during operations and such systems were employed on British naval vessels with the intention to dazzle pilots of attacking aircraft during the Falklands War.[23] Hand-held laser devices are now available in a range of colours from violet to near infra-red with powers from one to hundreds of mW, i.e. within the range to cause retinal injury.[24]

1.3.3 Pathophysiology of retinal injury following laser exposure

Primary cellular injury occurs as a result of the direct absorption of laser energy. The three major mechanisms underlying the process of cellular destruction following laser exposure are highlighted in this section, namely photothermal, photomechanical and photochemical injury. The cause of each type of mechanism is broadly dependent on the pulse duration as follows: pico to nano seconds, photomechanical; 100µs to several seconds, photothermal; and in excess of 100s, photochemical. Laser energy is primarily absorbed by melanin (Figure 1.2) within the RPE and choroid although a small proportion (≈ 5%) will be absorbed by the visual pigments of the eye.[25]

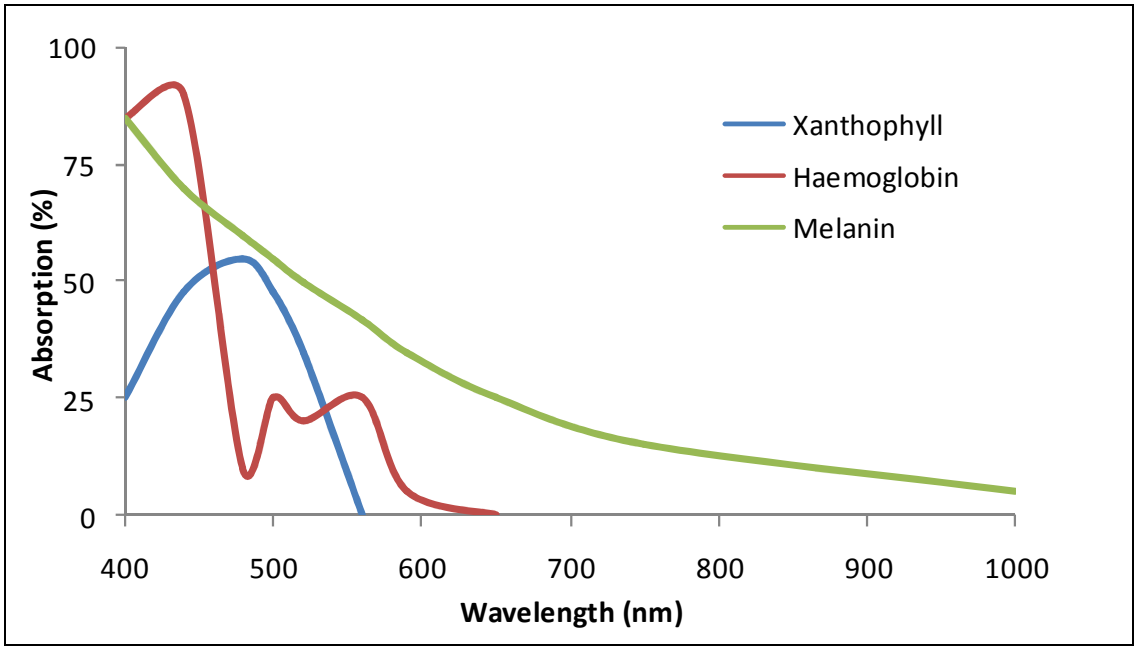

Figure 1.2. Main visual pigments of the RPE and choroid. Melanin absorbs green, yellow, red and infrared wavelengths; xanthophyll (in the macula) absorbs blue but minimally absorbs yellow or red wavelengths; hemoglobin absorbs blue, green and yellow with minimal red wavelength absorption.*

Absorption of photon energy by a chromophore results in either a change of vibrational modes of the molecule (vibration transition, near IR) or in a change in the distance between charges (electron transition, UV or visible spectrum). Increase in the vibrational component will be experienced as increase in heat content. Conduction of heat energy to adjacent structures, primarily the photoreceptor outer segments, may result in their permanent structural damage. This will be manifest as cellular vacuolation and coagulation or denaturation of protein components.[26] Although the immediate site of injury following laser photocoagulation is limited to an area including and adjacent to the irradiating beam, there will be an extension of

*Adapted from Lock, J. H. and Fong, K. C. S. Retinal Laser Photocoagulation. *Med J Malaysia* 2010 65(1):88-95.

this injury due to the suprathreshold degree of damage to surrounding neurons, even if that be partial damage. For instance, injury to only the photoreceptor outer segment may result in loss of the entire photoreceptor. A suprathreshold injury of sufficient energy may cause heat dissipation throughout the neural retina resulting in damage to the retinal ganglion cell layer. Injury to this layer will not only affect transmission of signal from this region of injury but also to retinal areas from which RGC axons pass through this site.[27] Not all laser injuries cause clinically significant or irreversible damage. Peripheral injuries for instance, do not necessarily result in significant visual defects and will only do so if gross retinal damage has occurred, as opposed to the case with macular and especially foveal injuries. Laser exposures that are near threshold can result in a reversible injury with resolution of a visual scotoma. The reason for this is not due to the renewal of photoreceptors as this cell type does not regenerate but is due to the proposed sliding across of viable retina to the area of injury.[28]

The key additional pigments that absorb (laser) light resulting in release of thermal energy are haemoglobin, that is present in the retinochoroidal vasculature, and xanthophyll, a member of the carotenoid group that is localised as a yellowish pigment to the macula lutea.[29] Although absorption by other pigments is made use of in certain therapeutic modalities, absorption by xanthophylls is only ever hazardous to the visual sensitive area comprising the macula.

In terms of the immediate injury that occurs following a laser pulse, cell death is related to a lipid peroxidation process. Following absorption of laser energy, a transient temperature rise occurs in the melanosomes of the RPE. This is thought to

occur at the level of the melanosome membrane which comprises a lipoprotein structure in common with most biological membranes.[30] Energy absorption by melanin within the melanosomes results in generation of free radicals which consist of membrane components or species of superoxide. These radicals attack the lipid-rich structures within the cytoplasmic compartment resulting in the formation of lipid radicals. Given the highly oxygenated state of retinal cells, rapid oxygenation of lipid radicals causes the formation of lipid peroxyl radicals.[31] When the number of radicals overwhelms the natural defensive capabilities of enzymatic scavengers such as glutathione peroxidise and nonenzymatic scavengers such as α-tocopherol, this causes changes in membrane permeability and resultant cell death.

In the case of retinal damage post laser, secondary neuronal injury occurs due to toxin release from neighbouring damaged cells. This neuroinflammatory injury involves the excessive production of proinflammatory mediators, reactive oxygen species, nitrogen intermediates and excitotoxins which cause further damage to injured neurons.[32] Production of these metabolites is enhanced by activation of microglial cells which, as described before, are the resident immune effector cells in the CNS that are stimulated in response to injury.[33] Naturally occurring or experimentally-induced animal models of retinal degeneration have been shown to elicit activation of retinal microglia. On activation, in addition to migrating from the inner retina to the outer retina and subretinal space, these cells undergo a conformational change from their resting state to an amoeboid configuration. Aside from phagocytosing debris from damaged photoreceptor cells, they also release

proinflammatory cytokines, such as IL-1β and tumor necrosis factor (TNF)-α, that can prove lethal to neuronal cells.[34,35]

1.3.3.1 Photothermal injury

Uptake of laser irradiation by the highly-absorbing melanin contained within melanosomes found in the RPE and choroid is responsible for the temperature rise that occurs upon exposure. As explained previously, retinal damage is believed to begin with melting of the lipoprotein membrane of the melanosomes.[36] This membrane rupture has been shown experimentally to change the melanosome from a protective free-radical scavenger to a free-radical producer.[37] Fluorescence spectroscopic and molecular dynamics studies of lipase derived from the fungus, *Humicola lanuginose*, suggest that these reactions occur at a rate in the order of 10^{-2} to 10^{0} s.[38] Lipofuscin, a product of the oxidation of unsaturated fatty acids which is present in the retina as lipophilic granules, may also give rise to deleterious radicals, derived from superoxide anions, lipids, and $NADH_2$.[39-42]

A 10^{o}C temperature rise above baseline is sufficient to cause irreversible tissue damage, with cell death occurring by either necrosis or apoptosis. A study of keratocytes exposed to heat injury showed that a temperature increase to 55-58^{o}C resulted in apoptotic cell death whilst 60-68^{o}C caused apoptosis or necrosis and above 72^{o}C resulted in immediate cell death.[43] These results approximate to the effects of heat injury on all cells. A temperature rise above threshold for injury but below 100^{o}C causes tissue coagulation. This process is used clinically, e.g., to induce photocoagulation in diabetic retinopathy or treat a retinal break. The effect appears immediately as a grey-white spot which fades over time leaving a scar with

hyperpigmentation of the RPE. Lasers operating in the VIS or near-IR range are most commonly used to maximise tissue penetration. Typically, such lasers have an irradiation of 100W/cm^2, since higher irradiation approaching 1000W/cm^2 causes a temperature rise above 100^{o}C resulting in immediate tissue vaporisation.[44] Though this is employed clinically during photoablative procedures, e.g., during corneal refractive surgery or for cutting tissue in general surgery, the process is far too damaging to be employed for retinal therapy.

1.3.3.2 Photomechanical injury

Exposure of tissue to a rapid temperature rise up to 10,000^{o}C results in photomechanical damage.[45] Injury is caused by mechanical stress as a result of compressive or tensile forces induced by thermoelastic expansion. The effect of tensile forces produces microcavitation bubbles which can prove lethal to cells.[46] Following photomechanical injury, the full-thickness of the retina may be subject to damage at the ultrastructural level due to bulk-tissue displacement. This results in a wave of energy absorption from its maximal point, usually at the RPE, extending towards the inner retina. This mode of injury is employed in procedures such as the peripheral iridotomy which uses a neodymium:yttrium argon garnet (Nd:YAG) laser to ablate the iris. Due to the excessive temperature rise generated by this method of laser application and the potential for collateral damage, it is not routinely used for retinal treatment. However, there are instances of the Nd:YAG laser having been used for posterior segment therapy, e.g. to dissipate preretinal haemorrhages.[47] Of greater relevance to this thesis, there are reports of retinal injury following accidental use of this type of laser.[48,49]

1.3.3.3 Photochemical injury

Photochemical or 'photo-oxidative' damage occurs following interaction of light energy with a chromophore. In the human retina, endogenous chromophores comprise the visual photopigments, melanin, lipofuscin, haem- proteins and flavoproteins. Interaction of these proteins with light results in their excitation to a triplet state which constitutes a reactive species.[50] Low-wavelength light of 550nm or shorter results in this type of damage due to the high-energy state of individual photons required to drive the chemical reactions. A widely recognised example of photochemical injury is solar retinopathy in which short wavelength VIS light of low irradiance is absorbed by retinal chromophores. Theoretical modelling has shown that following solar exposure, retinal cells sustain a temperature rise of 4^{o}C which is less than the 10^{o}C required to produce a permanent thermal injury.[51] The underlying mechanism of damage involves the generation of reactive oxygen species. These initiate a chain of events leading to lipid peroxidation and ultimately cell death. The effects are particularly marked in the retina since the choroid, being the most vascularised tissue in the human body, is highly oxygenated and thus serves as a large reservoir for free radical formation. Also, photoreceptor outer segments have large cell membranes which accentuate the damage resulting from lipid peroxidation. Rodent studies of light exposure have shown that pretreatment with free-radical scavengers and antioxidants can limit the cell death arising from photo-oxidative stress.[52]

1.4 Mechanisms of cell death

Cell death may occur by physiological or pathological means and by programmed or

non-programmed mechanisms. The classification described in this section relates to these modes of cell death. In broad terms, these are defined as necrosis versus apoptosis. Critical to these mechanisms is the potential for treatment at appropriate points in the pathway, in order to inhibit cell loss. This is especially the case for intervention in apoptosis, a form of programmed cell death (PCD), wherein neuroprotective therapies have shown promise.

1.4.1 Necrosis

Necrosis is a form of uncontrolled cell death that results from a disturbance in ionic homeostasis. The central events behind necrosis are a rapid loss of plasma membrane integrity and bioenergetic failure. These are caused by a chain of events involving increased mitochondrial production of reactive oxygen species, channel-mediated calcium uptake, impaired ATP production, and activation of non-apoptotic proteases. Disruption of ion channels and diminished ATP levels result in distension of cells and organelles. There is subsequent membrane rupture with release of lysozomal enzymes causing non-specific inflammation in the surrounding tissue.[53] Necrosis is immuno-stimulant whereby molecules, e.g., high mobility group protein B1 (HMGB1) and hepatoma-derived growth factor (HDGF) may be released by dying cells thus initiating an immune response or activating wound repair.[54,55] The characteristic features of necrosis are summarised as follows[56]:

1. Energy independent mechanism;
2. Involves the loss of plasma membrane integrity – additional morphological changes include swelling of cellular organelles and presence of an electron-lucent cytoplasm;

3. Results in random DNA degradation products;
4. Stimulation of the immune system;
5. Initiation of cell growth and repair.

1.4.2 Apoptosis

As a form of PCD, apoptosis is classified according to cytological morphology and specific molecular signalling. *In vivo*, apoptotic cells lose connection with adjacent cells, reduce in size and show evidence of chromatin condensation. DNA undergoes fragmentation by an endogenous endonuclease into internucleosomal fragments of 180-200 base pairs (bp) or multiples of this.[57] This regular spacing is exploited for the identification of apoptosis using techniques such as agarose gel electrophoresis or Terminal dUTP Nick End-Labeling (TUNEL).

Integrity of the cell membrane is maintained by transglutaminase activity which results in cross-linkage of membrane proteins. Resultant apoptotic bodies are rapidly recognised and digested by phagocytes thus avoiding the inflammatory response that is seen following necrosis.[58,59] Apoptosis is immuno-suppresive whereby molecules, e.g., lysophosphatidylcholine, are secreted to inhibit an immune response, and others, e.g., phosphatidylserine, are exposed on the cell membrane to facilitate phagocytic recognition and engulfment.[60,61] In contrast to necrosis, apoptosis is characterised by the following features[56]:

1. Energy dependent mechanism;
2. Maintenance of plasma membrane integrity;
3. Formation of organised DNA degradation products;

4. Inhibition of the immune system;
5. Cell elimination.

The principal pathways of this form of PCD involve two groups of proteins, the *caspases* (Cysteinyl aspartic acid-proteases) and the *Bcl-2* (B-cell lymphoma protein-2) *extended family*. *Bcl-2* is the first apoptotic gene to have been cloned and has a principal role in cell survival.[62] Possessing a single transmembrane domain, *Bcl-2* is localised to the outer mitochondrial, nuclear and endoplasmic reticulum membrane. The *caspases* constitute the initiator and effector molecules in the apoptotic pathway and their activation is common to most cell-death programmes. Apoptosis occurs by either the extrinsic or intrinsic pathway (Figure 1.3). The extrinsic pathway involves *caspase-8*, which is activated on binding of the death-receptor superfamily (e.g., TNF or CD95) to their cell membrane receptors.[63] Binding results in formation of a death-inducing signalling complex (DISC) which recruits procaspase-8 via the adaptor molecule, Fas-associated death domain protein (FADD), resulting in *caspase-8* activation.[64] This cycle can be blocked by the caspase homologue, cellular FLIP.[65] The intrinsic pathway involves *caspase-9* activation, which occurs at the mitochondrial membrane, following activation of a pro-apoptotic member of the *Bcl-2* family, including *Bax*, *Bad*, *Bim* and *Bid*. Pro- and anti-apoptotic *Bcl-2* family members compete for release of cytochrome *c* exit from the mitochondria. On its release, cytochrome *c* binds with the protein co-factor, Apaf-1, and other proteins, including procaspase-9, to form the apoptosome, resulting in *caspase-9* activation.[66,67] These initiator *caspases* (*caspase-8* and *-9*) stimulate a set of downstream effector *caspases* (*caspase-3*, *-6* and *-7*) that subsequently cleave

proteins in different cell compartments. This cleavage is responsible for the characteristic morphological events occurring in apoptosis in the form of apoptotic bodies. *Caspase-3* activity is blocked by the inhibitors-of-apoptosis (IAP) proteins, which themselves are inhibited by SMAC / DIABLO.[68]

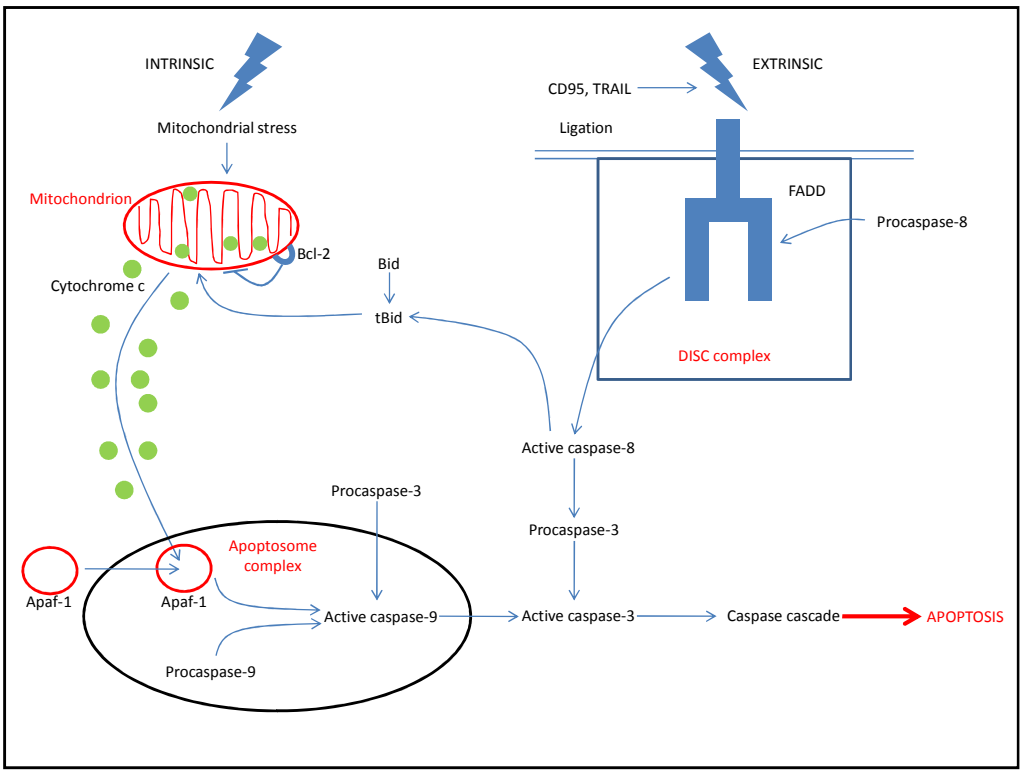

Figure 1.3. Schematic of events in apoptosis involving the intrinsic and extrinsic pathway.*

The extrinsic pathway involves triggering of the cell surface death receptors, CD95 and TNF-related apoptosis-inducing ligand (TRAIL). This results in activation of the initiator, caspase-8, following its recruitment to a receptor-ligand complex (DISC) through the adaptor molecule Fas-associated death domain protein (FADD). The intrinsic pathway involves release of mitochondrial proteins, such as cytochrome *c*, from the inter-mitochondrial membrane space, under the control of Bcl-2 family members. On release, cytochrome *c* binds to apoptotic protease-activating factor 1 (Apaf-1), which results in formation of the Apaf-1–caspase-9 apoptosome complex and activation of the initiator caspase-9. The activated initiator caspases-8 and -9 then activate the effector caspases -3, -6 and -7, resulting in the characteristic apoptosis phenotype.

* Adapted from MacFarlane, M. and Williams, A. C. Apoptosis and disease: a life or death decision. *EMBO Rep* 2004 Jul;5(7):674-8.

1.4.3 Autophagy

Autophagy is a form of cell death involving the disposal of intracellular organelles. The course of events is similar in organisms from yeasts to mammals. Macrophagy constitutes the main process during autophagy which involves membrane engulfment with sequestration of cytoplasmic fragments within double membrane vesicles known as autophagosomes. Subsequent processing of such autophagosomes is divided into four steps: packaging; formation; docking and fusion; and breakdown.[69] Induction of autophagy is controlled by the nutrient sensing mammalian target of rapamycin (mTOR) kinase (Figure 1.4). Overlaps in signal transduction pathways occur whereby the phosphoinositide 3-kinase (PI3-K) and mTOR pathways can influence shared intermediates, such as p70S6K, indicating that autophagy and apoptosis are indeed coordinated events. Autophagy can be induced pharmacologically by inhibiting negative regulators such as TOR with rapamycin. Conversely, autophagy can be inhibited pharmacologically, for instance by targeting the class III PI3K involved in autophagosome formation with 3-methyladenine.[70]

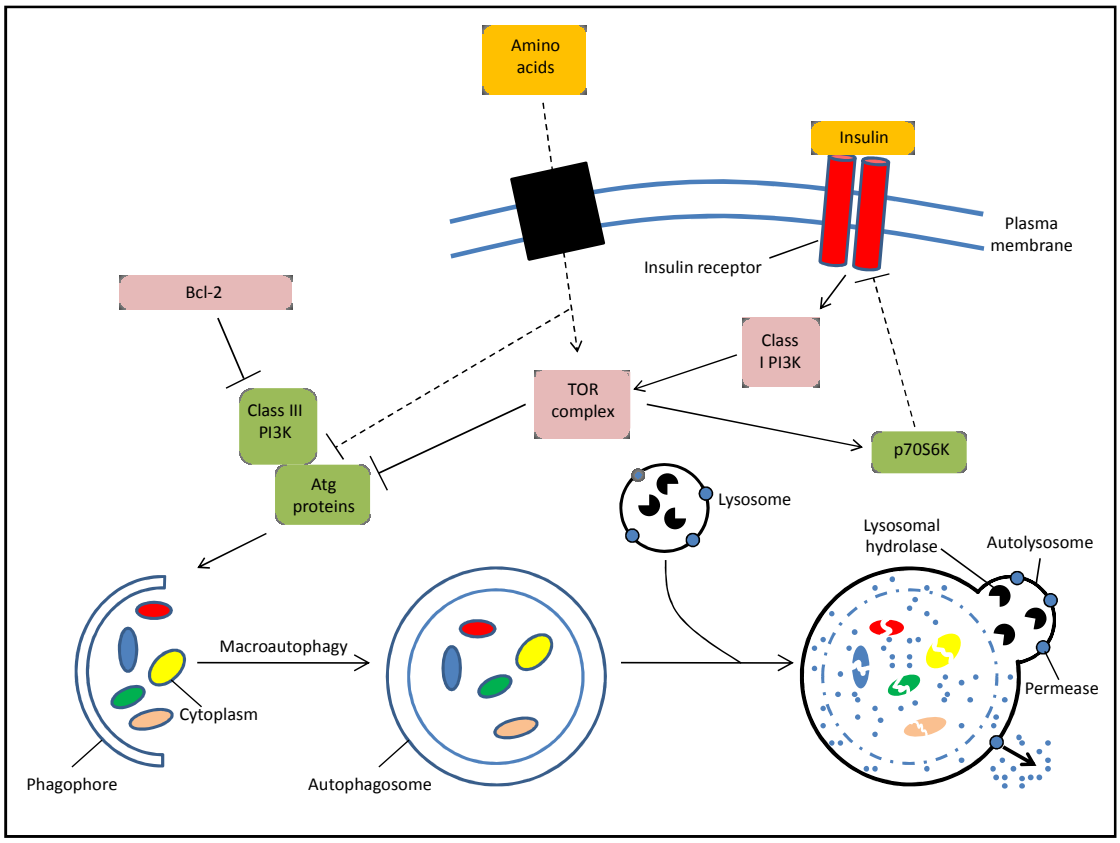

Figure 1.4. Pathways involved in autophagy.* A class III PI3K is required for activation of autophagy. TOR activity is regulated through feedback loops to prevent insufficient or excessive autophagy. p70S6 kinase, which is a substrate of TOR, may act to limit TOR activity, ensuring basal levels of autophagy. PI3K and TOR act to inhibit autophagy.

1.4.4 Necroptosis

Nectroptosis is differentiated from necrosis as a form of PCD with specific signal transduction pathways (Figure

1.5). Until recently, necrosis was thought to be a purely accidental, uncontrolled form of cell death. However, a number of molecular cues have been identified indicating that the process may be initiated as a deliberate mechanism, in the form of necroptosis. This is explained by the death domain receptors (e.g., TNFR1,

* Adapted from Mizushima, N., et al. Autophagy fights disease through cellular self-digestion. *Nature* 2008 Feb 28;451(7182):1069-75.

Fas/CD95 and TRAIL-R) and Toll-like receptors (e.g., TLR3 and TLR4) that have been shown to initiate necrosis, particularly in the presence of caspase inhibitors. Receptor-interacting protein kinase 1 (RIP-1) and its homolog, RIP-3, have been shown to be integral to TNFR1-, Fas/CD95-, TRAILR- and TLR3-mediated cell death.[71,72] Necroptosis, at the biochemical level, is therefore described as a process that can be prevented by inhibition of RIP-1/RIP-3.[73,74]

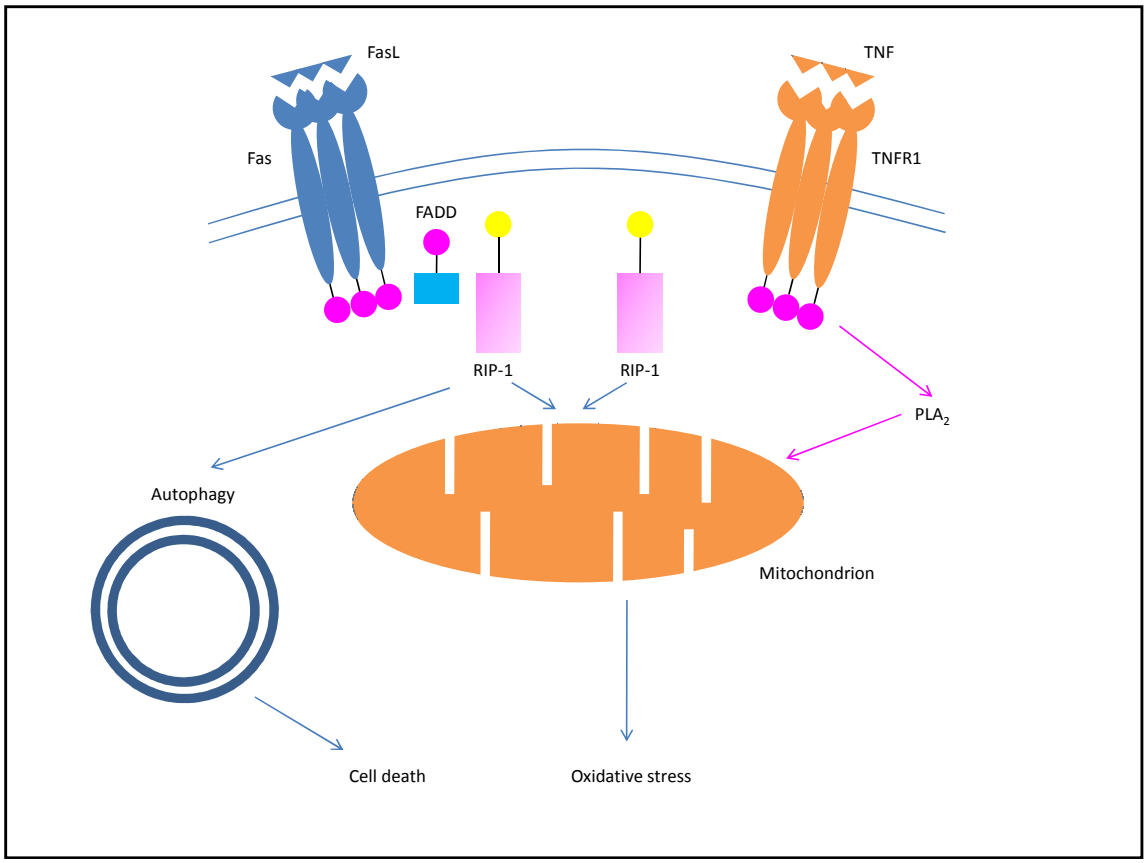

Figure 1.5. Cascade of events in death-receptor induced necroptosis.* Blockage of caspase activity results in death receptor activation which drives necroptosis through the upregulation of PLA_2 activity that subsequently causes oxidative stress. RIP-1 kinase is also activated causing necroptosis via direct action on mitochondrial function. PLA_2, phospholipase A_2.

* Adapted from Tait, S. W. and Green, D. R. Caspase-independent cell death: leaving the set without the final cut. *Oncogene* 2008 Oct 27;27(50):6452-61.

1.5 Neuroprotection

Neuroprotective therapy is aimed at inhibiting the secondary cell death that occurs following an insult, whether the cause is due to an ischaemic, mechanical, or radiation injury. In neuronal cells, it has been shown that an insult will result in loss not only of the primarily injured cells but also of neighbouring cells due to a change in the extracellular environment.[75] This change may occur as a result of increased neurotransmitter release or decreased reuptake, the release of endogenous destructive mediators, or due to alterations in synaptic binding. Due to the delayed nature of such secondary injury, this provides a window of opportunity for therapeutic intervention aimed at targeting these processes. As an example, Alzheimer's disease is characterised by increased activity of glutamate, the major excitatory neurotransmitter in the brain. Increased glutamate activity in this disease leads to sustained activation of *N*-methyl-D-aspartate (NMDA) receptors, impairing neuronal function. Memantine, a non-competitive NMDA antagonist, has been shown to have potential neuroprotectant properties by protecting neurons from glutamate-mediated excitotoxicity.[76]

Aside from neuro-excitatory factors such as glutamate, a number of mediators have been indentified that may cause secondary neuronal death. These include free radical formation, nitric oxide, lipid peroxidation products, and eicosanoids. However, all mediators will involve a common downstream pathway to cause cell death, namely PCD. Neuroprotection would be aimed at inhibiting PCD, where this occurs via the process of apoptosis.

1.5.1 Neurotrophic factors

Cell-cell communication is established through the production and release of intracellular signalling molecules. These take the form of peptide hormones, cytokines and growth factors. Peptide hormones are produced by endocrine cells and secreted into the bloodstream to reach their target organs. Cytokines and growth factors, which can have overlapping functions, are produced by different cell types not limited to the nervous system. Cytokines and growth factors differ primarily in that cytokine production may be induced whilst growth factor production is constitutive.[77] Cytokines are a group of polypeptides or glycoproteins that may be produced in response to an immune or inflammatory response.[78] Cytokines constitute a variety of families including the neurotrophins, neuropoietins, interleukins, and tumour necrosis factors (TNFs). Neurotrophic factors are a group of proteins that regulate development, survival and function of neurons. Their classification in mammalian systems is summarised in Table 1.1:

Neurotrophins (NTs)	Nerve growth factor (NGF) Brain-derived neurotrophic factor (BDNF) NT-3 NT-4 NT-5
Neuropoietic cytokines (neurokines)	Ciliary neurotrophic factor (CNTF) Leukaemia inhibitory factor (LIF) Cardiotrophin-1 (CT-1) Neuropoietin Oncostatin M
Glial cell line-derived neurotrophic factor (GDNF) family	GDNF Neurturin Osteogenic protein-1 Artemin Persephin
Insulin-like growth factor (IGF)	IGF-1 IGF-2
Fibroblast growth factors (FGFs)	FGF-1 through to 23
Hepatocyte growth factor	Neuregulin (NRG)
Proteins involved in synapse formation	Agrin, laminin 2, and ARIA (ACh-inducing activity)
Angiogenesis growth factor	
Pigment epithelium-derived factor	
Platelet-derived growth factor	
Ligands for epidermal growth factor receptor family (p185erbB2, p160erbB3, p180erbB4)	

Table 1.1. Classification of neurotrophic factors.[*]

[*] Adapted from Jain, K. K. The handbook of neuroprotection. New York: Humana Press; 2011. p. 25.

1.5.1.1 Actions

Neurotrophic factors are released by the cells that manufacture them although not all are secreted. For instance, CNTF and FGF do not have the N-terminal signal sequence necessary for secretion. It is possible that both these molecules are released by an alternative mechanism or on disruption of the cell. Each neurotrophic factor can produce different phenotypic actions, a property known as 'pleiotropism'. A single neurotrophic factor may be responsible for differentiation, survival or repair. This property may be explained by the environment in which the result is seen (e.g., the central versus peripheral nervous system), the timing of release and effect, and the receptor type, as certain receptors can produce variable responses to the same ligand.[79,80] NGF, for example, can activate non-neuronal cells such as cardiovascular and endocrine cells, whilst CNTF can stimulate glial cell proliferation.[81]

1.5.1.2 Neurotrophins (NTs)

NGF, which was first described In 1951, remains the prototypic neurotrophin.[82] However, since then, four others have been described in mammalian systems: BDNF, NT-3, NT-4, and NT-5. NTs share at least 50% sequence homology and all are generated as pre-pro-NT precursors with an approximate length of 240–260 amino acids. After further processing, these are secreted into the extracellular space as homodimeric proteins with a monomer length of 118–129 amino acids.[83] NT expression is regulated during development and in response to neuronal electrical activity and follows a variable course with age. For instance, during the perinatal stage in mammals, NT-3 expression is high and is primarily localised to the

hippocampus, neocortex, and cerebellum.[84] In contrast, BDNF expression is low in the perinatal stage but increases rapidly following birth, localising to the hippocampus, neocortex, amygdala and cerebellum.[85]

NTs activate two types of receptors: the tropomyosin-related kinase (Trk) family of receptor tyrosine kinases (TrkA, TrkB, and TrkC) and the p75 neurotrophin receptor (p75NTR), the latter a member of the TNF receptor superfamily (Figure 1.6). Via these receptors, NTs activate various signalling pathways, including those mediated by Ras and members of the cdc-42/ras/rho G-protein families, and the mitogen-activated protein kinase (MAPK), phosphatidylinositol 3-kinase, and Jun kinase cascades.[86] P75NTR binds all NTs whereas NGF binds selectively to TrkA, NT-3 to TrkC, and both BDNF and NT-4/5 to TrkB.

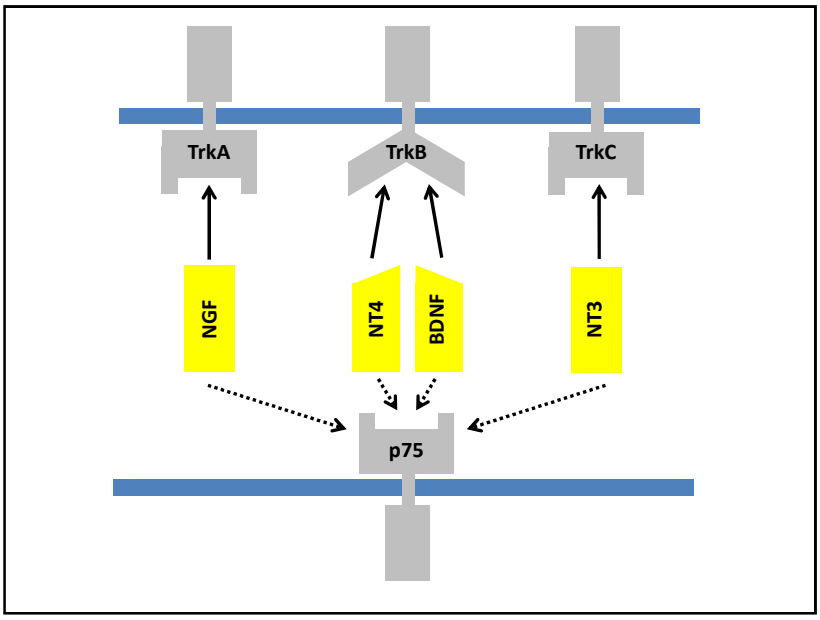

Figure 1.6. Neurotrophin family and receptor composition. All neurotrophins bind to the p75NTR whereas NGF binds selectively to TrkA, NT-3 to TrkC, and both BDNF and NT-4/5 to TrkB. *

* Adapted from von Bohlen und Halbach, O. Involvement of BDNF in age-dependent alterations in the hippocampus. *Front Aging Neurosci* 2010;2.

1.5.1.3 Neuropoietic cytokines (neurokines)

The neurotrophic cytokines belong to the IL-6 family of cytokines and include ciliary neurotrophic factor (CNTF), leukaemia inhibitory factor (LIF), cardiotrophin-1 (CT-1), neuropoietin and oncostatin M. CNTF will be discussed in greater detail later. LIF has diverse actions, including its role in neuronal differentiation, bone resorption and the stimulation of hepatic acute-phase responses.[87] LIF is present in the CNS in very small amounts whereas in peripheral nerves, Schwann cells are the primary source of this cytokine.[88] LIF is involved in regulating the inflammatory response by the immune, nervous and endocrine systems.[89] Following axotomy, LIF is retrogradely transported to the spinal cord motor neurons and to dorsal root ganglia. Due to the structure of LIF and the CNTF-receptor complex, it is probable that CNTF-responsive cells also respond to LIF.[88]

CT-1 is expressed at high levels in embryonic limb buds. It has been shown to improve survival of cultured fetal motor neurons and to prevent neuronal degeneration following axotomy of the neonatal sciatic nerve.[90] Unlike CNTF and LIF, to which CT-1 has weak homology, CT-1 does not require a glycophosphatidylinositol (GPI) component to mediate its action. CT-1 has been shown to bind to the LIF receptor in human and mouse cell lines.[91]

1.5.1.4 Glial cell line-derived neurotrophic factor (GDNF) family

The GDNF family, consisting of GDNF, neurturin, osteogenic protein-1, artemin and persephin, are distant members of the transforming growth factor-beta (TGF-β) superfamily. GDNF has pleiotropic actions exemplified by the fact that GDNF-knockout mice are born without kidneys and deficient in enteric neurons.[92] GDNF is

expressed in limb buds, Schwann cells, and cultured embryonic myotubes, from where it is retrogradely transported to motor neuron perikarya.[93] Persephin, which is approximately 40% homologous at the amino acid level to GDNF and neurturin, is generated in skeletal muscle and in the spinal cord.[94] It has been shown to improve the survival of ventral midbrain dopaminergic neurons and motor neurons in culture and *in vivo* after sciatic nerve axotomy and ureteric bud branching.[95] The GDNF receptor complex comprises two components: a non-transmembrane component, the GDNF receptor-α (GDNFR-α), which resembles the CNTFR-α (ciliary neurotrophic factor receptor-α) in its GPI-linked cell attachment; and a transmembrane tyrosine kinase component, c-Ret (Figure 1.7).[96] GDNF family ligands activate intracellular signalling via the receptor tyrosine kinase Ret, unlike other members of the TGF-β superfamily which signal through the receptor serine-threonine kinases.

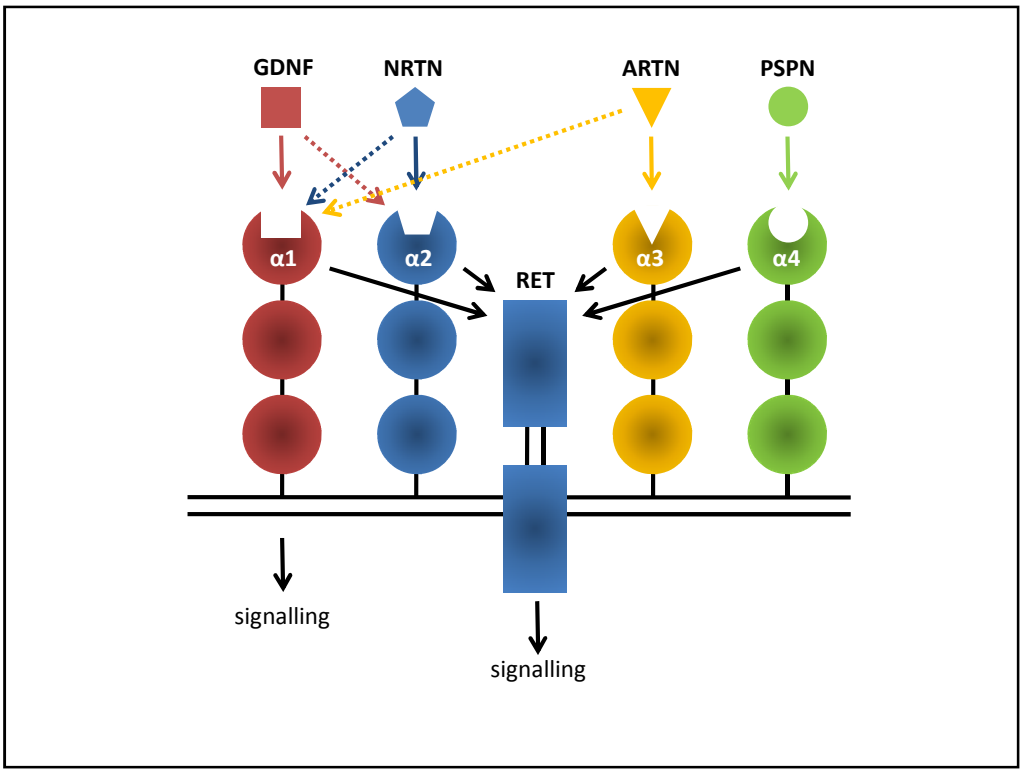

Figure 1.7. Receptor interaction with the GDNF ligand family. Following initial binding to GPI-linked GDNFRα receptors, GDNF family ligands activate the transmembrane Ret tyrosine kinase (RET). Respectively, GDNF binds to GFRα1, neurturin (NRTN) to GFRα2, artemin (ARTN) to GFRα3 and persephin (PSPN) to GFRα4.*

1.5.1.5 Insulin-like growth factors (IGFs)

The IGF family, which comprises IGF-1 and IGF-2, are polypeptide hormones which share homology to each other and to insulin. The IGFs are distributed throughout the body with a serum concentration 1000 times greater than that of insulin.[97] IGF-1 is an anabolic factor that stimulates DNA synthesis, cell proliferation, and has been shown to improve regeneration but not survival of cultured sensory neurons.[98] The actions of both IGF-1 and IGF-2 are mediated via the IGF-1 receptor (IGFR-1), a

*Adapted from Saarma, M. GDNF - a stranger in the TGF-beta superfamily? *Eur J Biochem* 2000 Dec;267(24):6968-71.

tyrosine kinase receptor belonging to the insulin receptor family. IGFR-1 activates mitogenesis via an almost identical pathway to that involving insulin, whereas the IGFR-2 pathway differs completely. Receptor binding results in activation of the PI3-K pathway and downstream phosphorylations. Subsequent involvement of the phosphokinase B and mTOR pathways leads to activation of a large number of transcription factors.[99]

1.5.1.6 Fibroblast growth factors (FGFs)

FGFs are polypeptide growth factors with diverse functions and comprise 23 members of which 10 are expressed in the developing CNS.[100] Human FGFs are structurally related proteins sharing 30-60% homology and contain 150 to 300 amino acids.[101] FGFs are essential for perinatal development and in the postnatal stage, exhibit homeostatic functions in response to injury or in regulating the electrical excitability of neurons amongst other cells.[102]

1.5.1.7 Other neurotrophic factors

Several other neurotrophic families are summarised in Table 1.1. These include less frequently distributed or more recently discovered molecules. One such example is hepatocyte growth factor, a pleiotropic factor which stimulates cell migration in addition to promoting cell survival and differentiation. This factor has been shown to have a synergistic action with NGF in stimulating axonal outgrowth of sensory neurons.[103]

1.5.2 Ciliary neurotrophic factor

Ciliary neurotrophic factor (CNTF) is an endogenously occurring protein with a molecular mass of approximately 22 kDa. It is a member of the neuropoietic cytokine family, and is structurally and functionally related to its counterparts, leukaemia inhibitory factor, cardiotrophin-1 and IL-6. Initially identified as an agent that enhances survival of embryonic chick ciliary ganglion neurons, it has since been purified to homogeneity from sciatic nerves.[104,105] Although not causally related to neurological disease, CNTF deficiency is found in 2-3 % of the human population due to a frameshift mutation in exon 2.[106] CNTF has a role in CNS development and injury, and supports survival of retinal, hippocampal, striatal and sensory neurons.[107-110] CNTF knockout mice develop a progressive loss of motor neurons whereas CNTFR-α knockout mice do not survive postnatally due to severe motor neuron defects.[111,112] In terms of its use as a neuroprotective therapy in the eye, delivery of the agent is via the intraocular route directly into the vitreal or subretinal space, as the blood–retinal barrier restricts access from the bloodstream to the neural retina.

1.5.2.1 CNTF receptor signalling

The CNTF receptor tripartite complex is composed of the following components which constitute members of the class I hematopoietin receptor family:

1. A CNTFR-α subunit;
2. An IL-6 receptor gp-130b subunit;
3. A LIF receptor–β (LIFR-β) subunit of the LIF receptor.

A characteristic feature of this receptor family is the presence of a cytokine binding domain (CBD).[113] The latter is composed of two fibronectin III domains bridged by a proline-rich residue. The C-terminal fibronectin III domain is composed of a conserved WS*X*WS sequence whereas the N-terminal domain is characterised by the presence of two disulfide bridges. Cytokine binding occurs at the boundary of either fibronectin domain.[114]

CNTF activates signalling by inducing heterodimerisation of its α-receptor components, the gp130 subunit and the LIFR-β subunit, respectively.[115]. Dimerisation of the α-receptor components results in activation of receptor-associated tyrosine kinases and subsequent downstream janus kinases (JAK) and tyrosine kinases (Tyk). Activation of JAK and Tyk enzymes initiates phosphorylation of intracellular signalling molecules, including the MAPK pathway, NFκB and STAT family of transcription factors (Figure 1.8).[116] Induction of JAK-Tyk kinases by LIF/CNTF cytokine family members results in varied responses according to cell type. This is due to activation of distinct patterns of JAK-Tyk phosphorylation with transduction of cell-specific second messenger cascades.[117] Of the STAT family, CNTF preferentially activates STAT-3. Upon activation, STAT-3 dimerises with itself or other STAT proteins (e.g. STAT-1). The resultant complex translocates to the nucleus where it binds to a DNA sequence found in the promoters of genes responsive to CNTF, inducing transcriptional activity.[118]

As the CNTFR-α subunit lacks a transmembrane or cytoplasmic domain, it is anchored to the plasmalemma by a glycophosphatidylinositol (GPI) linkage. Via phospholipase C-mediated cleavage, the CNTFR-α subunit can be released from the

plasma membrane as a soluble protein.[119] The latter hybridises with CNTF to form a CNTF–CNTFR-α complex in a 1:1 ratio, which further forms a hexameric complex, consisting of CNTF, CNTFR-α, gp130 and LIFR-β in a 2:2:1:1 ratio.[120] Soluble CNTFR-α has been detected at high levels in human cerebrospinal fluid and serum and enhances signalling capabilities in cells which are otherwise unresponsive to CNTF alone.[121,122] The CNTFR-α subunit has been localised to tissues outside of the CNS, including skeletal muscle where it is highly expressed, with lower expression in the adrenal gland, skin, liver, kidney, lung, bone marrow and testis.[123-127] Via the CNTF receptor-mediated signalling pathway, exogenous CNTF has been shown to activate the immediate-early gene, *tis-11*, in celiac ganglion neurons, peripheral and central neurons (septal, hippocampal, spinal cord), in addition to non-neuronal cells from skeletal muscle and the adrenal gland.[122,128]

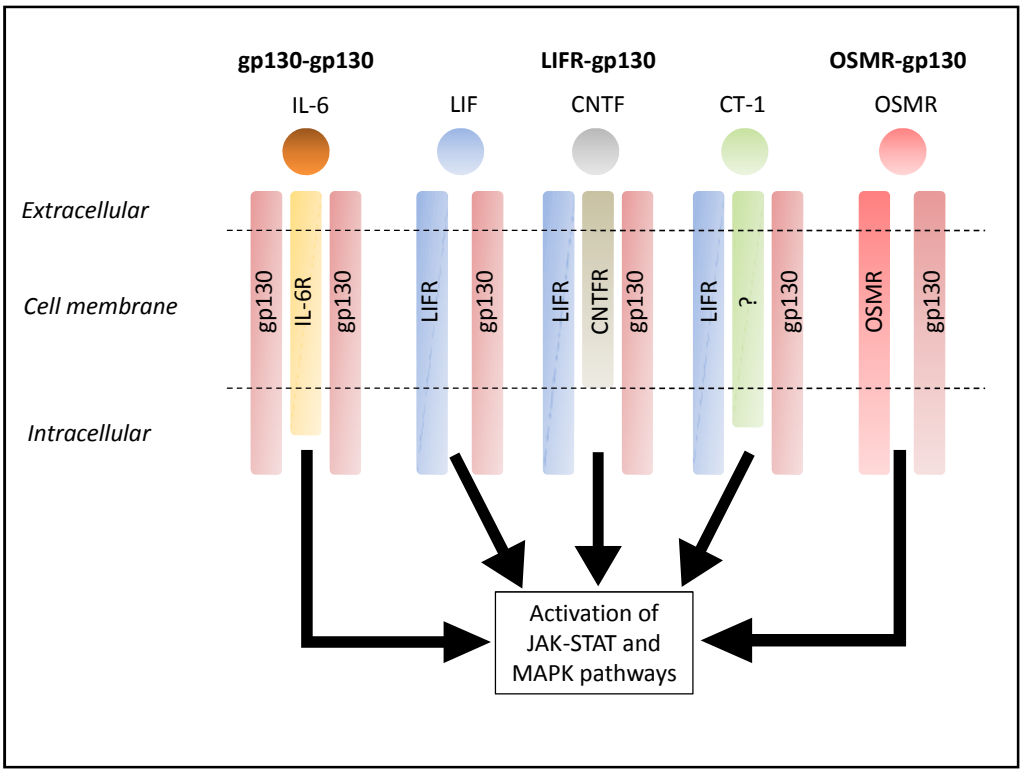

Figure 1.8. Signalling via the IL-6/LIF/CNTF receptor superfamily. The receptors are composed of two subunits: a subunit with ligand specificity towards CNTF, interleukin-6 (IL-6), leukaemia inhibitory factor (LIF), cardiotrophin-1 (CT-1) or oncostatin M (OSM) and a gp130 subunit, common to all family members. Receptor activation leads to activation of the Janus-activated kinase–signal transducer and activator of transcription (Jak–STAT) and the mitogen-activated protein kinase (MAPK) pathways.*

1.5.2.2 Biological interactions of CNTF

The Müller cell hypothesis of neuroprotection

The Müller cell is a primary target for the action of CNTF. CNTF is expressed by Müller cells and other glial cells of the retina.[129] CNTF expression is upregulated in response to stressors such as mechanical injury or light damage.[130,131] Direct activation of the Jak/STAT and MAPK pathways by increased CNTF expression in

* Adapted from Bauer, S., et al. The neuropoietic cytokine family in development, plasticity, disease and injury. *Nat Rev Neurosci* 2007 Mar;8(3):221-32.

Müller cells has been shown to improve photoreceptor survival in light-damaged and neurodegenerative disease models.[108,132,133] In contrast to the neuroprotective property on photoreceptors following intravitreal CNTF, one study showed that this effect was lost if CNTF was given in conjunction with a MAPK/ERK inhibitor. It was also seen that knockdown of STAT-3 expression significantly reduced Müller glia proliferation in the CNTF-injected undamaged retina. CNTF has been shown to control proliferation and differentiation of progenitor cell populations in the developing mammalian retina via the activation of the Jak/STAT, MAPK, and Akt signalling pathways.[108,134-138]

Although the precise mechanism of Müller-cell mediated protection of photoreceptors following CNTF delivery is unknown since photoreceptors themselves lack CNTF receptors, it may involve the release of specific survival factors.[139] Similarly, the Müller cell hypothesis of neuroprotection may have a role in RGC survival following CNTF delivery. In a similar way to that proposed in photoreceptors, enhanced RGC viability may be mediated by the release of RGC-specific survival factors.[129,140-144]

While Müller glia possess a limited ability to proliferate in the damaged mammalian retina, the action of CNTF has been shown to induce Müller glia proliferation.[145] This proliferation is likely to be related to STAT-3 expression analogous to the activation of STAT-3 as occurs in the CNTF-dependent control of stem and neuronal progenitor proliferation in the developing CNS.[146] Increased proliferation of Müller glial cells would enhance the production of endogenous neurotrophic factors (e.g. CNTF) that attenuate photoreceptor damage.

A recent study examined the ameliorating effect of electrical stimulation (ES) on photoreceptor degeneration in a rat photic injury model.[147] ES was found to stimulate production of the neurotrophins, BDNF and CNTF, in Müller cells cultured with light-reared photoreceptor cells, enhancing their survival. Additionally, ES had an inhibitory effect on the secretion of the proinflammatory cytokines, IL-1β and TNF-α in microglia.

Effect on photoreceptors

The direct interaction between CNTF and photoreceptors is debated with certain reports showing the presence of the CNTFR-α on outer segments whilst others argue against this.[139,148] There is nevertheless much evidence to support the protective effect of CNTF on rod and cone photoreceptors. Although the exact mechanism of neuroprotective action on photoreceptors is unknown, a number of hypotheses have been proposed, including: 1) a direct action on photoreceptors to inhibit apoptosis; 2) the activation of Müller cells to produce photoreceptor survival factors[139]; 3) the enhanced metabolism of circulating glutamate via increased synthesis of glutamate transporters to reduce its toxic effects[149]; 4) the increased resistance to toxic metabolites.[150] LIF, a cytokine related to CNTF, has been shown to have a direct effect on photoreceptors. Intravitreal LIF did not protect photoreceptors in photoreceptor-specific *gp130* KO mice but did improve photoreceptor survival in Müller cell-specific *gp130* KO mice.[151] It is possible that CNTF may act in a similar way to LIF. The protective effect of CNTF on photoreceptor

cells *in vitro* has been demonstrated in previous studies and the proposed mechanism involves activation of the PI3K or CREB1/ATF1 signalling pathway.[152,153]

Initial *in vivo* studies found that CNTF protected normal albino rat retinas from the damaging effects of constant light. Following intravitreal injection of CNTF at a concentration of 1 µg/µl, albino Sprague-Dawley rats were placed into constant fluorescent light at an illuminance of 115-200 footcandles. After one week in constant light, CNTF-injected eyes showed greater ONL thickness with preservation of normal morphology in surviving photoreceptors.[154] A protective effect on photoreceptor survival was also seen between one to four weeks following intravitreal CNTF injection (500ng/µl) in *Pde6b*$^{rd1/rd}$, *nr/nr*, and rhodopsin Q344ter mutant mice carrying naturally-occurring retinal degenerations.[155] In a feline model of rod-cone dystrophy, repeated intravitreal injections of a human CNTF analogue from postnatal day 10, significantly prolonged photoreceptor survival and reduced the presence of apoptotic cells.[156] However, certain models did not show a protective effect following intravitreal CNTF which may be explained by the bioavailability of the agent and response according to species/strain differences.[157]

Prolonged delivery of CNTF in retinal degeneration models has been achieved using recombinant virus gene therapy. Delivery of CNTF with a recombinant adenovirus delayed photoreceptor degeneration and increased the amplitude of scotopic ERGs in *Prph2*$^{Rd2/Rd2}$ mice.[158] Intravitreal injection of an adeno-associated virus (AAV) carrying CNTF with a green fluorescent protein (GFP) marker slowed photoreceptor degeneration in early postnatal *Prph2*$^{Rd2/Rd2}$ mice and in adult P23H and S334ter rhodopsin transgenic rats.[159] The postulated mechanism for photoreceptor

protection following intravitreal injection was due to diffusion of secreted CNTF across the retina with protection of photoreceptors occurring indirectly via activation of retinal ganglion, Müller, and other non-photoreceptor cells.[133] Importantly, this report showed either unchanged or reduced ERG amplitudes in eyes administered with rAAV.CNTF.GFP.

Encapsulated cell-based technology (ECT) is another technique that has been employed to provide a sustained release of agent. To date, the ECT implants contain human RPE cells that have been transfected with the CNTF gene to produce CNTF protein *in situ*. Use of this semi-permeable membrane allows controlled and sustained diffusion of CNTF without eliciting an immune reaction against the inert membrane by the host eye. Animal studies showed that CNTF-secreting cells in the form of ECT delayed photoreceptor degeneration in the *rcd1* dog, which carries a rapidly progressive retinal degeneration due to a stop mutation in *Pde6b*.[160] Human CNTF trials involving use of ECT have shown promising results. A Phase I clinical trial of CNTF delivered by ECT for retinal degeneration found that CNTF was safe for the human retina even with severely compromised photoreceptors.[161] Although determination of clinical efficacy was not a primary outcome of the trial, of seven eyes for which visual acuity could be measured by conventional means, three eyes reached and maintained improved acuities of 10–15 letters at six months post-implantation. More recently, a Phase 2 clinical trial in humans has employed encapsulated cell intraocular implants to deliver CNTF for the treatment of geographic atrophy in age-related macular degeneration (ARMD).[162] This trial

showed that CNTF delivered by the ECT implant slowed the progression of vision loss in geographic atrophy.

As stated earlier in this section, a potentially negative property of CNTF which has been reported is the suppression of both photopic (cone-dominated) and scotopic (rod-dominated) ERG responses following its intraocular delivery. This effect follows a dose-dependent response.[163] The continuous release of CNTF has been shown to reduce ERG amplitudes in normal mice and rabbits.[164,165] A single bolus intravitreal injection of CNTF has been associated with a transient reduction of ERG amplitude in normal rats.[166] This effect, which was evident at one week following delivery, resolved with return to normal ERG amplitude by three weeks post-injection. Therefore, CNTF is associated with ERG alterations but whether these correlate to a negative functional effect is open to question. Although most cases of inherited retinal degeneration are associated with suppression of ERG, this is not always the case. For instance, reduced or absent ERG amplitudes, as seen in Duchenne muscular dystrophy, have minimal effect on vision.[167,168] Experimental evidence to support the functional effect of CNTF has been reported in rat eyes injected with AAV-CNTF. At therapeutic doses that provided protection from constant light damage, no ERG suppression was seen in AAV-CNTF injected eyes, although at higher doses, both ERG amplitudes and optokinetic responses were decreased.[169]

CNTF has been shown to stimulate the regeneration of cone outer segments in mice carrying a retinal degeneration which involves secondary cone loss.[170] In this study, S334ter mice received an intravitreal injection of CNTF protein either as bolus or in the form of ECT to provide long-term delivery. CNTF-treated eyes showed a greater

density of PNA-positive or red/green (RG) opsin-positive cells and greater cone b-wave amplitude than control eyes. The precise mechanism of secondary cone loss in such retinal degenerations is unclear although the following hypotheses have been proposed[171]:

1) Release of toxic byproducts following rod degeneration;
2) Loss of purported "rod-derived cone viability factors" (RdCVFs);[172]
3) Loss of structural support due to rod degeneration;
4) Altered cone morphology with new and abnormal synaptic connections;
5) Alterations in RPE and Müller cells following loss of rods.

A point of note in models of CNTF injection is the neuroprotective effect on photoreceptors which arises as a result of the mechanical injury itself. Previous studies have shown that stress to either the eye or brain can induce a low level of neuroprotection.[108,131,173] In one study to investigate the effects of a variety of stress-mediated, conditioning stimuli, Injection of control solutions demonstrated a small increase in STAT-3 expression.[108] This factor needs to be taken into account in analyses involving inter-eye comparisons between CNTF treatment and saline vehicles.

Effect on retinal ganglion cells (RGCs)

CNTF receptors have been localised to RGCs.[174] *In vitro* studies on neuronal populations which include RGCs, have shown that CNTF can promote neurite growth.[175] Following axotomisation, RGCs grow only local sproutings rather than regeneration of complete axonal extensions. Although this is primarily due to the

failure of mature neurons to regrow axons, an additional contributory factor is the formation of a gliotic scar which acts as a mechanical and biological barrier. Intravitreal CNTF has been shown to promote RGC survival and axonal regrowth following axotomisation of RGCs whilst repeated administration of CNTF can cause axon regeneration via a peripheral nerve graft or into the optic nerve.[140,176,177] More sustained expression of CNTF using an AAV-CNTF-GFP vector was shown to protect 25% of the adult rat RGC population at seven weeks after peripheral nerve transplantation with axon regeneration reaching as far as the optic chiasm.[142] Regeneration of RGCs also occurs following intravitreal injection of lens-derived β/γ-crystallins or release of these proteins from the injured lens or introduction of the yeast wall extract zymosan into the vitreous body.[178,179] The underlying mechanism for the protection of RGCs is due to generation of CNTF from retinal astrocytes. In terms of pathways, neuroprotection of RGCs in rodents has been shown to result from STAT-3 activation in Müller glial cells.[180-182] This was confirmed *in vitro* in dissociated cell cultures of adult rat retinas showing that CNTF stimulated axon outgrowth of mature RGCs via the Jak/STAT-3 and PI3K/Akt-signalling pathway.[183] *In vivo*, this study showed that the mode of RGC survival following intravitreal CNTF involved the MAPK/ERK-signalling pathway, since the concurrent use of MAPK/ERK pathway inhibitors significantly reduced the neurite growth-promoting effects of exogenous CNTF.[183]

Effect on RPE

Expression of CNTF has been localised to the RPE, in addition to the presence of the CNTFRα, LIFRβ and gp130 receptors on the apical membrane of RPE, indicating that this cell type can respond to CNTF and related cytokines.[184] Following retinal injury, CNTF expression is increased and a contribution to this may arise from increased production by the RPE. The subsequent activation of the Jak/STAT-3 pathway may result in secretion of growth factors, cytokines, and neurotrophic factors to the subretinal space, with the release of these factors acting in conjunction with Müller cell secretion to provide a protective effect for photoreceptors. Human RPE cell lines have been shown to secrete a host of neurotrophic factors such as CNTF, LIF, GDNF, BDNF, and BNGF.[185] Activation of the CNTF receptor can cause alterations in RPE cell physiology, with an increase in RPE cell survival, a change in the polarised secretion of neurotrophic factors and cytokines, and an increase in fluid absorption across the RPE. In conjunction, these homeostatic functions serve to maintain the health of the neuroretina, RPE, and choriocapillaris.

1.6 Photoreceptor transplantation

Due to its well-defined characteristics and the ability to provide objective measures of function, the eye represents a unique model to observe the effects of neural degeneration and repair. Similar to other neural tissue, the retina has a limited regenerative capacity, particularly so following injury. Indeed, reparative mechanisms following retinal injury in higher vertebrates can have a deleterious effect on function. For example, damaging effects to neural tissue may occur following retinal detachment due to the development of proliferative vitreoretinopathy or in exudative ARMD which may be accompanied by the formation of a fibrovascular scar.[186] Therefore, the absence of endogenous mechanisms to replace lost retinal neurons, and in particular photoreceptors, requires restoration of new cells by transplantation. Retinal repair via cell transplantation has been investigated during the course of the last century with the vast majority of work having been conducted in animal models. However, not all animal studies serve as adequate models for human disease, due to inter-species biological variability and due to the lack of an appropriate model for certain diseases, especially the absence of a lower vertebrate model of macular degeneration.

In all cases, the aim of transplantation experiments has been to restore viable cells into the subretinal space. Under normal circumstances, the retina and RPE are closely apposed with maintenance of a potential space between both structures dependent on diffusion gradients across cells. If compromised, this space may accumulate fluid with resultant separation of neural retina from the RPE. This space

is exploited in transplantation studies as it provides a plane in which to deliver donor cells in order to replace photoreceptors on one side or RPE on the other. Recent human trials involving subretinal implantation of a photosensitive electronic chip in cases of photoreceptor degeneration have confirmed the proof-of-principle concepts that: a) the subretinal space provides a viable plane in which to deliver treatment modalities; and b) direct stimulation of inner retinal neurons can establish an electrical pathway and therefore restore a visual signal in the absence of functioning photoreceptors.[187,188] Transplantation success in animal models is dependent on a number of factors related to both the host and donor. In particular, donor cells are required to originate from a source that will provide sufficient numbers to enhance transplantation efficiency. This factor, in the light of transplantation studies, is described in more detail in the following sections. In order to broadly classify donor cell types according to stage of maturation, the following terms will be used to refer to cells with a range of self-renewing and differentiation potential: a “progenitor” is a generic term to describe a cell that has not undergone terminal differentiation; a “stem cell” is a form of progenitor cell that is capable of both self-renewal and generation of any germ cell line; a “precursor” is a form of progenitor cell downstream of a stem cell that is normally unipotent and has therefore lost its stem cell multipotency.

1.6.1 Donor cells

A primary issue in transplantation biology is the choice of donor material and with regards suitable donor cell selection, the key factor that determines survivability is the stage of maturation. Early retinal transplantation studies used what was

determined to be the most appropriate donors at an early stage of development in the form of embryonic retinal tissue. With the more recent identification of stem cells in both CNS and non-neural tissue, this specialised niche of pluripotent cells has been employed as retinal donor material. Promising results have been seen in animal models using embryonic stem (ES) cells as donors. However, a major concern with the use of ES cells is the potential for tumorigenesis. With respect to retinal transplantation, another risk is that ES cells may give rise to non-neural lineages. Also, the use of non-neural stem cells has lost favour due to the concept of fusion occurring between donor and host cells rather than actual transdifferentiation of donor cells.[189] Additionally, different stem cell sources have been shown to result in a variable degree of differentiation towards retinal and RPE cells.

1.6.1.1 Embryonic stem cells

Photoreceptor and RPE development begins in the embryonic stage and continues into the early postnatal phase. In the human retina, for instance, photoreceptor development begins at approximately 13 weeks, although the retina is not completely developed until 3–4 months after birth with formation of the macula. Beyond this stage, the neural retina, comprising the RPE and photoreceptors, has almost negligible regenerative capacity. For this reason, the most logical source of donor cells is the embryonic retina. ES cells are derived from the blastocyst stage which occurs between fertilisation and implantation. The blastocyst contains an inner cell mass of approximately 100 cells which are an abundant supply of pluripotent stem cells. This pluripotent capacity allows ES cells to form any of the three germ cell lines - ectoderm, mesoderm and endoderm – and therefore produce

any cell which forms the organism. Although the duration between pluripotency and designated differentiation is relatively short-lived, under optimal conditions, stem cells can be cultured to produce a line of self-renewing stem cell progeny which allows the potential to derive any type of cell *in vitro.* An example related to ocular biology is a recent study which showed the ability to grow an optic cup from cultured mouse ES cells.[190] This optic cup formation demonstrated generation of stratified neural retinal tissue showing *Rx* (or *Rax*) expression, in a regulated manner mimicking *in vivo* development.

Although much of the work on stem cell technology has been conducted on mouse ES cells, it is important to realise that different molecular cues operate in human ES cells. Maintenance of an *in vitro* mouse ES cell line capable of self-renewal involves the following factors: 1) LIF via the STAT-3 signalling pathway; 2) bone morphogenetic protein (BMP)[191]; and 3) the canonical Wnt signalling pathway.[192] Conversely, human ES cells are able to self-replicate in the absence of LIF or STAT-3 whereas BMP stimulates them to produce endodermic progeny.[193-195] In view of these fundamental differences, it is necessary to regard human ES cell technology as a separate field to that derived from animal models.

1.6.1.2 Embryonic neural stem cells

Embryonic neural stem cells (NSCs) are an additional source of progenitor cell which provide some benefit over ES cells. Embryonic NSCs are differentiated towards neural cells and do not show tumorigenicity following transplantation. Also, the lack of an MHC class I or class II receptor on embryonic NSCs offers a significant degree

of immune privilege thus reducing the risk of rejection or graft versus host disease.[196] Embryonic NSCs have a number of unique properties that include:

1) Species-specific variation – as an example, murine progenitors divide for extended periods while rat progenitors originating from the developing striatum may undergo a period of senescence at approximately one month in culture.[197]
2) Spatial variation - embryonic NSCs generate different types of cells depending on their site of origin. Spinal cord cells give rise to spinal cord progeny.[198] Cultured basal forebrain stem cells produce more GABA (γ-amino butyric acid)-containing neurons, indicative of their basal-specific region, than dorsal stem cell neurons.[199] Neurospheres derived from the CNS express region-specific markers, indicating that their originating stem cells were regionally specified.[200]
3) Temporal variation - embryonic NSCs exhibit different behaviour depending on their stage of maturation. Murine forebrain embryonic NSCs proliferate in the presence of FGF but not epidermal growth factor whereas this situation is reversed at later stages of development.[201] Embryonic NSCs give rise to interneurons and projection neurons whereas their adult derivatives generate interneurons only.[202] Embryonic NSC cell activity decreases with age.[203]

1.6.1.3 Retinal progenitor cells

In vertebrates, the bilateral evagination of the diencephalon in the early neurula marks the earliest morphological sign of ocular development. Formation of the optic

vesicles results from the continued evagination of the optic primordia. Extension of the optic vesicles towards the overlying, non-neural surface ectoderm results in formation of the lens and cornea. The subsequent invagination of the lens placode and optic vesicle gives rise to a lens vesicle and a double-layered optic cup that defines the final shape of the eye. The inner layer of the optic cup generates the neural retina whilst the outer layer forms the RPE.[204] The presence of surface ectoderm is critical to development of neural retina, as confirmed by explant studies showing that the neural retina failed to differentiate in the absence of surface ectoderm.[205] Similarly, this role is confirmed by the finding that 180^{o} rotation of the amphibian optic cup such that the presumptive RPE abuts the surface ectoderm results in it forming a secondary neural retina.[206]

During the period of close apposition with the surface ectoderm, the earliest defined transcription factor expressed by the presumptive neural retina is the paired-like homeobox gene *Chx10*.[207] Although not essential for determining retinal cell fate, *Chx10* plays a major role in regulating cell proliferation as evidenced by mutant *Chx10* mice which show reduced proliferation of retinal progenitor cells (RPCs).[208] This transcription factor is critical for normal ocular development and human mutations in *Chx10* have been shown to cause microphthalmia, cataracts and iris abnormalities.[209] Although at an early stage RPCs express the transcription factor *Six3*, they continue to express *Chx10* at a later stage along with, *Crx*, *Rx*, *Pax6*, and *Otx2*.[210]

A major role in the development of the neural retina is provided by the FGF family. Presumptive frog and chick RPE have been shown to transdifferentiate towards

neural retina in the presence of FGF in culture conditions.[211] Additionally, culture of chick optic vesicles in the presence of FGF-2 neutralising antibodies causes inhibition of neural retinal development.[212] In terms of RPC derivation, human ESCs have been shown to differentiate towards RPCs with high efficiency in the presence of noggin, dkk1 and IGF-1.[213] Similarly, murine ESCs are able to generate RPCs using a combination of dkk1, lefty (a nodal antagonist), fetal calf serum, and activin, although noggin was not found to be effective in this derivation.[214]

The temporal sequence of retinal histiogenesis is generally conserved across species and is summarised as follows:

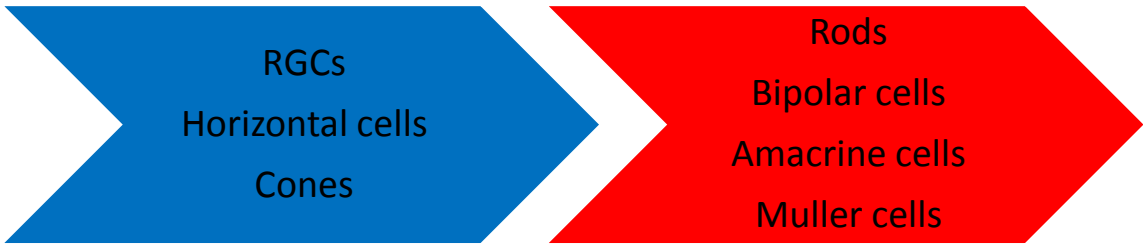

RGCs and horizontal cells develop first, followed by cones, amacrine cells, rods, bipolar cells, and finally Müller cells in overlapping phases. This chronological sequence is reflected in the type of progenitor cells from which they are derived. One colony of RPCs is responsible for early retinal cell development whilst another forms retinal cells at late stages of the embryonic period and in the postnatal phase.[215] These early and late RPCs co-exist as a distinct population, each with a time-ordered activation. Early RPCs generate neurons whereas late progenitors are generally directed towards producing glial cells.[216] However, a degree of plasticity

exists within these subtypes as evidenced by the derivation of early-born RGCs from late RPCs *in vitro*.[217]

1.6.1.4 Adult neural stem cells

It is a well-established fact that glial cells, which constitute the predominant cell within the CNS, continue to proliferate beyond the postnatal stage into adult life. Although glial proliferation and migration primarily occurs following degeneration, it has been shown to occur in oligodendrocyte precursors following demyelination restoring a functional population of myelinated nerve sheaths.[218] As discussed earlier, proliferation and migration of retinal glial cells occurs in response to a variety of insults, such as in proliferative vitreoretinopathy.

However, a key advance in stem cell biology has come from recent work showing that a degree of regenerative capacity is also found in a number of adult neuronal tissues. The most widely reported of these areas, or "niches", are located in the subventricular zone (SVZ) of the lateral walls of the lateral ventricles of the brain and the subgranular zone (SGZ) of the dentate gyrus, within the hippocampus.[219] These niches contain adult neural stem cells (NSCs) of astroglial morphology, which under normal conditions, give rise to neuronal precursors, or "neuroblasts". SVZ-derived neuroblasts reach their target area, the olfactory bulb, via a long migratory route whilst SGZ-derived neuroblasts extend a short distance of a few millimetres to reach the granular cell layer of the dentate gyrus. In keeping with the classical definition of stem cells, adult NSCs derived from the SVZ and SGZ show common properties with their ancestral cell of origin, the embryonic stem cell. They retain the capacity of self-renewal, which they exhibit over the course of the lifespan of the organism.

Also, under *in vitro* conditions, they demonstrate their multipotentiality through the generation of neurons, astrocytes, and oligodendrocytes.[220]

The pluripotent nature of adult NSCs was demonstrated in an *in vitro* study showing that SGZ-derived adult NSCs could be expanded as neurospheres to generate all germ layers in chimeric chick and mouse embryos.[221] Similarly, SGZ-derived adult NSCs could generate cells of haematopoietic lineage when transplanted into the bone marrow of irradiated mice[222] and into muscle cells *in vitro* and *in vivo*.[223] The pluripotentiality of SVZ-derived adult NSCs has not been studied in great depth although they have been shown to demonstrate similar properties to their SGZ-derived counterparts when transplanted in the rostral migratory stream of the rat brain.[202]

The potential to derive retinal neurons from SGZ-derived NSCs has been explored in a rat mechanical injury model.[224] This study showed engraftment of NSCs in injured adult retinas with differentiation into neuronal lineage and establishment of graft-host contacts with the formation of synapse-like structures. However, the NSCs failed to differentiate into retina-specific phenotypes as evidenced by the absence of HPC-1, calbindin, and rhodopsin expression.

1.6.1.5 Mesencymal stem cells

A key factor in the generation of retinal neurons from adult stem cells is the production of sufficient cell numbers. Given the relative paucity of adult NSC sources, another possibility for the generation of neural cells that has been explored is via the transdifferentiation of non-neural cells. Mesenchymal stem cells (MSCs), are one such example that have been reported to differentiate into neurons[225] and

specifically, retinal neurons, both *in vitro* and *in vivo*.[226,227] MSCs have been shown to express photoreceptor proteins following subretinal injection and in the *in vitro* setting, the latter through the expression of rhodopsin in cultured rat MSCs.[228,229] However, other studies have disputed the potential of MSCs to differentiate into neural retinal cells and, moreover, have demonstrated their transdifferentiation towards glial components.[230] Additionally, although certain reports have shown successful integration of MSCs into host retina, the integration rate is limited to small numbers. Integration of MSCs has been demonstrated in the setting of retinal laser injury,[75] ischaemia,[231] and following injection into the RCS rat tail-vein of bone marrow-derived MSCs.[232]

The main benefit of MSCs appears to derive from a trophic response on host cells. Both the subretinal[233] and intravenous[232] administrations of MSCs have been shown to delay photoreceptor loss and preserve function in animal models of retinal degeneration. A role for the neuroprotective property of MSCs was evidenced by the upregulation of CNTF expression following their intravenous delivery.[232]

1.6.1.6 Induced pluripotent stem cells

A major breakthrough in stem cell technology has come from the discovery that ESC-like cells, termed "induced pluripotent stem cells" (iPSCs), could be generated from mouse fibroblasts by the simultaneous induction of four genes: *Klf4*, *Sox2*, *c-Myc*, and *Oct4*.[234] This was successfully repeated using human fibroblasts to generate human iPSCs.[235]

Although iPSCs share properties with ESCs such as the capability of self-renewal, pluripotency, morphology, and gene expression, they do differ in important

respects. ESCs are derived from the blastocyst stage prior to separation of the soma and germ cell lineages whereas iPSCs are derived from somatic cells. Unlike the germ cell which passes on its genetic material to the next generation and is therefore immortalised, the life of the somatic cell is finite as it ends with the death of the organism. Due to this, mutations in the germ cell are subject to evolutionary selective pressures, including natural selection, whereas somatic cells escape these potentially beneficial forces.[236] The genomic integrity between ESCs and iPSCs may differ as a result, with iPSCs acquiring genetic alterations at a number of phases. The reprogramming required to generate iPSCs from a limited number of transcription factors has also been shown to be responsible for the introduction of copy number variations (CNV) on passage, which may induce mutations.[237,238] The observation that human iPSCs contain *de novo* mutations that are not present in ESCs in addition to the detection of CNVs indicates the inherent genomic instability and tumorigenic potential of these cells.[239] Further differences are seen in that human iPSCs differentiate to neural lineages at a much lower rate compared to ESCs irrespective of their origin whilst reduced survival of RPE cells derived from iPSCs has also been shown.[240]

Importantly, the recent finding that retinal cells could be derived from human iPSCs paves the way for future therapeutics using this technology.[241] The culture of iPSCs in the presence of recombinant Dkk-1, a Wnt antagonist, and recombinant Lefty A, a Nodal antagonist, generated the production of RPE cells as well as the induced expression of markers of retinal progenitor cells. The further addition of taurine and retinoic acid generated cells with positive expression of photoreceptor markers as

seen in the majority of human cell lines. ES cells and iPSCs have also been shown to differentiate into optic vesicle- and optic cup-like structures exhibiting a degree of lamination.[190,242-244] The potential for the aforementioned techniques not only lies in obviating the need for embryonic sources, an understandably controversial area, but also means that patient-specific therapies may be devised with derivation of iPSCs from autologous sources thereby reducing the risk of immune rejection.

1.6.1.7 Cilliary-derived stem cells

In ananmniotes, a highly specialised area located at the anterior retina, termed the "ciliary marginal zone" (CMZ), provides a continual source of retinal progenitors and multipotent cells that generate all types of neurons throughout the life of the organism.[245] In the adult mammalian retina, the area of the CMZ is much reduced in size and is localised to the pars plana, a flat sheet of cells connecting the ciliary body and the retina. This latter CMZ is believed to remain a vestigial source of stem cells with an extremely limited capacity to undergo cell proliferation and to regenerate neuronal cells.[246,247] These cells have been shown to form clonogenic neurospheres *in vitro* in keeping with stem cell characteristics and to divide with the addition of FGF-2[247] as well as the ability to generate progeny that express retinal cell markers.[216] Additionally, these cells have been shown to express several markers seen in NSCs including Nestin and LeX/SSEA-1[216] and low levels of pan-neuronal markers such as beta-III-tubulin. Conversely, the stem cell nature of these cells has been disputed by other authors who have instead found that these cells originate from differentiated pigmented ciliary epithelial cells whilst demonstrating ectopic

upregulation of pan-neuronal markers.[248] This study found that the ciliary epithelial cells did not form retinal neurons or glia, *in vitro* or *in vivo*.

Recent work has demonstrated the finding of a novel mammalian retinal stem cell niche in the planoretinal junction that is adjacent to the vestigial CMZ.[249] Cells derived from this area were shown to migrate bidirectionally into the pars plana and the retina. These progenitor cells demonstrated neurogenic activity through the generation of RGCs as evidenced by the increased numbers of *Atoh7*^{LacZ}-expressing cells in this region, the latter providing a marker of RGC specification.

1.6.1.8 Müller glial cells

Following injury or degeneration, Müller cells undergo reactive gliosis, characterised by their proliferation and migration and associated with morphological and molecular changes.[250,251] As a result, Müller cells are capable of dedifferentiation and of generating retinal progenitors with some cells even giving rise to retinal neurons. The process of neurogenesis derived from Müller cells is particularly well-preserved in fish which is able to repair large areas of retinal damage whilst in higher order animals, this capacity is almost negligible.[6,252-254] However, *in vitro* studies have shown the capacity to increase Müller cell proliferation with the addition of exogenous growth factors[255] and the characterisation of Müller cells outside of their natural environment has led to the suggestion that they exhibit stem cell-like properties when cultured in sphere aggregates. This is further evidenced by the fact that reactivated Müller cells can be used to derive retinal neurons, astrocytes, and oligodendrocytes.[256]

Injury to RGCs and amacrine cells from *N*-methyl-D-aspartate (NMDA)-mediated excitotoxicity can result in transdifferentiation of Müller cells into other retinal cell types in chickens.[145,257] Recent work has shown that human Müller cells can be used to derive rod photoreceptors which exhibit similar electrical properties to their normal adult rod counterparts as confirmed by patch-clamp recordings.[258] This property may be related to the expression in Müller cells of the transcription factor, paired homeobox gene 6 (*PAX-6*), which is critical in eye development. *PAX-6* positive Müller cells give rise to neural progenitor cells that originate in the inner nuclear layer. Following migration of these cells from the inner to the outer nuclear layer, *PAX-6* becomes downregulated whilst another transcription factor, cone-rod homeobox gene (*CRX*), that is responsible for photoreceptor specification, is upregulated.[6] Conversely, other studies have found that Müller cells are unable to generate photoreceptors in the injured mouse retina, instead resulting in a non-proliferative gliosis.[259] The suggested hypothesis was that the blockade of DNA synthesis during the S-phase of the cell cycle prevented the transdifferentiation of Müller cells into photoreceptors in the mammalian retina.

1.6.2 Photoreceptor transplantation studies

A number of therapeutic approaches have been explored to replace lost photoreceptors involving the transplantation of embryonic stem cells, progenitor cells, total retina, neural retinal cells, and photoreceptors. The aim has been to restore photoreceptors that form functional connections between the donor cells and host inner retinal neurons thereby re-establishing the retinal circuitry. The first described report of successful transplantation of ocular tissue *per se* was almost a

century ago and conducted in the spotted rat,[260] whilst the earliest description of retinal transplantation, in 1959, followed the transplantation of fetal rat retinas into maternal eyes.[261] A broad range of studies were conducted by one group over 40 years to investigate different treatment modalities in animal models of retinal degeneration, including the use of rodent fetal retina[262-266], human RPE cells[267,268] and human neural progenitor cells.[269,270] These landmark studies, amongst others, have formed the basis of retinal transplantation research as discussed in the following section.

1.6.2.1 Barriers to photoreceptor integration

Rosette formation

A major obstacle to successful integration of transplanted cells is the formation of retinal rosettes. As their name suggests, these aggregrates of retinal cells form a characteristic rosette-like histotypic pattern. Rosettes occur *in vivo* in retinal malignancies and are a hallmark feature in retinoblastoma. They may also be seen in developmental disorders such as retinal dysplasia, and occasionally occur in retinal detachment. The precise mechanism of formation is unknown. In terms of rosette formation in experimental conditions, they are more commonly seen following transplantation from embryonic sources. Although their formation follows that of normal retinal development, the retinal layers are inverted, with photoreceptor outer segments aligned toward the centre of the rosette and synaptic connections toward the exterior.[271-274]

Rosettes are able to form connections with host neurons, although these synapses are limited in number and do not demonstrate the presence of functional

responses.[275-277] Aside from this limited synaptic formation, a further mechanical effect is the obstruction of other cellular interaction between donor and host tissue. This may be due to the physical barrier of the outer limiting membrane of the rosette that inhibits interaction between the donor photoreceptors and the RPE.[278-281] Additionally, the membrane and rosette structure itself may affect cell adhesion that is critical to the normal migration and integration of cells in retinal development. An associated issue with rosette development is the risk of tumour/teratoma formation with murine experiments involving ESC donors showing tumour formation within weeks following transplantation.

Retinal architecture

The normal outer retina presents a challenge for donor cell integration due to the presence of the outer limiting membrane and the distance required for extension of the inner fibre towards a synapse in the outer plexiform layer. It may also be the case that the adult retinal environment is unable to provide the biological cues required for retinal neuronal development. Some groups have developed methods to disrupt the outer limiting membrane by genetic[282] or pharmacological means.[283] Certain functional disorders affecting the photoreceptors do not result in loss of photoreceptors in which case it may be difficult for the donor cell to traverse the outer retina. However, loss of the photoreceptor layer, as may occur in certain inherited degenerations or following a laser injury, may provide a more suitable environment for cell replacement as the long-distance connectivity is not required to achieve functional integration. Certain groups have developed a pharmacological

model to induce degeneration of the photoreceptor layer using a biodegradable implant.[284]

Immune rejection

The transplantation of embryonic retina has been shown to result in long-term survival of the graft in part due to the relative immunoprivileged status of the subretinal space. However, immune rejection can occur due to general host mechanisms following introduction of antigen or specifically due to compromise of the blood–retina barrier. Techniques to surmount this problem are being developed in the way of stem cells that show reduced human leukocyte antigen expression.[285]

1.6.2.2 Embryonic and postnatal retinal cell transplantation

The key factor in transplantation medicine is the restoration of function following introduction of the donor cell, tissue, or organ. With respect to photoreceptor transplantation, successful transfer of donor material, irrespective of source or stage of maturation, is characterised by the process of integration. An integrated photoreceptor is defined as having the following characteristics:

1. The ability to survive in the transplanted host;
2. The formation of direct contact between its outer segment and the RPE;
3. The development of synaptic connections with the inner retinal neurons.

Fetal retinal tissue has been shown to survive after transplantation in studies of mice, rats, rabbits, monkeys[261,286-291], and more recently, humans.[292-295] Increased survival, differentiation and integration of donor cells were observed when using

donors before embryonic day 15, indicating that progenitor cells within the embryonic tissue donors had a significant role in retinal transplantation.[296-298] However, even adult photoreceptors could integrate into the ONL of normal mouse retina at two weeks post transplantation although the long-term survival of such transplants is not expected.[299]

Photoreceptor-sorted transplantation

Cone integration occurred following transplantation of FACS-sorted embryonic donor tissue from CRX-GFP mice that express GFP in all photoreceptor progenitors. Successful integration was shown in two genetic models of Leber's congenital amaurosis (*Crb1*$^{rd8/rd8}$ and *Gucy2e*$^{-/-}$ mice) and was highest in the cone-deficient *Gucy2e*$^{-/-}$ retina.[300]

The survival of donor cells with evidence of preserved morphology and laminar organisation of the host retina has been shown in a number of reports. However, the key factor that has limited functional restoration has been the demonstration of successful integration of donor cells. A proof of concept study relating the stage of maturation of donor cells to integration efficiency demonstrated that rod precursor integration was related to the temporal expression of the transcription factor, *Nrl* (specific for post-mitotic rod precursors and persisting in adult rods).[301] This study identified the optimal ontogenetic stage of donor cells for transplantation by showing that successfully integrated rod photoreceptors were derived from post-mitotic rod precursors (postnatal 1 to 7 days) and not from proliferating progenitor cells. The establishment of downstream synaptic connections by these integrated

cells was demonstrated by the generation of positive functional responses. The Nrl-GFP$^{+/+}$ mouse model has also been used in a recent study showing functional rescue in retinal degeneration. Following transplantation of Nrl-GFP$^{+/+}$ sorted rod precursors into *Gnat1*$^{-/-}$ mice that lack rod transducin, transplanted mice could elicit light-evoked responses in the brain and demonstrated visual improvements in dark-adapted optokinetic and water maze testing in mesopic conditions.[302] One criticism of this paper however is that these responses can all be generated from residual cones which are fully functional in this mouse model. It is unclear why the researchers did not present pupillometry data, which has a much stronger input from rods compared to cones.

Paracrine effect

Almost all studies on retinal transplantation have been conducted in animal models with a much higher proportion of rods than cones. For instance, the mouse retina comprises almost 97% of rods as a proportion of its photoreceptors. For this reason, it could be argued that most murine studies have been observing primarily the effects of rod transplantation. Despite this, studies show relatively low numbers of successfully transplanted rod photoreceptors (less than 1000 cells on average). Over the last two decades, a series of studies showed successful integration of fetal retina into degenerate host retina with restoration of visual function.[303-310] However, the number of integrated donor cells was relatively low, in part due to the formation of rosettes of photoreceptors from the transplant. For this reason, the functional rescue of vision is suggested to be due in part to a paracrine effect, as evidenced by

studies confirming this following the subretinal injection of wild-type (WT) and human neural progenitor cells in Royal College of Surgeons (RCS) rats.[269]

A recent study suggested the presence of a paracrine neuroprotective effect on residual host cones following the transplantation of photoreceptors or total neural retina in the P23H rat, a model of dominant retinitis pigmentosa (RP).[311] This work showed that following transplantation, a significantly greater improvement in functional effect was observed than the effect on cell counting, suggesting that cone survival was dependent on preservation of cone function. A similar effect of host cone rescue has been observed after photoreceptor sheet transplantation[312,313] and retinal sheet transplantation in rd mice.[314] Conversely, other rat models of retinal degeneration have shown no cone rescue effect after transplantation of retinal sheets.[315-318]

Embryonic and early postnatal donors have been shown to result in a visual improvement in light-damaged rat retinas[297,319,320] with demonstration of synaptic connections occurring between transplanted embryonic retina and host retina.[321-325] A typically used animal model of retinal degeneration, akin to the equivalent phenotype in humans causing RP, is the rd mouse which has a mutation in the gene encoding the β-subunit of rod photoreceptor cyclic GMP phosphodiesterase, resulting in the rapid loss of rods from the retina shortly after birth whereas the inner retina remains. Following transplantation of dissociated early postnatal mice retinas into the subretinal space of rd mice, donor cells were shown to survive and integrate into the host retina.[326,327] Although an improvement in behavioural function[328] and a positive electrophysiological response[329] were shown, due to the

low number of integrated cells compared to the theoretical number that would be required to achieve this, the responses were thought to be due to a rescue effect of the host retina. The possibility of a trophic effect was further argued in studies that also saw the occurrence of rosette formation following transplantation. The development of photoreceptor rosettes in the rd mouse was reduced by the transplantation of flat sheets of embryonic retina that also resulted in an improvement in retinal function.[314] Interestingly, a greater functional improvement was seen in eyes with a disorganised retina than a more regular retinal structure and a further suggestion was that this improvement was due to a trophic effect.

Clinical translation

In 1995, the first human trial of photoreceptor restoration using the aforementioned principles, involved the subretinal transplantation of dissociated human embryonic retinas in patients with RP and AMD. Aside from demonstrating the technique to be safe and feasible, the results showed a significant improvement in visual acuity up to six months post procedure.[330] A post-mortem was conducted of one patient with AMD from this study who had received subretinal transplantation of microaggregates and retinal sheets from a 16-week old foetus.[331] The areas of microaggregate transplantation showed rosette formation with incomplete photoreceptor differentiation. The region of retinal sheet transplantation showed good integration but also with incomplete photoreceptor differentiation. The poor photoreceptor differentiation may have been related to the underlying disorder affecting the RPE. A separate case has also been reported of a patient with RP who

underwent subretinal transplantation of full-thickness sheets of embryonic retina and RPE.[332] Although this patient reported a subjective improvement in vision at the six year examination[308], scanning laser microperimetry did not show a parallel result. Whilst microperimetry testing demonstrated increased detection of the target at the edges of the grafted area, there was no improvement overlying the graft, indicating that the visual improvement may have been due to a trophic mechanism. A similar hypothesis for a trophic effect is suggested for the improvement of retinal function seen in the areas surrounding but not overlying the photosensitive subretinal implant that has been subject to clinical trial in patients with RP.[333]

1.6.2.3 Stem cell transplantation

Embryonic stem cells

The transplantation of neurons derived from ESCs in other regions of the CNS has shown some promising results. In animal models of Parkinson's disease, successful integration into the brain and partial restoration of function has been shown following transplantation of dopaminergic neurons generated from mouse, monkey, and human ESCs.[334,335] ESC-derived oligodendrocytes have been shown to partially repair neuronal damage following spinal cord trauma and in mouse models of spinal cord demyelination.[336,337]

With respect to retinal transplantation, there is plentiful data to suggest that ES cells can produce retinal cells and RPE. Following transplantation of ES cells, a particular issue that has generated interest is the phenomenon of cell fusion.[320,338] Cell fusion may explain the results of certain transplantation experiments and allows host cells to acquire some of the characteristics of the donor cells, e.g. gene expression or

morphology. ES cells have even been shown to integrate into host retina following intravitreal injection. One study showed that at 5 days post intravitreal delivery, integration was absent whereas at 30 days, a proportion of cells towards the inner retina had formed synapses with host inner retinal neurons at the inner plexiform layer. Other ES cells had acquired ganglion cell-like characteristics whilst others that had not integrated, had formed teratomas.[339] Intravitreal injection of ES cells pretreated with retinoic acid to enhance neural differentiation has been performed in rd host mice.[340] Results at six weeks post transplantation showed the formation of a cellular network on the retinal surface expressing neural and glial markers but not those of oligodendrocytes. Some of these cells had migrated towards the inner plexiform layer but not further than the inner nuclear layer.

Neural stem cells

Transplantation of cells targeted towards retinal cell fate, e.g. NSCs, has been shown to enhance integration efficiency. Human NSCs pretreated with transforming growth factor and injected intravitreally into rats were seen to migrate and differentiate into opsin-positive retinal cells.[341] The plasticity of NSCs towards generating retinal progeny has been shown in a number of studies. An additional major benefit of NSCs is their lack of causing tumour and rosette formation. The subretinal transplantation of rat embryonic forebrain-derived NSCs resulted in retinal cell formation[342] whilst another study using neonatal brain-derived NSCs generated neuronal and astrocytic cells in normal and retinal degenerate mice.[343]

Adult NSCs have been used as donors in transplantation experiments. Hippocampal-derived adult NSCs were shown to develop immature retinal cell characteristics following transplantation into neonatal or damaged host eyes.[344] Integration occurred after transplantation into a host with mechanical injury[345], ischaemic retinal injury[346], or in a genetic dystrophic retina.[347] Intravitreal injection of hippocampal-derived adult NSCs into adult RCS rats with RPE and retinal degeneration demonstrated appropriate integration and synapse formation, although retinal cell expression of HPC-1 and rhodopsin was limited.[347]

Retinal progenitors and induced pluripotent stem cells

Improved differentiation towards retinal cell lineage is seen following transplantation of stem cells derived from retina. RPCs have been shown to integrate with host retinas in a mouse model of Leber's congenital amaurosis caused by a mutation in the *Aipl1* gene that results in photoreceptor degeneration.[213] The Brazilian opossum serves as an ideal model for studying retinogenesis as it is born in an immature state.[348] This model was used as a host for subretinal transplantation of neonatal murine brain progenitor cells cultured as neurospheres.[349] Results showed donor cell integration into younger retinas with expression of retinal cell markers, including calciretinin and recoverin.

Recent work found that transplantation of mouse iPSC-derived retinal progenitors into rhodopsin knockout mice showed an increase in the ERG b-wave by 95 μV.[350] Subretinal transplantation of embryonic retinal stem cells in the presence of epidermal growth factor showed better integration in injured or diseased hosts[217,351]

than in normal hosts.[352] In a comparison between stem or stem-like cells derived from the limbal epithelium, ciliary epithelium, and retina, better integration was seen following transplantation of neural ciliary and retinal stem cells than of limbal epithelium.[353] Results showed appropriate localisation of staining for opsin, amacrine and bipolar cell markers. Following transplantation of human ESC-derived photoreceptor precursors into CRX knockout mice that have no ERG response, a small photopic ERG response could be elicited, correlating with the number of integrated photoreceptor precursor cells.[213] Forebrain-derived progenitor cells sustained photoreceptors for prolonged periods and slowed the deterioration of visual function following transplantation into Ush2a mice, a model of retinal degeneration resulting in a deletion of the Usherin protein.[354] This effect was hypothesised to be due to a trophic role of the donor cells or their phagocytic role in removing shed outer segment material.

1.6.2.4 Retinal pigment epithelial cell transplantation

The aim of RPE transplant studies has been to observe the effect in conditions affecting the RPE primarily, such as ARMD or certain types of RP. Transplantation of RPE is more straightforward than its neuronal counterparts as it does not require the same degree of neural connectivity or synapse formation. Embryonic RPE delivered subretinally in the form of sheets or dissociated cells has been shown to prevent photoreceptor loss in the RCS rat.[355-359] Abnormal changes in photoreceptor morphology and metabolic function were reversed with restoration of vision, suggesting a rescue effect following RPE transplantation. Transplantation of gelatin-embedded sheets of human RPE with fetal retina into light-damaged minipigs

showed an improvement in multifocal ERG, although the transplant showed only glial with no photoreceptor differentiation, suggesting a rescue effect of host retina.[360]

Translational work to investigate the effect of RPE transplantation has been conducted in patients with RPE degenerations. Subretinal transplants of human fetal RPE (13-20 weeks of gestational age) were shown to survive following transplantation in patients with dry ARMD demonstrating the feasibility of this approach even though there was no visual improvement. [294,361]

RPE cell lines are a specific source of donor cells but carry an associated risk of tumorigenicity and immune rejection.[362] One approach therefore, has been to use autologous adult RPE[363-365] or iris pigment epithelial cells[366]. Although these studies have shown a visual improvement following transplantation, it must be appreciated that these cells are derived from an already diseased organ often carrying an RPE gene defect. An alternative technique that has been performed over the last decade with mixed results involves the autologous translocation of an RPE-choroid complex. Although a recent review of 130 patients with exudative ARMD that received an RPE-choroid graft showed maintenance of vision for up to seven years post procedure, the results were confounded by factors such as variations in follow-up duration and vision testing.[367]

Another approach to reduce the risk of tumorigenicity and non-specificity of primitive ES cells has been to derive RPE from ES cells[368,369] or iPSCs that have a committed fate and are less likely to differentiate into non-neural cells or form tumours. ESC-derived RPE cells have been shown to rescue visual function in

dystrophic RCS rats[370,371] and in RPE65 knockout mice.[372] On the basis of these findings, a Phase I clinical trial has been conducted by Advanced Cell Technology (ACT; Santa Monica, CA) to transplant dissociated human ESC-derived RPE cells to patients with ARMD and Stargardt's disease, the results of which are awaited.[373]

CHAPTER 2

MATERIALS AND METHODS

2.1 Animals

2.1.1 Mouse strains

All animal experiments were performed in accordance with the Association for Research in Vision and Ophthalmology (ARVO) Statement for the Use of Animals in Ophthalmic and Vision Research and UK Home Office guidelines. All animals were kept in a 12 h light (<100 lux)/12 h dark cycle, with food and water available ad libitum. Adult mice were defined as at least six weeks old. For WT mice, the *C57Bl/6* model was provided by the Biomedical Sciences division of the University of Oxford whilst the following mice models were obtained from external suppliers:

1) *B6.Cg-Tg(OPN1LW-EGFP)85933Hue/Mmmh* transgenic mice (referred to herein as Opn1-EGFP) in which enhanced green fluorescent protein (EGFP) expression is restricted to medium wavelength-sensitive cones (M cones).
2) *Tg(CAG-dsRed*MST)1Nagy/Tg(CAG-dsRed*MST)1Nagy* transgenic mice (referred to herein as dsRed) in which all tissues of homozygotes fluoresce red. Mice hemizygous for the transgene express red fluorescent protein less intensely than homozygotes. This strain also carries the retinal degeneration *Pde6b*$^{rd1/rd}$ (referred to herein as *rd1*) mutation.
3) *OPN4*$^{-/-}$ *GNAT1*$^{-/-}$ *CNGA3*$^{-/-}$ transgenic mice [referred to herein as TKO (triple knockout)], which lack melanopsin and functional rods/cones and therefore have no significant pupil-light reflex, circadian photoentrainment or masking responses.
4) *Tg(Nrl-l-EGFP)Asw/Tg(Nrl-l-EGFP)Asw* transgenic mice (referred to herein as Nrl.GFP) in which EGFP expression is restricted to rod photoreceptors.

5) *BALB/c* mice which are tyrosinase-deficient albino strains with depigmented RPE cells.
6) *C3H/He* mice (referred to herein as C3H) which carry the retinal degeneration *Pde6b*$^{rd1/rd}$ mutation.

Intercrosses were setup between OPN1-EGFP and dsRed mice to establish an F2 generation (referred to herein as OPN1-EGFP-dsRed) with GFP-expressing M cones, a ubiquitous dsRed reporter and an *rd1* mutation.

2.1.2 Anaesthetics and mydriatics

Mice were anaesthetised by a single intraperitoneal injection containing a mixture of medetomidine (Dormitor 1 mg/mL; Pfizer, Sandwich, UK), ketamine (Ketaset 100 mg/mL; Fort Dodge, Southampton, UK) and sterile water at a ratio of 1:0.6:84 for P1 pups and 5:3:42 for adult mice. Pupil dilatation was achieved with tropicamide (Mydriaticum 1%; Bausch & Lomb, Kingston-on-Thames, UK) and phenylephrine (phenylephrine hydrochloride 2.5%; Bausch & Lomb) eye drops.

2.2 Laser experiments

2.2.1 Retinal laser photocoagulation

Mice were anaesthetised by intraperitoneal injection of 1 mg/kg medetomidine (Dormitor 1 mg/mL; Pfizer, Sandwich, UK) and 60 mg/kg ketamine (Ketaset 100 mg/mL; Fort Dodge, Southampton, UK). Mice were anaesthetised as described previously (see 2.1.2 Anaesthetics and mydriatics). Pupil dilatation was achieved with tropicamide (Mydriaticum 1%; Bausch & Lomb, Kingston-on-Thames, UK) and phenylephrine (phenylephrine hydrochloride 2.5%; Bausch & Lomb) eye drops.

Preliminary experiments identified the optimal settings required to create a threshold injury in the experimental set up, that resulted in a consistent window of GFP-positive cone loss visible by *in vivo* imaging. A frequency-doubled 532 nm Nd:YAG laser (Novus Spectra, Lumenis, USA) mounted on a slit lamp biomicroscope (Haag-Streit, Switzerland) was applied directly through a flat contact lens (9mm circular cover glass, VWR, UK) with the aid of a coupling medium (Viscotears, Novartis, Switzerland) to the retinas of recipient mice for *in vivo* study, histological confirmation of injury and molecular analysis.

2.2.2 Intravitreal injection

For in vivo study, human ciliary neurotrophic factor (CNTF) (Peprotech, UK) was delivered by intravitreal injection into the left eye, whereas a sterile PBS sham injection was made into the right eye of OPN1-EGFP mice to control for the release of endogenous growth factors as a result of generalised eye injury. In both cases, 1µl injections were performed after confocal scanning laser ophthalmoscope (cSLO) imaging (within 30 minutes of retinal laser injury) using a similar technique to that described in greater depth in section 2.3.2. However, on visualisation of the bevel of the needle in the subretinal space, the tip was advanced to perforate the retina and enter the vitreous cavity, wherein the substance was delivered.

2.2.3 *In vivo* imaging

The effects of laser injury on mice retinas and following subretinal transplantation were observed using the 488 nm autofluorescence (AF), 790 nm, and 820nm reflectance modes of a Spectralis HRA cSLO (Heidelberg Engineering, Heidelberg,

Germany). A custom-made 3.2 mm diameter polymethyl methacrylate (PMMA) contact lens was used for all recordings (Cantor and Nissel, Brackley, UK), with lubricating eyedrops (Hypromellose BPC 0.3 %; Martindale Pharmaceuticals, Romford, UK) as coupling fluid. All images were recorded in a standardised manner by initially focusing on and centralising the optic disc in the reflectance mode. This mode was used to localise the outer retina as indicated by areas of high reflectivity. At this point, the AF and 790nm modes were used to image the photoreceptor layer. For quantitative analysis, non-normalized images were recorded with a detector sensitivity of 95 in all cases.

2.3 Photoreceptor precursor cell transplantation

2.3.1 Dissociation of retinal cells

Dissociated cells were prepared from embryonic (E15) and early postnatal (P1) mice. Mice were sacrificed by cervical dislocation and neural retinas dissected free from surrounding tissues in warm media. Cells were dissociated using a papain-based kit (Worthington Biochemical, Lorne Laboratories UK) and either suspended in media for culture/transplantation experiments or fixed in 4% paraformaldehyde (PFA) for immunocytochemistry. For transplantation experiments, cells were re-suspended at a concentration of $2x10^5$ cells/µl in Neurobasal A media with the following additives: L-glutamine (0.08 mM), penicillin (100 U/mL), streptomycin (100 U/mL), B27 supplement (2%), and N2 supplement (1%, all Invitrogen Ltd., Paisley, UK).

2.3.2 Subretinal transplantation

Intraocular surgery was performed under direct visualisation using an operating microscope. Following anaesthesia of recipient mice, a 1.5 cm, 34-gauge hypodermic needle (Hamilton, Switzerland) was loaded with cells before penetrating the sclera tangentially. Once the bevelled tip was seen to enter the subretinal space as guided by the overlying retinal vessels, the needle was advanced slowly and directed posteriorly to prevent penetration of the retina. Cell suspensions (2µl per eye for adults and 1 µl for P1 pups) were injected in a controlled fashion to produce a consistent retinal detachment in the superior and/or inferior hemisphere. The needle was removed from the eye slowly leading to a self-sealing tunnel thereby preventing the reflux of cells.

2.3.3 Pupillometry

An infrared-digital camera was used to assess the pupil light reflex (PLR) in un-anaesthetised mice that had been dark adapted for at least 1 hour. PLR recordings were taken from the right (unoperated) eye whilst the left (operated) eye was exposed to a 100ms duration white light with an illumination intensity of 9000 Lux, emitted from a 100-W xenon arc lamp (LOTOriel) via a light guide. A Ganzfeld sphere was used to ensure reproducible and directionally independent full field retinal illumination. The light exposure was synchronised with the image capture using an electronic shutter. Each left eye was stimulated for 24 seconds with capture of 254 frames of the eye at 10 Hz. ImageJ software was subsequently used to analyse the pupil area at each frame.

2.3.4 Behavioural light aversion (BLA)

BLA was assessed using a light-/dark-chamber apparatus. The latter consisted of a 26 x 26 x 26 cm cube that was divided in half into a light "front" chamber and a dark "back" chamber. A central divider had a 4 x 5 cm opening midway to allow transition of the test animal. Before each test, the chamber was dismantled to enable thorough cleaning with 70% (vol/vol) ethanol. White light illumination was provided by background room lighting and a Philips Energy Light (Philips, Guildford, UK) suspended 0.45 m above the front chamber (irradiance at floor level 1200 Lux). A video camera (Logitech, Switzerland) was suspended directly above the whole arena.

All animals were light adapted for at least one hour and each animal was naïve to the test so as to exclude variable responses due to learning or anxiety-related behaviour. In order to start the test, the animal was held in the palm rather than by the tail, to reduce potential anxiolytic effects, and was lowered into the front chamber with the head facing the front in opposite direction to the dark chamber. The lid was replaced immediately and each trial lasted 24 minutes. Analysis was conducted offline using ANY-maze software (Stoelting, USA) for automated measurement of tracking. A transition between chambers was accepted if at least the front half of the animal crossed chambers. Animals that did not cross chambers during the first five minutes of the trial were excluded from analysis.

2.3.5 Calcium imaging

Under dim red light, neural retinas were dissected free from surrounding tissue in cold Ringer's solution containing (in mM) 119 NaCl, 2.5 KCl, 1 KH_2PO_4, 1.3 $MgCl_2$, 2.5

$CaCl_2$, 26.2 $NaHCO_3$, and 11 D-glucose, equilibrated with 95% O_2/5% CO_2 (pH 7.4). Retinas were nicked at four equidistant points, flat-mounted onto a 13mm cover slip photoreceptor side-up where they were held taut under a nylon-strung platinum wire harp and transferred to the stage of an upright microscope (Olympus BX). After loading with 10 µM Fura 2-AM (Molecular Probes) in Ringer's solution (0.5% DMSO; 0.1% pluronic acid dispersant) for 45 minutes at 30°C, retinas were washed in Ringer's solution for 5 minutes. The fluorescent dye was excited alternately at 340nm and 380nm for 400 and 250 ms of exposure, respectively, via a monochromator (Cairn Research Ltd, UK). The ratio of the emissions at those wavelengths directly correlated to the amount of intracellular calcium. Emission at 510nm was captured with an intensified CCD camera (IPentamax, Princeton Instruments) and images were acquired at 2 second intervals. Drugs were applied by micro-pipette injection into the bathing solution. DCPG ((S)-3,4-dicarboxyphenylglycine) (20µM; final concentration in bath), CPPG ((RS)-alpha-cyclopropyl-4-phosphonophenylglycine) (100µM) were supplied by Tocris (UK), and KCl (100µM) was supplied by Sigma (UK).

2.4 *In vitro* characterisation of cone photoreceptors

2.4.1 Retinal cell culture and cell counts

Following papain dissociation, retinal cells were cultured in 24-well plates at $5x10^5$ cells/well in the following media: 1) Neurobasal A, L-glutamine (0.08 mM) containing penicillin (100 U/mL), streptomycin (100 U/mL), B27 supplement (2%), and N2 supplement (1%, all Invitrogen Ltd., Paisley, UK); or 2) Dulbecco's Modified Eagle

Medium (DMEM) containing 10% fetal bovine serum, , L-glutamine (0.08 mM), penicillin (100 U/mL), streptomycin (100 U/mL). Media changes were carried out every 48 hours and with minimal disturbance of adherent cells. Experiments were performed in triplicate and cell counting was conducted at five areas per well, centrally and at four cardinal points, in order to derive an average. Images were captured using a fluorescent camera (Leica, Microsystems GmbH, Germany) and analysed off-line.

2.4.2 Fluorescence activated cell sorting (FACS)

Papain-dissociated retinas were suspended in Neurobasal A media at 37^{o}C at <1x10^{7} cells/ml. The GFP positive cone population was isolated by FACS (Beckman Coulter MoFloTM XPD) at 37^{o}C. FACS gates for any given sample were determined using stage-matched WT control cell suspensions. The sorted cells were resuspended in either RNAlater for mRNA analysis or warm media for culture experiments. Flow-sorted cells were isolated after centrifugation at 300g for 10min and cell viability was determined based on Trypan Blue staining.

2.4.3 Magnetic-activated cell sorting (MACS)

Dissociated retinal cells (up to 5 x 10^{7}) were suspended in 500µl Neurobasal A media at 37^{o}C. To prepare the magnetic beads, Dynabeads Protein G (Invitrogen, UK) were rotated on a daisy wheel for 5 minutes at room temperature (RT) from which 50µl were transferred to a 1.5ml tube. These were washed three times with PBS/0.02% Tween-20 by using a magnet to separate the beads and the supernatant. 20µl rat anti-mouse CD73 (Lot no. 550738, BD Pharmingen, UK) (0.5mg/ml) was added to the

beads in 480µl PBS/0.02% Tween-20 and rotated on a daisy wheel for 1 hour at RT. The mixture was washed twice with PBS/0.02% Tween-20 and then once with Neurobasal A media, using a magnet to separate beads from supernatant, thereby removing any unbound antibody. The supernatant was discarded and 500µl Neurobasal A media containing dissociated cells added to the antibody/bead complex before rotating on a daisy wheel for 2 hours at RT. The mixture was washed 3 times with 500µl Neurobasal A media by using a magnet to separate the antigen (potentially rods in this case)/antibody/beads complex from the supernatant (potentially containing all retinal cells minus rods). The supernatant washes from each step were pooled together into a separate 2ml tube, centrifuged at 300g for 5 minutes and the resultant pellet suspended in 500µl for RNA analysis. The remaining cells attached to the beads were removed by adding 500µl of elution buffer (50mM glycine, pH 2.8), incubating at RT for 2 minutes, followed by centrifuging at 300g for 5 minutes and suspending the resultant pellet in 500µl for RNA analysis.

2.5 Polymerase chain reaction (PCR)

2.5.1 Principles of PCR

The principle of PCR is to exponentially amplify a DNA product and is based on the mechanism of DNA replication that occurs *in vivo*. Double-stranded DNA (dsDNA) is denatured to single-stranded DNA (ssDNA) and duplicated, with repetition of this process throughout the course of the reaction. There are three steps to a PCR reaction (Figure 2.1) as follows:

1. Denaturation at 94^{o}C – during this stage, dsDNA melts open to ssDNA, and all enzymatic reactions stop (i.e. the extension from a previous cycle);
2. Annealing at 50-65^{o}C – at this temperature, annealing of primers to ssDNA takes place. Oligonucleotides used as primers usually consist of relatively short sequences (15-25 nucleotides) complementary to recognition sites in the target DNA. The annealing temperature is typically 3-5^{o}C below the melting temperature (T_m) of the primers used. Adequate binding results in the formation of strong ionic bonds between the ssDNA template and primer, allowing the polymerase to attach and begin copying the template in the next step;
3. Elongation at 72^{o}C - during this step a heat-stable DNA polymerase synthesises a new DNA strand complementary to the DNA template strand resulting in a duplication of the starting target material. This occurs in the presence of $MgCl_2$ by the addition of dNTPs in the 5' to 3' direction. With extension of the primers by a few bases, this strengthens the ionic bonds to the template, reducing the chance of unbinding.

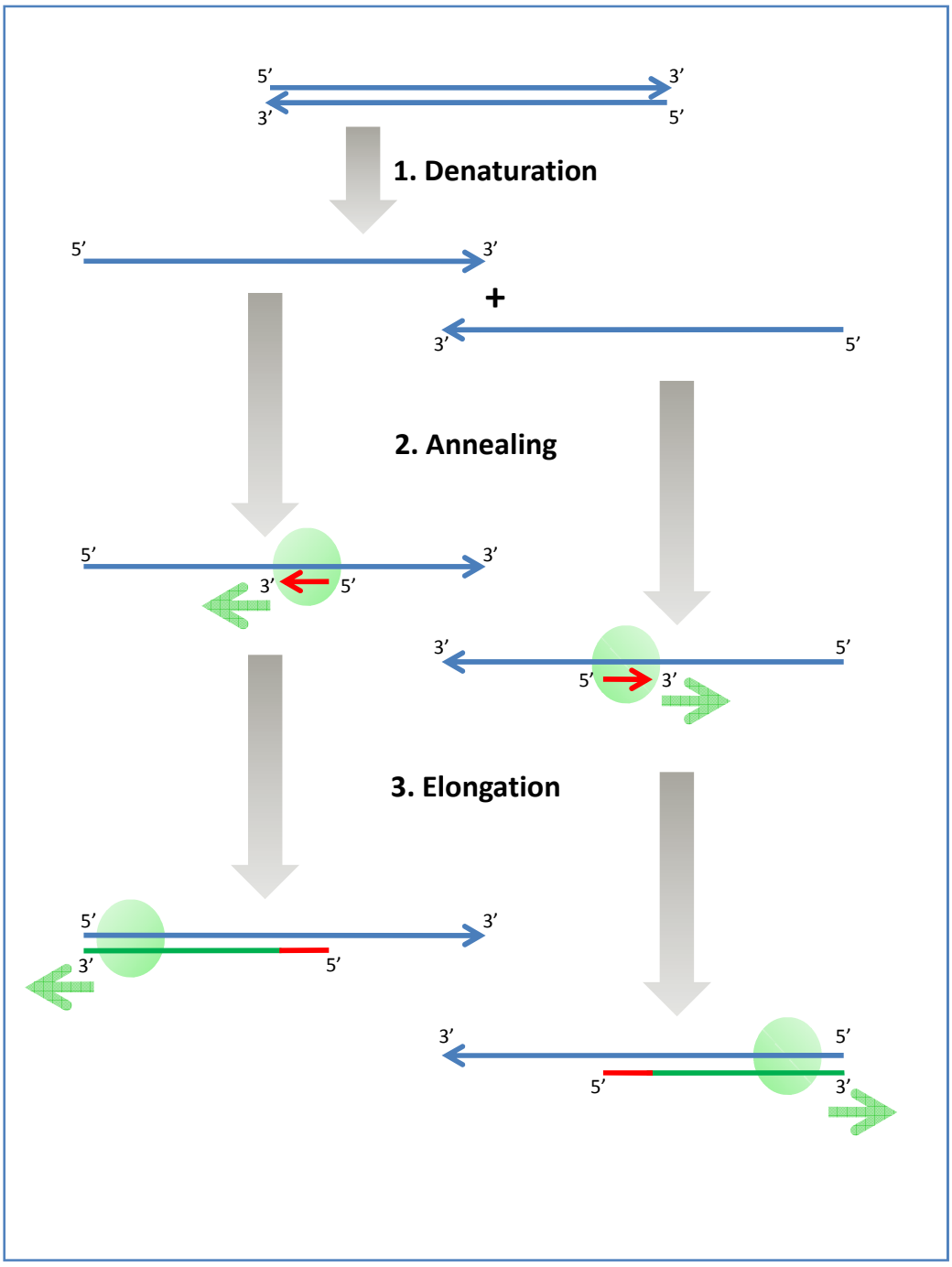

Figure 2.1. Schematic drawing of the PCR cycle showing the key steps: (1) Denaturation (2) Annealing (3) Elongation. The primers (red arrows) anneal to the DNA template (blue lines) and are extended by the DNA polymerase (light green circles) to give shorter DNA products (green lines), which themselves are used as templates in the proceeding PCR cycles.

At the end of each cycle, the newly synthesised DNA strands serve as the template in the next cycle. Since both strands are duplicated during PCR, there is an exponential increase of the number of copies of the gene. Therefore, assuming 100% efficiency during each cycle, after 40 PCR cycles there will be a 2^{40}-fold amplification.

2.5.2 Methodology of conventional PCR

Tissue isolation and DNA preparation

DNA samples were required for genotyping animals and were obtained from tissue pieces from the ears of adult mice or from the tail tips of P1 pups. Tissue samples were immersed in 100µm 50mM NaOH and kept on a heat block at 95^{o}C for 1 hour. Following this, samples were vortexed and centrifuged at 13000rpm for 2 minutes with subsequent addition of 10µl 1M Tris-HCl buffer and repeat centrifuge at 13000rpm for 2 minutes. The resultant suspension was immediately stored on ice.

PCR amplification of DNA

Individual DNA samples (2µl) were amplified in a reaction mixture containing 12.5µl Immomix Red, 1.25µl each of forward and reverse primer (each at 10µM), and 8µl RNase-free water. Initiation of PCR reactions was conducted in incubating tubes at 94^{o}C for 10 minutes (a pre-PCR thermal requirement to activate the Immomix Red). Thereafter, samples were amplified while avoiding saturation using an appropriate (normally 30 to 40) number of cycles that had been previously determined for each set of primers. Moreover, all of the PCR products yielded single bands corresponding to the expected size in base pairs and had previously been sequenced to ensure

their validity. Following an activation step at 95°C for 10 minutes, each cycle consisted of denaturation at 95°C for 10 seconds, hybridisation (annealing temperature) at 55°C for 30 seconds, and extension at 72°C for 30 seconds, using a Hybaid PCR Sprint thermal cycler (Ashford, Middlesex, UK). A final extension was performed at 72°C for 10 minutes. PCR products were visualised by gel electrophoresis as described in Section 2.6. The sequences of primers used for genotyping by conventional PCR are shown in Table 2.1:

Gene	Forward (5' to 3')	Reverse (5' to 3')
GFP	CAATTAAGAGATCAGGTAGTGT	AGTTCACCTTGATGCCGTTCTT
Pdeb^{rd1}	GTAAACAGCAAGAGGCTTTATTGGGAAC*	TGACAATTACTCCTTTTCCCTCAGTCTG
	TACCCACCCTTCCTAATTTTTCTCACGC†	
CNGA3	TGCACGACTCTCCCGGAAGTACA	ACCGGATAACCCGAGTCTCCAAG
Rhodopsin	GAGGGCTTCTTTGCCACACTTG	AGCGGAAGTTGCTCATCGGCTT
MW opsin	TCTGCTACCTCCAAGTGTGGCT	GCAGTATGCGAAGACCATCACC
S opsin	GTCGCCATGTTTGTGCTCTGGA	GCTTGGAGTTGAAGCGGATGCT

Table 2.1. Oligonucleotides used for genotyping by conventional PCR. *Forward primer used to detect mutant allele, †Forward primer used to detect WT allele.

2.5.3 Methodology of quantitative real time PCR (qPCR)

In conventional PCR, detection and semi-quantification of amplified products take place at the end of the reaction following the final PCR cycle, and involve post-PCR analysis such as gel electrophoresis and image analysis. In comparison, qPCR measures the amount of PCR product at each cycle, whereby quantification during the exponential phase of the reaction may be used to determine the initial amount of target product.

Tissue isolation and RNA preparation

For RNA samples, retinas were dissected free of all surrounding tissues under a microscope in RNAlater (Ambion, Huntingdon, United Kingdom), before being transferred to and homogenised in 500µl TRIzol (Invitrogen, Basel, Switzerland). The suspension was kept at RT for 5min before addition of 100µl chloroform. The mixture was vortexed for 15 seconds and kept at RT for 2 minutes. The suspension was centrifuged at 10000rpm and -4^{o}C for 15 minutes causing separation of the sample into three phases: a top colourless aqueous phase containing RNA, an inter-phase containing DNA and a bottom organic phase containing protein. 300µl of the RNA-containing phase was carefully removed and transferred to a new 1.5ml tube containing 300µl of 70% ethanol, following which total RNA was then extracted using a Qiagen RNeasy Micro Kit, according to the manufacturer's instructions (Qiagen, Germany). Traces of DNA were removed by incubation with DNase I at RT. The final step resulted in a sample of total RNA in 14µl of RNase-free water in a 1.5ml tube which was immediately placed on ice.

The concentration and purity of RNA was measured by spectrophotometry using a NanoDrop (Thermo Scientific, USA). Purity was determined by the ratio of sample absorbance at 260 and 280nm. A ratio of approximately 2.0 indicated good quality RNA with much lower values indicating the possibility of protein, phenol or other contaminants.

Reverse transcription

Oligo dT-primed complementary DNA (cDNA) was synthesised from 1µg total RNA,

using SuperScript III Reverse Transcriptase, according to the manufacturer's procedure (Invitrogen, Paisley, UK). For each reaction, a 30.5µl mixture was prepared consisting of 5µl Oligo dT, 1µg total RNA (in 5µl water), and 20.5 RNase-Free water. This was heated at 85^{o}C for 15 minutes and then chilled on ice for 2 minutes. Added to each sample were 10µl 5x First Strand buffer, 5µl 0.1M DTT, 2.5µl dNTP mixture (containing 10mM of each nucleotide), and 1µl RNAseOUT Inhibitor. The mixture was left at RT for 2 minutes followed by the addition of 1 µl SuperScript III Reverse Transcriptase and further incubation at RT for 5 minutes. After incubating at 50^{o}C for 1 hour, another 1 µl SuperScript III Reverse Transcriptase was added to the mixture followed by further 1 hour incubation at 50^{o}C. Upon completion, the cDNA samples were stored at -80^{o}C if not used immediately.

PCR primer design and qPCR conditions

The equivalent of 150ng cDNA was used to PCR amplify transcripts expressed by the following genes implicated in apoptosis: B-cell lymphoma protein-2 (*Bcl-2*); Bcl-2 associated protein X (*Bax*); Cysteinyl aspartic acid-protease-3 (*Caspase-3*); cellular oncogene FBJ murine osteosarcoma viral oncogene homolog (*c-Fos*); cellular oncogene V-jun avian sarcoma virus 17 oncogene homolog (*c-Jun*); mitogen-activated protein kinase-11 (*Mapk-11*); *Mapk-12*; *Mapk-13*; *Mapk-14*; and signal transducer and activator of transcription-3 (*STAT-3*) genes. In murine tissues, the *Bcl-2* gene is expressed as two isoforms, whereas the *Bax* gene is transcribed as a single mRNA transcript. Being related genes, *Bcl-2* and *Bax* encode for transcripts that share a high sequence identity. To ensure cross-hybridisation would not occur

during the qPCR experiments, primers for these genes were carefully designed with specific 3'-ends, such that polymerisation would only occur to amplify a specific product. All reactions used a SYBR® Green PCR Master Mix (Applied Biosystems, Warrington, UK) and 5µM of each forward and reverse primers (Table 2.2). All primer pairs were designed to span an intron of the target gene to minimise genomic DNA (gDNA) contamination. All qPCR experiments were performed in triplicate using a StepOnePlus real-time PCR system (Applied Biosystems, DE, USA) with the following settings: an initial denaturation step of 95^{o}C for 10 minutes, followed by 40 cycles of 95^{o}C for 30 seconds, an annealing temperature of either 55^{o}C (all genes except *Bcl-2*) or 60^{o}C (for *Bcl-2*) for 30 seconds, and extension at 72^{o}C for 30 seconds. Values obtained for the target genes were normalised to the geometric mean of three housekeeping genes, namely acidic repeat protein (*Arp*), *beta-actin*, and glyceraldehyde-3-phosphate dehydrogenase (*Gapdh*). Primer sequences were designed using Primer3 software and standard curve analysis was performed to ensure primer efficiencies were close to 100%.

Gene	Forward (5' to 3')	Reverse (5' to 3')
Bax	CATGTTTGCTGATGGCAACTTC	CACAAAGATGGTCACTGTCTGC
Bcl-2	GATGACTTCTCTCGTCGCTACC	CGGTTCAGGTACTCAGTCATCC
Caspase-3	CTCTACAGCACCTGGTTACTATTCC	ACAATACACGGGATCTGTTTCTTTG
c-Fos	GAACCCTTTGATGACTTCTTGTTTC	AAAGGAAGACGTGTAAGTAGTGCAG
c-Jun	AGAACTCGGACCTTCTCACGTC	TGTTCTGGCTATGCAGTTCAGC
Mapk-11	GATCATGCTAAACTGGATGCACTAC	GAGGCAGAGACTGGATGTATGTC
Mapk-12	AGACAGTGAGATGACAGGATATGTG	CTCTGCACTCTGTAGCTTCTGAAC
Mapk-13	GTCCAGTACTTGGTGTACCAGATG	GTCGACTGTCTGGTTGTAATGC
Mapk-14	TCAGTTTCTCATCTACCAGATCCTC	TGTCTGGTTATAGTGCATCCAATTC
STAT-3	AAGAACGTGAACTTCTTCACTAAGC	ATATTGTCTAGCCAGACCCAGAAG
Arp	GATCATCCAGCAGGTGTTTGAC	GTGTACTCAGTCTCCACAGACAATG
Beta-actin	GCTGTGCTATGTTGCTCTAGACTTC	CATAGAGGTCTTTACGGATGTCAAC
Gapdh	CTTCATTGACCTCAACTACATGGTC	GTGGTGAAGACACCAGTAGACTCC

Table 2.2. Oligonucleotides used for qPCR analysis of apoptotic gene expression.

2.6 DNA electrophoresis

Principles

Electrophoresis is a technique used to separate macromolecules - in particular nucleic acids and proteins - of differing size, charge or conformation. When placed in an electrical field, these molecules will migrate towards either the positive or negative pole depending on their charge. Whilst proteins carry either positive or negative charge, nucleic acids are negatively charged due to their phosphate backbone and therefore migrate towards the anode. The gel is composed of the polysaccharide, agarose, which is typically used at concentrations of 0.5 to 2%,

depending on the size of DNA fragments. Ethidium bromide, a fluorescent dye that intercalates between bases of DNA and RNA and is thus used to stain nucleic acids, is added to the agarose gel mixture before it sets. A loading buffer, which is denser than the agarose, is added to the DNA sample to allow it to sink to the bottom of the well.

Methods

Gel electrophoresis was employed for DNA and cDNA samples. DNA or cDNA products were separated on 2% (w/v) agarose gels with 1% (w/v) ethidium bromide using a 1 x TBE buffer. A 1kb DNA ladder was run in parallel to provide size markers. Samples were loaded using gel loading buffer. Gels were run at 100 volts for various times depending on the size of the DNA bands and were photographed on a UV transilluminator.

2.7 Histological analysis

2.7.1 Cryosections

Following sacrifice and enucleation at relevant time points, eyes were fixed in 4% (w/v) paraformaldehyde (PFA). After corneal excision and lens extraction, remaining eyecups were fixed in 4% PFA overnight, before being transferred to 30% (w/v) sucrose for two hours and embedding in OCT compound (VWR, Lutterworth, UK). Blocks were serially sectioned on a cryostat at 20 µm thickness on to polylysine-coated glass slides. All sections were stained with 4',6-diamidino-2-phenylindole (DAPI) (Invitrogen, Paisley, UK) with or without prior antibody staining, and

subsequently imaged using either an inverted fluorescence microscope (Leica Microsystems GmbH, Wetzlar, Germany) or confocal microscope.

2.7.2 Immunohistochemistry

Principles

Immunohistochemistry (IHC) is the process used to demonstrate the presence and location of proteins in tissue sections. IHC utilises labelled antibodies to localise specific cell and tissue antigens that are visualised by a marker such as a fluorescent dye, enzyme, radioactive element or colloidal gold. There are two principal techniques to IHC that involve either of the following:

1. Direct method – this involves a labelled antibody (i.e. fluorescein isothiocyanate (FITC) conjugated antiserum) reacting directly with the antigen in tissue sections. Although this method uses a single antibody and is relatively quick, it is insensitive due to little signal amplification and therefore has been superseded by the indirect method.
2. Indirect method – this involves an unlabelled primary antibody which reacts with tissue antigen, and a labelled secondary antibody (against the IgG of the animal species in which the primary antibody has been raised) which reacts with the primary antibody. The secondary antibody can be labelled with a fluorescent dye such as FITC, rhodamine or Texas red, known as the indirect immunofluorescence method, or with an enzyme such as peroxidase, alkaline phosphatase or glucose oxidase, known as the indirect immunoenzyme method.

Methods

Retinal sections collected on polylysine-coated slides were rinsed 3 x 5 minutes with PBS and permeabilised for 20 minutes with 0.4% Triton-X in PBS. This was followed by a further rinse for 3 x 5 minutes with PBS and subsequent blocking for 1 hour with PBS containing 0.1% Triton-X and 10% normal donkey or goat serum, the latter depending on the host species of the secondary antibody. Slides were incubated overnight at 4^{o}C with PBS containing 0.1% Triton-X, 2% normal donkey or goat serum, and primary antibody at the appropriate concentration. After rinsing 3 x 5 minutes with PBS-Tween 20, slides were incubated at RT with PBS containing 0.1% Triton-X, 2% normal donkey or goat serum, and 1:200 secondary antibody. Slides were rinsed 3 x 5 minutes with PBS-Tween 20 and counter-stained with Hoescht 33342 (Molecular Probes, UK) for 5 minutes (1:1000 in PBS). The primary antibody was omitted from negative controls. The primary and secondary antibodies used are summarised in Table 2.3 and Table 2.4 respectively.

Antigen	Raised in	Source	Fixation	Dilution
Arrestin	Rabbit	Millipore (AB15282)	4% PFA	1 : 1000
R/G opsin	Rabbit	Millipore (AB5405)	4% PFA	1 : 1000
Recoverin	Rabbit	Abcam (AB5585)	4% PFA	1 : 1000
CNGA3	Rabbit	Kind gift (M.Biel)	4% PFA	1 : 3000
GFAP	Rabbit	Abcam (AB7779)	4% PFA	1 : 1000
GS	Mouse	Millipore (MAB302)	4% PFA	1 : 1000
GFP	Chicken	Abcam (AB13970)	4% PFA	1 : 1000

Table 2.3. Primary antibodies used for IHC. R/G, red/green; CNGA3, cyclic nucleotide gated channel alpha 3; GFAP, glial fibrillary acidic protein; GS, glutamine synthetase; GFP, green fluorescent protein.

Antigen	Raised in	Fluorescent dye	Source	Fixation	Dilution
Anti-Rabbit	Donkey	Alexa Fluor 568	Invitrogen (A10042)	4% PFA	1:200
Anti-Rabbit	Donkey	Alexa Fluor 635	Invitrogen (A31576)	4% PFA	1:200
Anti-Mouse	Donkey	Alexa Fluor 647	Invitrogen (A31571)	4% PFA	1:200
Anti-Chicken	Goat	Alexa Fluor 647	Invitrogen (A21449)	4% PFA	1:200

Table 2.4. Secondary antibodies used for IHC.

Lectin peanut agglutinin (PNA) staining

For lectin PNA staining, retinal sections on slides were washed with PBS before blocking for 30 minutes with 0.5mg/ml bovine serum albumin in PBS. Slides were again washed with PBS before incubation for 20 minutes with 1:500 lectin PNA in PBS. The types used were either lectin PNA, Alexa Fluor 568 Conjugate (L32458, Invitrogen, UK) or lectin PNA, Alexa Fluor 647 Conjugate (L32460, Invitrogen, UK). The final wash steps and counter-staining with Hoescht 33342 were identical to those described previously.

2.7.3 Immunocytochemistry (ICC)

Methods

The ICC protocol was similar to that used for IHC but with shorter steps and centrifugation. Following cell dissociation, the resultant cell pellet was immediately suspended in 2% PFA for 10 minutes at RT before centrifugation at 300g for 10 minutes. The cell pellet was permeabilised for 5 minutes with 0.4% Triton-X in PBS, followed by centrifugation at 300g for 10 minutes and re-suspension for 15 minutes with PBS containing 0.1% Triton-X and 10% normal donkey or goat serum. The cell pellet was incubated for 4 hours at 4^{o}C with PBS containing 0.1% Triton-X, 2% normal donkey or goat serum, and primary antibody at the same concentration as per the IHC protocol. After centrifugation at 300g for 10 minutes, the cell pellet was incubated at RT with PBS containing 0.1% Triton-X, 2% normal donkey or goat serum, and 1:200 secondary antibody, followed by a final centrifugation at 300g for 10 minutes. The resultant cell pellet was counter-stained with Hoescht 33342

(Molecular Probes, UK) for 2 minutes (1:1000 in PBS) and a drop of this suspension put on a polylysine-coated glass slide with an overlying coverslip

2.7.4 Terminal dUTP Nick End-Labeling (TUNEL) of fragmented DNA

Principles

TUNEL is a method for detecting DNA fragmentation that occurs due to apoptotic signalling cascades, by labelling the terminal end of nucleic acids. The underlying principle relies on the detection of characteristic nicks in the DNA that can be identified by terminal deoxynucleotidyl transferase (TdT). TdT is an enzyme that will catalyse the binding of dUTPs that are secondarily labelled with a marker such as Texas Red for downstream detection and quantification.

Methods

DNA strand breaks in retinal cell nuclei were detected by TUNEL assay on retinal sections between one to five days post laser application according to manufacturer's instructions (In Situ Cell Death Detection Kit, Roche, Switzerland). Sections were further counterstained with DAPI to identify photoreceptor nuclei. Apoptotic cells were counted from three sections of the central most area of maximal lesion damage and the resulting numbers were averaged.

2.7.5 Confocal microscopy

Retinal sections were viewed on a confocal microscope (Zeiss LSM710). Epifluorescence illumination was used to locate GFP- and dsRed-positive cells before

taking a series of XY optical sections. The fluorescence of Hoechst, GFP, dsRed, Alexa-555, Alexa-568, and Alexa-635 was sequentially excited using 350-nm UV, 488-nm argon, and the 543-nm HeNe lasers, as appropriate. A stack was generated to give an XY projection image, and images were processed using Volocity (Perkin-Elmer), ImageJ, and Adobe Photoshop CS4 version 11.0.2.

2.7.6 Counts of integrated cone photoreceptors

To establish the number of integrated cone photoreceptor cells in recipient retinas, animals that received injections were sacrificed between two to three weeks post-cell transplantation and the eyes prepared for analysis. Cells were counted as integrated if they displayed a whole cell body in addition to at least one of the following structures: pedicle synapse, inner processes, and/or inner segments. The number of integrated cones photoreceptors per eye was determined by counting all the integrated GFP-positive cells in all serial sections through each eye. Cell counts for individual eyes were excluded if there were GFP-positive cells present in the vitreous, indicating accidental penetration of the retina with resultant intravitreal injection. Also excluded were eyes with no subretinal donor mass and surgical notes recording the presence of excessive reflux or inadvertent intravitreal injection. Reflux of cells and accidental intravitreal injection occurred at a frequency of 1/15 and 1/25 eyes respectively.

2.7.7 Statistical analysis

Statistical analyses are presented as mean ± SEM (standard error of the mean); N, number of animals; n, number of eyes or sections examined, as appropriate. To

determine normality of distribution, the Shapiro-Wilk test was used with a significance threshold of 0.05. For normally distributed data, comparisons of cell counts and gene expression between contralateral eyes were analysed using paired two-tailed Student t-tests, with Bonferroni correction as appropriate, and a significance threshold of 0.05. For cell counts from paired animals, a paired two-tailed Student t-tests was used when all animals were present, otherwise an unpaired t-test was used to compare all the data, with a significance threshold of 0.05. Data sets with more than two groups were compared using an analysis of variance with a post hoc Bonferroni multiple comparisons test for groups of four or less and a Tukey post hoc test for greater than four groups, with a significance threshold of 0.05. For data that was not normally distributed, the non-parametric Mann-Whitney was used, with a significance threshold of 0.05. All analyses were conducted using SPSS version 19 (IBM) with charts prepared using Graphpad Prism version 5.00 for Windows (GraphPad Software, San Diego California USA, www.graphpad.com); *$P < 0.05$, **$P < 0.01$, ***$P < 0.001$.

CHAPTER 3

DEVELOPMENT OF A MODEL TO DETECT LOSS OF CONES FOLLOWING RETINAL LASER EXPOSURE

3.1 Introduction

3.1.1 Aim

To develop a reproducible *in vivo* model of retinal laser injury that shows the effect on cone photoreceptors.

3.1.2 Overview

The effects of laser injury on photoreceptors is well established with the loss of cells occurring due to either the conduction of heat energy to the photoreceptor outer segments, resulting in their permanent structural damage, or due to the loss of supporting RPE cells following their absorption of laser energy. The precise mechanism typically involves a rapid expansion of the RPE with the formation of gas bubbles, which results in dissipation of energy to the surrounding structures.

Historically, retinal laser studies have been conducted using histological methods. A number of these studies have shown that a delayed effect is seen to occur with the expansion of injury following laser exposure. Since necrosis is an immediate cause of cell death, the hypothesis would be that the delayed loss of photoreceptors would involve the process of apoptosis.

In vivo imaging of retinal laser exposure has typically involved either ophthalmoscopy or more recently, the use of devices such as the confocal scanning laser ophthalmoscope (cSLO) or optical coherence tomography scanner. The advantage of these methods is that they provide real-time imaging of the effects of laser exposure and therefore allow for longitudinal study whereas histological methods provide only cross-sectional information.

In order to investigate the effects of laser injury on individual cells of the retina, the optimal method is to localise a fluorophore to the cell of interest. This may take the form of an exogenously applied agent, such as fluorescein, or the use of a reporter that provides endogenous fluorescence, such as GFP. Using the property of fluorescence allows detection using the aforementioned techniques, as in the case of the cSLO that can excite and detect GFP signal using appropriate laser wavelengths. Specifically tagging the cone photoreceptors with a GFP reporter as seen in the OPN1-EGFP mouse, allows real-time imaging of individual cones by cSLO and therefore provides the ideal model in which to study the effects of laser injury.

3.1.3 Summary of results

The findings in these studies can be summarised as follows:

1) *In vivo* imaging using the cSLO detected the loss of M cones in the OPN1-EGFP mouse following laser injury, and the loss of this cone population increased with time.
2) Histology confirmed an area of photoreceptor attenuation coinciding with the site of laser injury and that the loss of photoreceptors increased with time.
3) TUNEL assay showed the presence of apoptosis occurring in the area of laser injury and that the proportion of apoptotic cell bodies decreased with time.
4) Analysis of gene expression following laser detected the upregulation of the *c-Fos* gene with trends seen suggesting the upregulation of *Bax* and *STAT-3* and inhibition of *Bcl-2*.

3.2 Experimental design

Experiments were conducted as follows:

In vivo imaging

Adult OPN1-EGFP mice were anaesthetised by intraperitoneal injection of 1 mg/kg medetomidine and 60 mg/kg ketamine and pupil dilatation was achieved with tropicamide 1% and phenylephrine 2.5% eye drops. Baseline images were obtained using the cSLO following which retinas received two to four equidistant burns approximately two disc diameters from the edge of the optic disc. This distance allowed for adequate imaging of GFP-positive cones without blur resulting from being too close to the optic disc. Retinas were again imaged by cSLO and mice recovered using atipamezole (1mg/kg). Mice were re-imaged at one, three, and six weeks.

Histology and TUNEL assay

For histology and TUNEL assay, WT mice received eight burns bilaterally (16 burns in total) in a similar distribution as described. For histology, mice were sacrificed at one, three, and six weeks post laser injury whilst for TUNEL assay, mice were sacrificed on consecutive days between one to five days post laser application. Eyes were prepared for sectioning as previously described. Sections were stained with DAPI (and by TUNEL assay as appropriate) and imaged using an inverted fluorescence microscope.

qPCR analysis

To investigate the effect of laser on retinal gene expression, WT mice received 20 pan-retinal burns unilaterally with the contralateral eye left untreated to serve as control. At three days post laser exposure, a comparison was made between gene expression (as previously described) in lasered versus non-lasered retinas.

3.3 Results

3.3.1 *In vivo* imaging

Threshold injury determination

Visible spectrum light fundoscopy was used to establish the settings required to create a minimum visible lesion (MVL). At low laser energy levels, a small homogenous patch of white developed a few seconds following laser application. Increasing the energy level created a larger lesion with immediate blanching of the retina (Figure 3.1). Use of even higher energy levels caused either a retinal haemorrhage or the formation of a vaporisation bubble, indicating the rupture of Bruch's membrane.

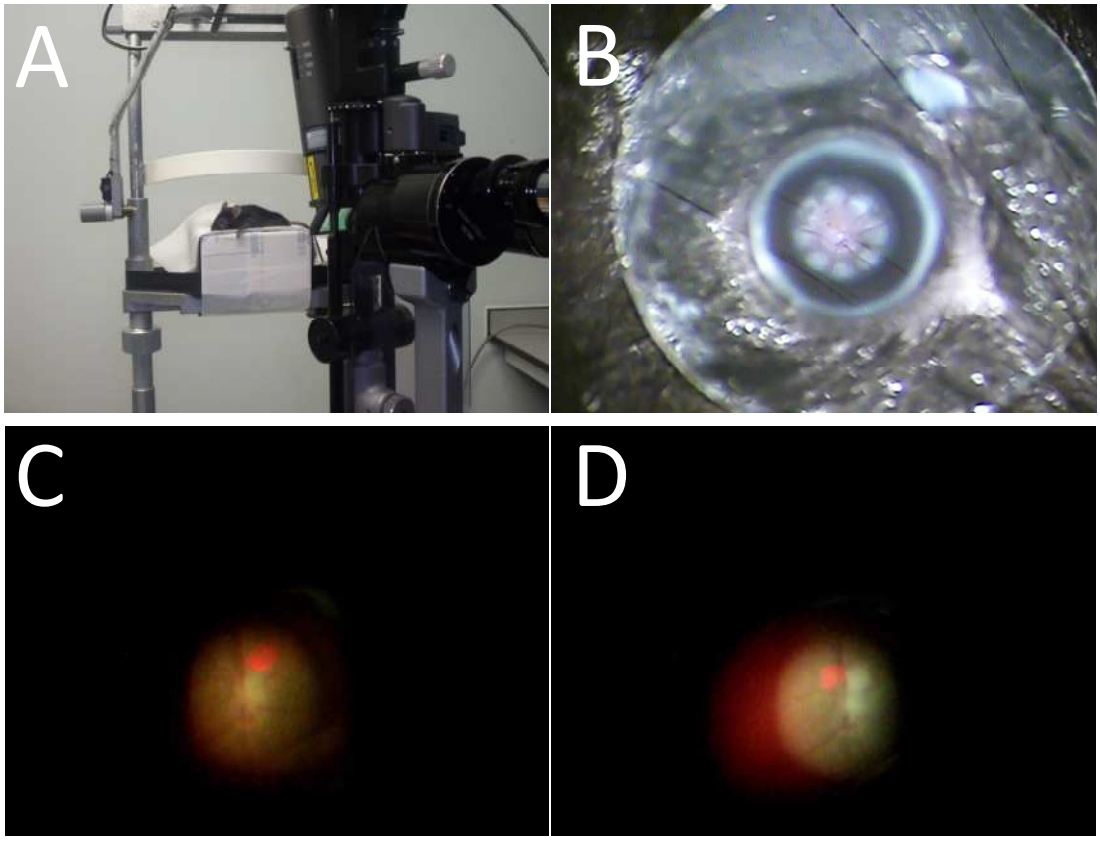

Figure 3.1. A colour photograph showing the set-up for laser application to the mouse retina. A slit lamp was used to deliver the retinal laser burn to the anaesthetised mouse that was placed on a platform in line with the viewing arm (**A**). A colour photograph of the mouse eye with an overlying coverslip showing the blanching effect of several retinal laser burns encircling the optic disc centrally (**B**). A view of the mouse retina as observed on the slit lamp showing the white optic disc centrally (**C**). A red aiming beam is seen superior to the disc which marks the point of laser delivery. The immediate response following laser application creates a blanching effect, as seen superior to the disc (**D**). The aiming beam has been moved adjacent to this spot in order to apply another burn.

Near-infrared reflectance imaging

Using the 820nm reflectance setting following laser application enabled localisation of the injured area which showed a discrete region that developed into an irregular pattern at later stages (Figure 3.2). Focusing at the plane of maximal reflectance coincided with the outer retina, and therefore allowed observation of the effects on the photoreceptor layer using AF imaging.

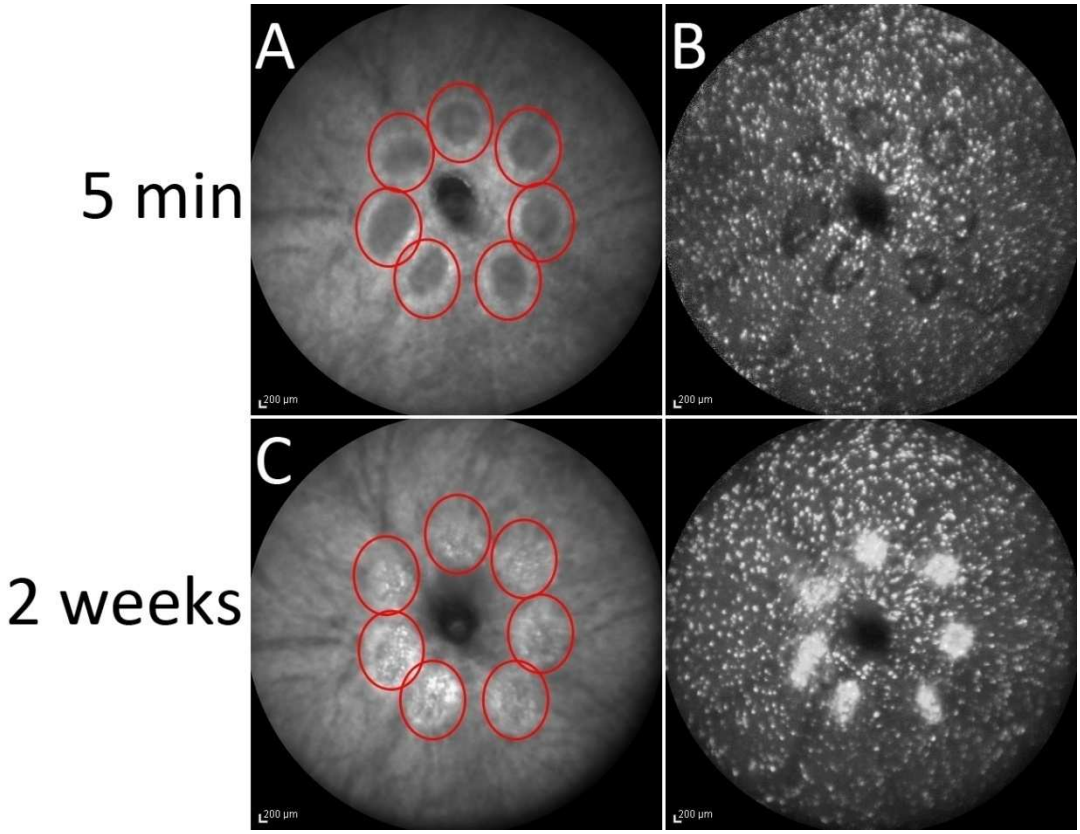

Figure 3.2. Reflectance and 488nm AF images post laser in the OPN1-EGFP retina. Reflectance images 5 minutes post laser showed well-defined lesions (red circles, **A**) that developed an irregular pattern at two weeks (red circles, **C**). Corresponding AF images at the same plane localised to the GFP-positive cones and showed no significant change immediately post laser (**B**), whereas at two weeks the lesions were defined by areas of hyper-autofluorescence (**D**).

488nm AF imaging

Contrary to the loss of AF signal from GFP-positive cones that was the aim of the model, initial qualitative experiments detected a hyper-autofluorescent 488nm signal within the lasered area from one day post exposure (Figure 3.3). This is in comparison to no hyper-autofluorescent areas in the non-lasered control retina (Appendix Figure 3).

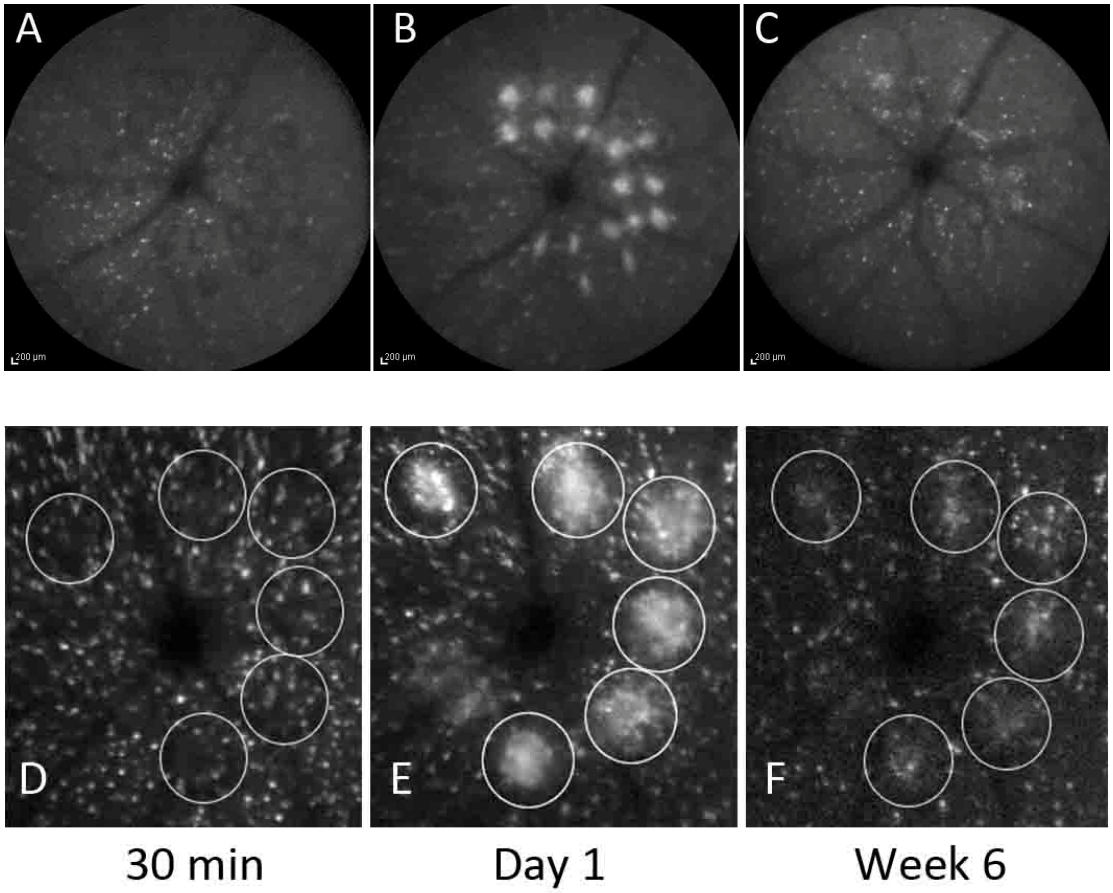

Figure 3.3. Two representative examples demonstrating changes in autofluorescence post laser in the OPN1-EGFP retina. Both upper (**A**-**C**) and lower (**D**-**F**) series of images show the changes in autofluorescence occurring at 30 minutes, one day, and six weeks post laser. Immediately (i.e. 30 minutes) post laser, the lasered area shows slight hypoautofluorescence whereas at one day, the same area shows a marked increase in autofluorescence that persists to a lesser degree at six weeks.

In order to test whether this hyper-autofluorescence was related to GFP, non-GFP mice were lasered and imaged the following day. A similar pattern of hyper-autofluorescence occurred at the same stage in adult C57Bl/6, $Rho^{-/-}$, and rd/rd cl mice but was absent from BALB/c mice which showed no increase in autofluorescence in the lasered area (Figure 3.4).

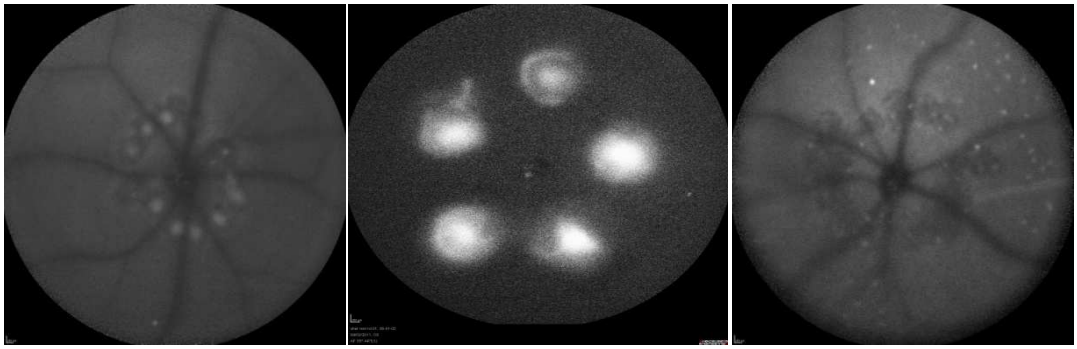

Figure 3.4. 488nm AF images of a wild type and BALB/c retina following laser application. Multiple lesions encircling the disc show a hyperautofluorescent signal in the wild type (far left) and rd/rd cl (middle) retina at one day post laser. However, BALB/c mice do not show this increase in autofluorescence within the lasered area (far right).

Near-infrared AF imaging

The area of laser injury was seen as a hypo-autofluorescent 790nm signal within the same site. Since the latter was a consistently discrete area with well-defined margins, images derived by the 790nm AF setting were used to delineate the lasered region. Using ImageJ software, a freehand outline of this area was transposed to the non-normalised image taken using the 488 nm AF setting (Figure 3.5).

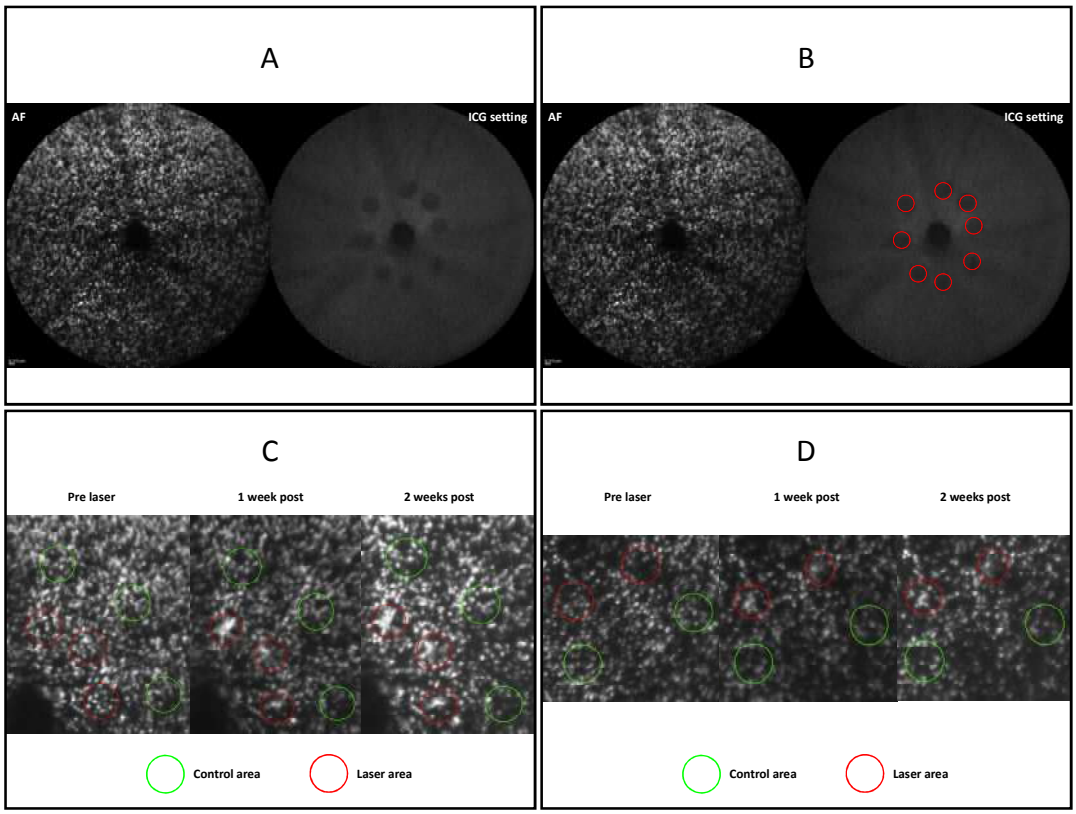

Figure 3.5. Baseline 488nm and post-laser 790nm AF images in the OPN1-EGFP retina. 790nm AF images show a series of concentric laser burns centred on the optic disc (**A**). An outline of each well-demarcated burn was transposed to the baseline 488nm AF image to derive the baseline GFP-positive cone count within the lasered area (**B**). Post laser 488nm AF images from the superior (**C**) and inferior (**D**) retina showed hyper-autofluorescent areas within lasered sites (red circles) whereas non-lasered internal control areas (green circles) remained unchanged between baseline and at one and two weeks post injury.

Loss of GFP-positive cones detected by AF imaging

In order to investigate the effects of different laser settings on lesion morphology, MVLs as observed by cSLO imaging (Figure 3.6) were shown to differ according to the following adjustments of exposure duration and spot size:

1) exposure duration – with a maximal spot size (500 µm), a MVL was produced at 160 mW. On infrared (IR) reflectance imaging, the lesion area increased from 1.34 ±

0.14 to 2.53 ± 0.22 disc areas (DA) at 0.5 s and 3 s, respectively (***t_5 = 9.31, P < 0.0001, N = 6).

2) spot size – with a fixed duration (3 s), a MVL was produced at 60 mW. The lesion area increased from 1.10 ± 0.04 to 1.36 ± 0.12 DA with a spot size of 100 µm and 500 µm respectively (**t_5 = 5.74, P < 0.01, N = 6).

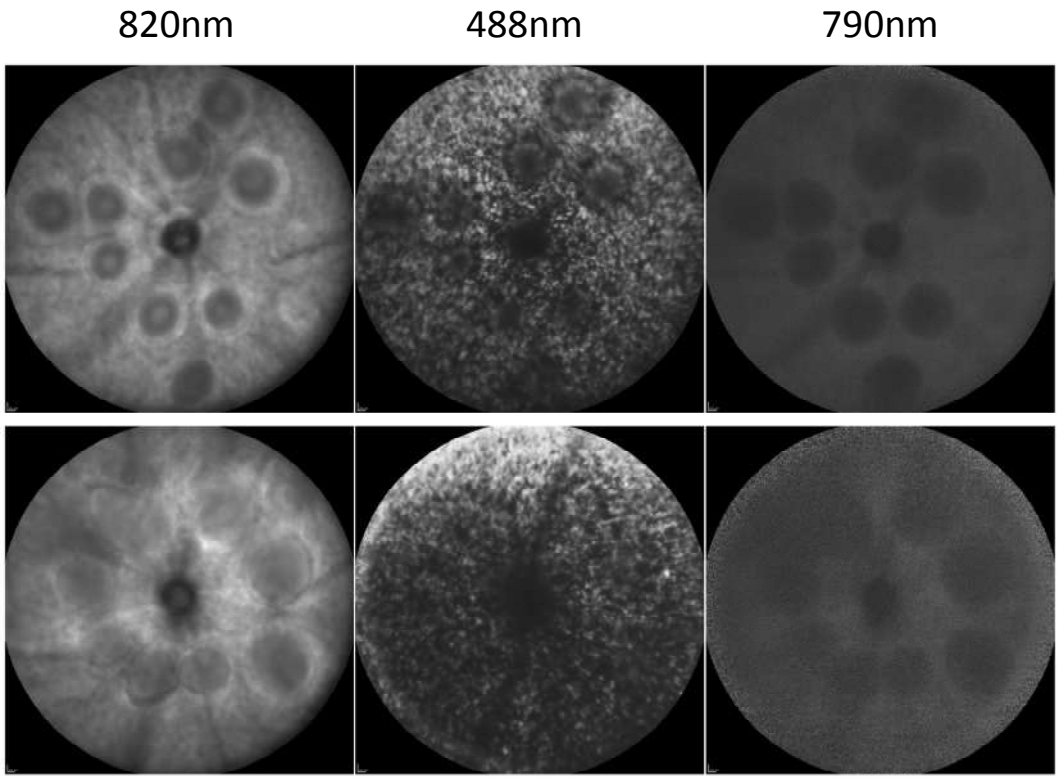

Figure 3.6. Laser dosimetry in the OPN1-EGFP retina as determined by cSLO imaging. The top row shows a single eye receiving three sets of laser lesions performed in triplicate. The images derived from the 820nm reflectance, 488nm, and 790nm laser sources are shown from left to right respectively. From the inferior set of burns going clockwise, lesion areas are seen to increase as the exposure duration is increased with equivalent loss of GFP signal. The bottom row shows four sets of laser lesions performed in duplicate. From the inferior set of burns going clockwise, lesion areas are seen to increase as the spot size is increased with equivalent loss of GFP signal although the effects on GFP signal are not as marked as with alteration of exposure duration.

Use of long duration, large diameter laser settings, produced lesions with the desired effect demonstrating a loss of GFP autofluorescence as detected by 488nm AF imaging (Figure 3.7).

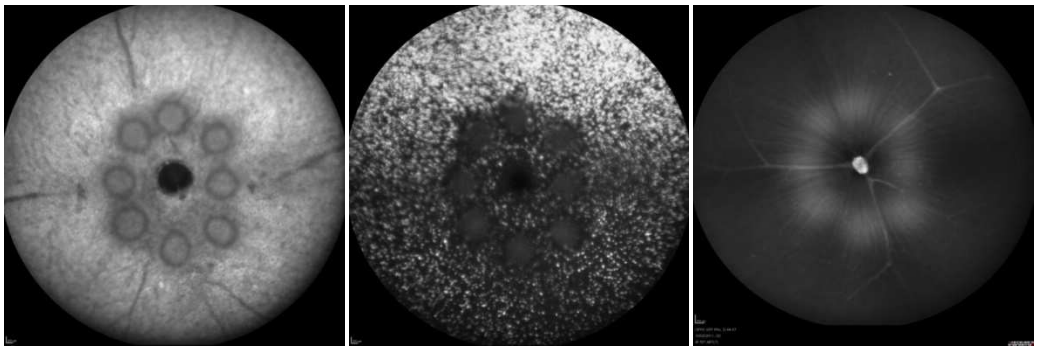

Figure 3.7. Optimal laser burn morphology for evaluation of cone loss. The images derived from the 820nm reflectance, 488nm, and 790nm laser sources at 5 minutes after injury are shown from left to right respectively. Eight concentric laser burns are shown centred on the optic disc, each with a width of approximately one disc diameter. The lesions are well-demarcated with loss of GFP-positive cones within the lesion area. The 790nm laser source has been focused towards the anterior retina in order to show less AF change within the inner retina and ganglion cell layer than is apparent at the level of the outer retina and RPE.

This hypo-autofluorescence persisted at all stages of follow-up, up to the six week point. Relative to the baseline, the number of GFP-positive cones decreased to 36.3 ± 2.7% (***t_{10} = 12.9, $P < 0.001$, $N = 11$) and 18.8 ± 3.8% (***t_{10} = 12.1, $P < 0.001$, $N = 11$) at three and six weeks post exposure, respectively. Similarly, the area of GFP-positive cone loss increased from 0.42 ± 0.19 DA to 0.94 ± 0.14 DA at three and six weeks post exposure, respectively (*t_{10} = 3.05, $P < 0.05$, $N = 11$). The effect of rupture through Bruch's membrane was characterised by changes in autofluorescence with increased 488nm AF signal and reduced 820nm reflectance (Figure 3.9). These eyes were excluded from analysis.

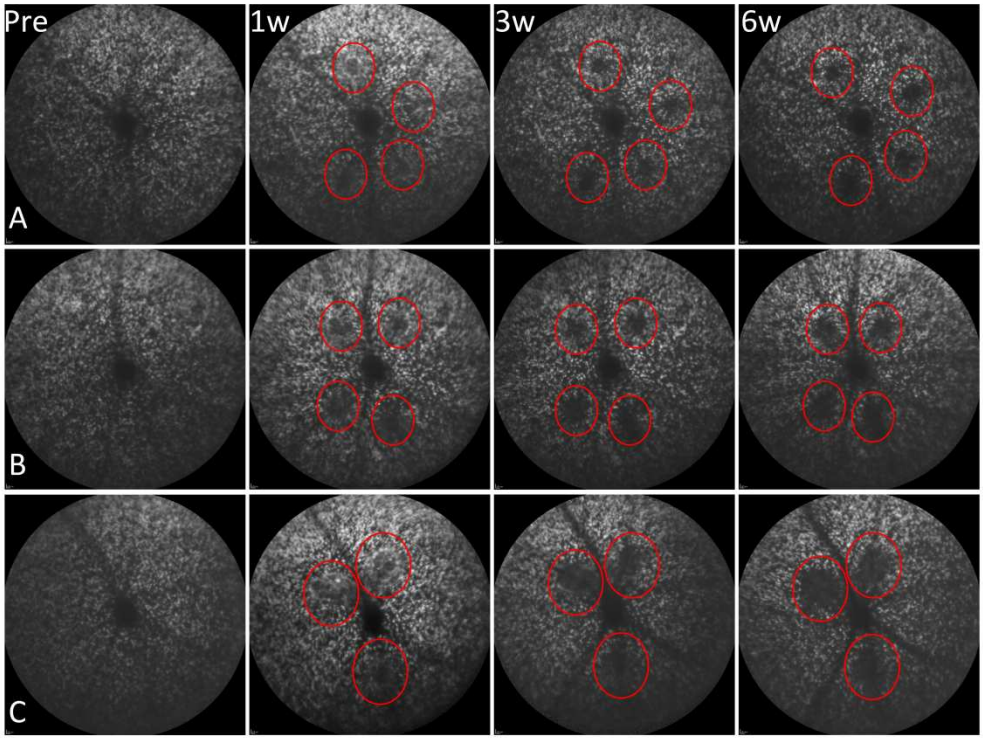

Figure 3.8. 488nm AF images of OPN1-EGFP retinas showing cone loss. The panel shows three representative examples (**A**-**C**) preceding and at one, three, and six weeks post laser application, with the time course for each eye shown in separate rows. Cone loss was more apparent from one week following laser exposure corresponding to the lesion area, with the zone of cone loss expanding over the ensuing weeks (within red circles).

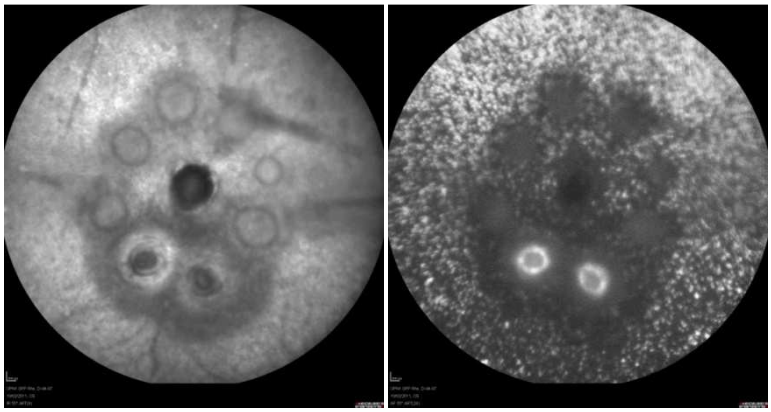

Figure 3.9. Reflectance and 488nm AF images demonstrating the effect seen on rupture of Bruch's membrane post laser in the OPN1-EGFP retina. Two burns with excessive energy causing rupture of Bruch's membrane can be seen inferior to the optic disc. Within each lesion, the 820nm reflectance image (left) shows the loss of central reflectance with surrounding subretinal or choroidal haemorrhage which also appears with loss of reflectance. The corresponding 488nm image (right) shows bright hyper-autofluorescence within the lesion area whereas other lesions that did not rupture Bruch's membrane appeared as hypo-autofluorescent areas.

3.3.2 Histology of photoreceptor loss post laser injury

Light microscopy was used to determine the site of laser injury with maximum cytoarchitectural damage. From one week post exposure, outer nuclear layer (ONL) attenuation was visible at the lesion centre with a loss of photoreceptor nuclei (Figure 3.10). A segment of detached RPE could be seen at the base of the lesion in most cases. The outer plexiform layer (OPL) was disrupted with thickening of the inner nuclear layer (INL), presumably due to oedema, whilst the retinal ganglion cell (RGC) layer was unaffected.

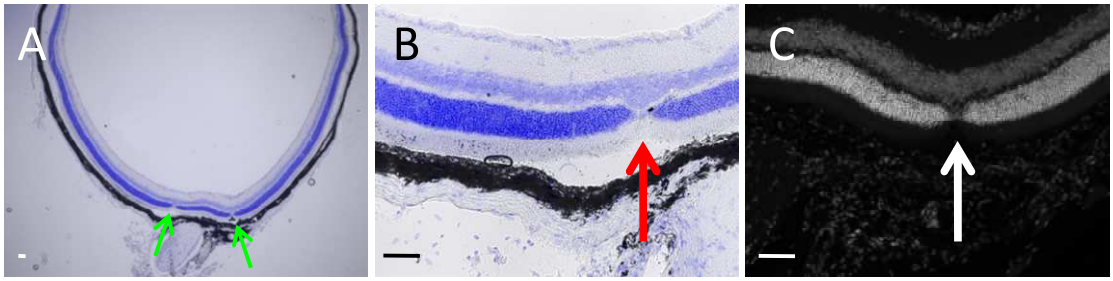

Figure 3.10. DAPI-stained sections post retinal laser. One laser lesion is seen either side of the optic nerve (**A** – green arrows). Higher magnification of both lesion areas shows loss of the ONL with thickening of the overlying inner nuclear layer and a segment of detached RPE at the level of the ONL (**B** and **C** – red and white arrows). Scale bar: 50µm.

In order to quantify photoreceptor density, the number of outer retinal nuclei in the lesion area were expressed as a percentage relative to a non-lasered internal control area of equal size at a distance of 100µm from the edge of the lasered region (Figure 3.11). At one week, the number of photoreceptor nuclei present at the centre of the lesions (124.3 ± 10.4 nuclei) was less than in non-lesioned internal control areas (200.7 ± 3.5 nuclei) (***t_5 = 9.22, P < 0.0001, N = 6). This was also the case at six weeks with less photoreceptor nuclei centrally (102.3 ± 6.8 nuclei) compared to the number in control areas (186.0 ± 16.4 nuclei) (***t_6 = 7.65, P < 0.0001, N = 7).

Bruch's membrane remained intact and no subretinal neovascularisation was evident at any time point post laser, confirming the consistency of the laser model.

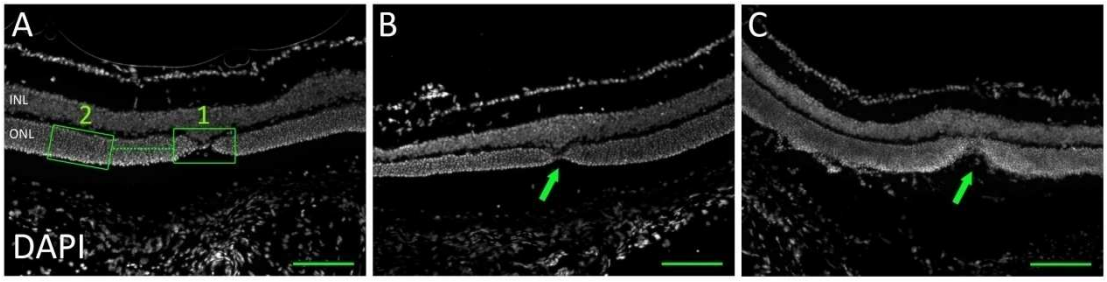

Figure 3.11. DAPI-stained sections of retinal laser lesions showing the central area of injury. Photoreceptor density was calculated by counting the number of outer retinal nuclei in the lesion area (Box 1 in **A**) and expressing this as a percentage relative to a non-lasered internal control area of equal size (Box 2 in **A**). Photoreceptor loss was greater at six weeks (**C**) than one week (**B**) post injury (arrows). Scale bar: 100 µm.

Detection of photoreceptor apoptosis post laser by TUNEL assay

The greater loss of photoreceptor nuclei at six weeks compared to one week implied another mechanism of cell death beyond necrosis might be active in the later stages following laser exposure. To assess the contribution of apoptosis histologically, TUNEL stain was applied (Figure 3.12) and was found to be confined to the ONL, confirming that photoreceptor death occurred via the activation of apoptotic pathways.

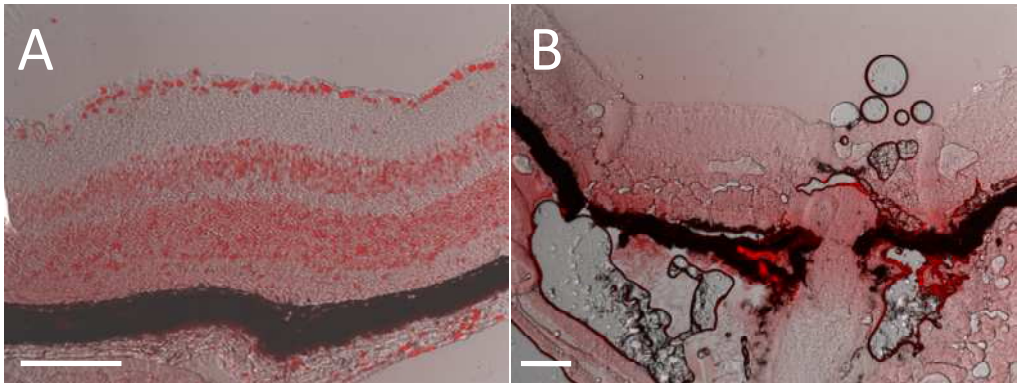

Figure 3.12. TUNEL staining in retinal sections. A positive control detects the presence of the TUNEL assay as indicated by the presence of Texas red staining within the nuclear layers of the retina. A negative control is shown alongside with absence of stain. Scale bar: 50µm.

Confocal microscopy showed that TUNEL staining was located at different depths of the ONL (Figure 3.13), reflecting rod apoptosis throughout the ONL and cone apoptosis that was limited to the outer region of the ONL close to the external limiting membrane, where cone nuclei typically reside. The area of maximal TUNEL staining coincided with the loss of GFP-positive cones. The number of TUNEL-positive cells decreased from one to five days post laser exposure ($F_{2,12}$ = 8.35, P < 0.01, N = 5 per time point, **P < 0.01 post-hoc, Figures 3.14, 3.15).

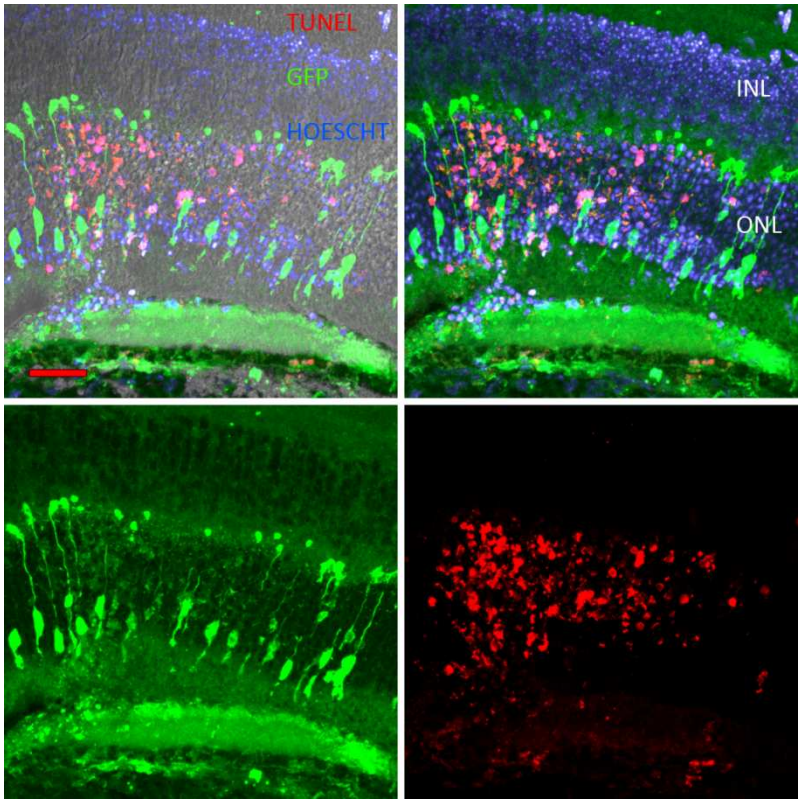

Figure 3.13. TUNEL stain following laser application in the OPN1-EGFP retina. A confocal micrograph showing the localisation of TUNEL stain predominantly to the photoreceptor layer. Loss of GFP-positive cones coincided with the area of maximal TUNEL staining. Scale bar: 20 µm.

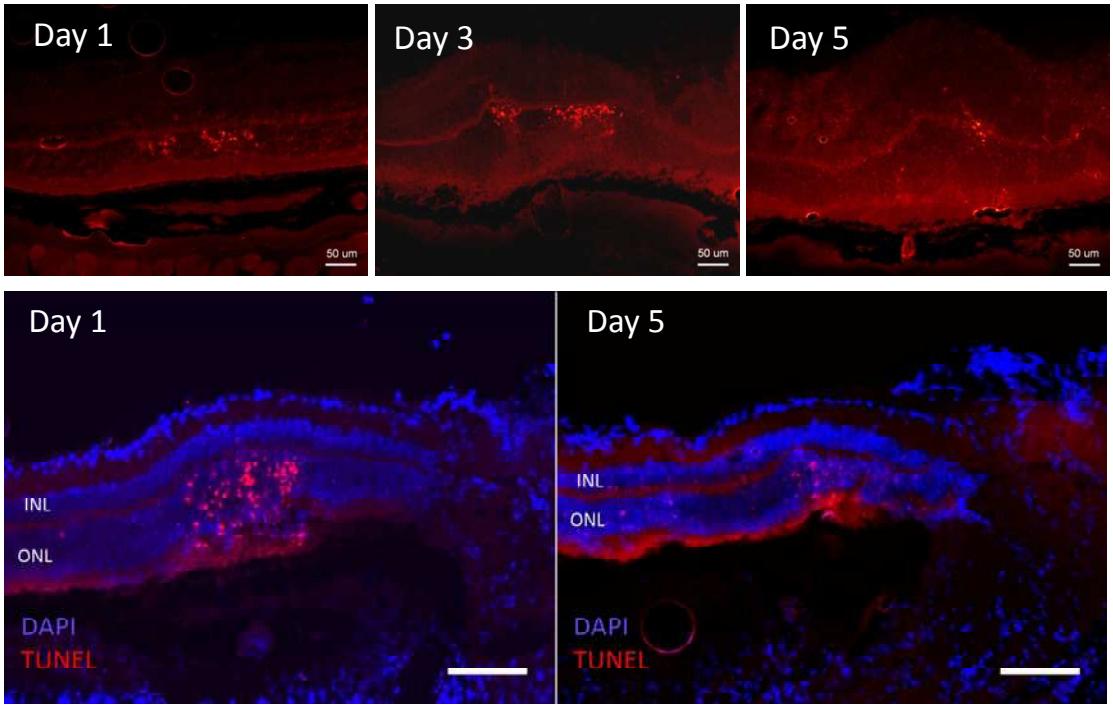

Figure 3.14. DAPI-stained sections with TUNEL assay post laser showing longitudinal changes. Two representative examples (top and bottom rows) are shown to

demonstrate the reduction in TUNEL-positive cells with time. Retinal laser lesions show more TUNEL-positive cells (red) at day one post laser compared to fewer cells at days three and five. Scale bar: 50 μm.

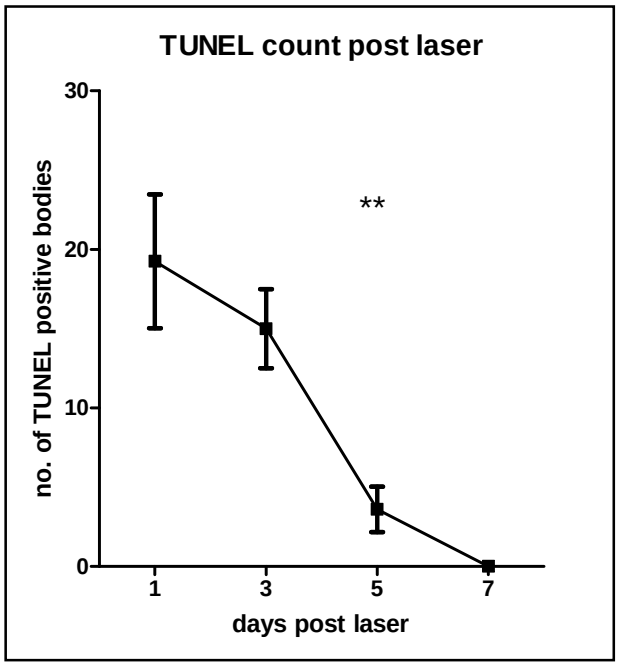

Figure 3.15. Analysis of TUNEL count post laser. This shows a reduction in the number of TUNEL-positive cells from one to five days post laser exposure (G). Error bar ± SEM, *N* = 5 per time point. ***P* < 0.01.

3.3.3 Validation of primers

Primer sequences were designed using Primer3 software. Sequences were designed according to the following parameters:

1) The base composition of primers to be between 40% and 50% GC;
2) The length for the PCR product of 200-250bp;
3) Oligonucleotides with lengths between 18 and 24 bases in order to increase sequence specificity;
4) The melting temperature (Tm) tolerance was set at +/- 2.5^{o}C thus availing more primers that fit into the five degree range;

5) The presence of G or C bases at the 3' end of primers (GC clamp) in order to promote correct binding at the 3' end due to the stronger hydrogen bonding of G and C bases.

The BLAST tool was used to check primers against the genome to assess their specificity to the region of amplification. A dual set of primers were designed for each gene of interest and each was checked against mRNA derived from 3 week old C3H mice that carry the *rd1* mutation thus acting as a positive control for apoptosis activity. All primers showed positive bands of expected size on agarose gel electrophoresis (Figure 3.16).

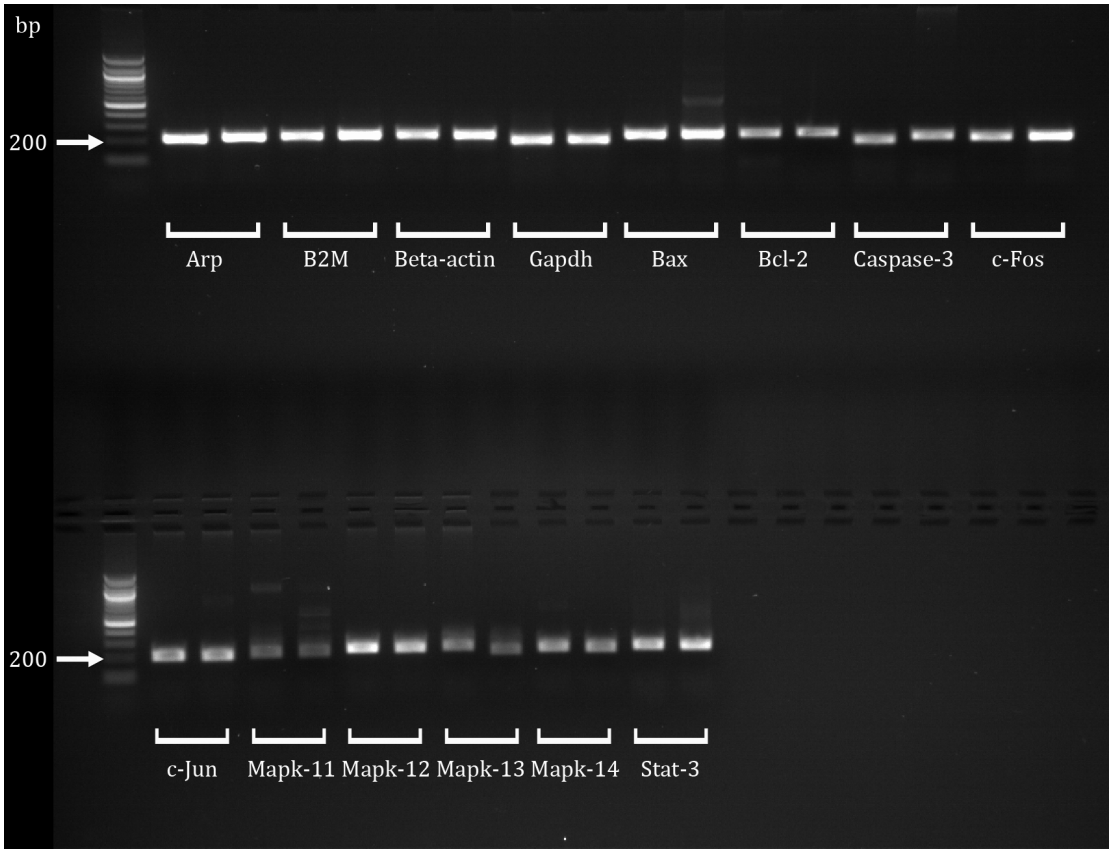

Figure 3.16. Amplification of housekeeping and apoptosis genes in C3H retinas. PCR products were separated on an ethidium bromide-stained agarose gel. Dual sets of primers for each gene were separated in adjacent wells. A single and clear band was observed in all sample lanes at the correct expected molecular size (≈200bp).

.

In order to normalise values against endogenous controls, the housekeeping genes, *Arp*, *beta-actin*, and *Gapdh* were used as internal standards. To optimise the primer set, the melt curve was obtained and Tm for each primer were determined. Optimal temperatures were then calculated (i.e. 2.5°C below Tm) for maximal fluorescence measurement during each cycle of qPCR. An example of the melt curve obtained for the *Bax* gene that has a size of 365bp is shown in Figure 3.17.

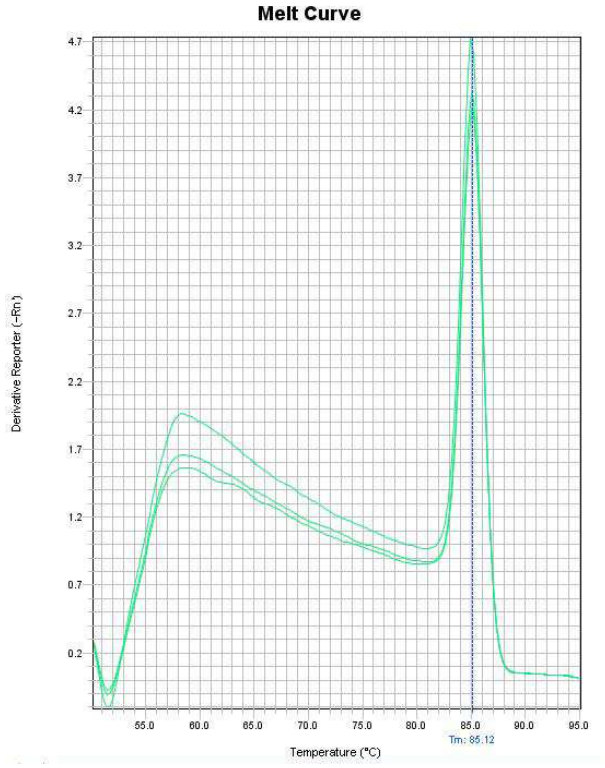

Figure 3.17. Amplication of the *Bax* gene. Graph showing a melt curve during primer optimisation for the *Bax* gene. One major peak was observed at 85.1^{o}C that indicated the specificity of the primers used, with no amplification of non-specific PCR products.

To perform standard curves in order to calculate primer efficiency and ensure that this was close to 100%, qPCR analyses were conducted to derive dilution curves for each primer. Efficiency (E) was calculated as:

$E = 100\ (10^{-1/M} - 1)$ where M is the gradient of the trendline.

Using the example for the *Arp* primers (Figure 3.18), the efficiency was calculated as:

$$E = 100\ (10^{-1/-3.324}-1) = 99.9\%$$

that indicates a highly efficient primer set for qPCR analysis.

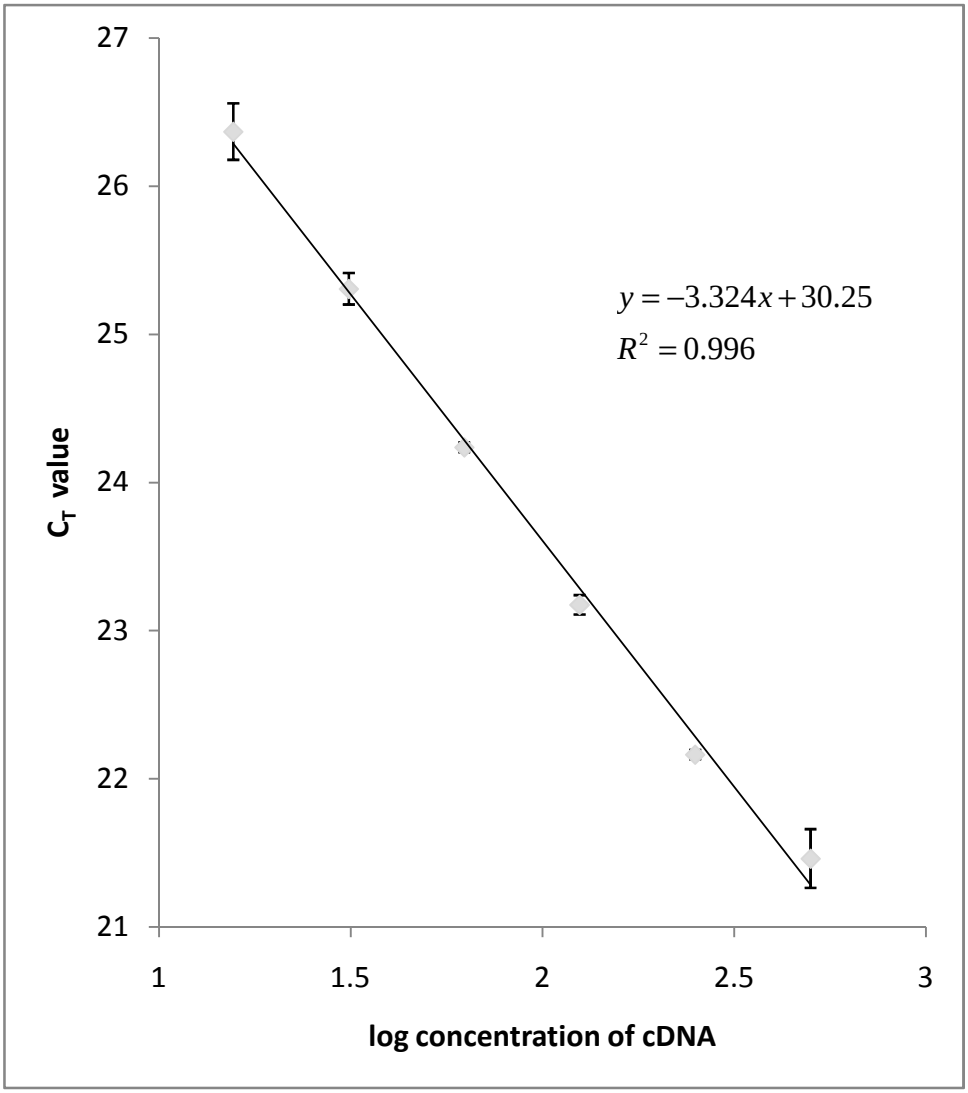

Figure 3.18. A qPCR standard curve for *Arp* primers. This shows log fold serial dilutions of cDNA from 500ng to 15.625ng. cDNA samples were derived from C3H retinas. Three replicate samples were performed for each input quantity of cDNA. The efficiency of *Arp* primers were determined using this standard curve (r = 0.998; PCR efficiency, 99.9%). The relationship between cycle threshold (Ct) and the absolute number of *Arp* genes (assuming one copy per cell) is expressed by the equation $\boldsymbol{y = -3.324x + 30.25}$, where $\boldsymbol{y}$ is Ct, −3.324 is the slope constant, and 30.25 is the $\boldsymbol{y}$ intercept.

3.3.4 qPCR analysis

To analyse the mechanism of photoreceptor cell death following laser injury, further experiments were performed to identify which molecular pathways of cell death might be involved. In order to do this, the left eye of C57Bl/6 mice received 30 retinal laser burns as previously described (Figure 3.19) whilst the contralateral eye was not lasered. Retinas were collected for mRNA extraction and cDNA synthesis, as previously described.

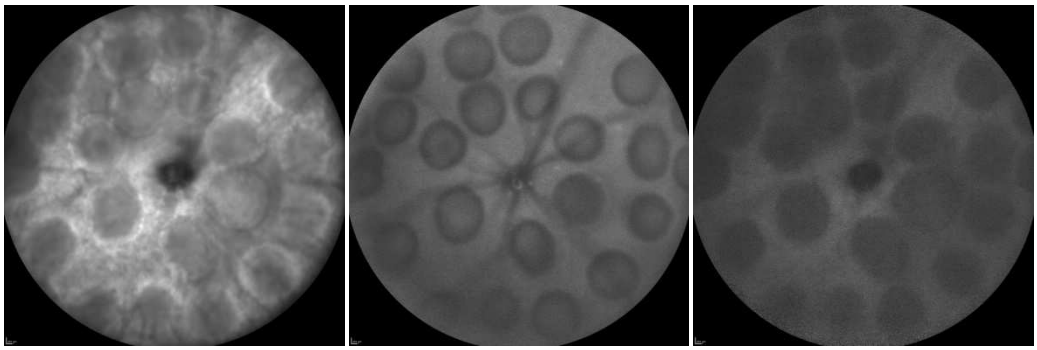

Figure 3.19. cSLO images showing multiple retinal laser burns prior to mRNA analysis. The use of multiple burns reduced the dilution effect of adjacent non-lasered retina on gene expression.

The expression of several candidate genes involved in the apoptotic pathway in 14 retinas three days after laser exposure was investigated by qPCR (Figure 3.20). Changes in gene expression were compared between lasered versus contralateral non-lasered eyes and the results normalised to wild type mRNA. The expression of retinal *c-Fos* mRNA was increased by 2.4-fold (*t_6 = 3.60, P = 0.01, N = 7) relative to the non-lasered group. A positive trend was seen for the pro-apoptotic gene, *Bax*, with relative induction in the laser compared to non-laser group. Notably a negative trend was observed for the anti-apoptopic gene, *Bcl-2*, in the laser-treated group

compared to non-laser controls. However, in both these latter cases, the trends were not statistically significant. Paradoxically, perhaps, the expression of *STAT-3* tended to increase three days after laser exposure, although this trend was also not statistically significant. Similarly, *Mapk-13* showed a trend towards increased expression whilst *Mapk-12* displayed an opposite trend to reduced expression at the same stage, although again, these were not statistically significant. No change in trend was seen in the expression of *Caspase-3*, *c-Jun*, *Mapk-11* or *Mapk-14*.

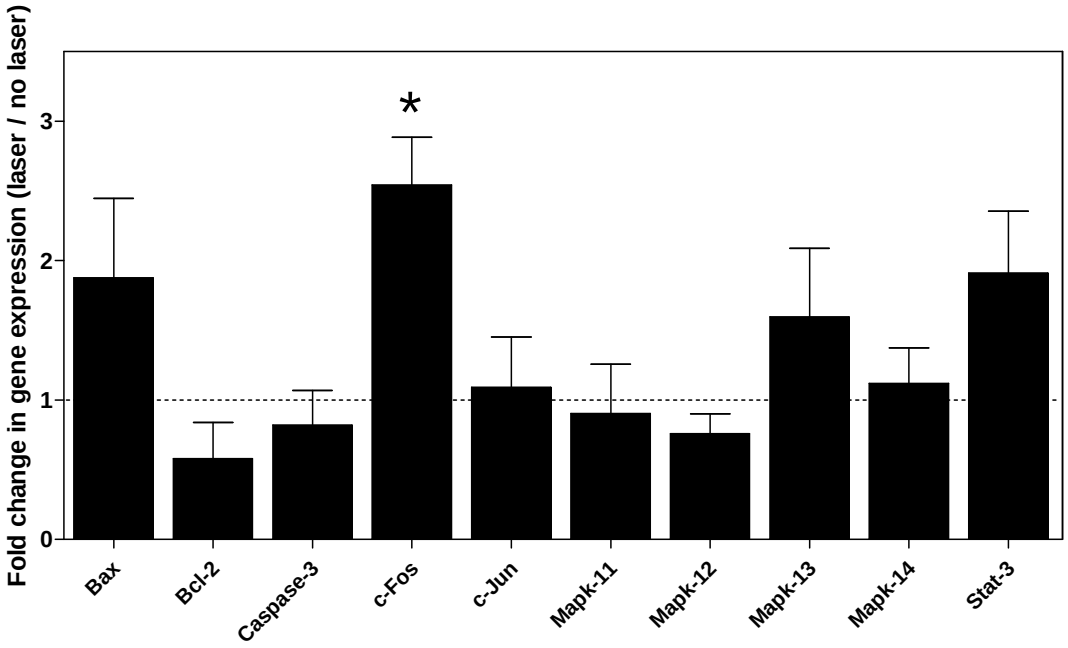

Figure 3.20. Apoptotic gene expression determined by qPCR in C57BL/6 retinae at three days post laser exposure. Results showed a significant increase in the transcriptional expression of pro-apoptotic *c-Fos*, and positive and negative trends for *Bax* and *Bcl-2* expression, respectively, in lasered eyes. Error bar ± SEM, $N = 7$ mice. *$P < 0.05$.

3.4 Discussion

The results of this study demonstrate a reproducible animal model to study secondary, apoptotic cone loss, following retinal laser injury. This model, which

enabled cone loss to be followed longitudinally, may simulate a human foveal laser injury that predominantly affects cone photoreceptors. The *in vivo* model described here provides a unique method of assessing photoreceptor damage, and specifically cone injury, post laser exposure, as it directly monitors the longitudinal effects on cones following laser.

Although fluorescein angiography, near infrared reflectance, white light fundoscopy, and electroretinographic techniques have been used to study the effects of laser injury in various animal models,[374-377] the mainstay of investigation has relied solely on histology. Aside from the benefits of non-invasive imaging helping to significantly reduce the number of experimental animals required, histological techniques are severely limited due to a number of factors, including the fact that such studies are necessarily cross-sectional and, therefore, subject to a source of biological and procedural error across animals and time points.[378] Quantification of photoreceptor nuclei or ONL thickness in a lasered area depends on localisation of a focal area of injury. This is potentially inaccurate due to asymmetry of the injured area, variability of laser exposure and selection bias. However, coupled with a longitudinal imaging method, the approach described in this chapter provides for a more robust method of analysis. A limitation of this *in vivo* study however, is that media clarity needs to be maintained in the presence of an agent delivered via the intravitreal route. This therefore, excludes certain opaque compounds (e.g. triamcinolone acetonide) from investigation that may otherwise be used in routine clinical practice via this route.

In the previously described *in vivo* model, hypoautofluorescence of the outer retina was observed immediately following laser with no changes in autofluorescence of

the inner retina. Two possible mechanisms to explain the hypoautofluorescent changes in the outer retina could be due to, firstly, the immediate damage of GFP positive cones that would occur as a result of photothermal injury or, secondly, due to the presence of oedema with resultant blockage of autofluorescence.[379] The finding that the loss of GFP fluorescence over six weeks as the lesion expanded indicates that cones are progressively lost following an initial injury in the *in vivo* model. This result is consistent with previous reports of enlargement of retinal laser lesions in humans over time, where lesion enlargement by 42% at 32 months[380] and 103% at 1 year[381] was determined by measuring the macular laser lesion diameter following treatment for choroidal neovacularisation.

By using the TUNEL assay, the results indicate that a mechanism of photoreceptor death occurring within the first week post injury is secondary to apoptosis. The localisation of TUNEL staining at different depths of the ONL indicates that apoptotic cell death occurs in both rods and cones, whereas the greater ONL loss occurring at six weeks, which again indicates the occurrence of both rod and cone death, correlates with the *in vivo* findings of progressive cone loss during this period.

In order to target this secondary cell death, neuroprotective treatment would need to be initiated in the acute phase of injury. Since the results suggest that maximal apoptosis occurs between one and three days post laser in line with previous reports investigating retinal laser injury,[382] this time period would provide the optimum window for therapeutic intervention.

Bcl-2, *Bax*, and *c-Fos* have all been identified as key components in the intrinsic or mitochondrial apoptotic pathway, with the latter being activated by toxic light

exposure.[383,384] Due to the high sequence identity that exists between *Bax* and *Bcl-2* orthologues, qPCR primers were designed to ensure no cross-hybridisation would occur between these genes. The three day time point was chosen to exclude changes associated with necrosis in the immediate aftermath of laser exposure. Previous reports have also shown that alterations in apoptotic gene expression occur three days post laser treatment.[385] Generally considered to be anti-apoptotic, *STAT-3* can also act to promote apoptosis,[386] and, as such, may support the increase in expression with laser treatment. The fact that some trends were seen which did not quite meet levels of statistical significance may, of course, reflect the fact that only a proportion (posterior pole) of the retina was treated with laser. This could result in changes that are real, but diluted against background levels.

CHAPTER 4

CNTF ATTENUATES CONE LOSS *IN VITRO* AND POST LASER EXPOSURE

4.1 Introduction

4.1.1 Aim

To investigate the effect of the neurotrophic cytokine, ciliary neurotrophic factor (CNTF), on cone photoreceptor survival *in vitro* and *in vivo*, the latter following retinal laser exposure.

4.1.2 Overview

CNTF is an endogenously occurring member of the neuropoietic cytokine family with a molecular mass of approximately 22 kDa, that has a role in CNS development and injury, and supports survival of retinal, hippocampal, striatal and sensory neurons.[107-110] CNTF has been shown to control proliferation and differentiation of progenitor cell populations in the developing mammalian retina via the activation of the Jak/STAT, MAPK, and Akt signalling pathways.[108,134-138] In terms of its use as a neuroprotective therapy in the eye, delivery of the agent is via the intraocular route, directly into the vitreal or subretinal space, as the blood–retinal barrier restricts access from the bloodstream to the neural retina. The intravitreal route of administration of CNTF protein was applied to the studies described in this chapter. Not only does this increase the bioavailability of the protein by allowing direct access to the retina but it also ensures targeting of the Müller cells, which span the retina with their footplates forming the inner limiting membrane. Assuming that photoreceptor survival is dependent upon Müller cell activity as described shortly, then the direct action of CNTF on this cell would best be achieved by intravitreal delivery.

Although the general actions of CNTF are understood, its precise role in the protection of photoreceptors is still poorly defined. For instance, it is known that CNTF is expressed by Müller cells and other glial cells of the retina and that the Müller cell is believed to be a primary target for the action of CNTF.[129] CNTF has been shown to induce Müller glia proliferation,[145] which would enhance the production of endogenous neurotrophic factors (e.g. CNTF itself) that ameliorate photoreceptor damage. Although a few studies propose the presence of the CNTFR-α on outer segments,[139] the majority of reports suggest that photoreceptors do not possess a CNTF receptor, therefore leaving open the question of the precise mechanism of Müller-cell mediated protection of photoreceptors following CNTF delivery. Proposed mechanisms of CNTF action on photoreceptor survival have included the release of specific survival factors,[139] the direct action on photoreceptors to inhibit apoptosis, the reduction of circulating glutamate,[149] or the increased resistance to toxic metabolites.[150]

The molecular mechanism of CNTF action involves, upon activation, the heterodimerisation of its tripartite receptor complex, which comprises its α-receptor components, the gp130 subunit and the LIFR-β subunit, respectively.[115] Resultant activation of receptor-associated tyrosine kinases (Tyk) and subsequent downstream janus kinases initiates phosphorylation of intracellular signalling molecules, including the MAPK pathway, NFκB and STAT family of transcription factors. Direct activation of the Jak/STAT and MAPK pathways by increased CNTF expression in Müller cells has been shown to improve photoreceptor survival in light-damaged and neurodegenerative disease models.[108,132,133]

The primary aim of this study was to investigate the neuroprotective effect of CNTF on cone photoreceptors. In order to establish an effective dose of CNTF in the murine retina, the experimental studies described in this chapter were based on previous reports of the use of intravitreal CNTF and its protective effect on photoreceptor survival. These included the finding of greater preservation of ONL thickness following intravitreal injection of 1 µg/µl CNTF in albino Sprague-Dawley rats when placed into constant fluorescent light[154] and the protective effect on photoreceptor survival following intravitreal CNTF injection (500ng/µl) in *Pde6b*$^{rd1/rd}$, *nr/nr*, and rhodopsin Q344ter mutant mice carrying naturally-occurring retinal degenerations.[155]

Specifically with regard to cone photoreceptors, CNTF has been shown to stimulate the regeneration of cone outer segments in S334ter mice that carry a retinal degeneration which involves secondary cone loss.[170] The protective effect may have reversed the causal factors of cone loss, that were hypothesised to include: the release of toxic byproducts following rod degeneration; the loss of purported "rod-derived cone viability factors" (RdCVFs)[172]; the loss of structural support due to rod degeneration; altered cone morphology with new and abnormal synaptic connections; or alterations in RPE and Müller cells following the loss of rods.

4.1.3 Summary of results

The findings in these studies can be summarised as follows:

1) CNTF supports the survival of GFP positive cones *in vitro*.

2) CNTF attenuates the loss of GFP positive cones within the lesion area following retinal laser exposure *in vivo*.
3) CNTF attenuates the loss of photoreceptors within the lesion area following retinal laser exposure as determined by histology.
4) The molecular mechanism of action of CNTF following retinal laser exposure involves inhibition of the pro-apoptotic *Bax* gene and activation of the anti-apoptotic *Bcl-2* gene.

4.2 Experimental design

Experiments were conducted as follows:

In vitro cell counting

The neuroprotective effect of CNTF on GFP positive cones was determined by adding CNTF to cultured cells. Following papain dissociation, OPN1-EGFP retinal cell suspensions were separated into 24-well plates with varying concentrations of CNTF (50ng/ml, 100ng/ml, and 200ng/ml). As a comparison, the effect of another neuroprotective agent, IGF-1, was observed at the same concentrations. Treatments were administered daily during a complete change of media and cell counting was performed daily using an inverted fluorescence microscope. Cell counting was performed from five points per well (central and four cardinal points) in order to avoid bias.

In vivo imaging

Following intraperitoneal anaesthetic injection, baseline retinal images were obtained from adult OPN1-EGFP mice using the cSLO. Thereafter, each retina received two to four equidistant burns approximately two disc diameters from the edge of the optic disc before re-imaging by cSLO. Subsequently, the left eye of each animal received an intravitreal injection of CNTF with the contralateral eye receiving an intravitreal sham injection of PBS. Retinas were re-imaged at one, three and six weeks.

Histology and TUNEL assay

For histology, WT mice received eight burns bilaterally (16 burns in total) and received an intravitreal CNTF versus contralateral PBS injection as per the previously described method. Following this, mice were sacrificed at one, three, and six weeks post laser. Eyes were sectioned, stained with DAPI, and imaged using an inverted fluorescence microscope.

qPCR analysis

To investigate the effect of CNTF on retinal gene expression post laser, WT mice received 20 pan-retinal burns bilaterally followed by an intravitreal CNTF versus contralateral PBS injection as per the previously described method. At 3, 7, and 14 days post laser exposure, a comparison was made between gene expression in CNTF-treated versus sham-injected retinas.

4.3 Results

4.3.1 In vitro

CNTF was shown to enhance the survival of GFP positive cones in a dose-dependent manner (Figure 4.1). Comparison between 50ng/ml, 100ng/ml, and 200ng/ml showed a dose-response with the highest dose (200ng/ml) associated with most survival of GFP positive cones at day 9 compared to PBS control ($P < 0.0001$, $n = 12$, two-way ANOVA with Bonferroni post-hoc test, dose and time as factors, Figure 4.2). Although 100ng/ml CNTF also led to the increased survival of cone photoreceptors ($P = 0.005$, $n = 12$, two-way ANOVA with Bonferroni post-hoc test), 50 ng/mL CNTF did not have a significant protective effect over PBS treatment at day 9 ($P = 0.127$, $n = 12$, two-way ANOVA with Bonferroni post-hoc test). Retinal culture with the addition of the neuropeptide, IGF-1, did not show a difference in the survival rate of GFP positive cones when compared to the PBS-treated group ($P = 0.620$, $n = 12$, two-way ANOVA, Figure 4.3).

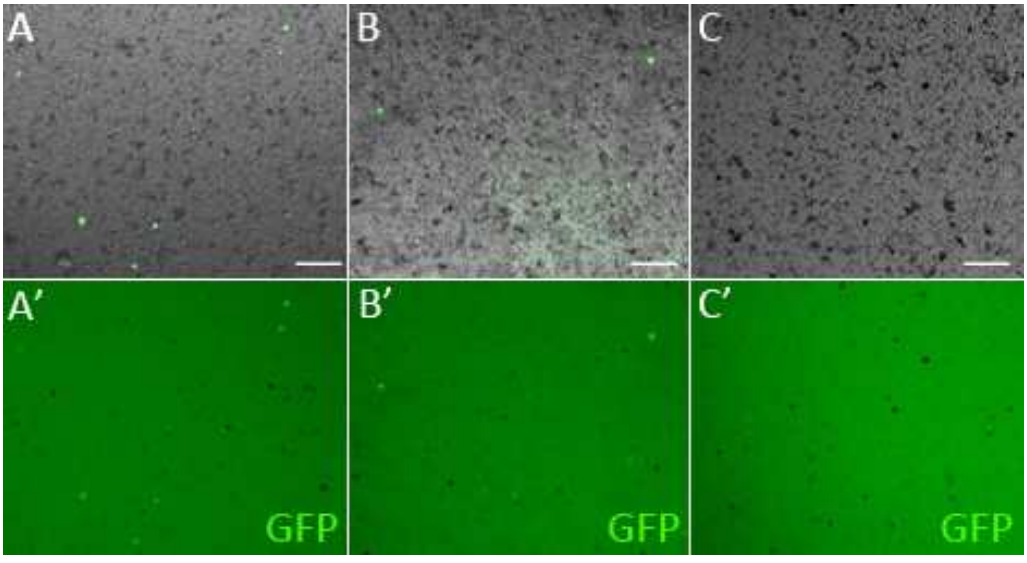

Figure 4.1. Cultured OPN1-EGFP cells in the presence of CNTF at day 9. Increased survival of GFP positive cells is seen at the higher 200ng/ml CNTF dose (A/A') than in

the lower 50ng/ml dose (B/B'). Few surviving GFP positive cones are seen in the PBS control plate (C/C'). Scale bar: 100 µm.

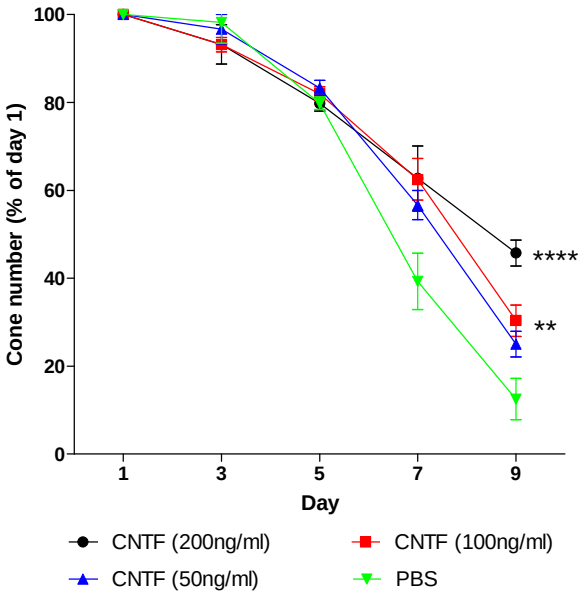

Figure 4.2. A dose response curve showing the effect of CNTF on survival of cultured GFP positive cones. Increased cone survival correlated with increasing CNTF dose. PBS control was associated with the lowest rate of survival. Error bar ± SEM, *n* = 12 per time point. ****$P < 0.0001$; **$P < 0.01$; two-way ANOVA with Bonferroni post-hoc test (time and dose as factors).

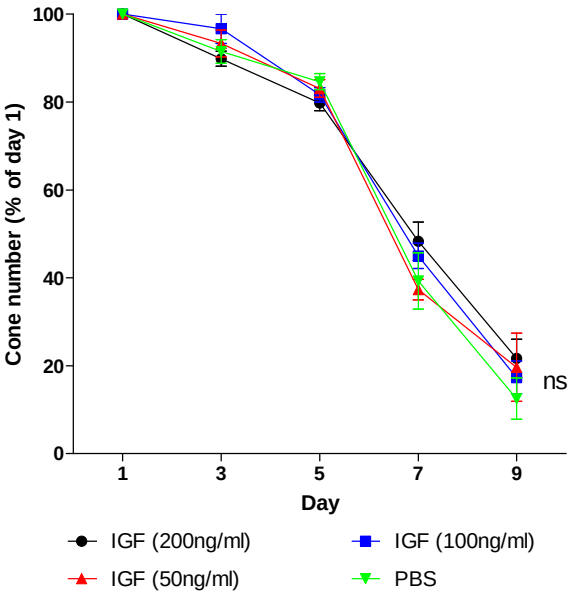

Figure 4.3. A dose response curve showing the effect of IGF-1 on survival of cultured GFP positive cones. IGF-1 did not show a protective response on cone survival. Error

bar ± SEM, *n* = 12 per time point. *P* = 0.620; two-way ANOVA with Bonferroni post-hoc test (time and dose as factors).

4.3.2 *In vivo* imaging

AF imaging showed a gradual attenuation of GFP-positive cones in eyes receiving either intravitreal CNTF or contralateral sham injection (Figure 4.4). However, at six weeks, the lesion area was smaller in CNTF-treated (44.6 ± 0.07%) than in sham-injected (59.5 ± 0.08%) eyes as determined by 790nm AF imaging (*t_{10} = 2.85, *P* = 0.017, *N* = 11, Figure 4.5). Furthermore, at three weeks after laser application, 488nm AF imaging showed that there were more surviving GFP-positive cones in CNTF-treated eyes (54.1 ± 5.15% of baseline count) than in sham-injected eyes (28.7 ± 4.4%) (**t_{10} = 3.81, *P* = 0.03, *N* = 11, Figure 4.6E). This difference in cone survival persisted at the 6 week point (treated, 39.6 ± 3.2% vs. sham, 18.0 ± 3.8%) (**t_{10} = 3.53, *P* = 0.005, *N* = 11, Figure 4.6A-E). There was no significant difference in the number of GFP-positive cones in non-lesioned internal control areas in either the CNTF or sham-injected experiments at any time point (paired t–test, *P* = 0.73 and 0.43 at 3 and 6 weeks respectively), showing that the effect on cone survival was specific for the presence of CNTF and not secondary to trophic effects due to the intraocular injection procedure.

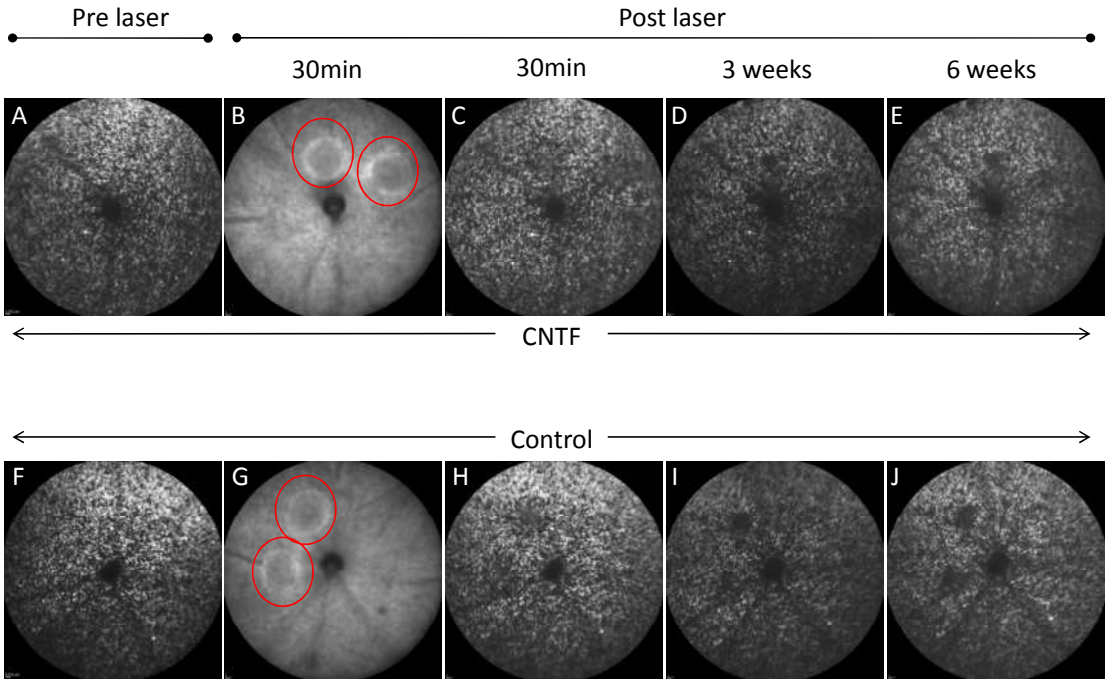

Figure 4.4. cSLO images of the OPN1-EGFP post laser injury following intravitreal CNTF versus sham. The upper row (**A-E**) shows the longitudinal result from a CNTF-treated eye and the lower row (**F-J**) from a sham-injected eye. A baseline 488nm AF image for each group is shown at the far left (**A** and **F**). 820nm reflectance imaging showed two similar, well-defined laser lesions in the superior retina of either eye close to the optic disc (within red circles, **B**, **G**). The loss of GFP positive cones, as detected by 488nm AF imaging, within the lasered area increased from 30 minutes (**C**, **H**) to 6 weeks (**E**, **J**) post injury in both groups. However, there was greater preservation of GFP positive cones within the lesion area in the CNTF-treated eye (**E**) compared to the sham-injected eye (**J**).

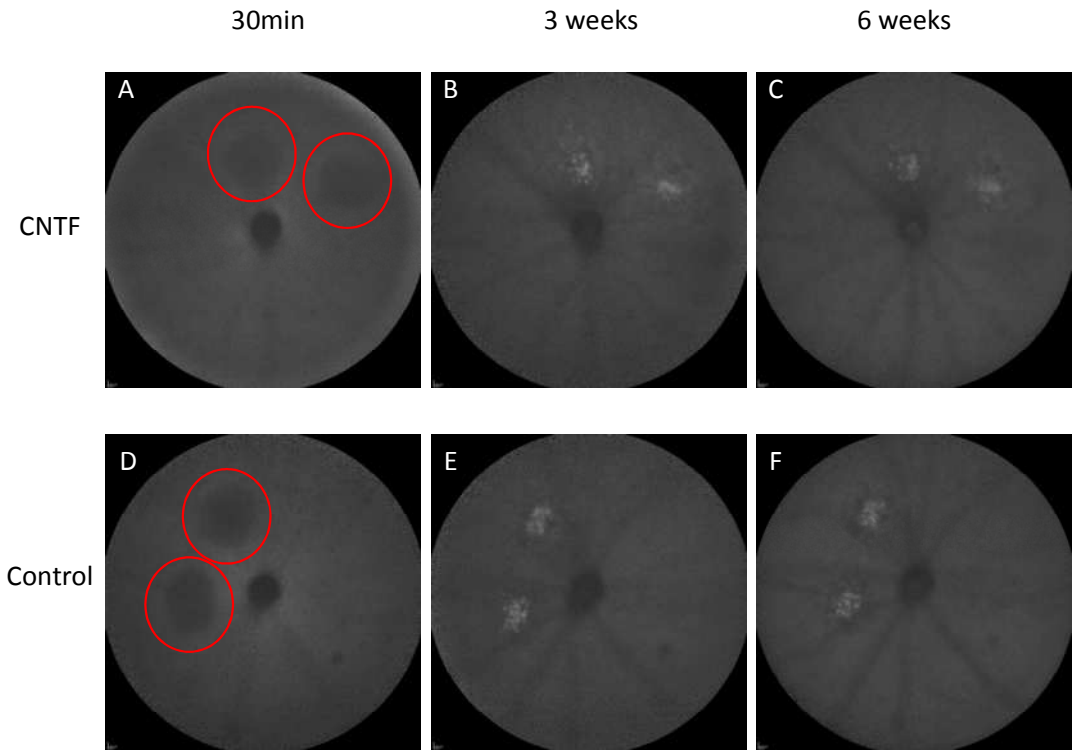

Figure 4.5. 790nm AF images post laser injury following intravitreal CNTF versus sham-injected eyes. These images correspond to the examples in Figure 4.4 with the upper row (**A-C**) showing the longitudinal result from a CNTF-treated eye and the lower row (**D-F**) from a sham-injected eye. At 30 minutes post laser, a similar hypoautofluorescent appearance was noted within the lesion area (within the red circles) in both CNTF-treated and sham-injected eyes (**A** and **D** respectively). However, at both the 3 and 6 week stage, the lesion area that was now marked by an increase in autofluorescence, was smaller in CNTF-treated eyes (**B** and **C** respectively) compared to sham-injected eyes (**E** and **F** respectively).

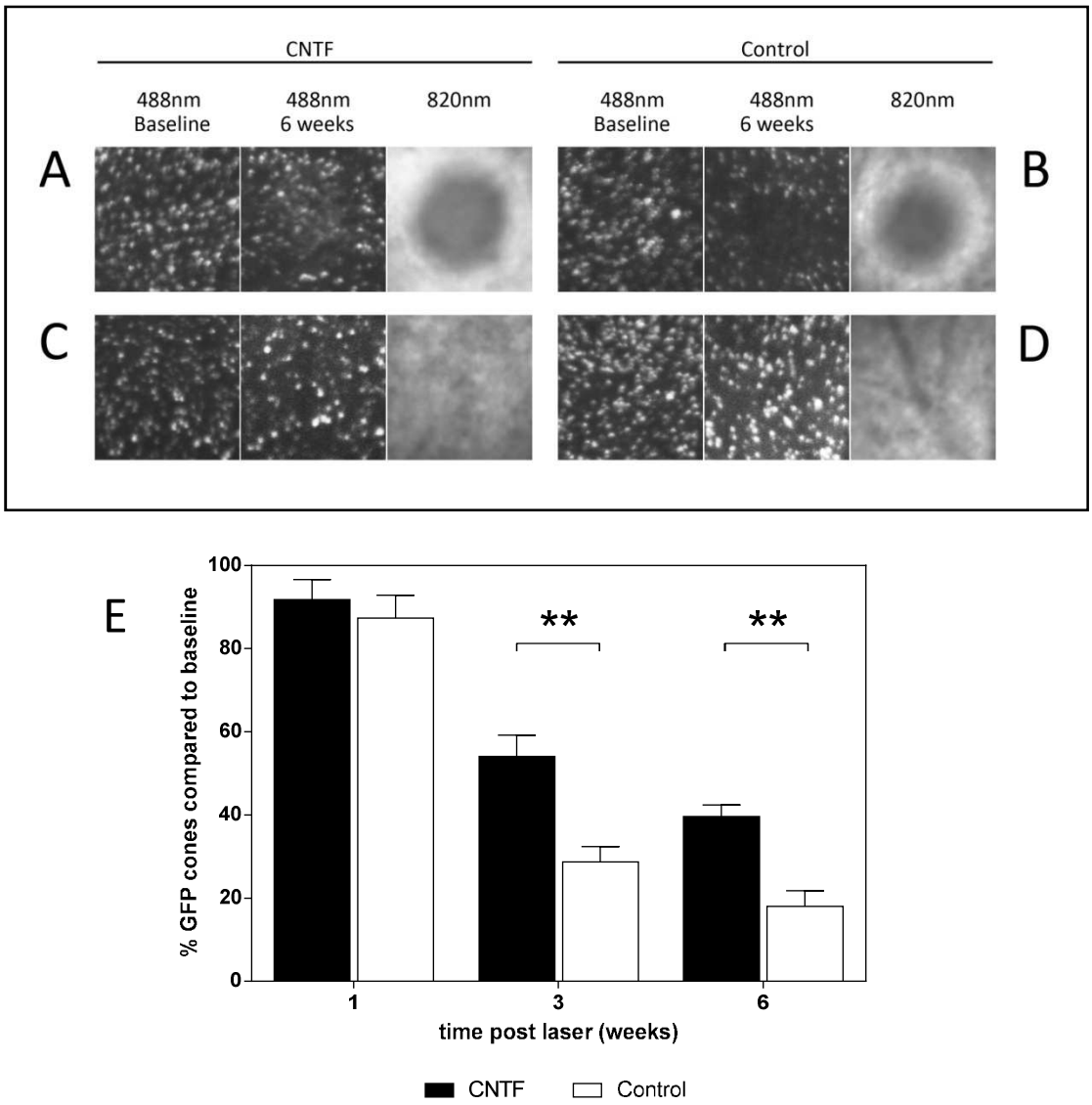

Figure 4.6. High power cSLO images immediately before ("baseline") and six weeks following intravitreal CNTF administration versus sham-injection post laser exposure. At six weeks, CNTF-treated eyes (**A**) showed greater preservation of GFP-positive cones on 488 nm imaging within the site of injury compared to contralateral sham-injected eyes (**B**). Areas of decreased reflectance seen on near-infrared imaging immediately following laser corresponded to the lesion area. Non-lesioned internal control areas remained unchanged between baseline and six weeks in both treated (**C**) and sham-injected (**D**) groups. Analysis of cone survival by cSLO imaging showing cone photoreceptor number (indicated by GFP counts), following intravitreal CNTF versus sham-injection post laser (**E**). The CNTF-treated group showed greater cone survival than sham-injected controls, equivalent to rescue of approximately 50% of cones at six weeks post laser. Error bar ± SEM, N = 11 eyes in each group at each timepoint. $^{**}P < 0.01$ for both groups.

4.3.3 Histology

As an additional validation, histological assessment (which includes cell counts of rod and cones) was also performed on retinal sections through the lesions at one, three and six weeks after laser exposure. In keeping with the *in vivo* imaging, there was a greater loss of photoreceptors with time, from one to six weeks, although as the data was derived from different eyes at different timepoints, it was cross-sectional and therefore subject to variability. Between treatment groups however, the proportion of surviving photoreceptors within lesions (normalised to the photoreceptor count in a non-lesion control area in each eye as described in Chapter 3) was significantly greater in CNTF-treated eyes compared to sham-treated eyes (63.4 ± 2.3% vs. 50.8 ± 3.4%, treated and sham-injected group, respectively by six weeks; $^{**}t_9 = 3.78$, $P = 0.004$, $N = 10$, Figure 4.7). Although there was a trend, no significant difference was detected in the photoreceptor count at one week post laser, possibly due to greater variability at this stage (Figure 4.7G).

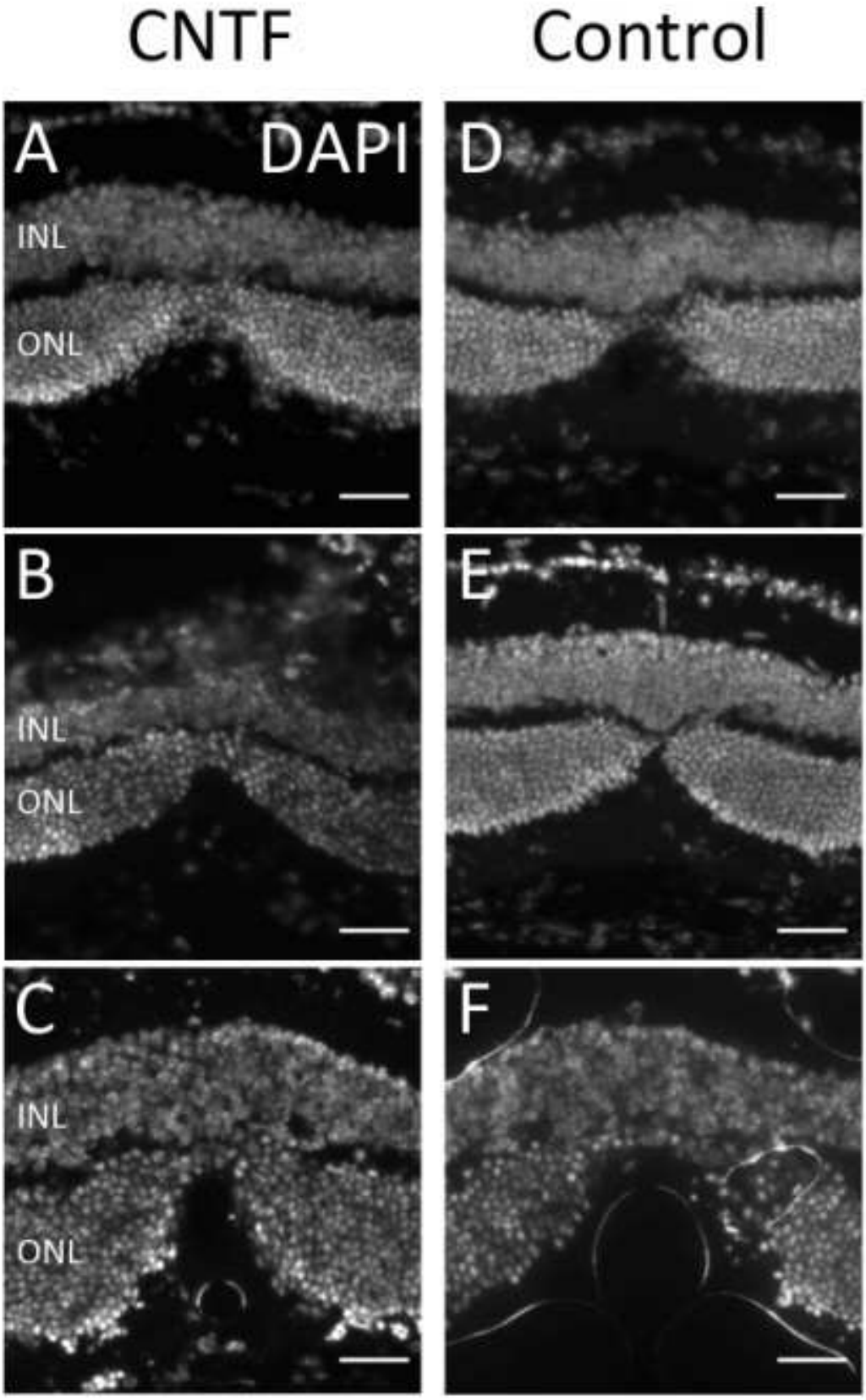
CNTF
Control
A
DAPI
INL
ONL
D
B
INL
ONL
E
C
INL
ONL
F

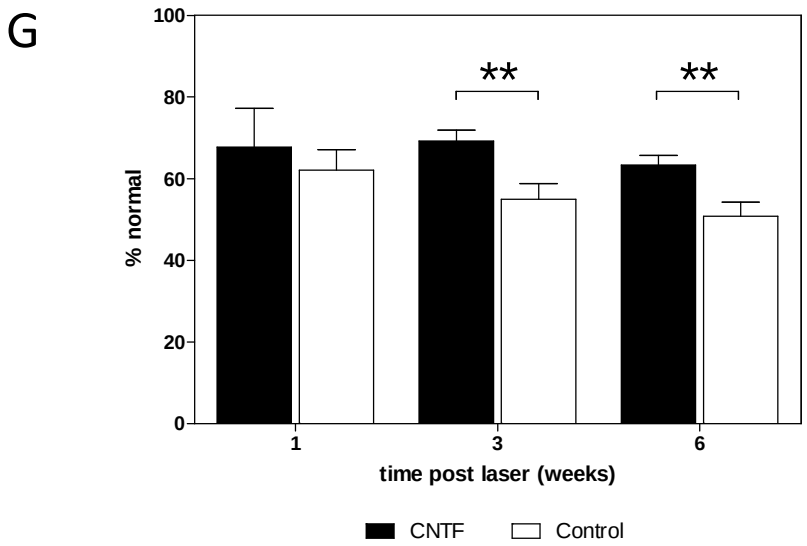

Figure 4.7. DAPI-stained sections of lesion centres at six weeks post retinal laser (A-F). A greater preservation of photoreceptors was observed within the CNTF group (A-C) compared to contralateral sham-injected (D-F) experiments. Scale bar: 50 µm. Analysis of rod and cone survival by comparing photoreceptor nuclei within the lesion centre following intravitreal CNTF versus sham-injection post laser (G). Photoreceptor density is given as a percentage within the lesion centre relative to a non-lasered internal control area. An overall increase in the survival of photoreceptors was seen within the CNTF-treated group relative to the sham-injected experiment at three and six weeks post laser. This result is consistent with the effect observed in cones by *in vivo* analysis. Error bar ± SEM, $N = 10$ eyes in each group at each timepoint. $^{**}P < 0.01$. INL, inner nuclear layer; ONL, outer nuclear layer.

4.3.4 qPCR analysis

As described in Chapter 3, the baseline levels of expression for genes involved in apoptosis were established following laser exposure. A further analysis was performed where eyes receiving intravitreal CNTF were compared to contralateral sham-injected eyes at three time points following laser exposure: three days, one week, and two weeks. These results are summarised in the heat map shown in Figure 4.8 and the temporal relationship for each gene is shown separately in Figure 4.9-4.16. In this case, only *Bax* and *Bcl-2* expression were significantly influenced by

CNTF, which led to a two-fold reduction in *Bax* expression at one week post laser exposure ($F_{2,27}$ = 5.68, P = 0.009, N = 30, $^{**}P$ = 0.006 post-hoc, Figure 4.9) and a four-fold increase in *Bcl-2* expression ($F_{2,27}$ = 7.51, P = 0.003, N = 30, $^{***}P$ = 0.0005 post-hoc, Figure 4.10) relative to the sham-injected group. Since both *Bcl-2* and *Bax* function via complementary actions, changes in their levels can be usefully expressed as a ratio. Following laser exposure, CNTF caused a marked elevation in the *Bcl-2*:*Bax* ratio relative to sham injection at one week ($F_{2,27}$ = 10.57, P = 0.0004, N = 30, $^{***}P < 0.0001$ post-hoc, Figure 4.11).

In addition, positive and negative trends were observed in the expression of other apoptotic genes in response to CNTF treatment: in particular, *c-Fos* expression decreased after three days; *c-Jun* expression increased after one week; *Mapk-11* expression decreased after three days and two weeks; *Mapk-14* expression increased after one week, and *STAT-3* expression decreased after three days and two weeks (Figure 7A). Although not statistically significant, the trends with CNTF treatment were inverse to those resulting with laser treatment alone, suggesting that this neuroprotective agent may act on similar cell stress-related pathways to reverse any changes in apoptotic gene expression that are induced by laser injury.

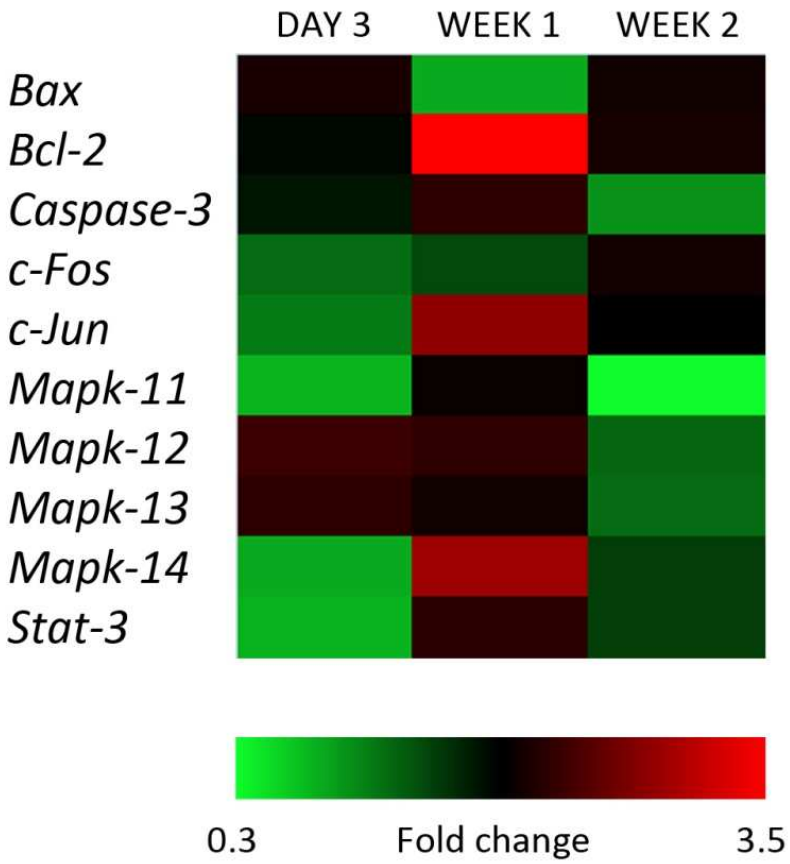

Figure 4.8. A heat map of differentially expressed apoptotic genes post intravitreal CNTF versus contralateral sham-injection following laser. The numbers used to generate the heat map are the mean fold changes (absolute values) in gene expression determined from sham-injected eyes compared to those calculated from the contralateral CNTF-injected group. Red and green indicate an increase or decrease in the mRNA level, respectively. The heat map colours represent the expression of each gene individually and are not comparable between genes.

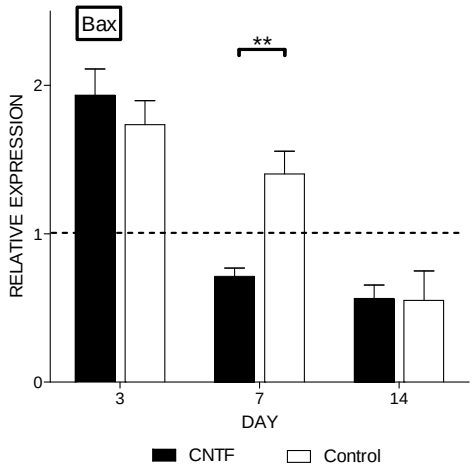

Figure 4.9. The expression of the *Bax* gene after intravitreal CNTF injection following laser treatment, compared to contralateral sham controls. qPCR analysis in C57Bl/6 retinae at time points post laser exposure (normalised to wild type). At one week post laser, *Bax* expression was inhibited (black columns) following intravitreal CNTF compared to controls (white columns). Error bar ± SEM, *N* = 30 mice. ***P* = 0.0062, two-way ANOVA with Bonferroni post-hoc test.

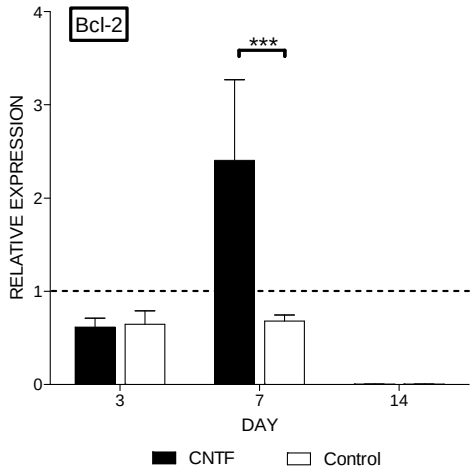

Figure 4.10. The expression of the *Bcl-2* gene after intravitreal CNTF injection following laser treatment, compared to contralateral sham controls. qPCR analysis in C57Bl/6 retinae at time points post laser exposure (normalised to wild type). At one week post laser, *Bcl-2* expression was induced (black columns) following intravitreal CNTF compared to controls (white columns). The unexplained absence of signal at 14 days in the treated and control arms but preservation of signal in the wild type group is likely due to experimental error rather than biological variation. Error bar ± SEM, *N* = 30 mice. ****P* = 0.0005, two-way ANOVA with Bonferroni post-hoc test.

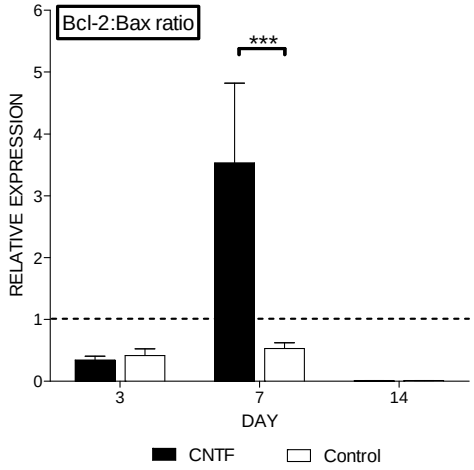

Figure 4.11. *Bcl-2*/*Bax* ratios after intravitreal CNTF injection following laser treatment, compared to contralateral sham controls. qPCR analysis in C57Bl/6 retinae at time points post laser exposure (normalised to wild type). At one week post laser, *Bcl-2*/*Bax* ratios were elevated following intravitreal CNTF compared to controls. Error bar ± SEM, *N* = 30 mice. ****P* < 0.0001, two-way ANOVA with Bonferroni post-hoc test.

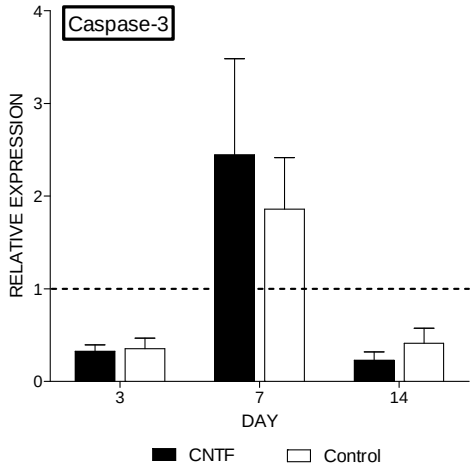

Figure 4.12. The expression of the *Caspase-3* gene after intravitreal CNTF injection following laser treatment, compared to contralateral sham controls. qPCR analysis in C57Bl/6 retinae at time points post laser exposure (normalised to wild type). No significant difference was detected between treated and sham-injected eyes. Error bar ± SEM, *N* = 21 mice. *P* = 0.478, two-way ANOVA with Bonferroni post-hoc test.

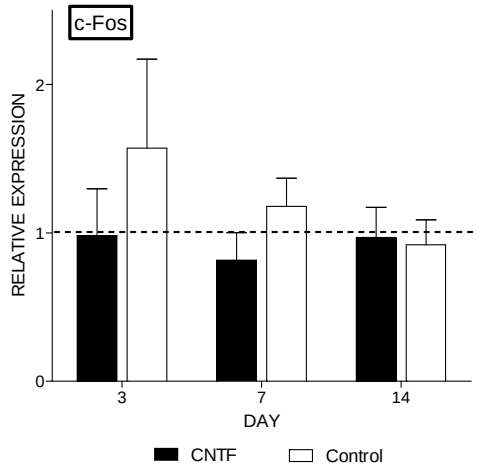

Figure 4.13. The expression of the *c-Fos* gene after intravitreal CNTF injection following laser treatment, compared to contralateral sham controls. qPCR analysis in C57Bl/6 retinae at time points post laser exposure (normalised to wild type). No significant difference was detected between treated and sham-injected eyes although a positive trend was seen in sham-injected eyes at day 3 post laser. Error bar ± SEM, *N* = 30 mice. *P* = 0.321, two-way ANOVA with Bonferroni post-hoc test.

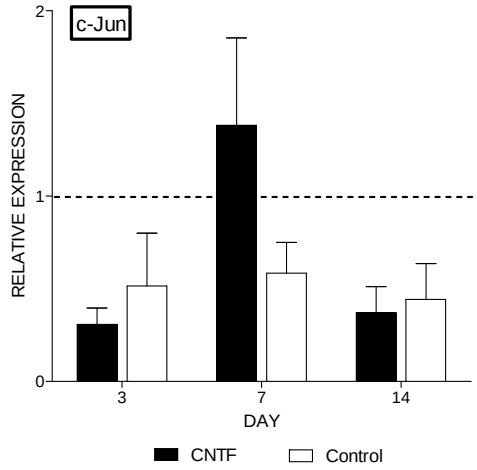

Figure 4.14. The expression of the *c-Jun* gene after intravitreal CNTF injection following laser treatment, compared to contralateral sham controls. qPCR analysis in C57Bl/6 retinae at time points post laser exposure (normalised to wild type). No significant difference was detected between treated and sham-injected eyes although a positive trend was seen in CNTF-injected eyes at day 7 post laser. Error bar ± SEM, *N* = 21 mice. *P* = 0.094, two-way ANOVA with Bonferroni post-hoc test.

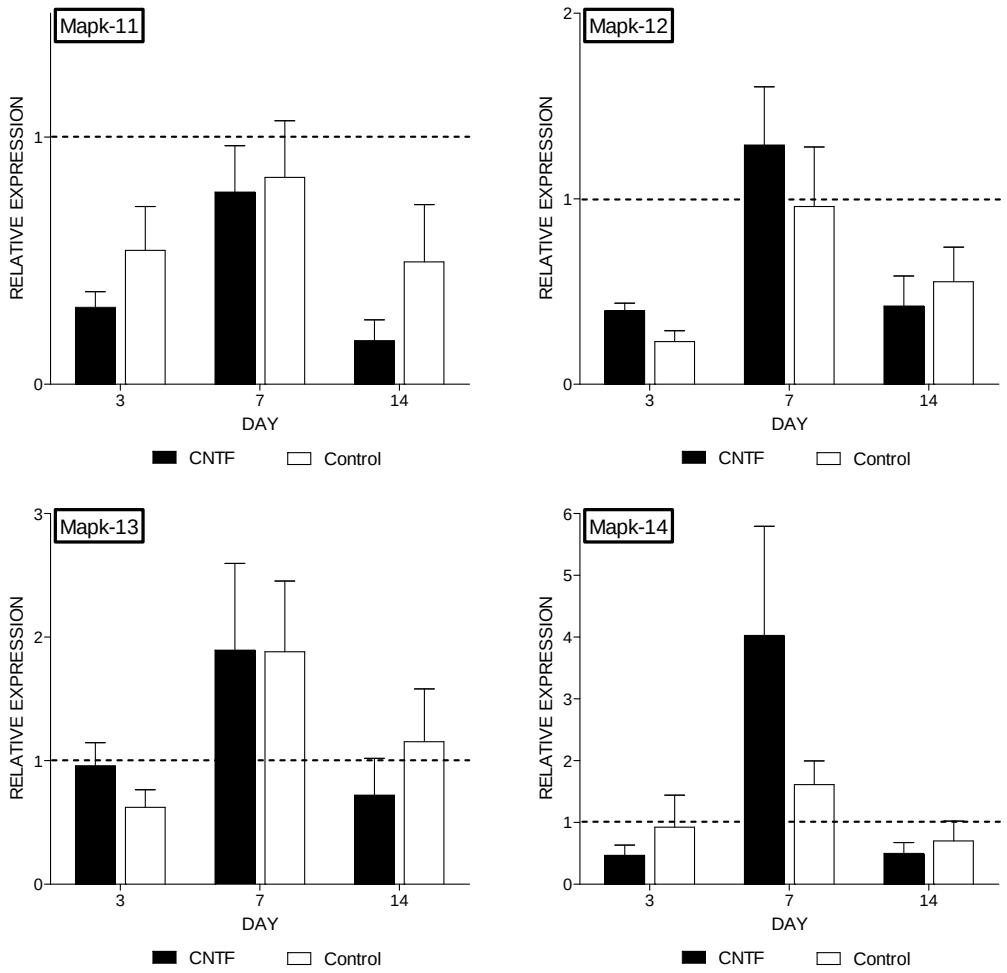

4.15. The expression of the *Mapk* gene family after intravitreal CNTF injection following laser treatment, compared to contralateral sham controls.qPCR analysis in C57Bl/6 retinae at time points post laser exposure (normalised to wild type). No significant differences were detected between treated and sham-injected eyes, however several trends were noted. *Mapk-11* showed a positive trend in sham-injected eyes at days 3 and 14, and *Mapk-14* showed a positive trend in CNTF-injected eyes at day 7 post laser. Error bar ± SEM, *N* = 21 mice.

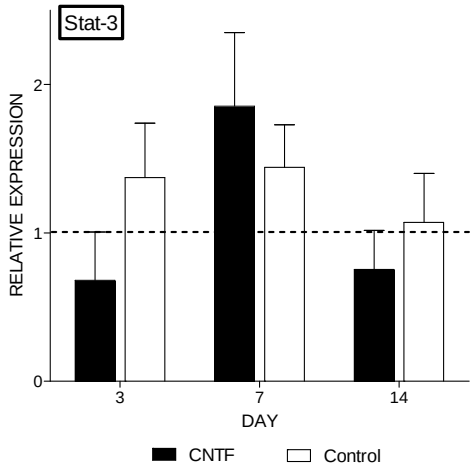

4.16. The expression of the *STAT-3* gene after intravitreal CNTF injection following laser treatment, compared to contralateral sham controls. qPCR analysis in C57Bl/6 retinae at time points post laser exposure (normalised to wild type). No statistical significance was found between treated and untreated eyes although a negative trend was noted in the CNTF-injected group at days 3 and 14 post laser. Error bar ± SEM, *N* = 29 mice. *P* = 0.437, two-way ANOVA with Bonferroni post-hoc test.

4.4 Discussion

In order to target the secondary cell death that occurs following laser exposure, neuroprotective treatment would need to be initiated in the acute phase of injury. Since the TUNEL data as described in Chapter 3 suggests that maximal apoptosis occurs between one and three days post laser in line with previous reports investigating retinal laser injury,[382] this time period would provide the optimum window for therapeutic intervention. The neuroprotective effect of CNTF has been demonstrated in previous rodent models of retinal injury.[387] On the basis of this work, CNTF was chosen as a potential therapeutic agent in this model of cone loss induced by laser exposure. By using a multimodal approach consisting of both *in vivo* imaging and *in vitro* histological and molecular techniques, the results confirmed the protective effect of CNTF in this model of laser injury.

Initial evidence for the protective role of CNTF on cone photoreceptors was confirmed by *in vitro* culture. Given that cones have not been shown to possess a CNTF receptor, it is unlikely that CNTF had a direct action on these cells. It is possible however, that the protective action may have been due to a paracrine effect, since cones were cultured with all retinal cells. In particular, the Müller cell may have had a fundamental effect given its suggested role in photoreceptor neuroprotection.[108,132,133] It is possible that survival of this subgroup of cells in the presence of CNTF had a subsequent impact on cone survival. The *in vitro* data as described in this chapter supports recent work demonstrating the protective effect of CNTF on cones in a retinal explant model of cone degeneration.[388] The latter study showed a dose-response relationship with the administration of high dose CNTF improving cone survival compared with the PBS-treated group, similar to the findings described in this chapter.

It is noteworthy that the histological studies described in this chapter were conducted in wild type (C57Bl/6) mice and not in OPN1-EGFP mice. The rationale for this was due to the recent finding that the OPN1-EGFP model has a dominant cone degeneration that is independent of GFP expression.[389] While this issue would also have been present in the *in vivo* study, the effect would have been smaller as the same animal was followed longitudinally. In contrast, histological study was conducted at different time points with different animals, in which case the additional loss of cones - that do, albeit, represent a small proportion of the outer nuclear layer - could have constituted a further source of error due to variability between animals.

Bax protein is a potent pro-apoptotic initiator in the cell death cascade. Following homodimerisation, the resulting configuration forms a channel across the mitochondrial membrane. This allows Cytochrome-C to exit the mitochondria and enter the cytosolic space, where it is involved in conversion of pro-Caspase-9 to Caspase-9 and subsequent initiation of apoptosis.[390] CNTF has previously been shown to inhibit Bax in studies of axotomized motor neurons following sciatic nerve transection.[391] The anti-apoptotic molecule, Bcl-2, which is an integral membrane protein localized to mitochondria, inhibits the activation of Bax following initiation of a death signal.[384] As such, the ratio between these two molecules reflects the susceptibility of cells to a death signal, with positive correlations having been shown between higher Bcl-2/Bax ratios and injury.[392,393] Additionally, the *c-Fos* gene, which encodes a nuclear phosphoprotein that constitutes the transcription factor activator protein 1 (AP-1), has been implicated as having a role in light-induced photoreceptor degeneration.[394] Upregulation of *c-Fos* gene expression has been demonstrated in rodent models of retinal cell apoptosis following photic injury.[383] The results described in this chapter are consistent with the aforementioned findings, showing a reduction of *Bax* and increase of *Bcl-2* mRNA respectively, an increase in the *Bcl-2*/*Bax* ratio, and a trend toward reduction of *c-Fos* mRNA following CNTF administration post laser trauma, thus suggesting that CNTF affects *Bax*, *Bcl-2*, and *c-Fos* at the transcriptional level.

Nonetheless, the precise mechanism by which CNTF improves photoreceptor survival is unknown. As discussed in the introductory chapter, CNTF has been shown to act on the alpha CNTF receptor (CNTFRα), the beta leukemia inhibitory factor

receptor (LIFRβ), and the glycoprotein 130 receptor (gp130R).[395] Photoreceptors lack a CNTF receptor, which is, however, found on inner retinal neurons including Müller cells. Based on this, the postulated mechanism underlying CNTF-dependent photoreceptor protection is thought to be related to Müller cell activation and anti-apoptotic Jak/STAT and MAPK signalling pathways.[108,132,133]

Aside from the targeted and immediate photothermal damage of cone photoreceptors post laser exposure, a further postulated mechanism for this effect in the described model is that RPE cell death leads to secondary cone loss, since direct RPE apoptosis has previously been shown under similar laser treatments.[396] In AMD, the RPE is primarily affected and results in significant loss of sight that arises from photoreceptor (predominantly cone) death. Thus, it is possible that similar molecular pathways are modulated, with accompanied pathophysiological changes, in the secondary cone death that occurs in both laser trauma and retinal degeneration or dystrophy. The wider application of the *in vivo* model as described, and the demonstration of the protective role of CNTF may, therefore, extend to other disorders affecting cone survival.

CHAPTER 5

REPLACEMENT OF CONE PHOTORECEPTORS BY TRANSPLANTATION

5.1 Introduction

5.1.1 Aim

To investigate the feasibility of cone transplantation and the factors that would enhance the survival of donor cones.

5.1.2 Overview

Loss of cone photoreceptor cells is the underlying cause of blindness in retinal laser injury, since the human, being diurnal, is predominantly cone-dependent. In terms of a photoreceptor proportion, the human fovea comprises almost exclusively of cones, hence the devastating visual deficit that occurs from an injury to this area and due to a loss of this cell type. As cones are incapable of regeneration, cell replacement offers the only conducive therapy to restore this population.

Due to the nature of rodent models used in retinal transplantation experiments, the major cell type from the donor is the rod photoreceptor, which comprises approximately 98% of the murine photoreceptor population. Therefore, whole retina donor transplants are predominantly composed of rods. Since cones are relatively few in number, the ability to sort this subpopulation from other retinal cells has provided a particular challenge in transplantation studies. Flow-sorting is one technique that has been used to separate fluorescent photoreceptors from other retinal cells but again this has been done in order to derive flow-sorted fluorescent rods and cones en masse.[300]

Much work has been done on rod transplantation as described in the introductory chapter, with recent evidence showing the successful restoration of visual function

in retinal degeneration.[397] However, there are no previous reports to investigate the transplantation of cones when isolated from rods. Questions remain on whether cones are capable of survival following transplantation, especially in the absence of rod donors. The aim of this chapter is to address the issue of cone survival following transplantation by employing a unique donor model of cone photoreceptors that obviates the confounding results arising from a combined rod/cone transplant.

Specifically, this model exploited the *rd1* (or *Pde6b*$^{rd1/rd}$) mutation in order to eradicate rods from the donor mass at the appropriate juncture. Therefore, by crossing the OPN1-EGFP with the dsRed mouse which carries the *rd1* mutation, an F2 progeny was generated that possessed GFP-positive cones and all dsRed-positive cells except rods, since the latter underwent degeneration typical of mice with the *rd1* mutation. In the *rd1* mouse retina, the vast majority of rods (98%) degenerate by 17 days of age, and no rods are left after the third or fourth postnatal week.[398] At later stages, rod death is followed by loss of cones.

5.1.3 Summary of results

The findings in these studies can be summarised as follows:

1) Cones survive in the absence of rods *in vitro*.
2) Fluorescence-activated cell sorting (FACS) and magnetic-activated cell sorting (MACS) are inefficient methods of deriving decent yields of cone photoreceptors.
3) Transplanted cones survive in the subretinal space of wild type hosts when delivered in conjunction with rod donors.

4) Transplanted cones survive in the subretinal space of "rod-less" degenerate retinas and in the absence of rod donors.
5) Transplanted cones survive in the subretinal space of retinas that have been subject to retinal laser exposure.

5.2 Experimental design

Experiments were conducted as follows:

In vitro cell counting

The *in vitro* survival of GFP-positive cones was determined under different culture conditions. Following papain dissociation (Figure 5.1), OPN1-EGFP retinal cell suspensions were separated into 24-well plates. Aside from determining the optimal conditions required to achieve single cell suspensions that would enhance transplantation efficiency, the following factors were investigated for their effect on cone survival: temperature, age, and co-culture with rods or RPE. Cell counting was performed daily using an inverted fluorescence microscope.

Figure 5.1. A colour photograph showing whole retinas removed from mouse eyes and suspended in media prior to dissociation. A lens removed from one mouse eye, as indicated by the green arrow, and a 25G needle are shown for comparison. Scale bar: 4mm.

Subretinal transplantation

Donor retinas were derived from the following strains:

1. OPN1-EGFP containing GFP-positive cones on a wild type background.
2. OPN1-EGFP-dsRed mice containing GFP-positive cones and a ubiquitous (beta actin promoter) dsRed reporter on an *rd1* background.

Following papain dissociation of P1 retinas, resultant donor cells ($2x10^5$ cells in 1µl) of either of the aforementioned strains were transplanted into the subretinal space of adult wild type or adult *rd1* mice (Figure 5.2). Host mice were sacrificed at three weeks by either cervical dislocation (for wild types) or perfusion fixation (for *rd1* strains). Eyes were processed for sectioning, immunohistochemistry, and imaged using the confocal microscope as previously described.

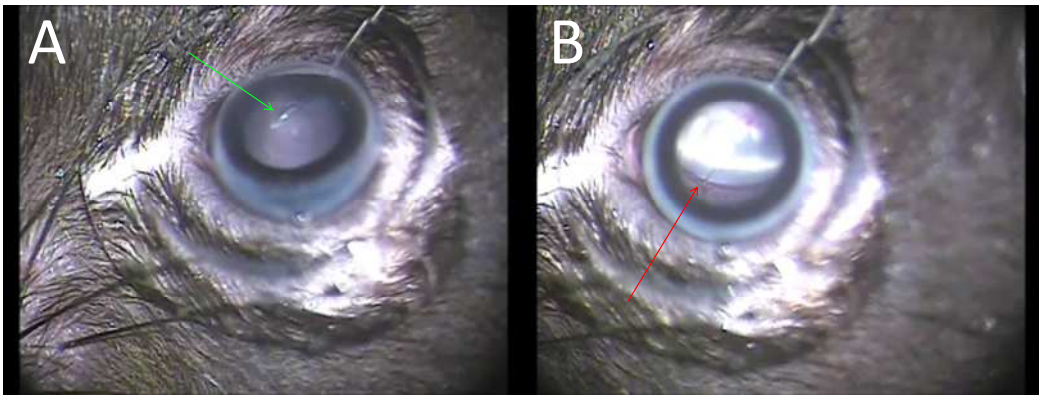

Figure 5.2. Colour photographs showing the technique of subretinal injection. Entry of the needle into the subretinal space was marked by penetration of the RPE by the bevel (green arrow, **A**). The subsequent injection of cell suspension aimed to create a subretinal bleb that extended to the optic disc (red arrow, **B**).

5.3 Results

5.3.1 Genotyping/phenotyping of donors

The initial step in the identification of donor cones was to characterise the morphology, stage of maturation, and protein expression in an appropriate model. The two models of choice that were used throughout all transplantation experiments were either the Opn1-EGFP (bearing GFP-positive cones on a wild type background) or the Opn1-EGFP-dsRed (bearing GFP- and dsRed-positive cones on an *rd1* background), the latter which is described in later sections.

The Opn1-EGFP model

Genotyping

Genotyping of Opn1-EGFP mice confirmed the presence of a transgenic GFP-positive band (641 bp, Figure 5.3).

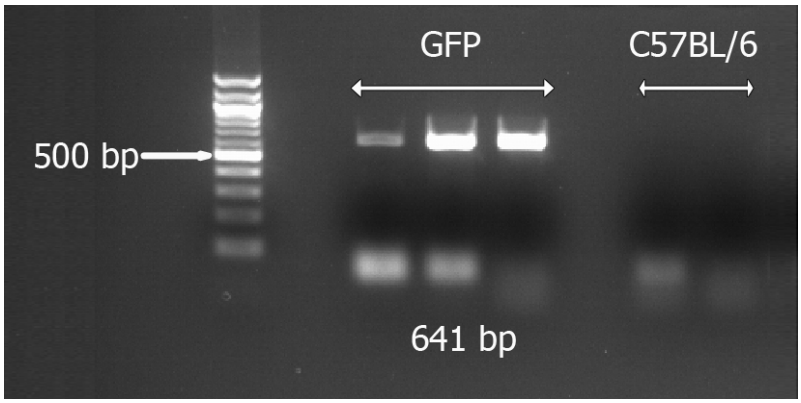

Figure 5.3. Agarose gel electrophoresis of PCR products to detect the presence of GFP. Genotyping of Opn1-EGFP mice detects a transgenic GFP-positive band in homozygous or heterozygous positive animals. Three consecutive positive bands identifying GFP are shown with a size of 641bp. Negative controls from wild type (C57Bl/6) genomic DNA are shown alongside.

Immunohistochemistry (IHC)

In the Opn1-EGFP retina, IHC methods identified the cone outer segments using anti-RG opsin and anti-CNGA3 antibody, the cone sheaths with PNA lectin, and the entirety of the cone with anti-arrestin antibody (Figure 5.4; no primary antibody controls shown in Appendix Figure 1).

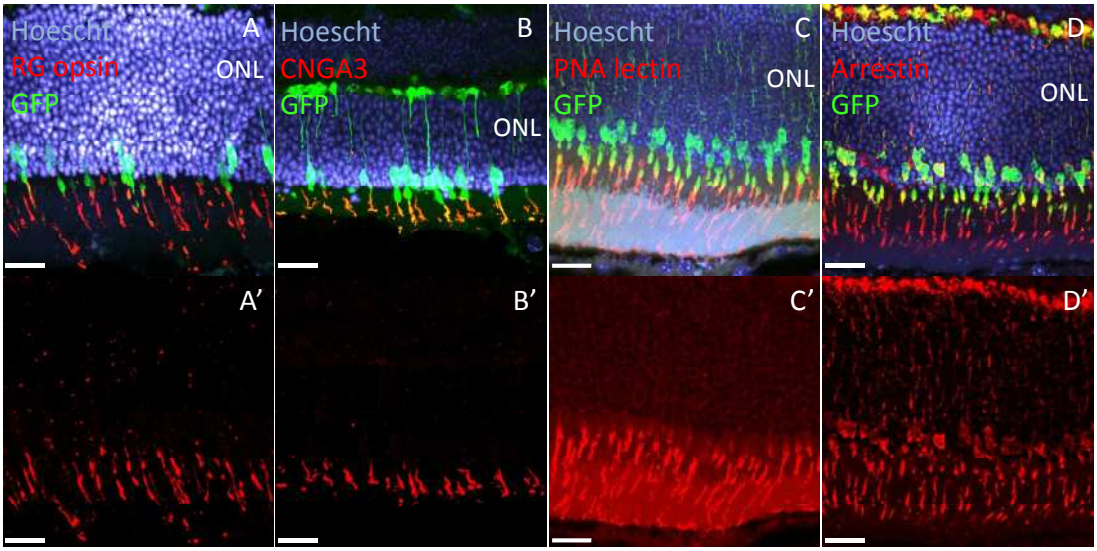

Figure 5.4. Immunohistochemistry (IHC) of GFP-positive cones in the *Opn1.gfp* reporter mouse. RG opsin (**A**, **A'**) and CNGA3 (**B**, **B'**) colocalise to the cone outer segments whilst PNA lectin (**C**, **C'**) stains cone sheaths. It is noteworthy that GFP does not enter the cone outer segments. Arrestin (**D**, **D'**) stains the entirety of the cone from the outer segment to the pedicle. Scale bar: 20µm.

Expression of PNA lectin

Expression of PNA lectin, indicative of the presence of cone sheaths, was correlated to the age of the cone photoreceptor and the onset of GFP (Figure 5.5). The stage of cone maturation in the Opn1-EGFP retina at P14 was similar to the adult in terms of PNA lectin and GFP quantification (n = 12, P > 0.999, one-way ANOVA with Bonferroni post-hoc test). Although PNA lectin expression was apparent at P5 and P8, few GFP-positive cones were present in relation to this (n = 12, P < 0.0001 for

both ages, one-way ANOVA with Bonferroni post-hoc test). These findings were used to determine the optimum stage post transplantation of early postnatal (P1) donor cones in which to observe the morphology of said cones and this was defined as three weeks.

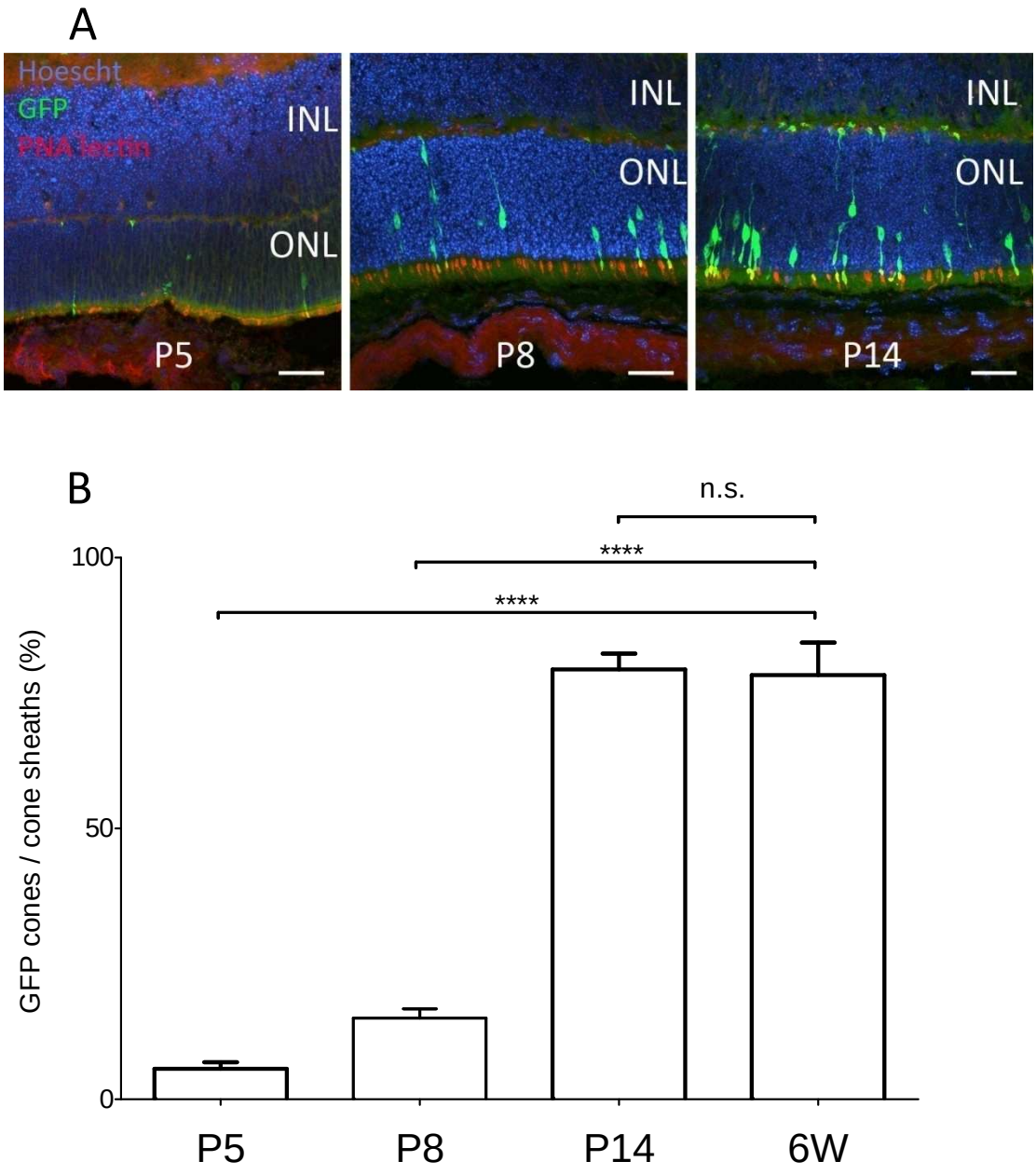

Figure 5.5. The expression of PNA lectin in the Opn1-EGFP retina according to postnatal age. Confocal images of the most densely populated part of the superior retina in terms of GFP-positive cones at three postnatal ages (**A**). Although cone sheaths, as determined by lectin staining, could be detected in the outer retina, few GFP-positive cones were seen at P5 and P8. Scale bar: 20µm. By P14 however, the

ratio of GFP-positive cones to cone sheaths reached adult levels (**B**). Error bar ± SEM, *n* = 12. ****P < 0.0001, one-way ANOVA with Bonferroni post-hoc test.

The Opn1-EGFP-dsRed model

Phenotyping

The presence of the dsRed reporter was detected by imaging the paws of mice using the 488nm AF setting on the cSLO. Using the same detector sensitivity, an intense hyperautofluorescence was present in dsRed-positive mice whereas no increase in autofluorescence was seen in dsRed-negative animals (Figure 5.6). The presence of GFP-positive cones could not be determined by AF imaging alone since the dsRed was detected at a lower sensitivity and, being a ubiquitous reporter, totally masked other signal from the retina. GFP positivity was therefore confirmed by genotyping as described previously (Figure 5.7).

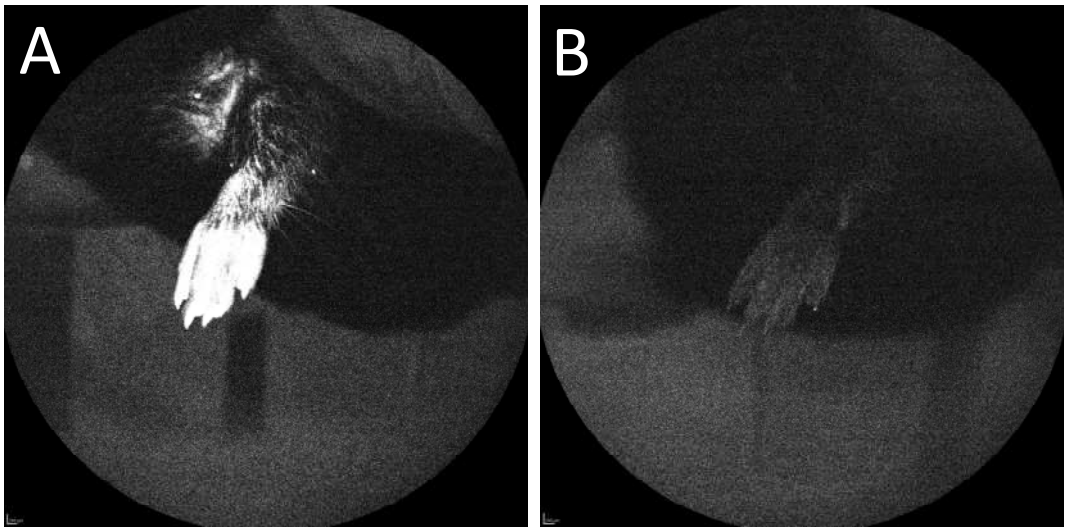

Figure 5.6. Phenotyping of dsRed-positive mice. The 488nm AF setting on cSLO showed hyperautofluorescent paws in positive animals (**A**) and no increase in autofluorescence in negatives (**B**). The same detector setting was used for both images as indicated by the similar appearance of the background area.

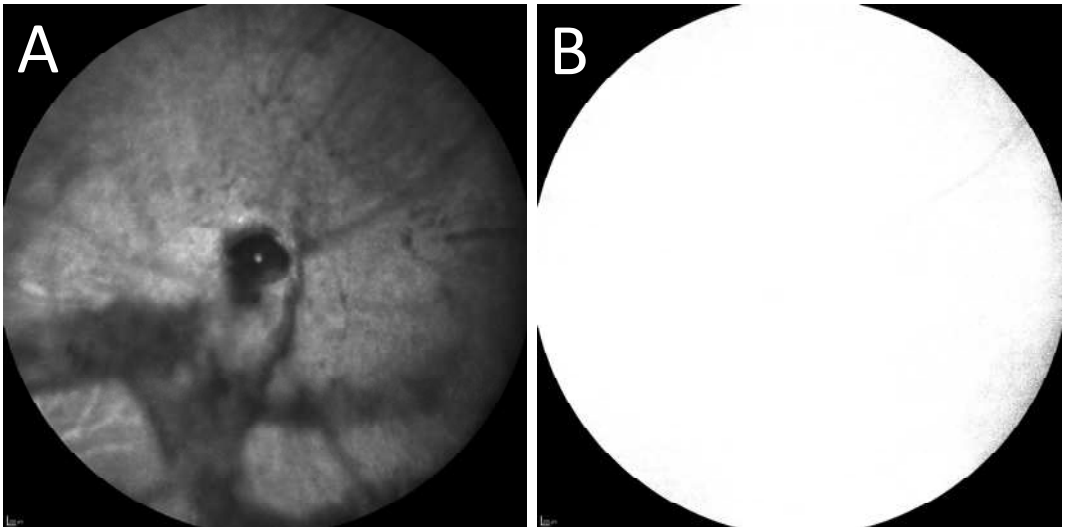

Figure 5.7. cSLO imaging of the Opn1-EGFP-dsRed retina. The reflectance image (**A**) shows the typical appearance of a retinal degeneration caused by the *rd1* mutation as in this mouse model. In the same eye, the 488nm AF image (**B**) demonstrates the result seen in the presence of a ubiquitous dsRed reporter. With the detector setting at the lowest sensitivity required to identify GFP-positive cones, the dsRed signal is too intense to allow visualisation of any other fluorescent signal.

Genotyping

A duplex genotyping system was used to identify the *rd1* mutation in Opn1-EGFP-dsRed mice showing the presence of a wild type versus mutant allele (Figure 5.8). Since the *rd1* phenotype is a recessive trait, homozygous recessive breeding pairs were established to ensure that all progeny inherited the mutant alleles.

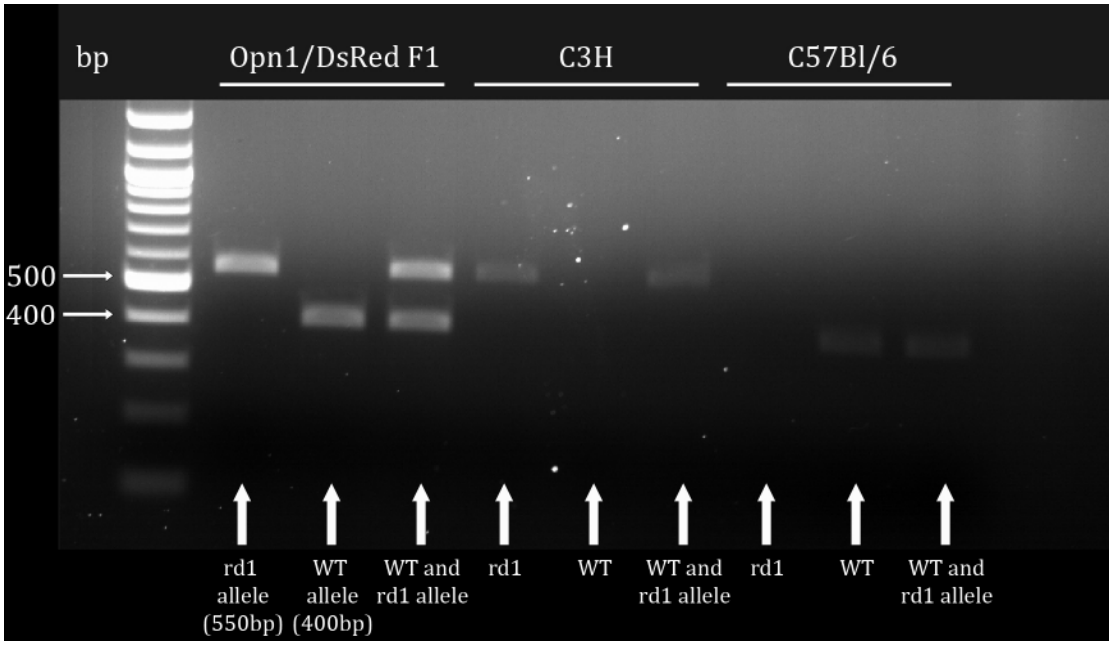

Figure 5.8. Genotyping of Opn1-EGFP-dsRed mice. Agarose gel electrophoresis of PCR products from tissue derived from the F1 progeny of the intercross between Opn1-EGFP and dsRed mice ("Opn1/dsRed F1"). After the DNA ladder at the far left, the first lane shows a 550bp fragment from the mutant (*rd1*) allele and the second lane shows a 400bp fragment from the wild type (WT) allele. The third lane shows a combination of all three primers used to identify both alleles in a single lane. The positive controls from C3H and C57Bl/6 mice are shown thereafter.

Histology

The histological findings in Opn1-EGFP-dsRed retinas are shown in Figure 5.9. The F1 progeny of the cross between Opn1-EGFP and dsRed mice had normal retinal thickness with preservation of the ONL since this generation carried only one *rd1* allele. GFP-positive cones were present as was the ubiquitous dsRed reporter (Figure 5.9A-B). Intercrossing of this F1 generation resulted in an F2 progeny of which one-quarter were homozygous recessive for the *rd1* mutation. In the latter, the loss of rod photoreceptors due to the retinal degeneration resulted in a collapse of the ONL to leave GFP-positive M and non-fluorescent S cones (Figure 5.9C-D). Again, the ubiquitous dsRed reporter could be seen in all layers. A comparison of retinal

morphology between Opn1-EGFP and Opn1-EGFP-dsRed early postnatal mice is shown in Figure 5.10, highlighting the marked attenuation of the ONL by postnatal day 14 in the latter model. These findings were used to determine the optimum stage post transplantation of early postnatal (P1) donor cones from Opn1-EGFP-dsRed mice in which to observe the morphology of transplanted cones and this was defined as three weeks. At this stage, rods had undergone almost complete degeneration due to the *rd1* mutation.

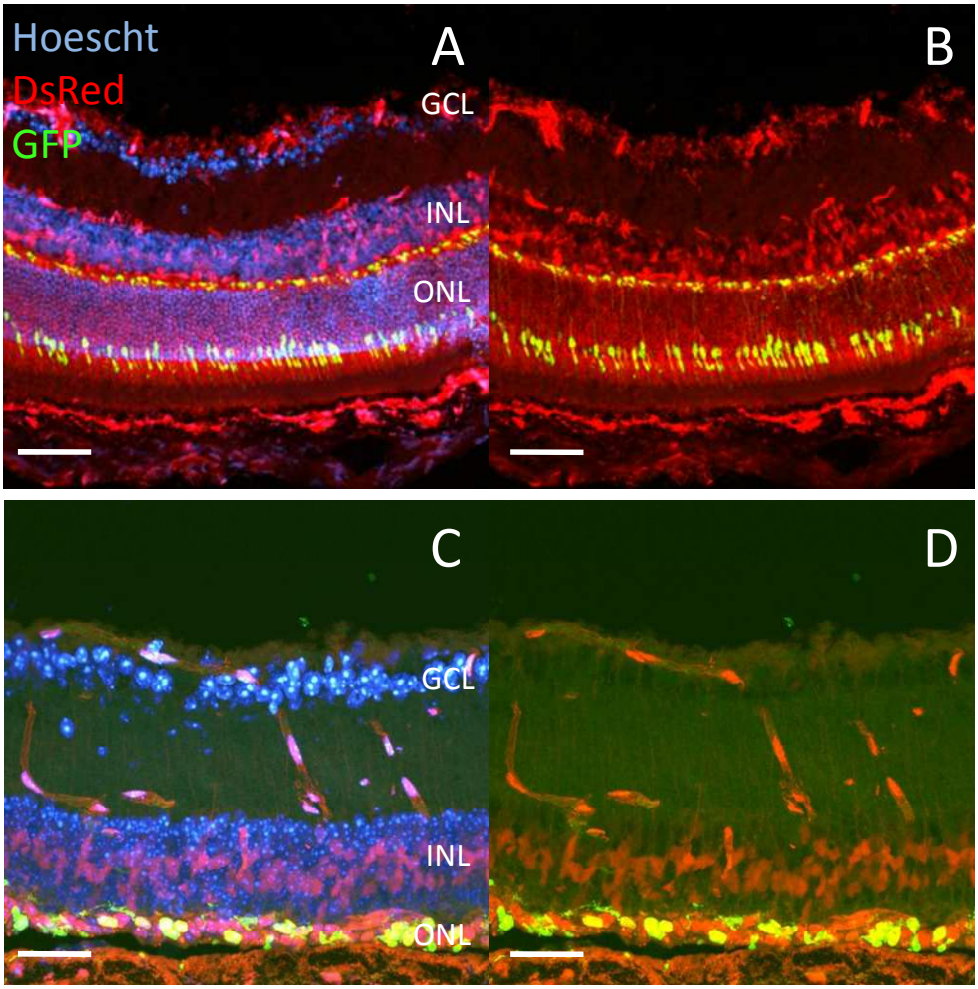

Figure 5.9. Retinal sections from six week old F1 and F2 progeny of the intercross between Opn1-EGFP and dsRed mice. The F1 sections (**A**, **B**) show a normal retinal morphology with the dsRed reporter present in all retinal layers and more prominent in the nuclear layers. The F2 sections (**C**, **D**) also demonstrate dsRed throughout but show marked attenuation of the ONL due to the loss of rods, although cones continue to survive at this level. Scale bar: 50µm.

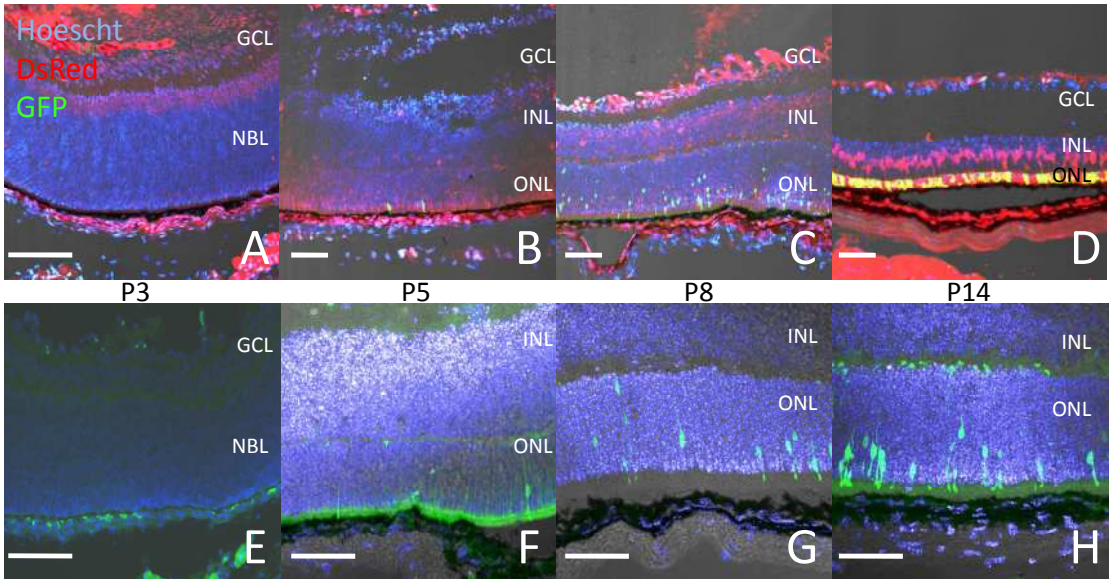

Figure 5.10. A comparison of outer nuclear thickness between the Opn1-EGFP-dsRed and Opn1-EGFP phenotype according to postnatal age. Histological sections from the superior retinal areas that are most densely populated with GFP-positive cones. Representative retinal images are shown of the Opn1-EGFP-dsRed in the upper row (**A**-**D**) and Opn1-EGFP in the lower row (**E**-**H**), from P3, P5, P8, and P14 mice (from left to right respectively). A similar structure of the ONL and of GFP-positive cones is apparent in both phenotypes between P3 to P8. However, attenuation of the ONL at P14 in the Opn1-EGFP-dsRed retina has left a remainder comprising predominantly of GFP-positive cones with few other nuclei within this layer. Scale bar: 20µm.

5.3.2 In vitro culture

Optimisation of cell dissociation

The survival of transplanted cells is dependent on several factors including the number of donor cells delivered at the time of transplantation. This number itself is dependent on the quality of cell dissociation, as a poorly dissociated sample will have few individual cells and instead will have areas of cell clumping thereby reducing the cell yield available for transplantation. In order to optimise cell dissociation, the process was assessed using different concentrations of DNAse (Figure 5.11). A comparison of 0.005%, 0.0025%, 0.001%, and no DNAse, showed

that the final cell yield was directly proportional to the DNAse concentration, with the highest concentration demonstrating the maximal yield ($F_{3, 6}$ = 239.3, n = 12, P < 0.0001, one-way ANOVA with Bonferroni post-hoc).

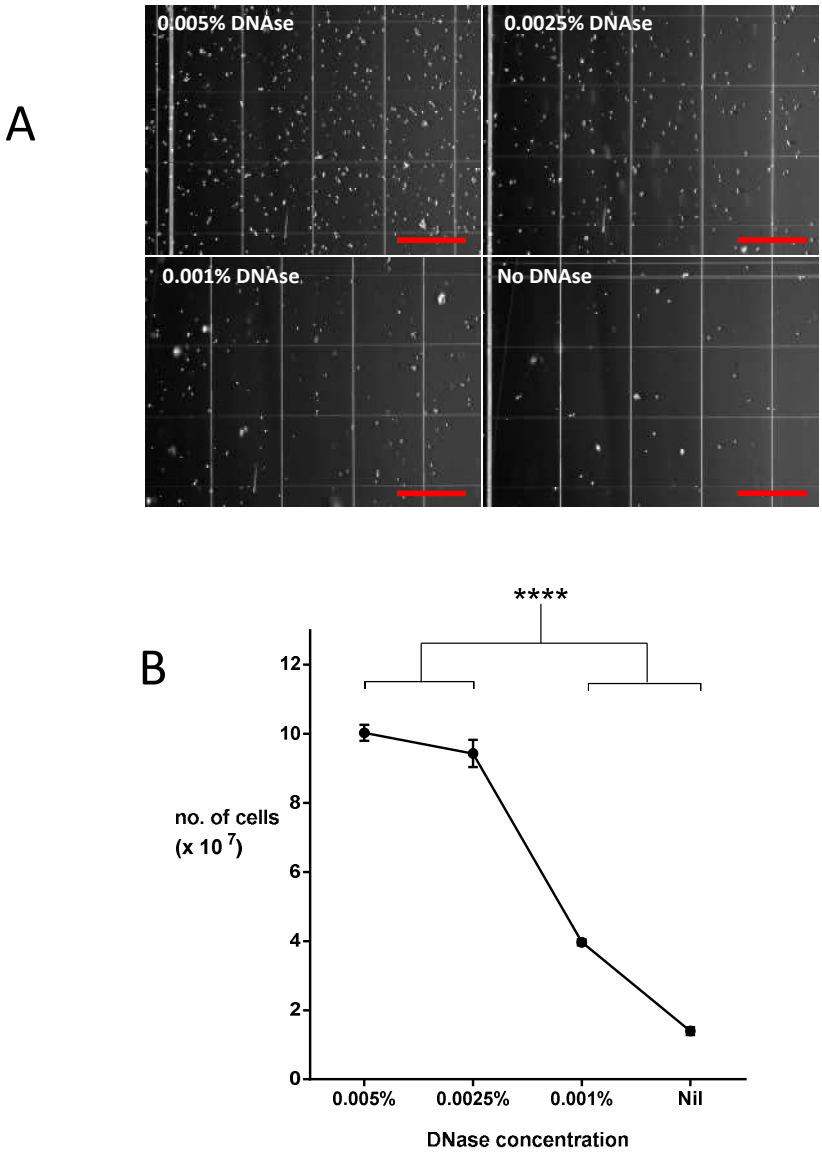

Figure 5.11. Micrographs demonstrating the difference in cell yield obtained by altering DNAse concentration during dissociation (**A**). Cells derived from Opn1-EGFP retinas are shown following dissociation with aliquots placed on a hemocytometer for cell counting. Scale bar: 0.25mm. Graphical representation of these findings show that higher DNAse concentrations (0.005% and 0.0025%) resulted in increased cell yields compared to a lower concentration (0.001%) or absence of DNase (**B**). Error bar ± SEM, n = 12. ****P < 0.0001, one-way ANOVA with Bonferroni post-hoc test.

Survival of cultured GFP-positive cones

In order to increase the viability of donor cones post transplantation, several factors were assessed for their influence on cone survival.

Temperature

Culturing dissociated Opn1-EGFP retinas at 37°C or 34°C did not show a difference in the survival of GFP-positive cones up to day 11 ($F_{1, 4}$ = 4.907, n = 6, P = 0.0911, two-way ANOVA with Bonferroni post-hoc, Figure 5.12).

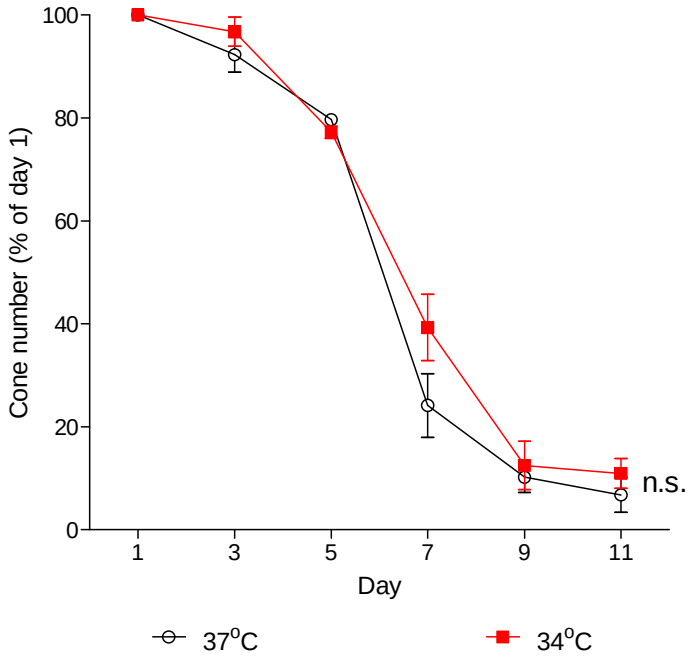

Figure 5.12. *In vitro* cone survival at different temperatures. No difference was found in cone survival between incubation at 34°C and 37°C. Error bar ± SEM, n = 6. P = 0.091, two-way ANOVA with Bonferroni post-hoc test.

Age

A greater proportion of surviving GFP-positive cones was shown at day 11 in cultured dissociated retinas derived from P7 compared to 4 weeks and 8 weeks old Opn1-EGFP mice ($F_{2, 35}$ = 26.36, n = 9, P = 0.002 and 0.018 respectively, two-way ANOVA with Bonferroni post-hoc, Figure 5.13).

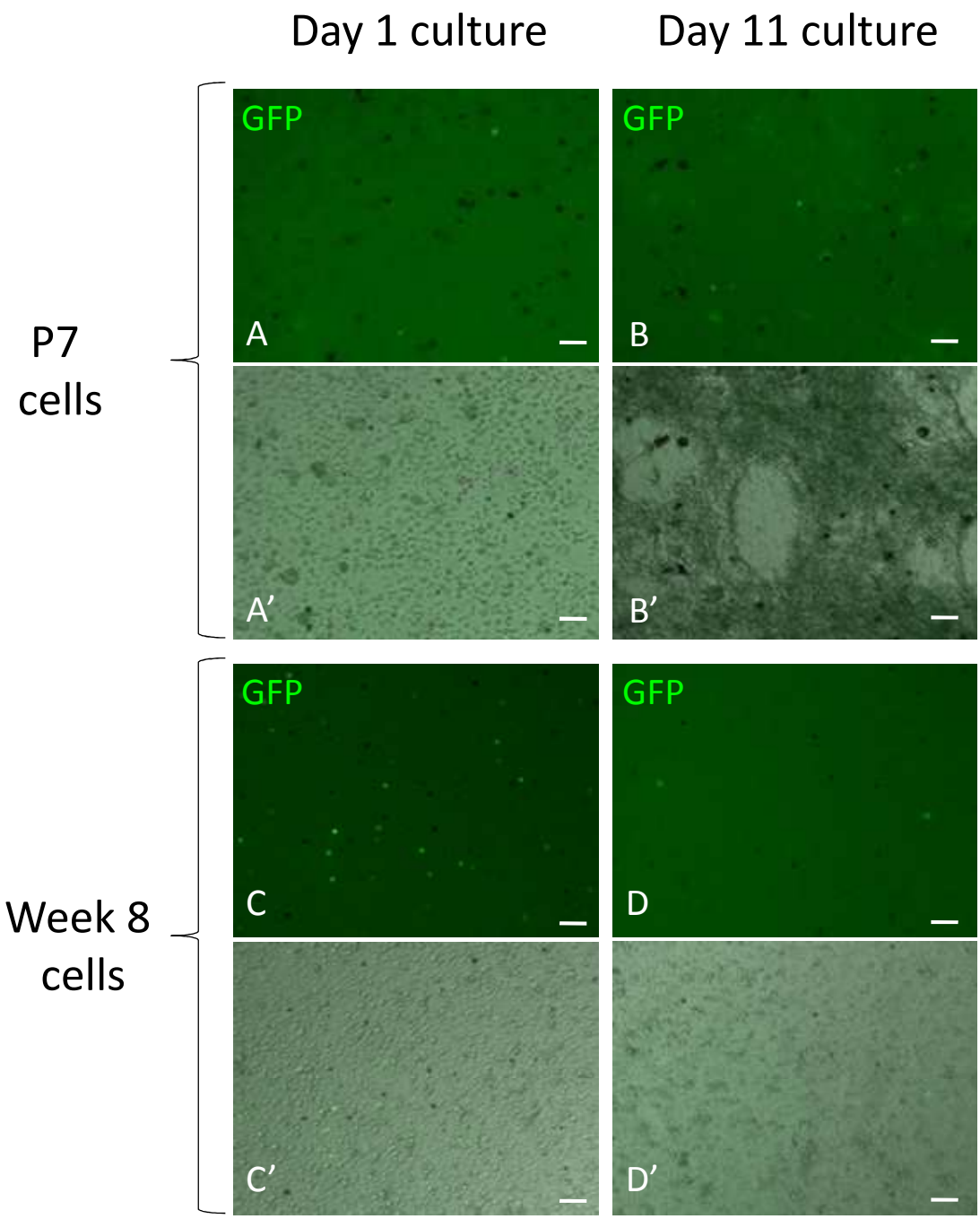

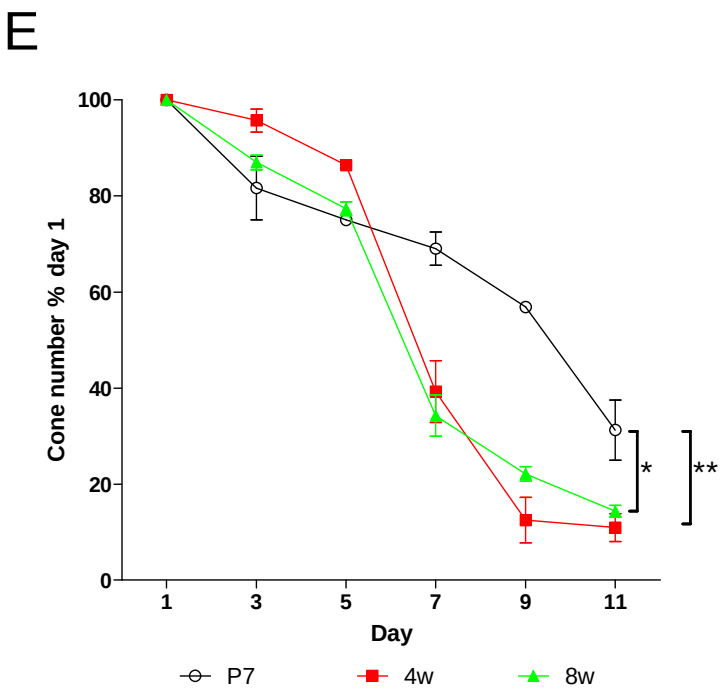

Figure 5.13. Micrographs demonstrating the difference in survival rate of cultured Opn1-EGFP cells according to donor age. Cells derived from the retinas of Opn1-EGFP mice aged P7 (**A**) and 8 weeks (**C**) are shown in comparison at day 1 culture ("baseline"). Although a similar total cell count (including GFP-negative cells) was seen at baseline in both specimens (**A'** and **C'**), the GFP count was higher in the older donor group. The surviving GFP-positive cones at day 11 culture are shown alongside (**B** and **D**). Despite evidence of cell clumping in the P7 group (**B'**), GFP-positive cells were still present at day 11 (**B**). In contrast, although no cell clumping was apparent in the 8 weeks group, the number of GFP-positive cells (**D**) had decreased markedly relative to baseline. Scale bar: 50µm. Graphical representation of these findings reveal that GFP-positive cones derived from P7 donors showed a higher survival rate at day 11 compared to 4 and 8 weeks old donors (**E**). Error bar ± SEM, n = 9. $^{**}P$ = 0.002, $^{*}P$ = 0.018, two-way ANOVA with Bonferroni post-hoc test.

Presence of rod photoreceptors

In order to observe the effect of the presence or absence of rods on cone survival *in vitro*, retinal cells derived from 6 weeks old Opn1-EGFP and Opn1-EGFP-dsRed mice were dissociated and cultured. At this age, Opn1-EGFP retinas had normal rods whereas Opn1-EGFP-dsRed retinas had no rods due to the underlying *rd1* mutation. At day 11 culture, the proportion of surviving GFP-positive cones was similar in both

the rod-containing and "rod-less" group ($F_{1, 12}$ = 2.487, n = 6, P = 0.141, two-way ANOVA with Bonferroni post-hoc, Figure 5.14).

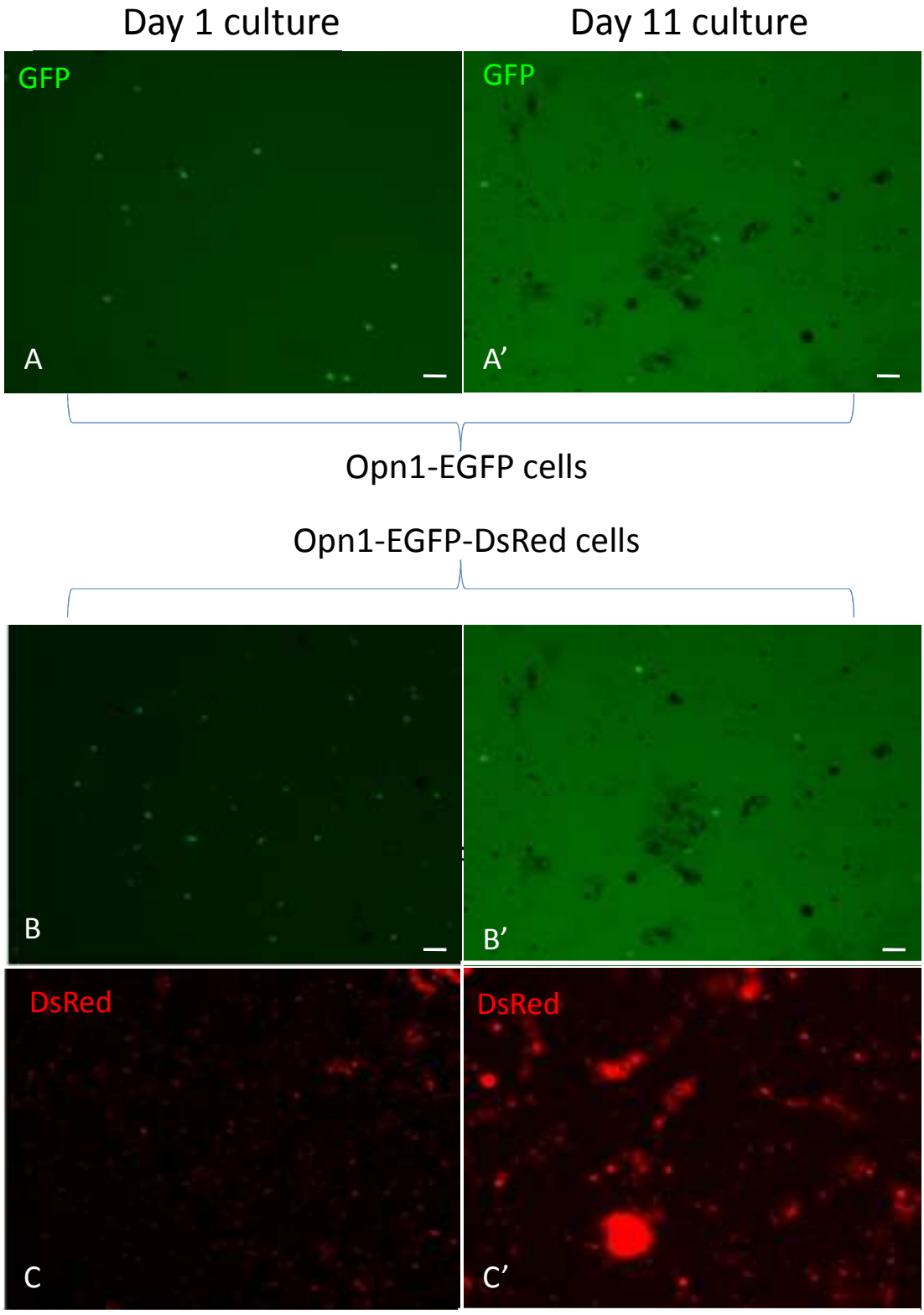

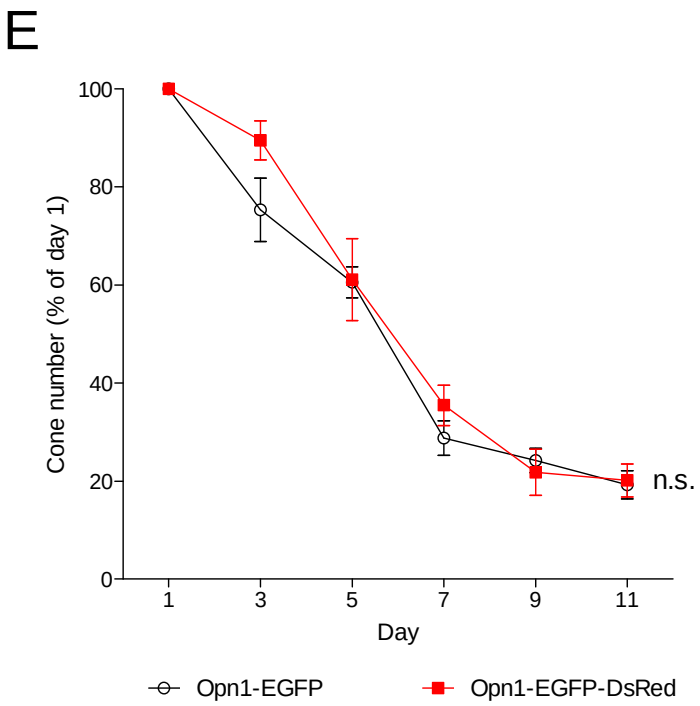

Figure 5.14. Micrographs demonstrating the survival rate of cultured GFP-positive cones derived from Opn1-EGFP ("rod-containing") cells and Opn1-EGFP-dsRed ("rod-less") cells. Cells derived from the retinas of 6 weeks old Opn1-EGFP (**A**) and Opn1-EGFP-dsRed (**B/C**) mice are shown in comparison at day 1 ("baseline") demonstrating an equivalent GFP-positive cell count. Although Opn1-EGFP-dsRed retinas had an almost complete loss of rods at this age group, cells were plated at baseline at an equal density in both groups. The surviving GFP-positive cones at day 11 culture are shown alongside (**A'** and **B'**), as are images demonstrating the ubiquitous dsRed reporter in the Opn1-EGFP-dsRed cells (**C** and **C'**). Scale bar: 100µm. Graphical representation of these findings showed a similar survival rate of GFP-positive cones in the rod-containing and "rod-less" group (**E**). Error bar ± SEM, *n* = 6. *P* = 0.141, two-way ANOVA with Bonferroni post-hoc test.

Presence of RPE

In order to observe the effect of the presence or absence of RPE on cone survival *in vitro*, retinal cells derived from 6 weeks old Opn1-EGFP and Opn1-EGFP-dsRed mice were dissociated and co-cultured with or without RPE. At day 11 culture, the proportion of surviving GFP-positive cones was similar in both the group with RPE and without RPE ($F_{3, 36}$ = 1.348, *n* = 12, *P* = 0.274, two-way ANOVA with Bonferroni

post-hoc, Figure 5.15). No difference was found on subgroup analysis of Opn1-EGFP and Opn1-EGFP-dsRed retinas ($F_{1, 12}$ = 0.370, P = 0.554 and $F_{1, 12}$ = 0.0840, P = 0.778 respectively, n = 6 per group, two-way ANOVA with Bonferroni post-hoc, Figure 5.15).

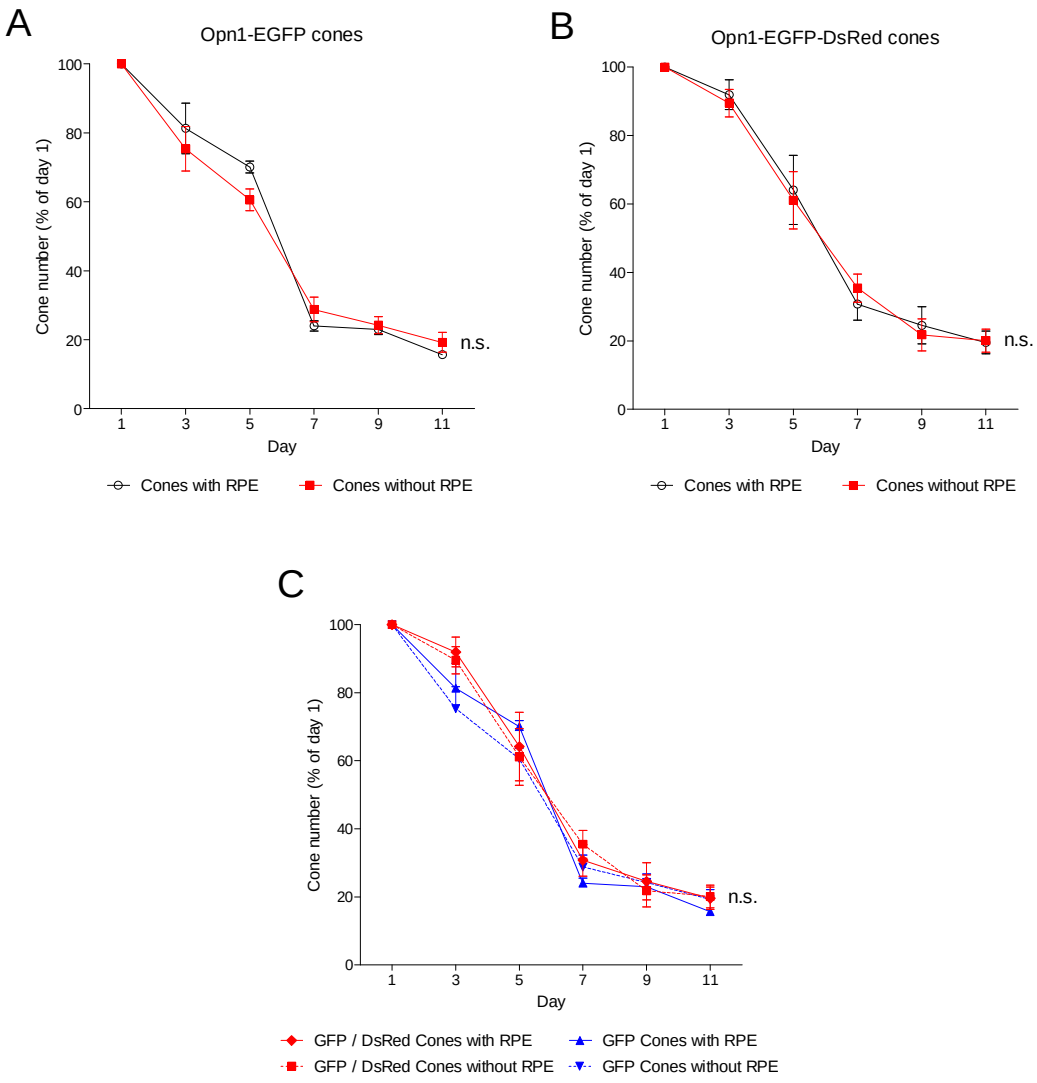

Figure 5.15. Survival rates of GFP-positive cones derived from Opn1-EGFP ("rod-containing") cells and Opn1-EGFP-dsRed ("rod-less") cells in the presence or absence of RPE. The presence of RPE did not affect the survival rate of GFP-positive cones derived from Opn1-EGFP (P = 0.554, Figure **A**) or Opn1-EGFP-dsRed retinas (P = 0.778, Figure **B**). The collective results across all groups showed no difference in survival rate (P = 0.274, Figure **C**). Error bar ± SEM, n = 6 in each group, two-way ANOVA with Bonferroni post-hoc test.

Fluorescence-activated cell sorting (FACS)

Genotyping

FACS was used to isolate a colony of GFP-positive cones. FAC-sorting was performed on dissociated retinas from 3 week old Opn1-EGFP mice that had been positively genotyped. RNA extraction and qPCR analysis were conducted on the resultant sorted sample to observe the expression of opsin genes. Agarose gel electrophoresis of the PCR products showed positive bands for *L-M opsin* and the housekeeping genes, *beta-actin* and *Gapdh* but no bands for *rhodopsin* or *S opsin*, implying the isolation of M cones (Figure 5.16). In contrast, the wild type control showed positive bands for all genes.

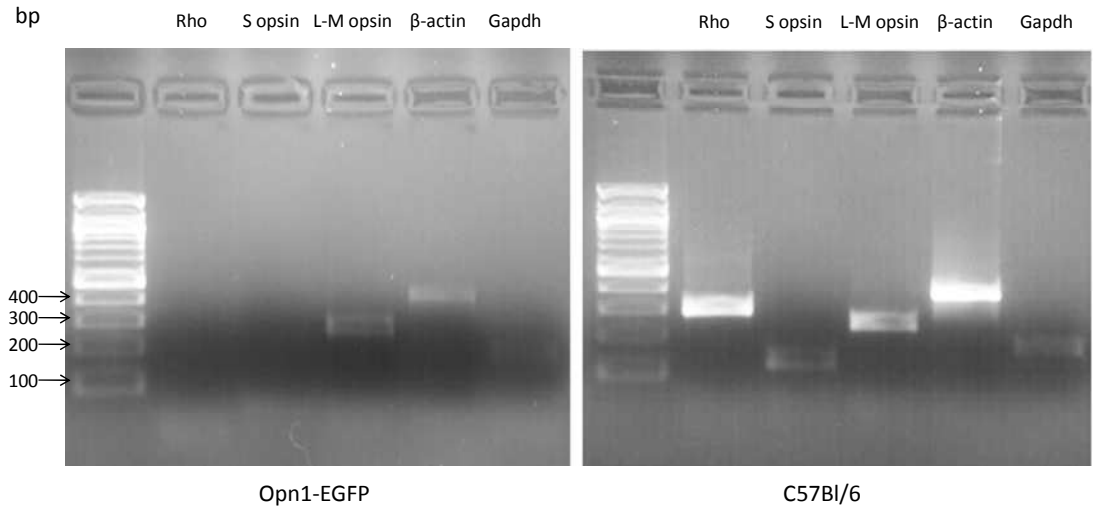

Figure 5.16. Agarose gel electrophoresis of PCR products derived from FAC-sorted Opn1-EGFP and C57Bl/6 retinas. FAC-sorted Opn1-EGFP retinas, that resulted in the isolation of GFP-positive (or M) cones, showed the presence of *L-M opsin*, *beta-actin*, and *Gapdh* but no *rhodopsin* or *S opsin*. In contrast, positive control C57Bl/6 retinas showed the presence of all of these genes.

FACS efficiency

The efficiency of FAC-sorting in terms of cell yield was determined by comparing the proportion of sorted cells from Opn1-EGFP versus Nrl-GFP retinas (Figure 5.17). For Opn1-EGFP retinas, the proportion of GFP-positive cones halved from 2.31 ± 0.18% before FACS to 1.13 ± 0.17% after FACS (***t_{10} = 4.67, P = 0.0009, N = 12, unpaired t-test). For Nrl-GFP retinas, the proportion of GFP-positive rods reduced threefold from 97.27 ± 0.46% before FACS to 30.07 ± 2.16% after FACS (***t_{10} = 30.43, P < 0.0001 , N = 12, unpaired t-test).

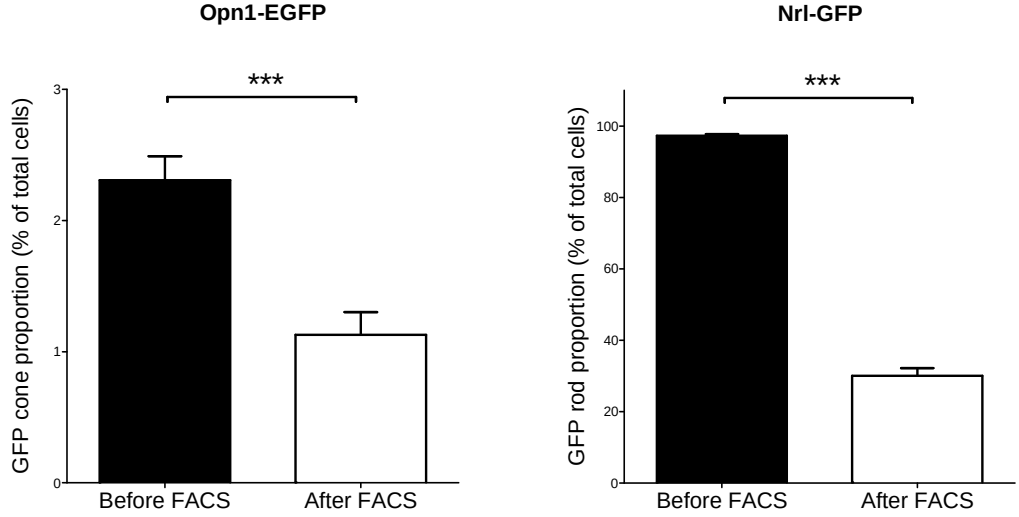

Figure 5.17. The proportion of GFP-positive cells from Opn1-EGFP and Nrl-GFP isolated after FACS. After FACS, the proportion of GFP-positive cones in Opn1-EGFP retinas was halved and the proportion of GFP-positive rods in Nrl-GFP retinas was reduced to a third, compared to before sorting. Error bar ± SEM, N = 6 in each group. ***P < 0.001, unpaired t-test.

Age of sorted cells

The number of GFP-positive cones derived from FAC-sorting was determined according to the age of the animal. FACS was performed on 1 x 10^7 cells per sample for each of P1, P3, P5, and P14 positively genotyped Opn1-EGFP retinas (Figure

5.18). Few GFP-positive events were derived from P1-5 retinas whereas a significantly higher yield was obtained from P14 retinas ($F_{3, 8}$ = 223.9, P < 0.0001, n = 12, one-way ANOVA with Bonferroni post-hoc test).

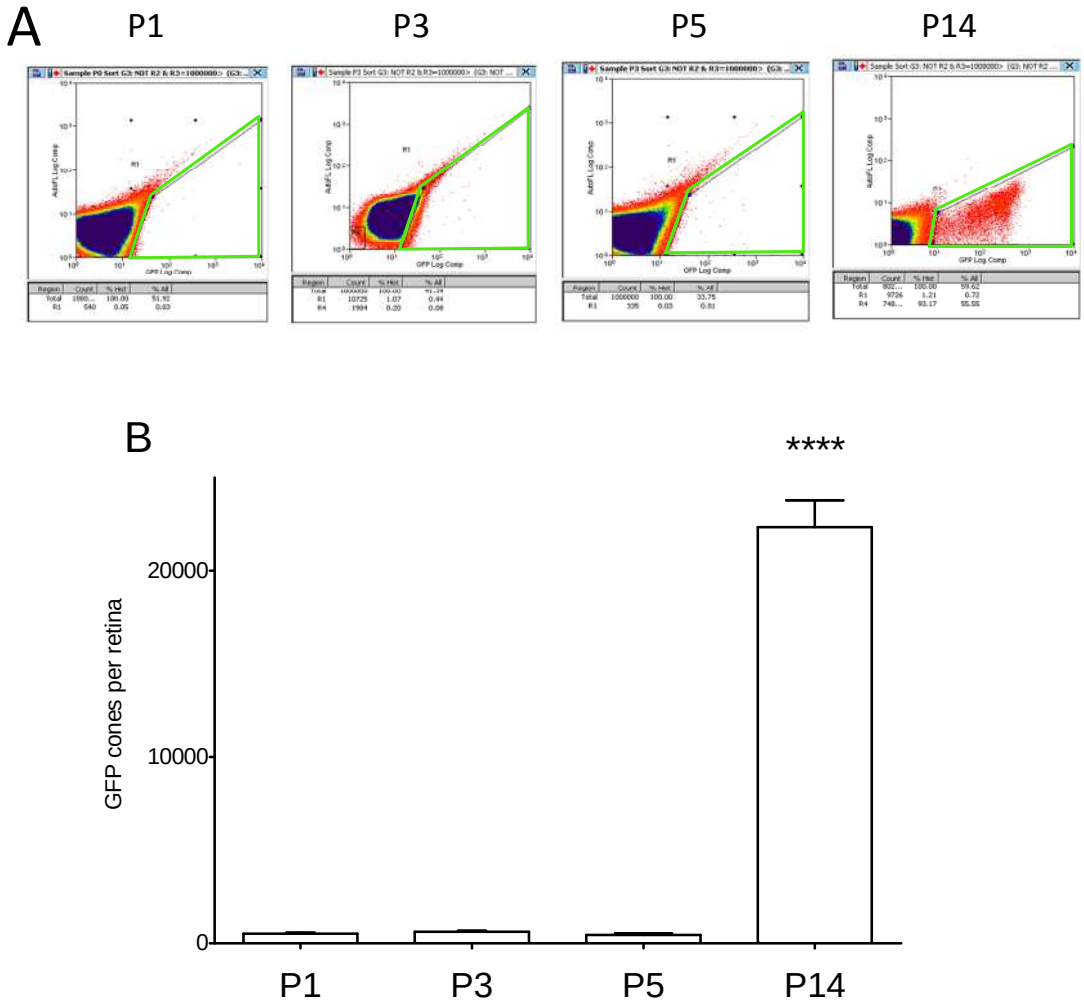

Figure 5.18. The number of GFP-positive cones from different ages of Opn1-EGFP retinas isolated after FACS. Illustrations demonstrate results of FACS for GFP-positive cells according to age (**A**). The green-bounded area delineates the gate used to determine GFP-positive cells with each red dot within this area representing a single GFP-positive event. For retinas from mice aged between P1 to P5, few GFP-positive events were detected whereas many events were observed for retinas from P14 mice. Graphical analysis confirming that a greater number of GFP-positive cones (synonymous with "events") were derived from P14 mice and few were detected at early postnatal stages (**B**). Error bar ± SEM, n = 12. ***P < 0.0001, one-way ANOVA with Bonferroni post-hoc test.

Phenotype of sorted cells

As further validation of the process, FACS was performed on GFP-positive and negative controls. Dissociated cells were derived from Rho$^{-/-}$.GFP$^{+/-}$ and Rho$^{-/-}$.GFP$^{-/-}$ mice aged 7 weeks and from Opn1-EGFP mice aged 6 months, the latter having been shown to exhibit a cone degeneration. GFP-positive events were only seen in retinas derived from Rho$^{-/-}$.GFP$^{+/-}$ mice whereas few events were seen in Rho$^{-/-}$.GFP$^{-/-}$ and Opn1-EGFP mice, confirming the specificity of the FACS parameters used ($F_{2, 6}$ = 445.5, P < 0.0001, n = 9, one-way ANOVA with Bonferroni post-hoc test, Figure 5.19).

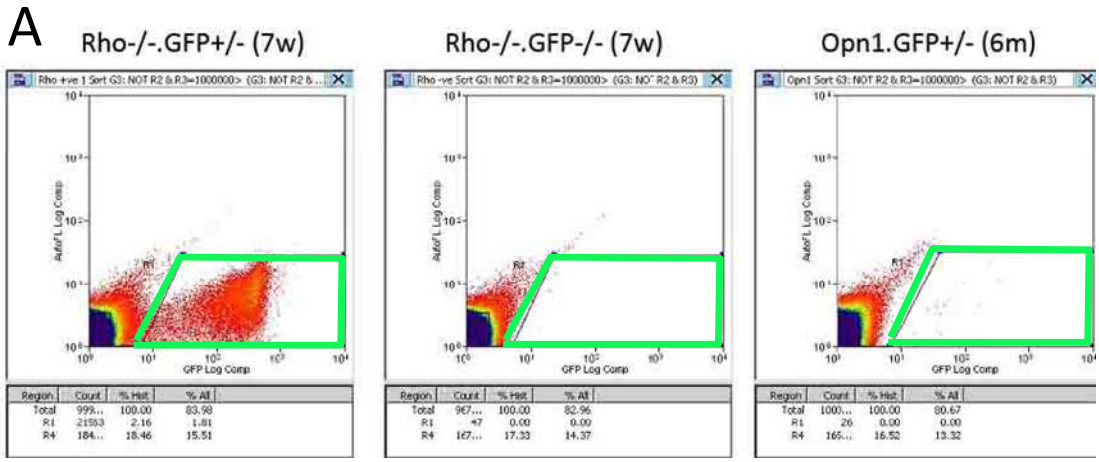

Figure 5.19. Illustrations demonstrating the results of FACS for GFP-positive cells according to phenotype. The green-bounded areas delineate the gate used to determine GFP-positive cells with each red dot within this area representing a single GFP-positive event (**A**). $Rho^{-/-}.GFP^{+/-}$ mice aged 7 weeks showed a large number of GFP-positive events as seen by the volume of red dots within the green bounded area whereas very few (presumably artefactual) GFP-positive events were detected in $Rho^{-/-}.GFP^{-/-}$ mice of the same age. Similarly, few GFP-positive events were detected in Opn1-EGFP mice aged 6 months. Analysis of FACS results showing a higher number of GFP-positive cones derived from $Rho^{-/-}.GFP^{+/-}$ retinas than from controls (**B**). Error bar ± SEM, *n* = 9. ****P < 0.0001, one-way ANOVA with Bonferroni post-hoc test.

Identification of cells post FACS

Although FACS resulted in a population of GFP-positive M cones as determined by gene expression, repeated experiments were unable to successfully deliver these sorted cells in culture. Following FAC-sorting, the GFP-positive population was suspended in warm media (Neurobasal A with additives as previously described). Centrifugation was conducted immediately at speeds of 70g, 300g, 1000g and for durations of 5, 10, and 20 minutes. However, no significant population could be identified post-centrifugation aside from an occasional scattered GFP-positive cell.

Magnetic-activated cell sorting (MACS)

A further method to isolate GFP-positive cones was investigated in the way of MACS. MAC-sorting of $1x10^7$ cells derived from positively genotyped Opn1-EGFP retinas was performed using anti-CD73 antibody. The “CD73-positive” sample was expected to contain rods since the antibody binds to the CD73 cell surface marker present on rods. Therefore, the sample of interest was the “CD73-negative“ portion. Although this sample showed 95% viability as determined by trypan blue staining, the GFP-

positive proportion was 1.5%, i.e. similar to that seen in unsorted cells (Figure 5.20). Following RNA extraction and PCR amplification of this sample, agarose gel electrophoresis of the PCR products showed a bright band for rhodopsin, indicating the presence of rods in this sample, thereby supporting the cell microscopy findings of a large proportion of cells other than GFP-positive cones (Figure 5.21). In addition, positive bands were present for L-M opsin, S opsin, and GFP. In contrast, the CD73-positive sample showed no bands for L-M opsin, S opsin or GFP but showed a bright band for rhodopsin, the former indicating the absence of cones and the latter the presence of rods.

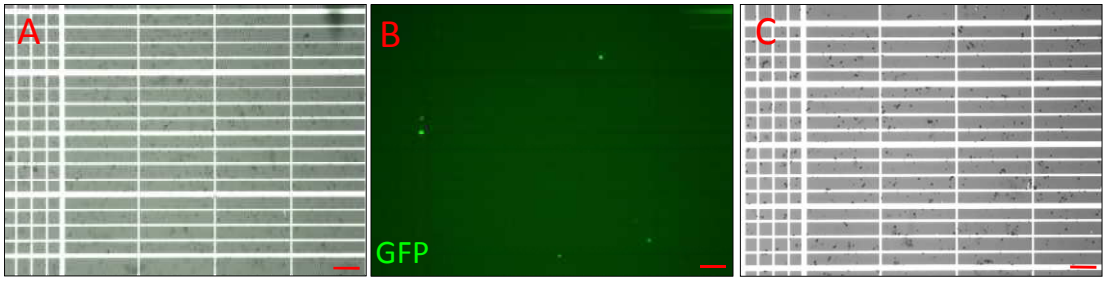

Figure 5.20. Micrographs showing the results of dissociated Opn1-EGFP cells post MACS. The hemocytometer image shows cells from the CD73-negative sample that were stained with trypan blue, indicating a 95% viability (**A**). However, the proportion of GFP-positive cones amongst this cell population was small (**B**). The hemocytometer image from the CD73-positive sample that were stained with trypan blue, showed a 5% viability and no GFP-positive cells (**C**). Scale bar: 100µm.

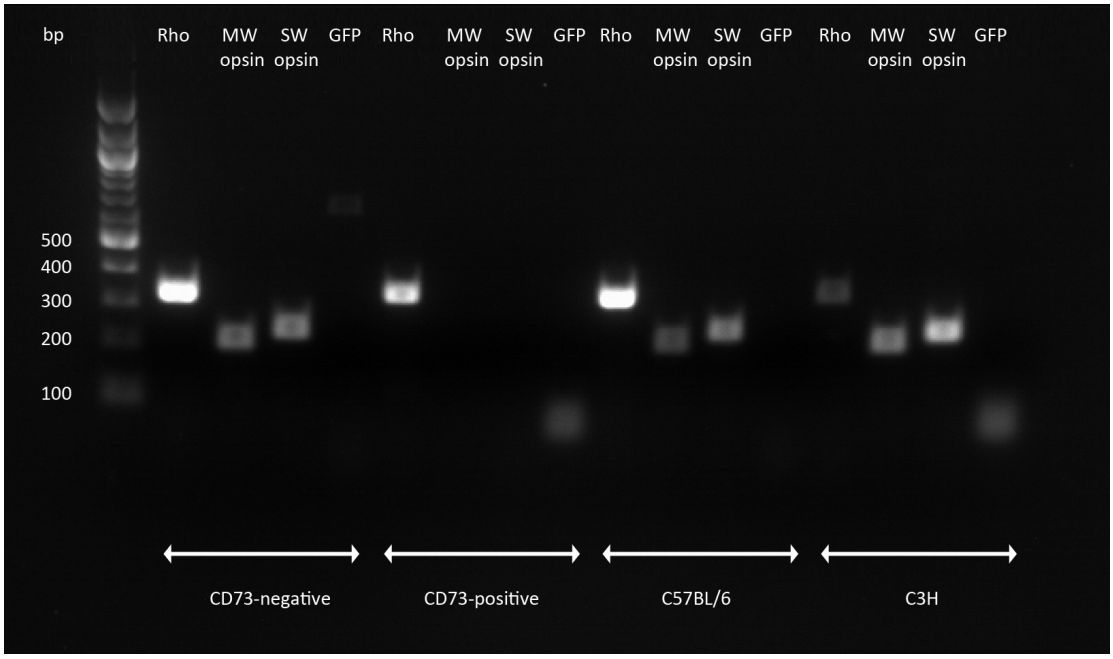

Figure 5.21. Agarose gel electrophoresis of PCR products from MAC-sorted Opn1-EGFP retinas. GFP was detected in the CD73-negative sample indicating the presence of M cones. This was supported by the presence of bands for MW opsin. GFP was absent from the CD73-positive sample which was again supported by the absence of a band for MW opsin. As expected, rhodopsin was present in the CD73-positive sample but was also detected in the CD73-negative sample. A weak band for rhodopsin was also seen in the C3H control even though the retinas were from 3 month old mice. Although there were no rods, it is possible that small amount of rhodopsin might be expressed by other retinal cell types, as true rod photoreceptors never form in this mutant mouse and this may lead to dysregulation of the normal developmental pathways.

5.3.3 Cone survival post transplantation

5.3.3.1 Opn1-EGFP donors in wild type hosts

The following results pertain to the subretinal transplantation of donor retinal cells from P1 Opn1-EGFP mice into adult C57Bl/6 mice.

In vivo imaging

At day 5 following transplantation, *in vivo* cSLO imaging showed (488nm) hyperautofluorescence within the injected area (Figure 5.22A). This region was well-defined with a clear demarcation from adjacent uninjected retina and had a varied configuration between scattered dots and confluent areas (compare to no autofluorescence in uninjected control retinas, Appendix Figure 3). The detector setting (at 95) required to identify this signal was identical to that used to assess GFP-positive cones in adult Opn1-EGFP mice. The injected area increased in AF signal by day 14 as measured by gray level whereas the uninjected area did not show a significant change ($F_{2, 63}$ = 17.81, P < 0.0001 and P = 0.591 respectively, N = 8, two-way ANOVA with Dunnett's post-hoc test, Figure 5.22B). The longitudinal increase in AF signal held true even for the corrected gray level that was determined by subtracting the level within the uninjected area from that within the injected area, thereby adjusting for an artefactual increase in signal (P = 0.002).

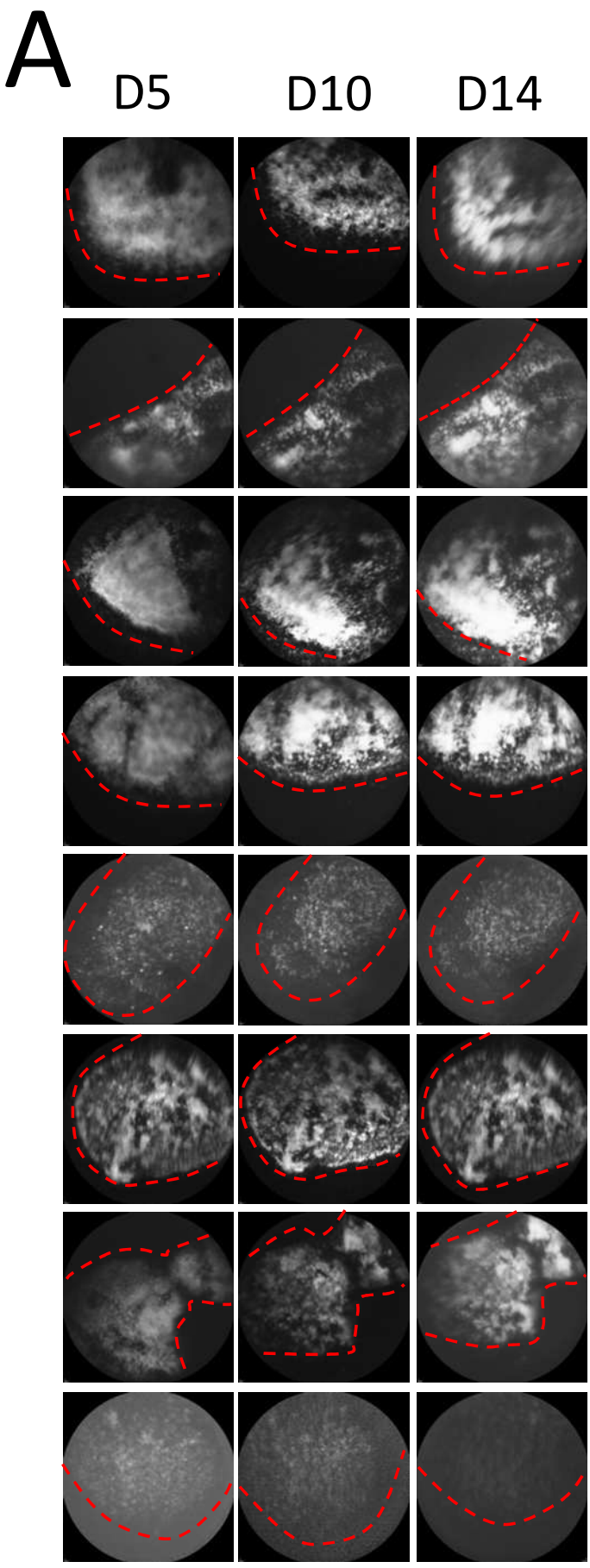
A
D5
D10
D14

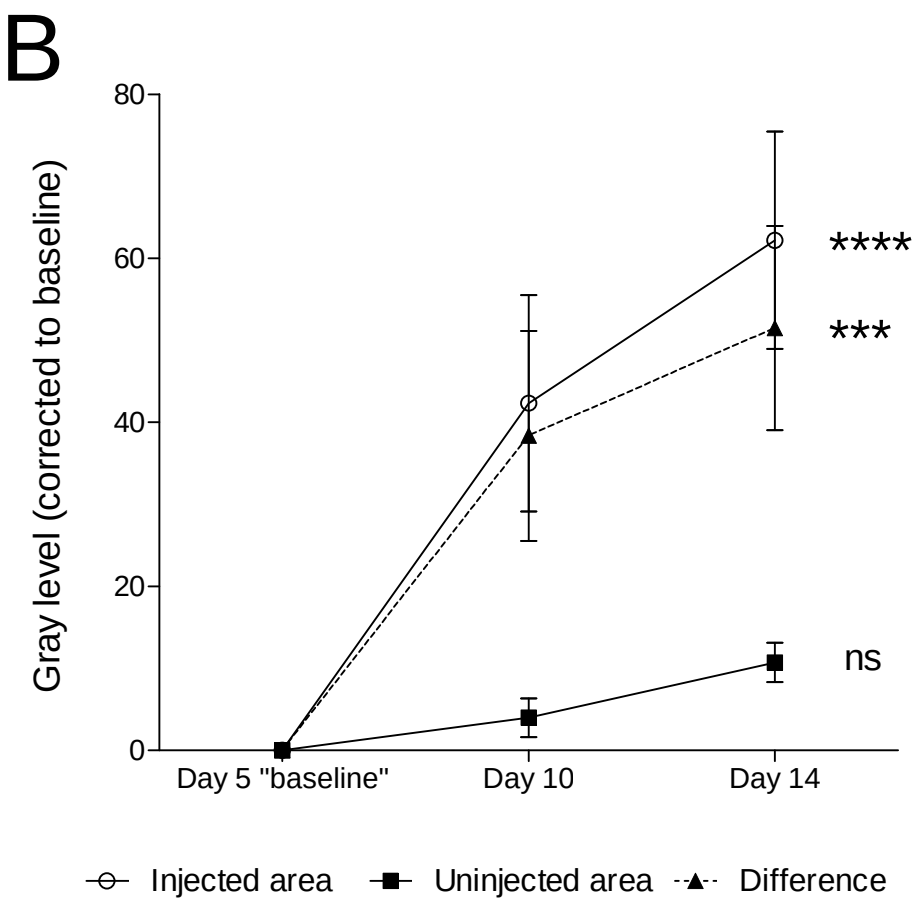

Figure 5.22. 488nm AF images showing the survival of transplanted cones. The result of transplantation of Opn1-EGFP retinal cells into the wild type subretinal space is shown in rows for eight eyes (**A**). The columns represent the findings at days 5, 10, and 14 post-transplantation. The injected area is autofluorescent at day 5 and in a number of eyes, this increases by day 14. A clear demarcation (as indicated by the dashed line) is apparent between the injected and uninjected area. Although mainly confluent, in certain areas, the autofluorescent signal is seen as individual dots. Analysis of gray level following transplantation of Opn1-EGFP retinal cells into the wild type subretinal space (**B**). The analysis confirms the cSLO findings showing that the autofluorescence within the injected area is increased from day 5 baseline to day 14. Error bar ± SEM, $N = 8$. ****$P < 0.0001$, ***$P < 0.001$, two-way ANOVA with Dunnett post-hoc test.

Histological sections

Donor retinal cells survived at three weeks following transplantation as evidenced by the formation of a Hoescht-staining subretinal mass containing GFP-positive cones

(Figure 5.23A-B). It has to be recalled that at the stage of transplantation, P1 cones did not express the GFP fluorophore. Therefore, at three weeks post transplantation, donor cones not only survived but expressed the appropriate reporter as per the equivalent age-matched Opn1-EGFP retina. Additionally, the fluorescent cones had processes that were, albeit, limited to the subretinal mass rather than extending through the host ONL towards the outer plexiform layer (Figure 5.23C-D).

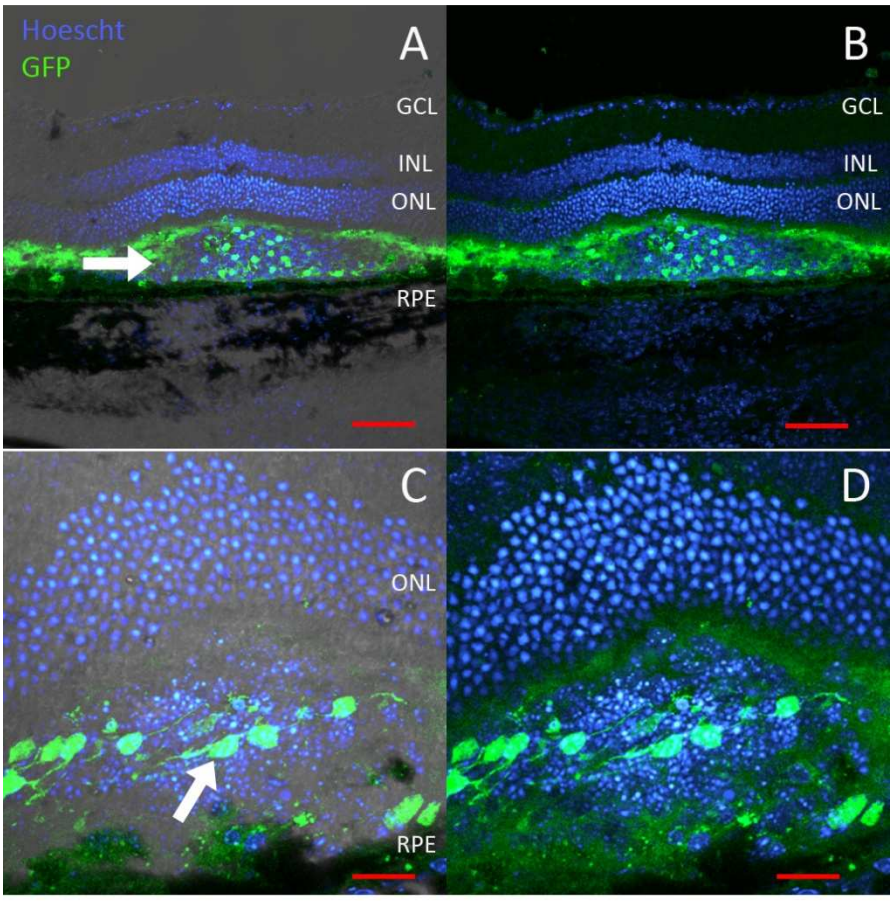

Figure 5.23. Retinal sections showing the survival of transplanted subretinal cones.

A mass of transplanted E15 Opn1-EGFP cells is shown in the subretinal space of wild type mice (arrow, **A**, **B**). A demarcation line is apparent between the donor mass and the host ONL. Although cones did not express GFP at the time of transplantation, at the stage of sectioning, GFP expression was present within the donor cells. The GFP-positive cones showed the formation of processes although their arrangement was irregular and limited to the subretinal mass rather than extending towards the host ONL (arrow, **C**, **D**). Scale bar: 100µm (**A**, **B**); 20µm (**C**, **D**).

Immunohistochemistry (IHC)

Anti-GFP antibody

As evidence of the identity of GFP-positive cones, anti-GFP antibody colocalised exactly to these cells (Figure 5.24-5.25). Any background autofluorescence or artefact that emitted at the same wavelength did not stain positive.

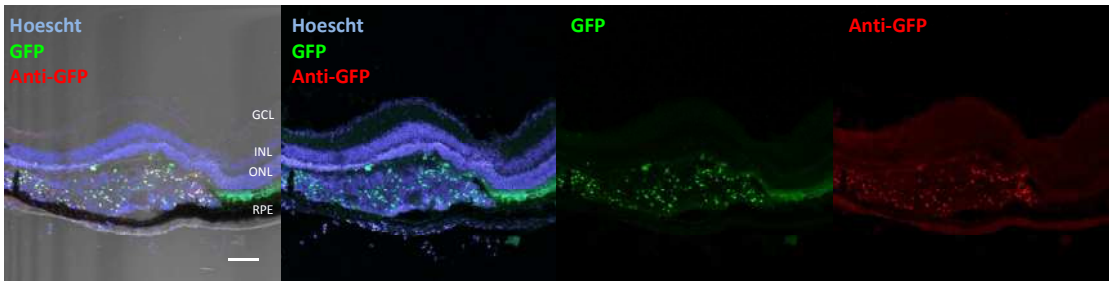

Figure 5.24. Anti-GFP antibody staining of transplanted cones. In order to confirm that the GFP signal was specific and not due to autofluorescence, anti-GFP antibody was used to stain GFP-positive cones. There was a 1:1 colocalisation of the antibody and fluorescent cone. Scale bar: 100µm.

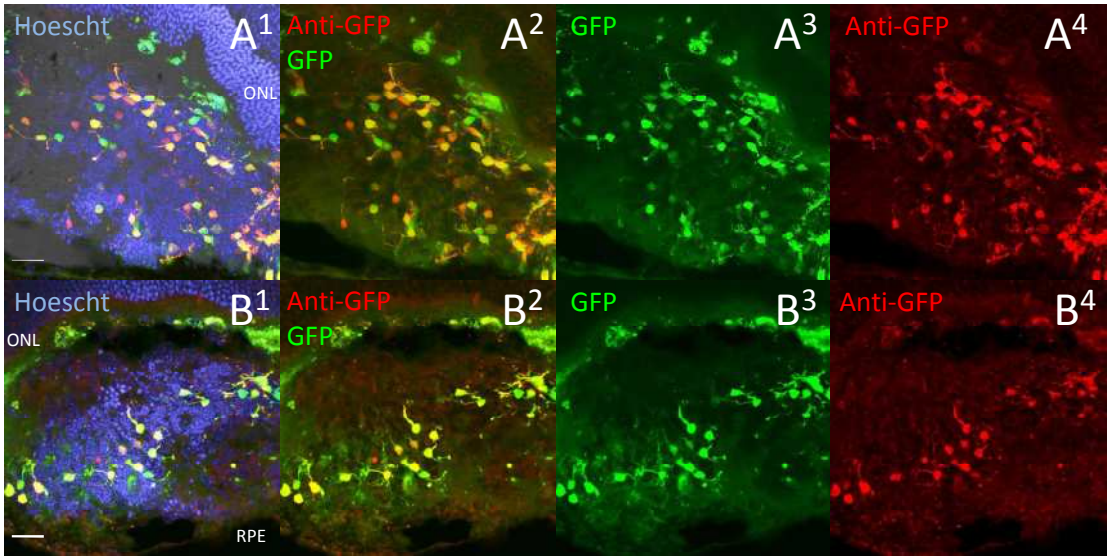

Figure 5.25. High power confocal micrographs showing anti-GFP staining. Two separate areas of anti-GFP staining are shown in the upper (**A**$^{1-4}$) and lower rows (**B**$^{1-4}$) respectively. Both demonstrate colocalisation of the anti-GFP antibody to GFP-positive cones. In areas of autofluorescence, there is no binding of antibody. Scale bar: 20µm.

Anti-arrestin antibody

GFP-positive donor cones stained positive for arrestin with a positive internal control provided by host cones (Figure 5.26). The antibody colocalised to the entirety of the cone and areas of positive staining with no GFP-positivity were seen, indicating the presence of non-fluorescent S cones.

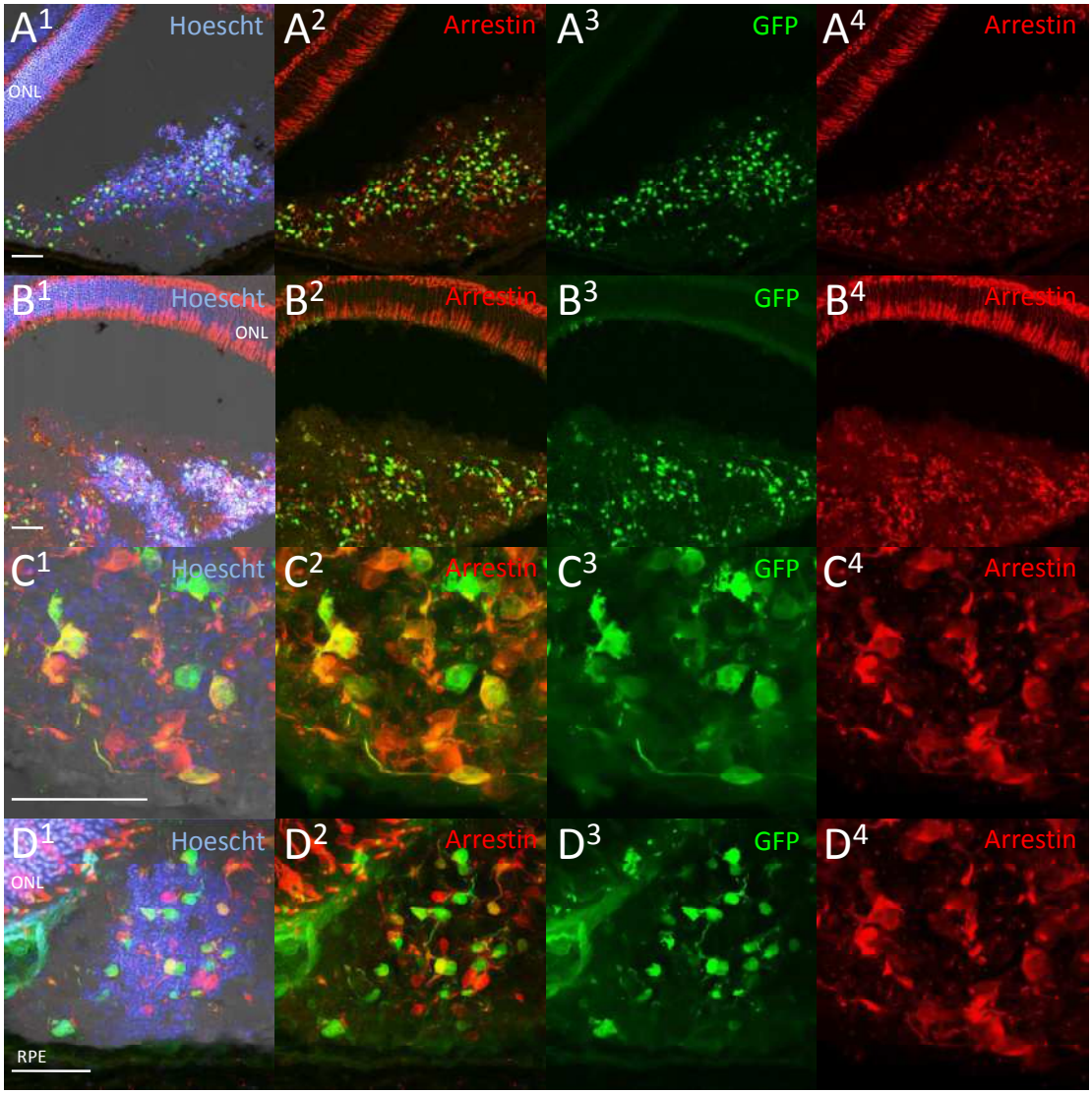

Figure 5.26. Arrestin staining of transplanted cones. Four areas of arrestin staining are shown in separate rows. A positive control for arrestin staining is provided by the host cones in images **A**$^{1\text{-}4}$ and **B**$^{1\text{-}4}$. Similar to anti-GFP, all images demonstrate colocalisation of the anti-arrestin antibody to GFP-positive cones in the subretinal donor mass. As per the pattern seen in host cones, arrestin stains the entirety of the donor cone, including the cell body and processes. Scale bar: 20µm.

Anti-RG opsin antibody and PNA lectin

Donor cones formed outer segments following transplantation as evidenced by positive staining with anti-RG opsin antibody (Figure 5.27). The latter was specific to M cones and therefore, in the donor model, was restricted to only those cones expressing GFP. Cone sheaths present in donor GFP-positive cones showed staining for PNA lectin.

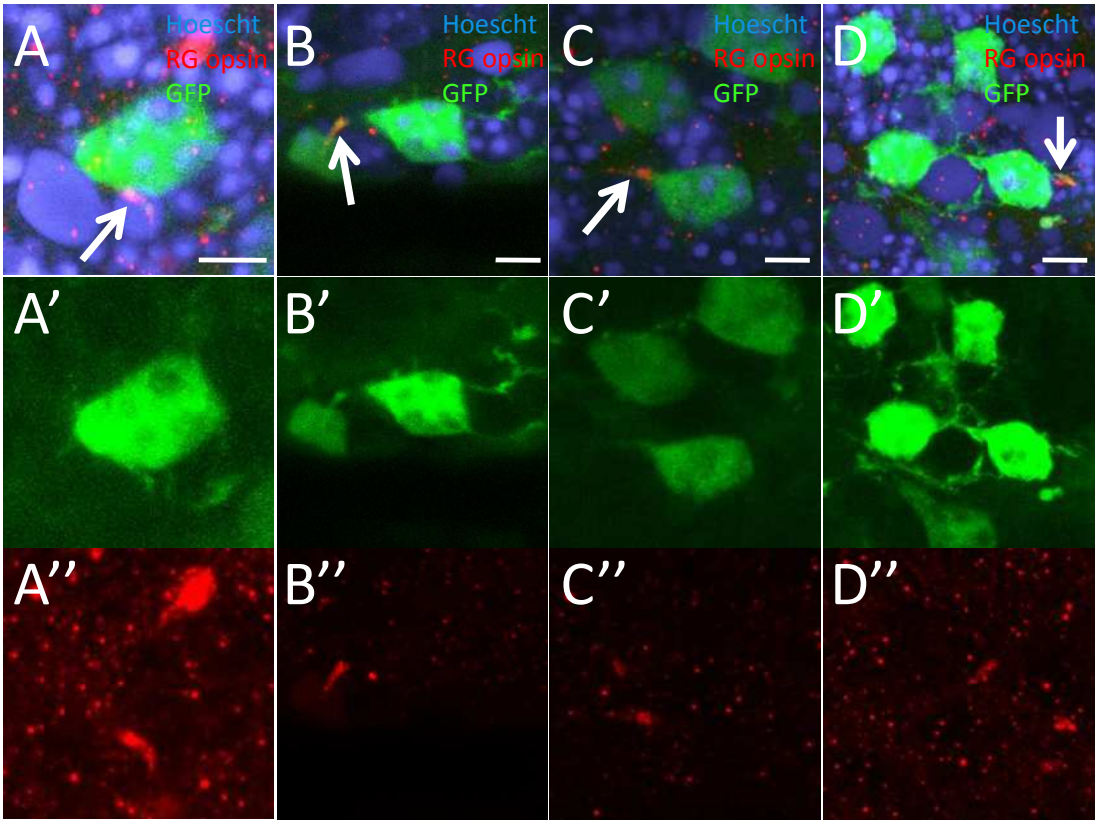

Figure 5.27. RG opsin staining of transplanted cones. Four areas of RG opsin staining are shown in separate columns. Anti-RG opsin antibody colocalised to the outer segment (arrow) of GFP-positive cones. Scale bar: 5µm.

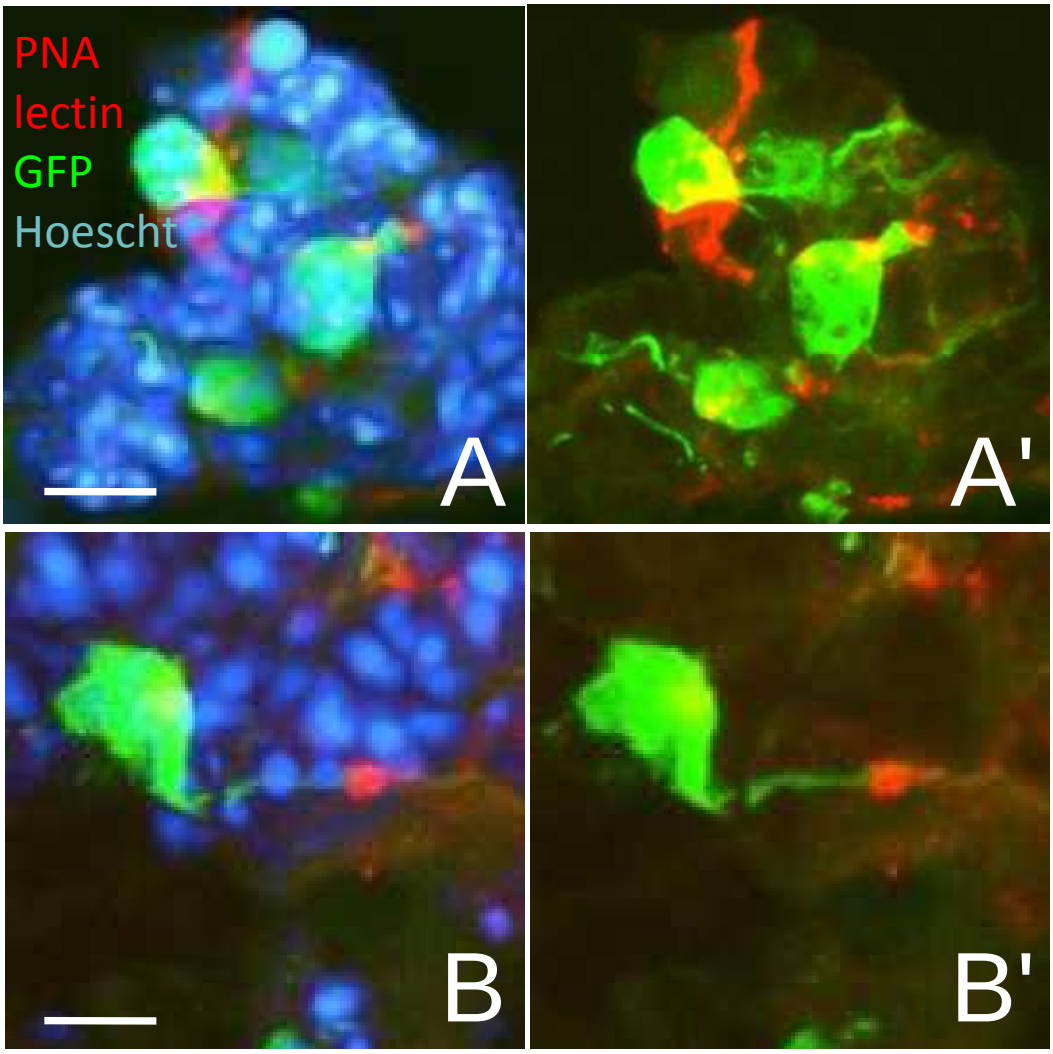

Figure 5.28. PNA lectin staining of transplanted cones. Two areas of lectin staining are shown in separate rows, demonstrating localisation of lectin to the cone sheath. Scale bar: 5µm.

Anti-PDE6B antibody

The presence of rods within the donor cell mass was shown by positive staining of rod outer segments with anti-PDE6B antibody (Figure 5.29). As expected, this did not colocalise to GFP-positive cones. A positive internal control was provided by the host rod outer segments.

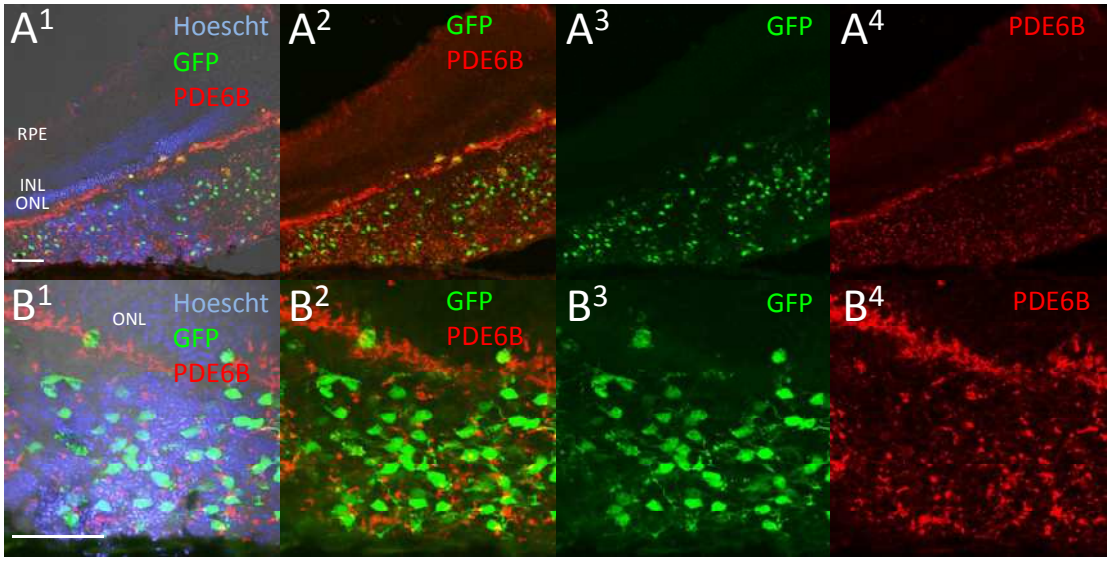

Figure 5.29. PDE6B staining of transplanted rods. Two areas of PDE6B staining are shown in separate rows, demonstrating localisation of antibody to the rod outer segment. An internal positive control is provided by the host rods. No staining of GFP-positive cones is seen, indicating the specificity of the antibody and confirming that the GFP donor cells are not rods. Scale bar: 50µm.

Retinal flatmounts

Another method used to investigate the results following transplantation was via retinal flatmounts at three weeks post procedure (Figure 5.30). This method offered the advantage of preserving whole cell structures that would otherwise be subject to deformation or cleaving during sectioning.

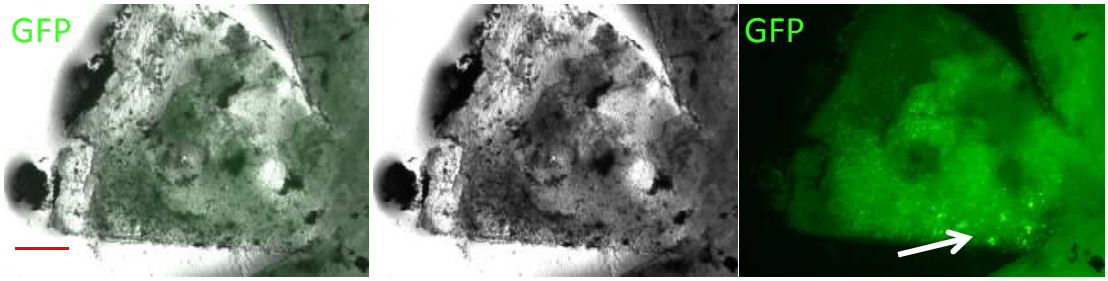

Figure 5.30. A light micrograph of a retinal flatmount with transplanted cones. The flatmount has been placed photoreceptor side up and shows GFP-positive cones localised to an area of one leaf with absence from surrounding regions (arrow, far right image). Scale bar: 0.5mm.

IHC

As per the results seen for histological sections, antibody staining was positive for the markers expressed by cone photoreceptors. However, a relative disadvantage of flatmounts was the observation of incomplete staining that may have been due to the more difficult penetration and permeabilisation of whole tissue rather than sections. This was particularly the case for RG opsin staining (Figure 5.31-5.32). On the other hand, arrestin staining remained efficient with staining of GFP-positive cones (Figure 5.33-5.34).

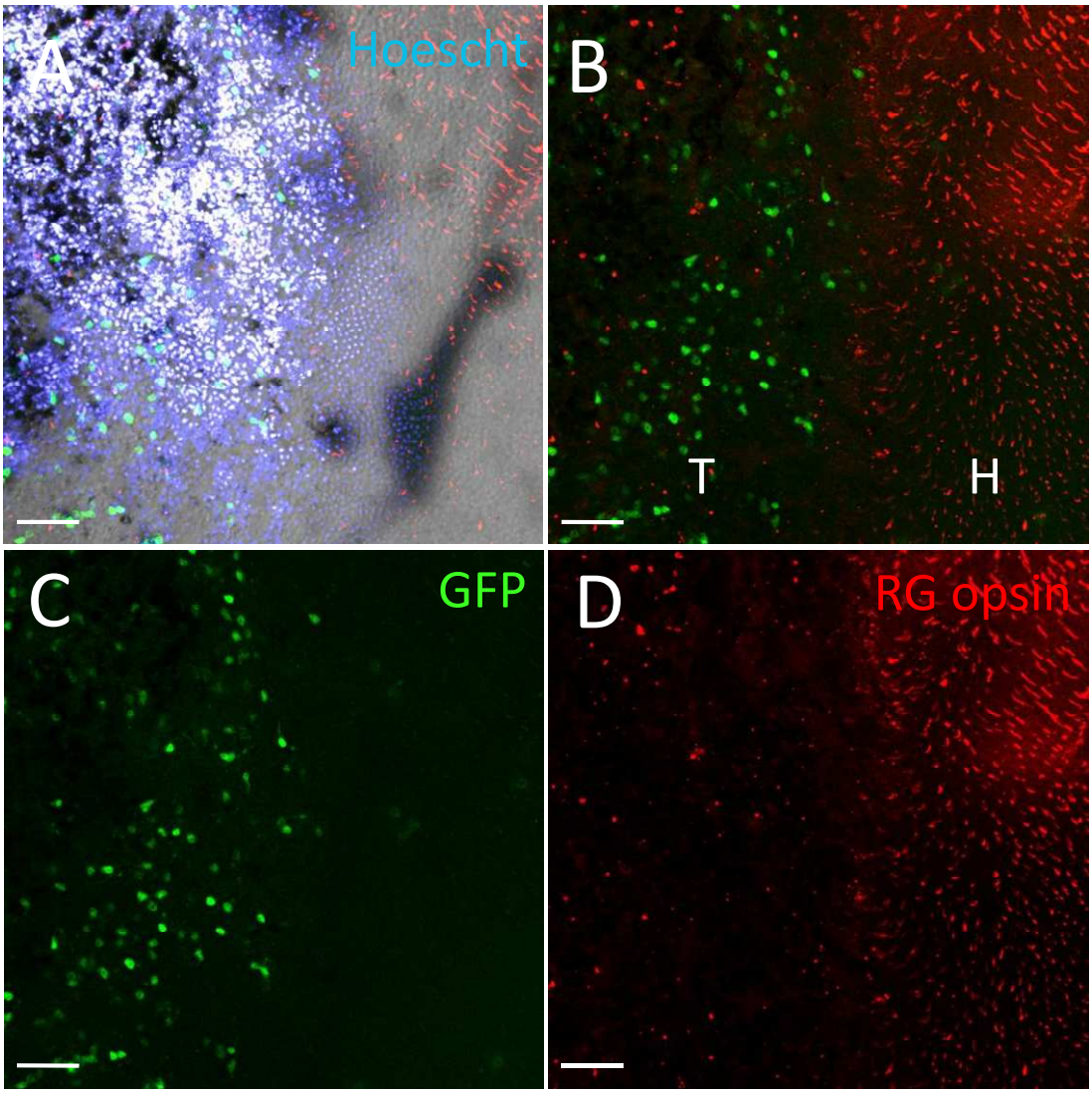

Figure 5.31. RG opsin staining of transplanted cones in a retinal flatmount. A clear demarcation is seen between the transplant (T) and host (H) retinal interface as

demonstrated by the donor GFP-positive cones which occupy only half of the field of view and terminate abruptly. The transplanted mass lies in a separate plane to the host ONL as reflected by the different pattern of nuclear staining in image **A** between donors and host. Anti-RG opsin antibody stains host cone outer segments (COS) more efficiently than donor COS as demonstrated by the scanty staining of donor cones in image **D**. Scale bar: 50µm.

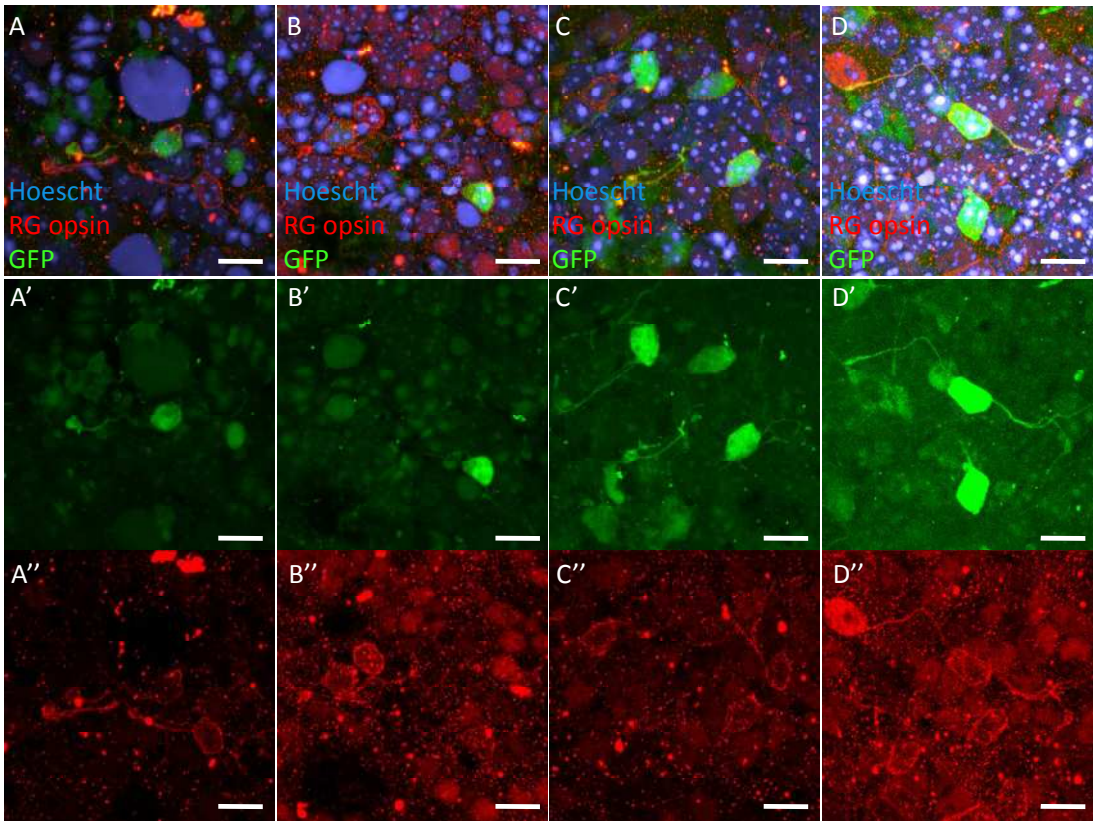

Figure 5.32. High power confocal micrographs of RG opsin staining of transplanted cones in a retinal flatmount. In this panel, four different areas of RG opsin staining are shown in columns. Anti-RG opsin antibody is seen to colocalise to GFP-positive cones, either to the outer segments or to the membrane or processes. Conversely, there are areas of RG opsin staining that are GFP-negative, reflecting either the variable expression of GFP due to the heterozygous Opn1-EGFP phenotype or due to the loss of GFP through photobleaching. Scale bar: 10µm.

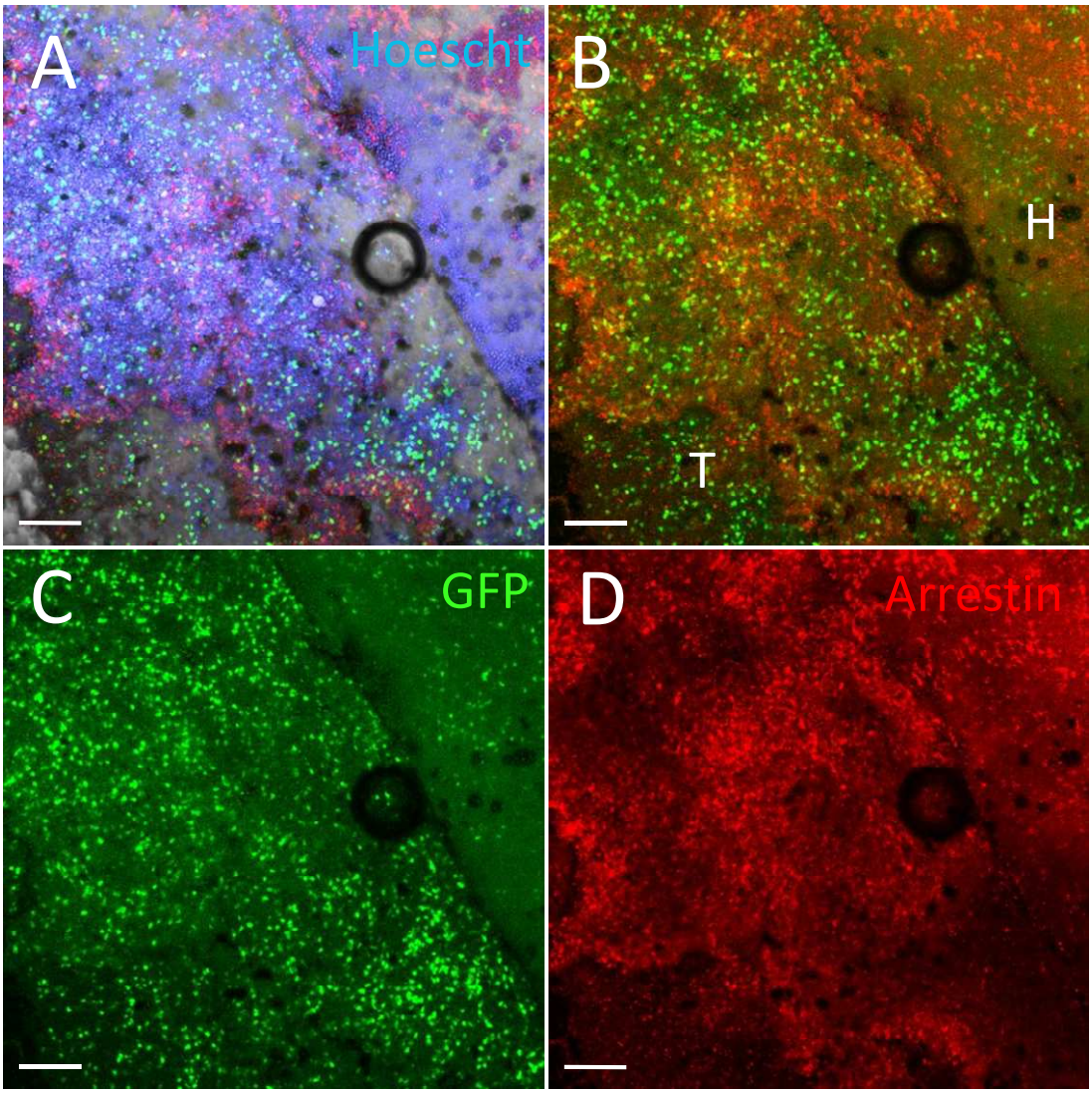

Figure 5.33. Arrestin staining of transplanted cones in a retinal flatmount. As with the previous figure, a clear demarcation is seen between the transplant and host retinal interface as demonstrated by the distribution of the donor GFP-positive cones. Anti-arrestin antibody colocalises to donor cones efficiently (**B**). Scale bar: 100µm.

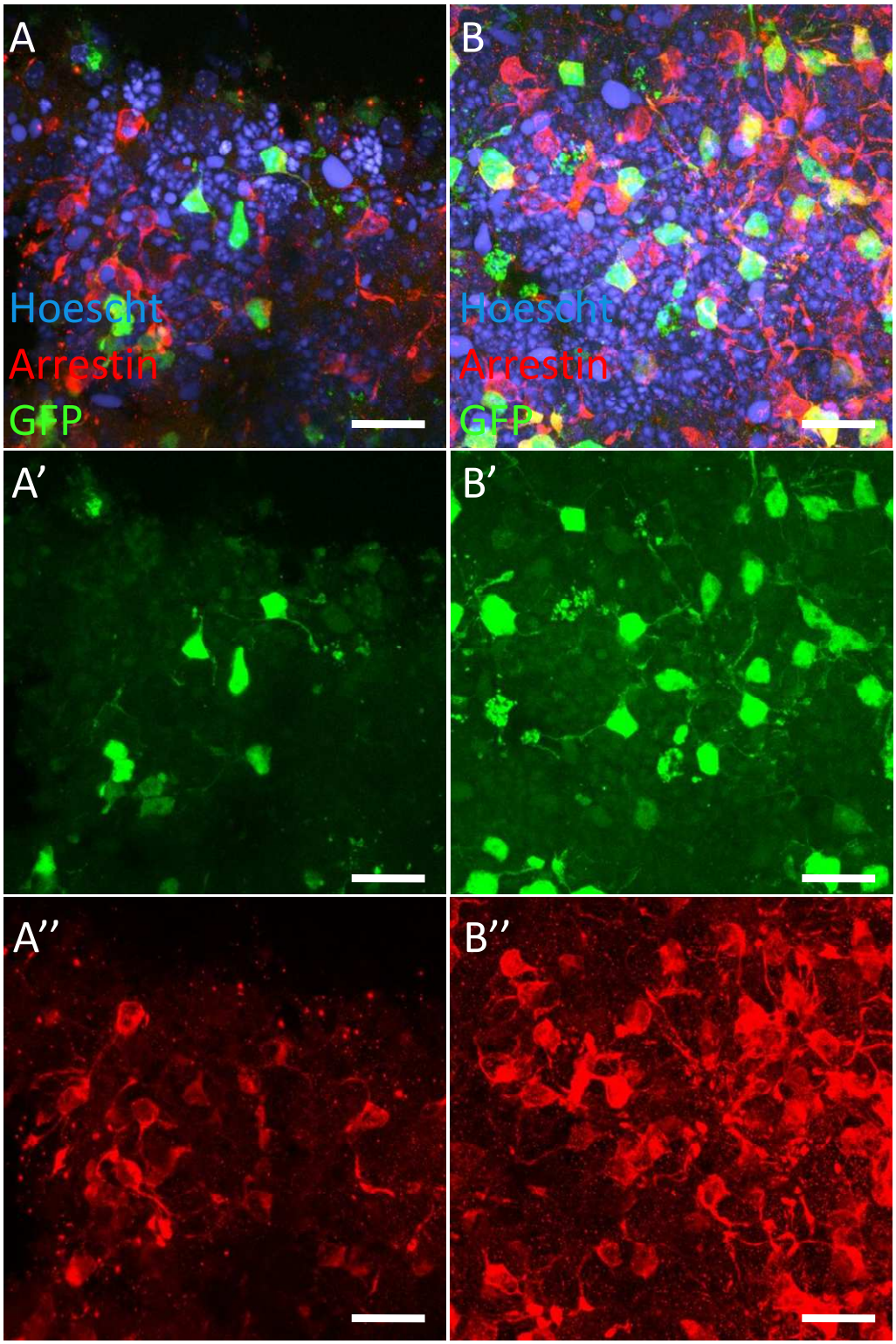

Figure 5.34. High power confocal micrographs of arrestin staining of transplanted cones in a retinal flatmount. In this panel, two different areas of arrestin staining are shown in columns. Anti-arrestin antibody is seen to colocalise to GFP-positive cones. Areas that are positive for arrestin but are GFP-negative occur due to the staining of S cones that lack GFP. Scale bar: 20µm.

5.3.3.2 Opn1-EGFP-dsRed donors in wild type hosts

The following results pertain to the subretinal transplantation of donor retinal cells from P1 Opn1-EGFP-dsRed mice into adult C57Bl/6 mice. The purpose of these experiments was to observe the survival of donor cones in the absence of donor rods, the latter having undergone degeneration due to the *rd1* mutation in donor Opn1-EGFP-dsRed mice.

Donor GFP/dsRed-positive (referred to herein as GFP-dsRed) cones were shown to survive in the subretinal space of adult wild type mice at three weeks post transplantation (Figure 5.35). The gross microscopic appearance of these cones was similar to that of transplanted GFP-positive cones derived from Opn1-EGFP mice as described in previous experiments in terms of size and formation of irregular arranged processes. Again, the transplanted cells were limited to a subretinal mass with a clear separation from the host ONL.

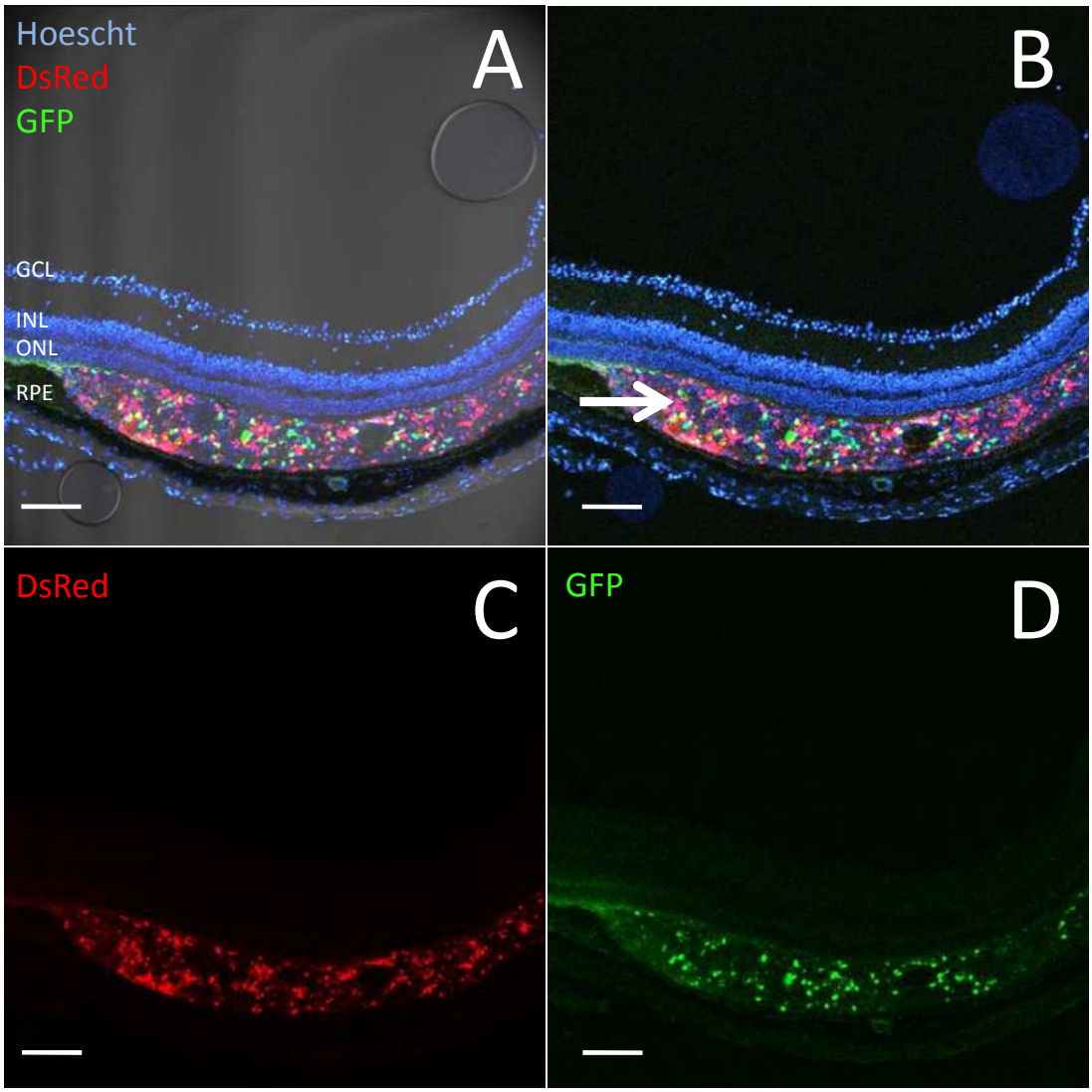

Figure 5.35. Survival of transplanted GFP-positive cones derived from Opn1-EGFP-dsRed donors. The confocal images show that donor cells derived from P1 Opn1-EGFP-dsRed retinas survive in the subretinal space of adult wild type hosts (arrow). Survival of M cones is evidenced by the expression of GFP that would have been absent at the time of transplantation but has 'switched on' at the point of sectioning at three weeks. Additionally, the expression of the ubiquitous dsRed reporter in donor cells indicates the survival of accompanying cells in the donor mass. Importantly, the latter excludes rod photoreceptors since these have undergone cell death due to the underlying *Pde6b* mutation in the donor retina. Scale bar: 100µm.

Immunohistochemistry

As per the findings using Opn1-EGFP donors, transplanted Opn-EGFP-dsRed retinal cells expressed the cone markers for arrestin (Figure 5.36), RG (M) opsin (Figure

5.37), and the pan-photoreceptor marker, recoverin (Figure 5.38). Regarding the latter, at three weeks post-transplantation, the absence of rods from the donor mass would have resulted in staining of surviving cones only. Evidence for the absolute nature of the subretinal donor mass and the lack of contamination or communication with the host photoreceptors was shown by the absence of PDE6B staining of donor cells but positive staining of host ROS (Figure 5.39).

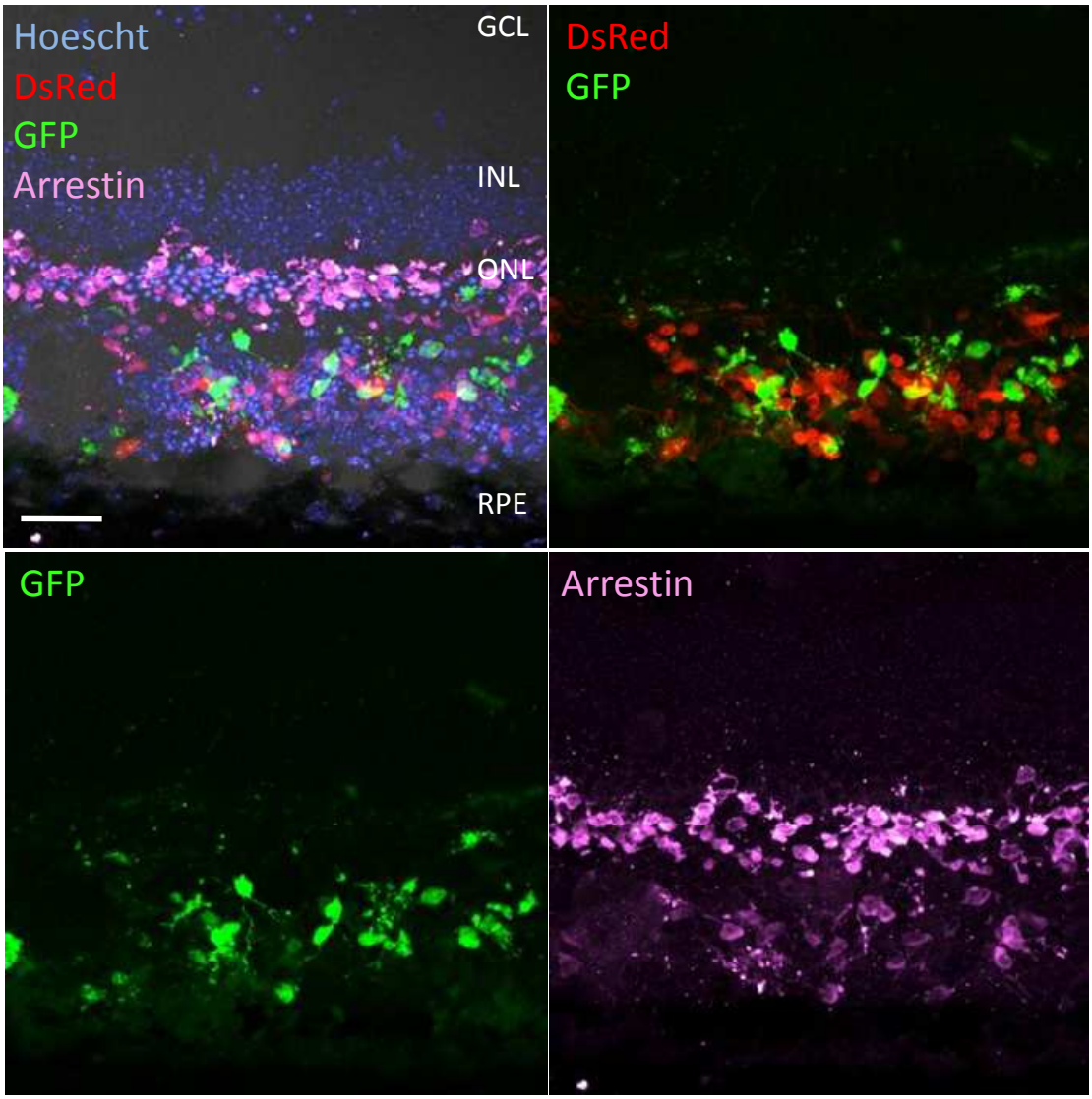

Figure 5.36. Arrestin staining of transplanted GFP-dsRed cones. The transplanted mass of Opn1-EGFP-dsRed cells is seen in the subretinal space of a wild type mouse. The GFP signal is apparent in the donor cells as is the ubiquitous dsRed reporter. Anti-arrestin antibody (which is shown in magenta) stains GFP-dsRed cones in addition to the positive internal control of host cones seen at the level of the ONL. Scale bar: 50µm.

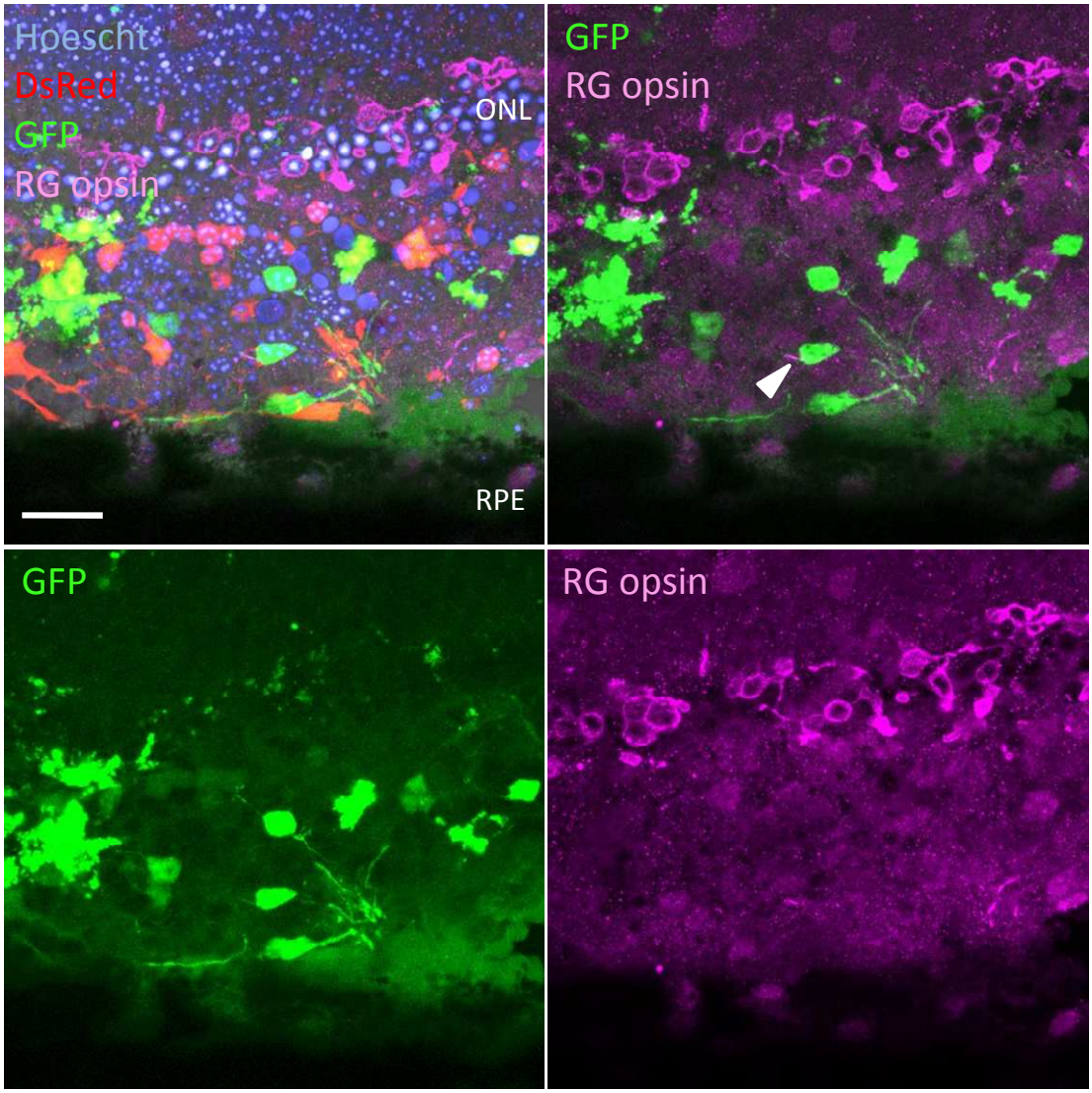

Figure 5.37. RG opsin staining of transplanted GFP-dsRed cones. The transplanted mass of Opn1-EGFP-dsRed cells is seen in the subretinal space of a wild type mouse. Anti-RG opsin antibody (which is shown in magenta) stains a GFP-dsRed cone outer segment in the middle image (white arrowhead). Additionally, the internal control of host cones seen at the level of the ONL demonstrates colocalisation of the antibody to the cell membrane. Scale bar: 20µm.

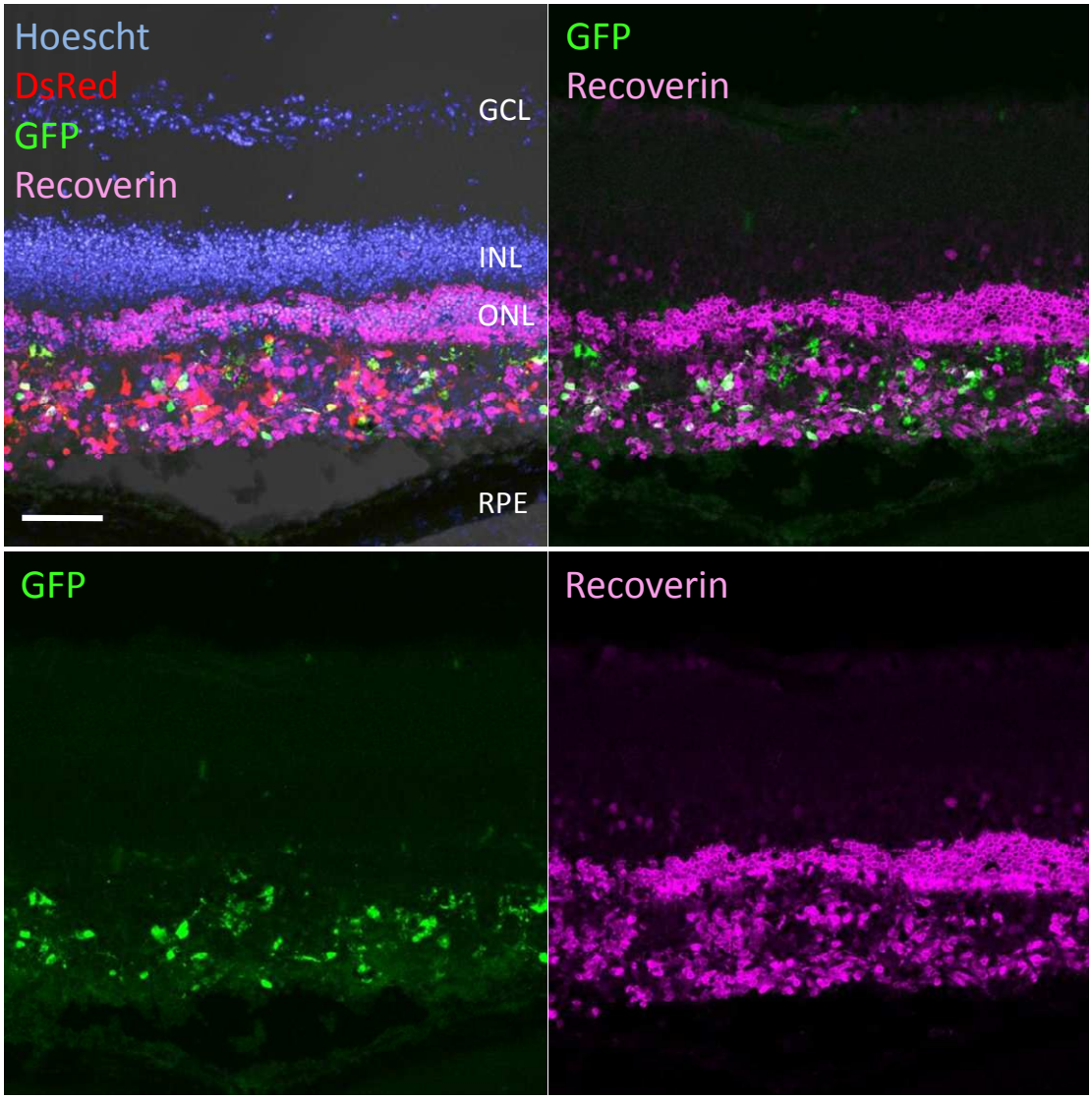

Figure 5.38. Recoverin staining of transplanted GFP-dsRed cones. The transplanted mass of Opn1-EGFP-dsRed cells is seen in the subretinal space of a wild type mouse. Anti-recoverin antibody (which is shown in magenta) stains all photoreceptors including GFP-dsRed cones. Since there are no rods in the transplanted cell mass due to the underlying *Pde6b* mutation in the donor retina, recoverin staining is specifically limited to S-cones and GFP-positive LM cones. The internal control of host rods and cones seen at the level of the ONL demonstrates colocalisation of the antibody to all photoreceptors. Scale bar: 50µm.

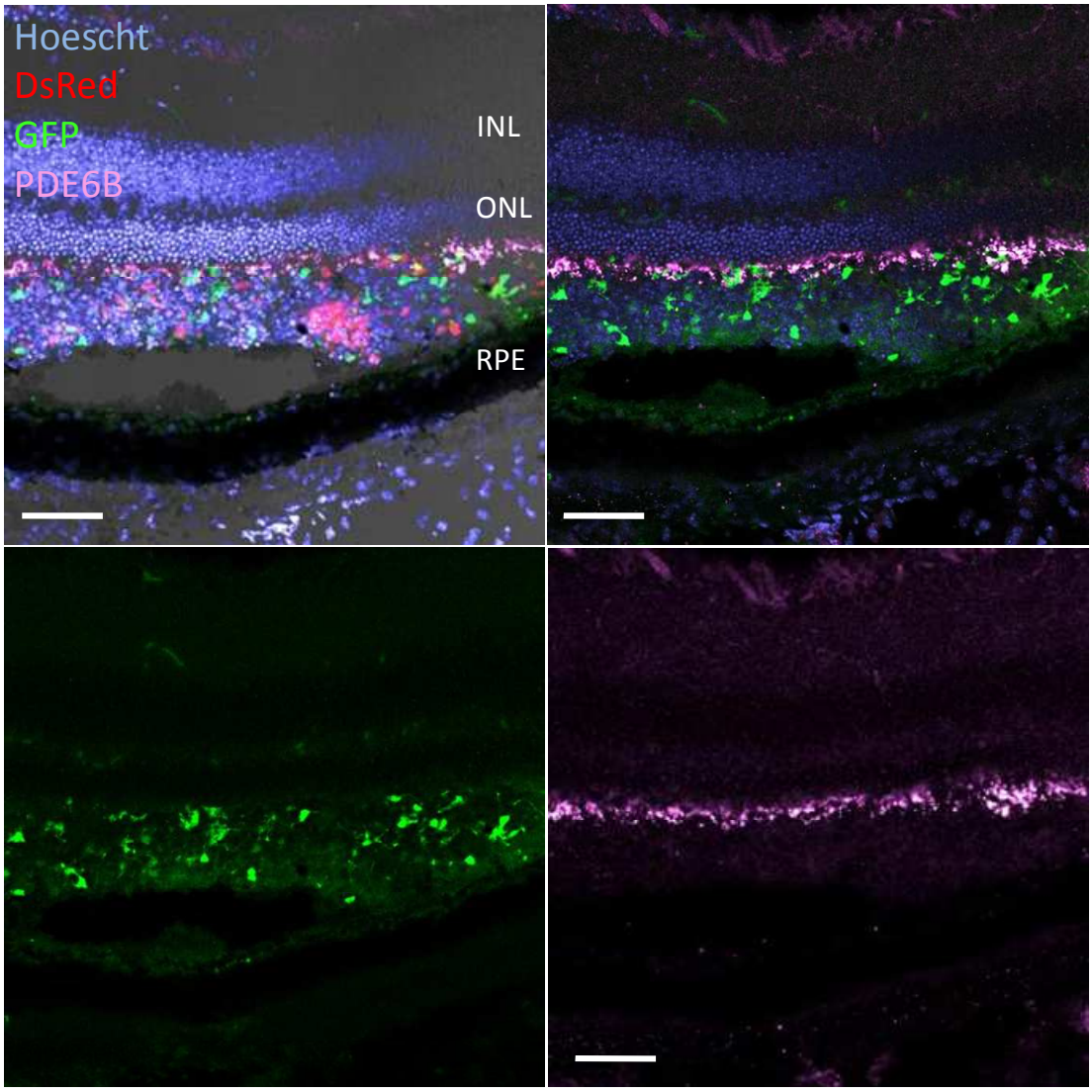

Figure 5.39. PDE6B staining of transplanted GFP-dsRed cones. The transplanted mass of Opn1-EGFP-dsRed cells is seen in the subretinal space of a wild type mouse. Anti-PDE6B antibody (which is shown in magenta) stains all host rod outer segments serving as a positive internal control. No staining is seen within the transplanted subretinal mass as this contains no rods due to the underlying *Pde6b* mutation in the donor retina. Scale bar: 50µm.

5.3.3.3 Opn1-EGFP-dsRed donors in rd1 *hosts*

In order to investigate the survival of transplanted cones in the absence of rods or rod-derived factors, donor Opn1-EGFP-dsRed retinal cells were injected into the subretinal space of adult (12-weeks old) C3H mice carrying the *rd1* mutation (Figure 5.40). Rods were absent from the host retina due to the age of the mice and had

degenerated by three weeks post transplantation in donor cells due to the same mutation. GFP-dsRed cones showed equivalent survival to that seen in transplanted wild type hosts and also to the number of GFP-positive cones following transplantation of Opn1-EGFP retinal cells into wild type hosts ($F_{2, 22}$ = 0.2129, P = 0.810, one-way ANOVA with Bonferroni post-hoc test, Figure 5.40E).

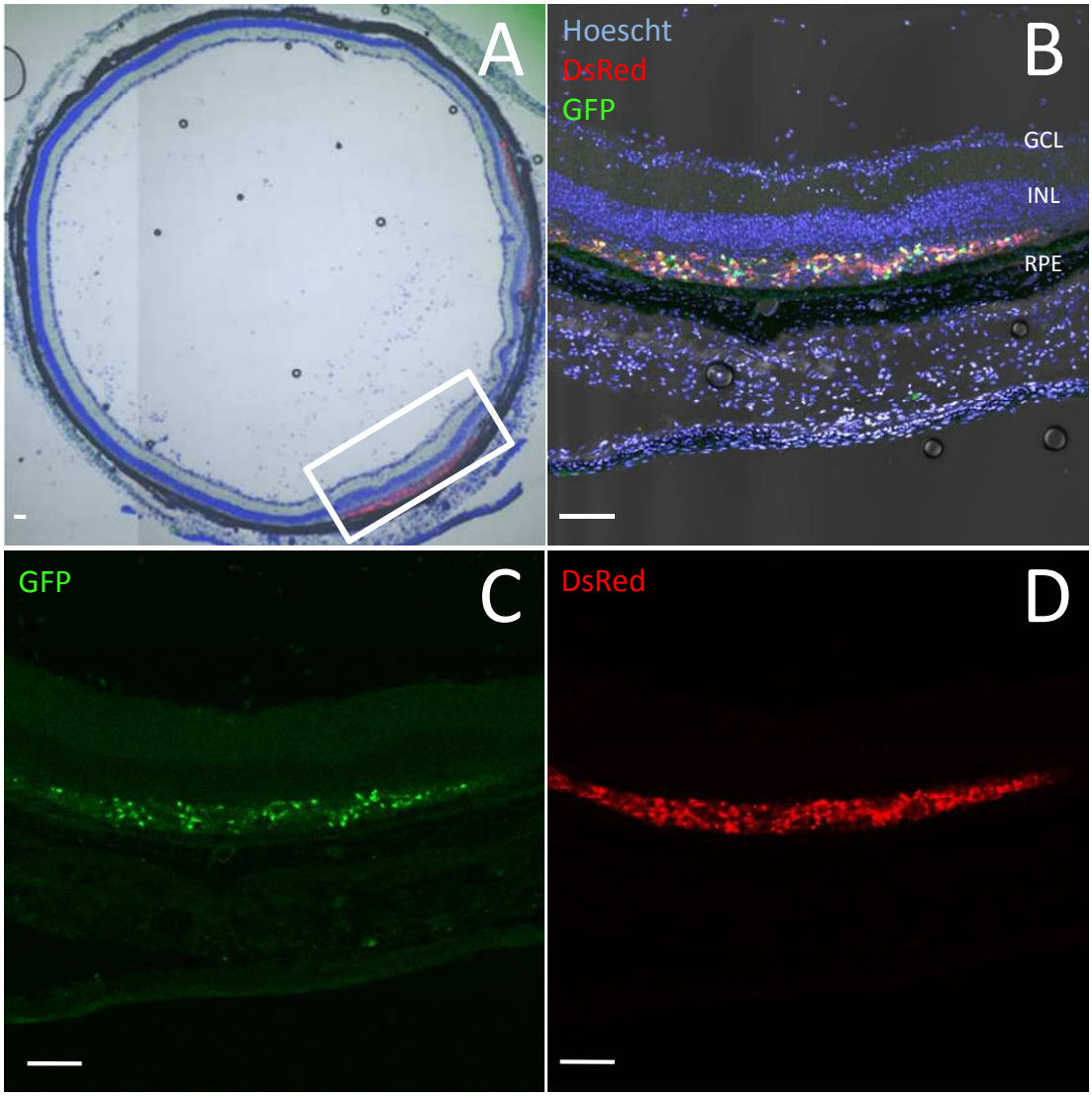

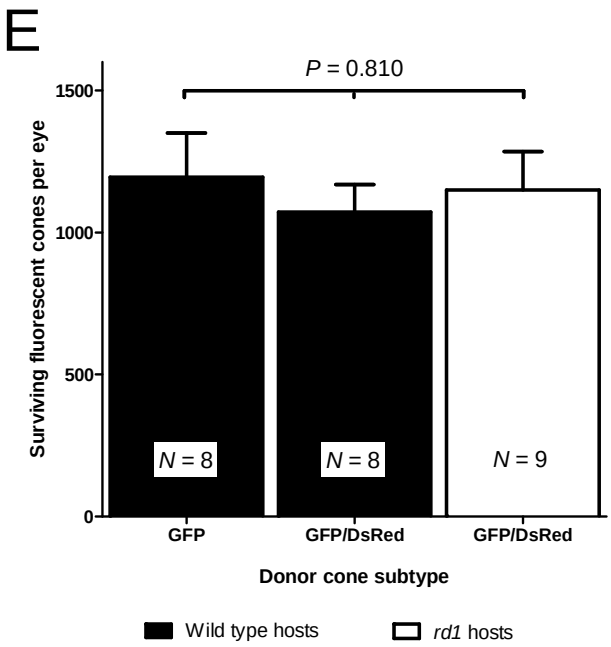

Figure 5.40. Retinal sections showing the survival of transplanted cones in the subretinal space of *rd1* mice. A mass of transplanted Opn1-EGFP-dsRed cells is shown in the subretinal space of mice carrying the *rd1* mutation (white rectangle in image **A** enlarged in **B**-**D**). As a result of this, both the donor and host contain no rods due to the underlying *Pde6b* mutation, which explains the lack of a host ONL. Although cones do not express GFP at the time of transplantation, at the stage of sectioning, GFP and dsRed expression is obvious within the donor cells. Analysis of GFP-dsRed cone survival following transplantation (**E**). Equivalent numbers of GFP-dsRed cones were shown to survive following transplantation into either wild type or *rd1* hosts. Error bar ± SEM, $P = 0.810$, one-way ANOVA with Bonferroni post-hoc test.

Immunohistochemistry

Antibody staining confirmed the expression of arrestin, RG (M) opsin, PNA lectin, and recoverin in transplanted GFP-dsRed cones (Figure 5.41). The localisation of cone opsin was consistent with the findings observed in donor cones derived from Opn1-EGFP retinas and therefore suggested the identification of outer segments. However, due to previous reports suggesting the mislocalisation of cone opsin in rd1 retinas, it is possible that the staining was not confined to the outer segments given the irregular structure of these cones.

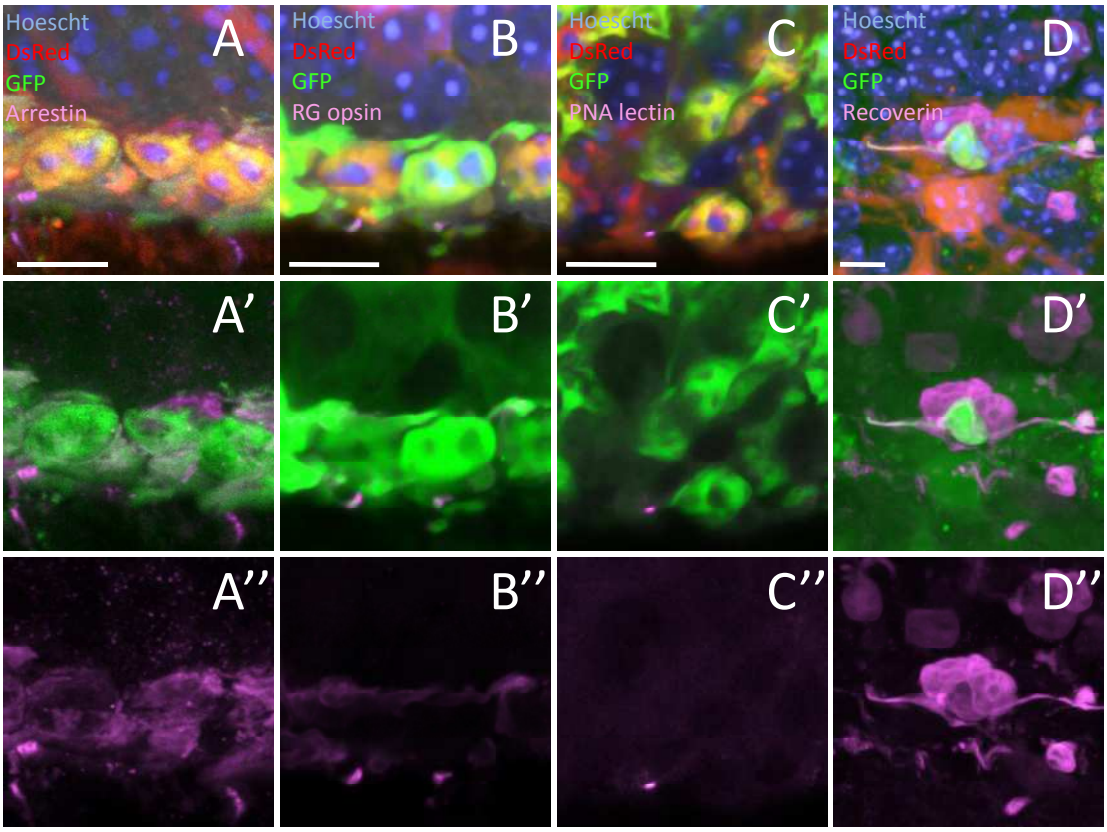

Figure 5.41. Immunohistochemistry of GFP-dsRed cones post transplantation into C3H mice. Opn1-EGFP-dsRed donor retinal cells were transplanted into the subretinal space of C3H mice carrying the *rd1* mutation. These images show staining of the donor GFP-dsRed cones. Anti-arrestin antibody is seen to colocalise to these donor cones (A-A''). Anti-RG opsin antibody (B-B'') and PNA lectin (C-C'') detect the presence of cone outer segments and cone sheaths respectively. Anti-recoverin antibody stains the fluorescent cone in addition to non-fluorescent S-cones (D-D''). Rods are absent from both the donor and host due to the underlying *rd1* mutation. Scale bar: 5µm.

5.3.4 Transplantation post laser

Dissociated P14 Opn1-EGFP retinas containing identifiable GFP-positive cones were injected into the subretinal space of adult wild type mice immediately following laser application. Longitudinal cSLO imaging was conducted between days 1 and 6 post procedure followed by histological examination.

In vivo imaging

cSLO reflectance imaging (Figure 5.42) showed a well-demarcated area indicating the site of injection on the first day post treatment (Figure 5.42C). The demarcation was less apparent by day 6 indicating that the subretinal bleb was diminishing with closer apposition of the retina to the RPE (Figure 5.42G). In the injected area adjacent to laser burns, 488nm AF imaging showed the presence of white dots at the photoreceptor level at day 1 post treatment. These were quantified at a point that was two disc diameters away from the edge of a laser burn and therefore in non-lasered retina. The resultant number of these dots in a given area the size of a laser burn increased from day 1 post laser but did not change between days 3 to 6 ($P < 0.0001$ and $P > 0.999$ respectively, $N = 8$, one-way ANOVA with Bonferroni post-hoc test, Figure 5.43).

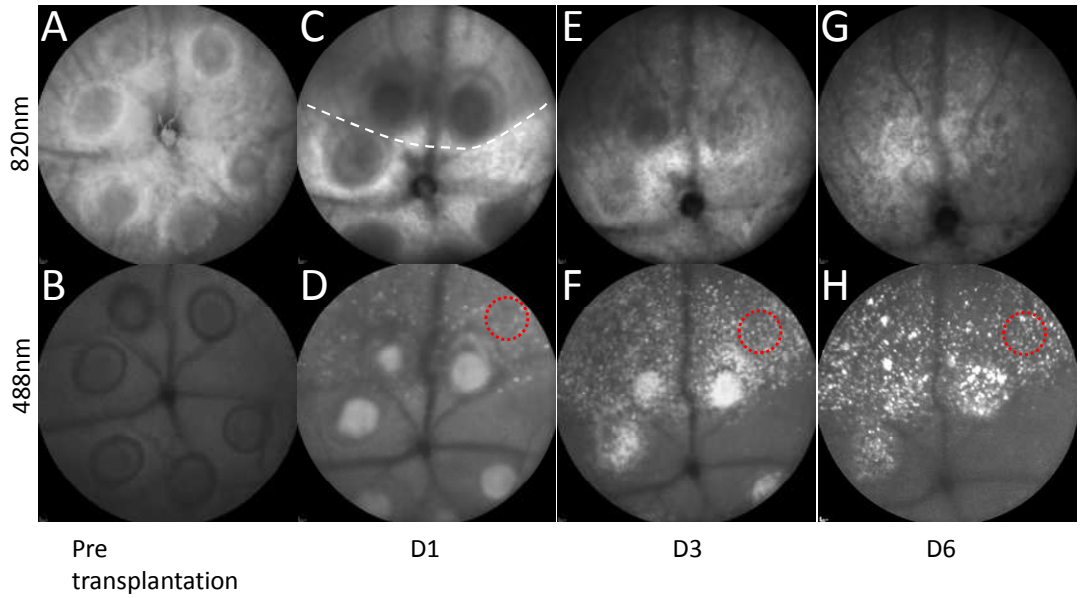

Figure 5.42. cSLO images of transplanted GFP-positive cones post laser. In the wild type retina, six laser burns were placed in a concentric distribution centred on the optic disc. The 820nm reflectance (**A**) and 488nm AF (**B**) images show well-demarcated burns before cell transplantation. Following laser, cells derived from Opn1-EGFP aged P14 were transplanted into the subretinal space. The appearance of a superior subretinal bleb can be seen at day 1 post transplantation creating a well-demarcated area of decreased reflectance (outlined by the white dashed line in

image **C**). The corresponding AF image shows the appearance of autofluorescent dots within the injected area that represent GFP-positive cones (**D**). At days 3 and 6, the injected area becomes less apparent on reflectance imaging (**E** and **G** respectively). However, the corresponding AF images demonstrate that the autofluorescent dots adjacent to the burns (red circles) become more obvious at days 3 and 6 (**F** and **H** respectively).

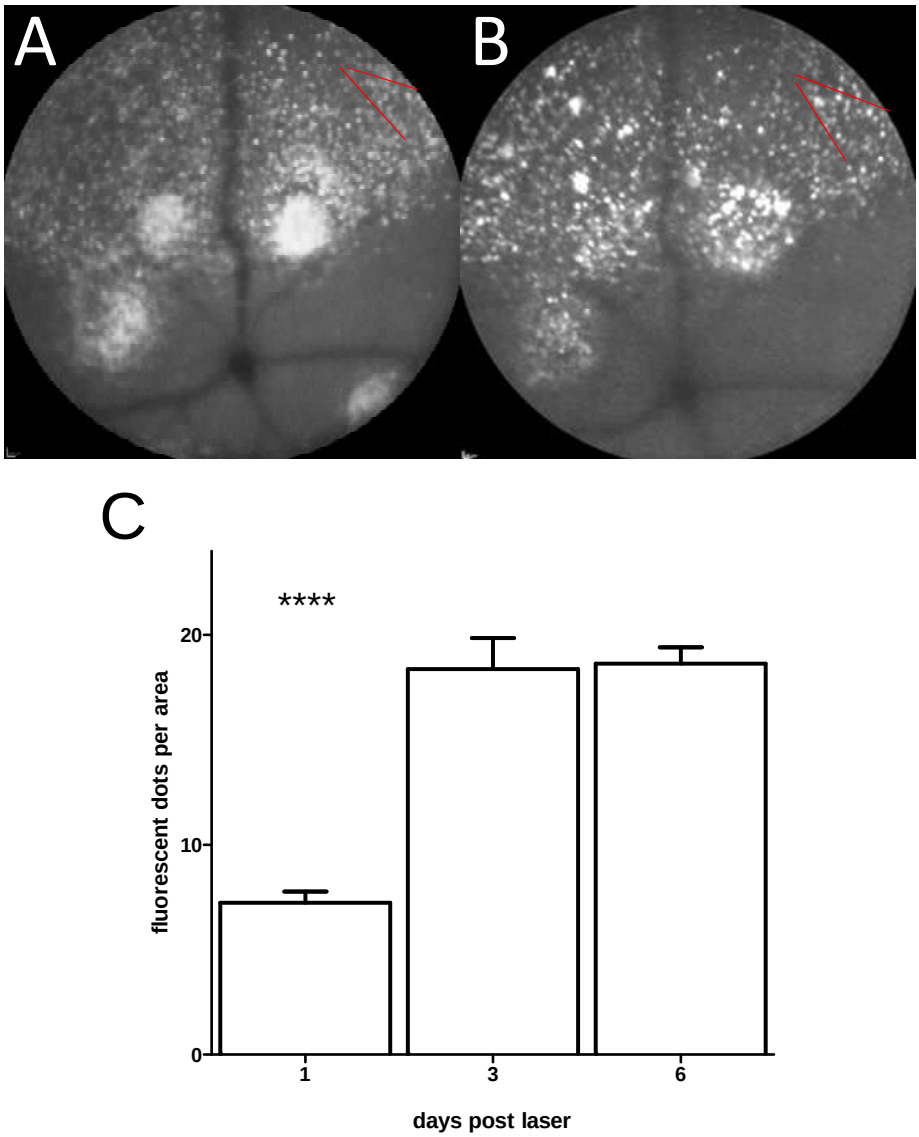

Figure 5.43. Autofluorescent cSLO images of transplanted GFP-positive cones post laser. These images show, at higher magnification, the appearance of autofluorescent (AF) dots following transplantation in the wild type subretinal space at days 3 and 6 (**A** and **B** respectively). Between the two red markings in each image, AF dots can be seen that have remained stationary, consistent with the expected nature of transplanted GFP-positive cones. Analysis of AF dots in a unit area the size of a laser burn (**C**). The number of AF dots increased from day 1 post laser and remained unchanged between days 3 and 6 (Error bar ± SEM, ****$P < 0.0001$ and $P > 0.999$ respectively, $N = 8$, one-way ANOVA with Bonferroni post-hoc test).

Histology

The characteristic features of a retinal laser injury with RPE disruption and ONL attenuation were identified within the area of subretinal cell transplantation. An additional marker to identify the lasered area was via the use of a TUNEL assay (Figures 5.44 and 5.45). As described previously, TUNEL stain localised to cells that had undergone apoptosis secondary to laser injury. Such cells were seen within the ONL of the lasered area. Transplanted cells did not stain positive for TUNEL assay.

In terms of cone survival with GFP as a marker of viability, cones were shown to survive within the area of laser injury. However, the number of cones was less within the injured area than in the adjacent non-lasered retina (Figure 5.46). This may also have reflected the overall reduction in donor cell survival in this area as evidenced by scanty recoverin staining of the transplanted mass within the lasered area compared to the periphery (Figure 5.47).

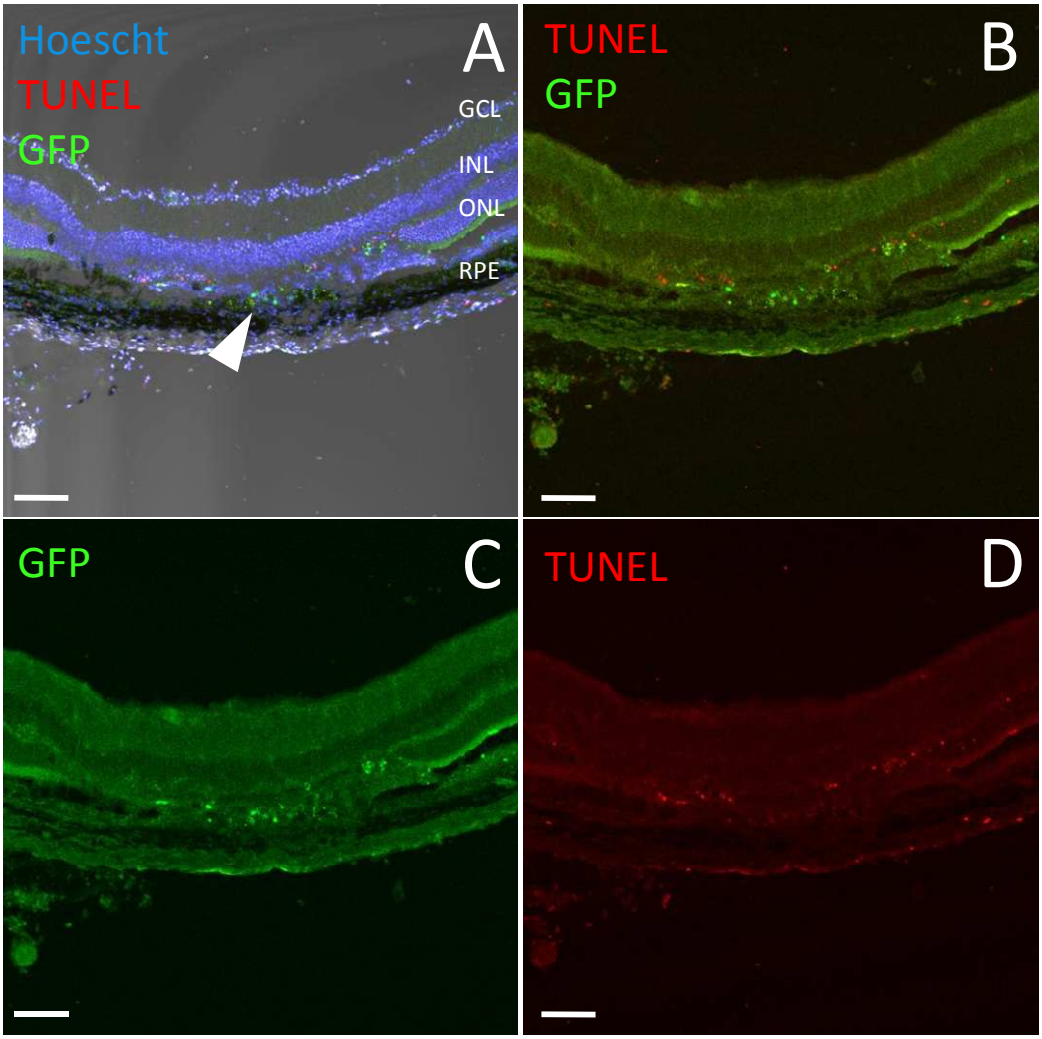

Figure 5.44. Histological sections showing transplanted GFP-positive cones in areas of laser injury. An area of RPE disruption with photoreceptor loss is shown, consistent with the effects of a laser injury (white arrowhead in image **A**). The area of deficient ONL has been replaced by the transplanted mass of Opn1-EGFP cells. There is no disruption of the overlying INL. Surviving GFP-positive cones are apparent in the area of laser injury (**B**, **C**) as are TUNEL-positive cells (**D**), the latter indicative of apoptosis. Scale bar: 100µm.

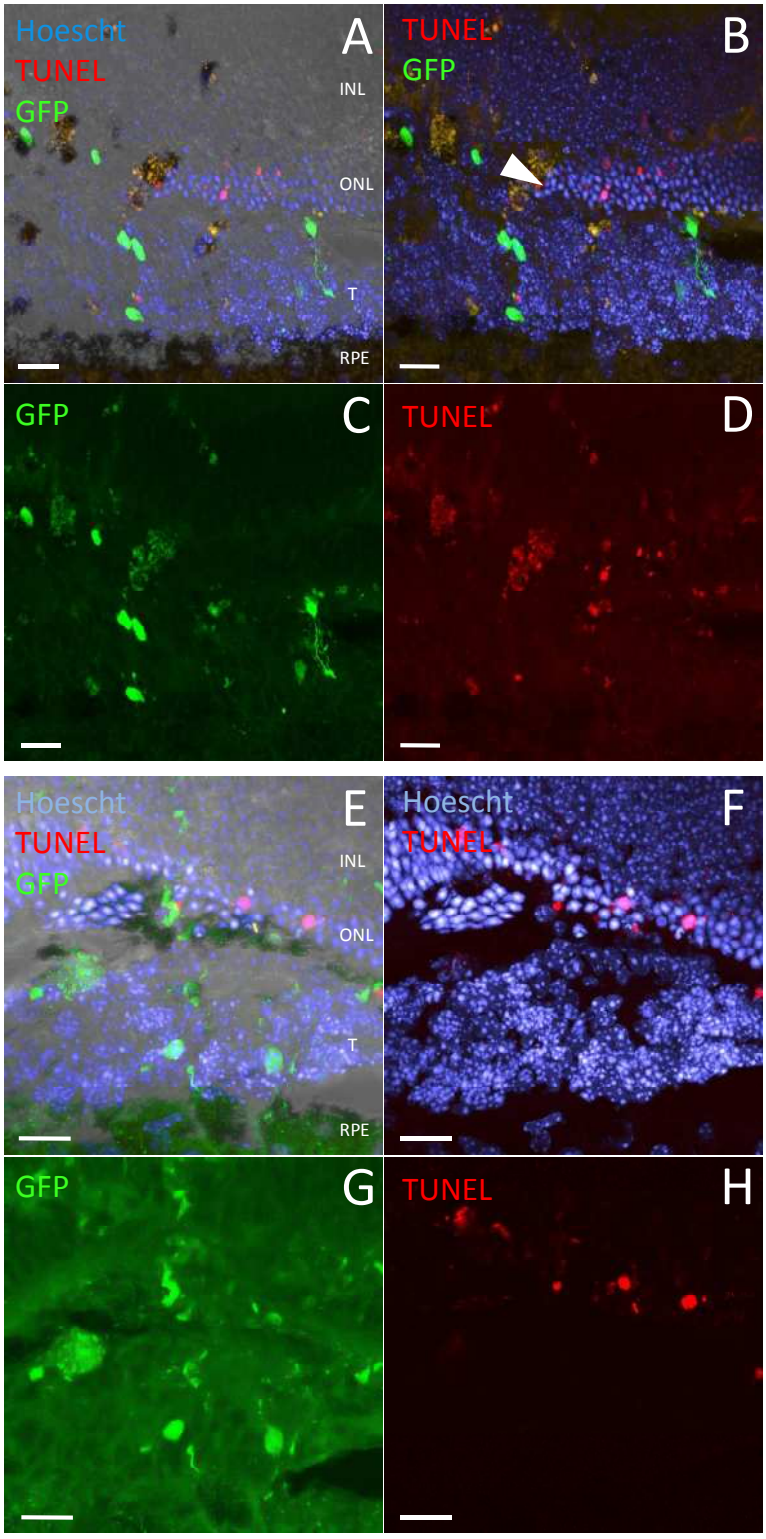

Figure 5.45. High power confocal images showing transplanted GFP-positive cones in areas of laser injury. Two representative areas of laser injury are shown in the upper (**A-D**) and lower (**E-H**) panel respectively. Consistent with laser injury, areas of disrupted RPE are apparent, in addition to loss (white arrowhead in **B**) or attenuation of the ONL (**F**). As confirmation of injury, TUNEL-positive cells are seen at the level of the ONL (**B**, **F**). Surviving GFP-positive cones are seen in the area of injury (**C**, **G**). Scale bar: 20µm. T, transplanted cell mass.

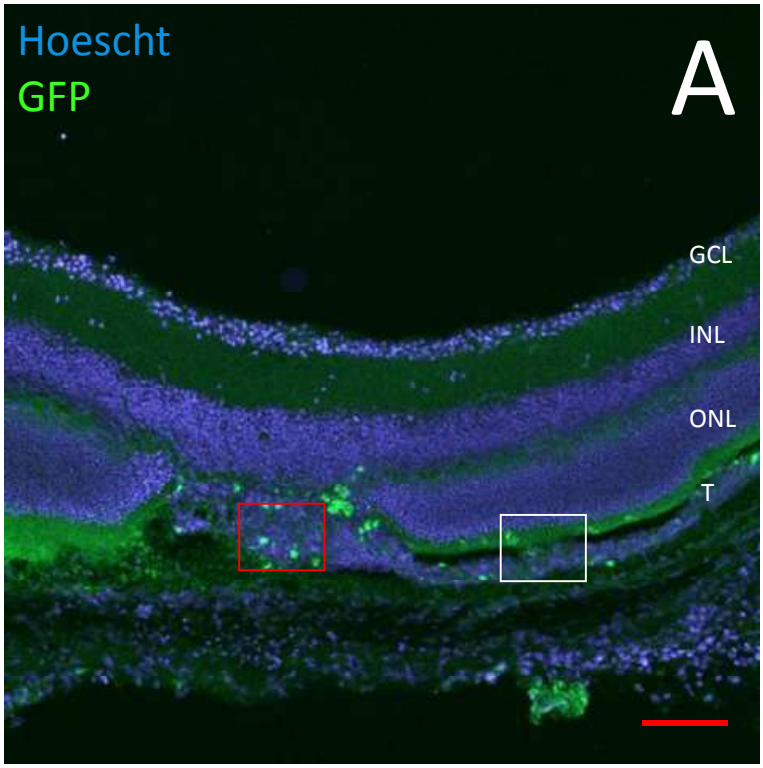

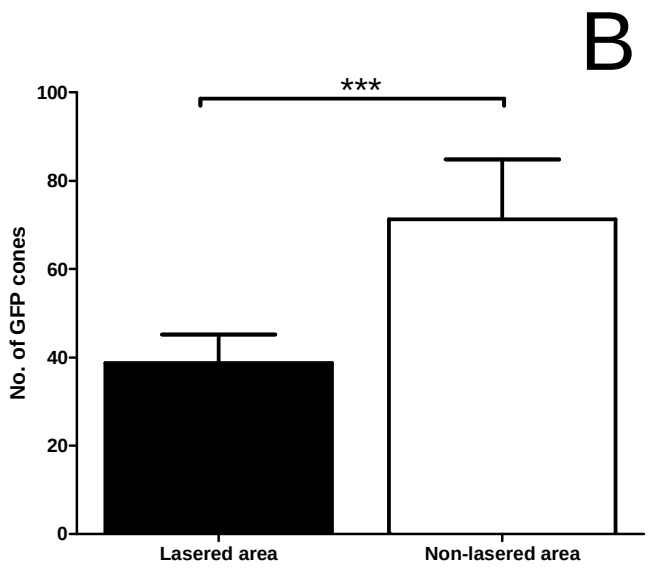

Figure 5.46. Quantification of transplanted GFP-positive cones post laser injury. The number of GFP-positive cones was counted in the lesion area (red box in **A**) and in an adjacent non-lasered internal control area of equal size (white box in **A**). Scale bar: 100µm. Analysis of cone survival by comparing the number of GFP-positive cones within the lesion centre to a non-lasered internal control area (**B**). A lower number of GFP-positive cones survived in the central area of laser injury relative to a peripheral non-lasered area. Error bar ± SEM, $N = 16$. ***$P < 0.001$, paired t-test.

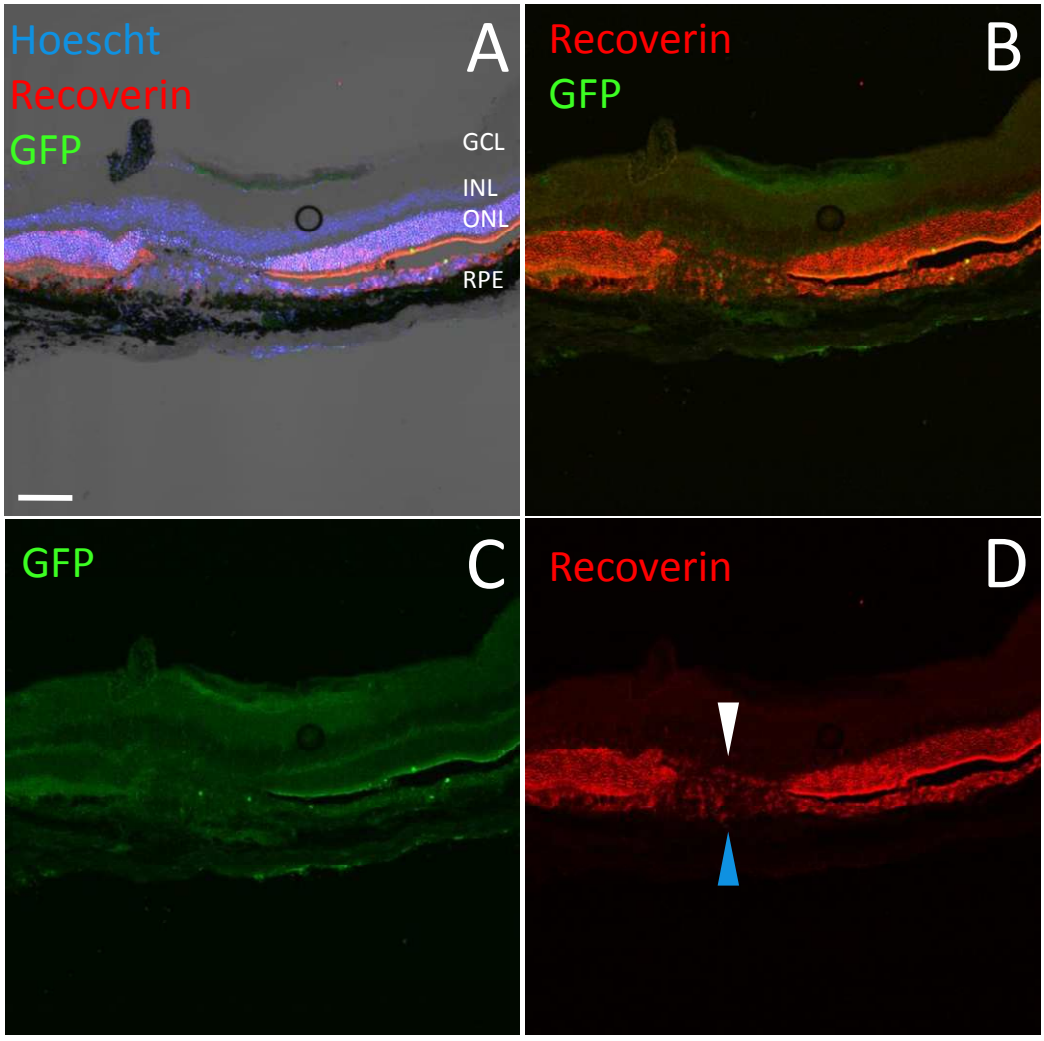

Figure 5.47. Recoverin staining following transplantation of GFP-positive cones post laser injury. This panel of low power micrographs shows that anti-recoverin antibody, which provides a pan-photoreceptor stain, colocalises to the host ONL as expected (**A**, **B**). Additionally, it identifies photoreceptors within the donor subretinal mass. There are few GFP-positive cones visible within the subretinal mass (**C**). Due to the laser injury, there is an area of host ONL loss that is reflected by the absence of recoverin staining (white arrowhead, **D**). This overlies an area of transplanted cells which show weak recoverin staining (blue arrowhead, **D**), even though either side of this area, the staining intensity is brighter. This area itself overlies the central region of laser injury with maximal RPE disruption. Scale bar: 100µm.

5.4 Discussion

The use of FACS to obtain a population of GFP-positive photoreceptors, both rods and cones, has been shown in a previous study using CrxGFP transgenic donors.[300]

However, from the methods described in this chapter, derivation of a cone population containing no rods from Opn1-EGFP mice was not possible by FAC-sorting to yield a sufficient numbers of cells. This is probably because Opn1 expression occurs later during post-natal development than Crx and hence the number of fluoresecent green cells available for FACS at P1 is substantially less. Additionally, the use of MAC-sorting, which has previously been used to enrich photoreceptor precursors for transplantation,[399] did not separate cones from rods in our experiments, as determined by the presence of rhodopsin within this isolate on PCR analysis. Therefore, a biological method was adopted to sort cones from rods in the Opn1-EGFP-dsRed model, which resulted in a rapid degeneration of rods due to a mutation in the *Pde6b* gene.

Cell culture results showed the improved survival of cones derived from younger animals than adults. This finding provided evidence for the selection of early postnatal mice as the source of donor cones in transplantation experiments. At birth, cones in the mouse retina are terminally differentiated but immature with cone genesis having started at embryonic day 11 and the expression of S opsin having begun *in utero*. Expression of M opsin follows that of the other opsins and begins at around postnatal day 6. [400] Evidence of this was seen in the Opn1-EGFP mouse by the absence of GFP until this postnatal stage, since in this model the transgene is composed of a regulatory sequence of the human red and green opsin genes containing the promoter and the GFP reporter cassette.[401] On the basis of this, the earliest postnatal age was used to provide donor retinal cells, this stage providing the optimal window to coincide the onset of GFP with the survival of

cones. Earlier (embryonic) donors would have required a longer period (> 3 weeks) following transplantation to show maximal GFP expression which would have risked the loss of donor cones due to host immune mechanisms.

Cones survived following transplantation into adult hosts. This was evidenced by the expression of GFP which was absent at the time of initial transplantation. The expression of other markers of cone function was also apparent in the way of M (or RG) opsin, arrestin, and recoverin. Importantly, cones survived when derived from the Opn1-EGFP-dsRed donor retina and transplanted into *rd1* hosts. This implies that cones survive in the absence of rods, the latter having degenerated from both donor and host, which concurs with the *in vitro* results of cone culture. This further indicates that the hypothetical paracrine effect of rods, in particular via the proposed Rod-derived Cone Viability Factor (RdCVF)[402] is not fundamental to cone survival. Of note, the identification of M opsin in transplanted cones demonstrated their formation of outer segments since the expression of opsin genes is delayed to P4–13.[403] As phototransduction takes place in the cone outer segments, the presence of these structures allowed for the possibility of a functional response following transplantation. This is explored in further detail in the next chapter.

Transplanted cones were shown to survive in the area of laser injury albeit to a lesser degree than in the surrounding non-lasered area. This difference in survival rate may be attributable to a number of reasons. Due to the intricate relationship between these layers, the damage to RPE cells due to the effect of laser injury would have an impact on overlying photoreceptors. Local release of inflammatory mediators from apoptotic or necrotic cells and recruitment of macrophages would

result in loss of potentially antigenic donor cells.[404] Additionally, the age of donor cells may have had an influence on the number of surviving cells. The justification for using the P14 donor retinas rather than from an earlier postnatal age was that donor cones needed to be observed at an early stage following transplantation. P14 donors were selected as the earliest postnatal stage at which GFP expression reached adult levels. This not only allowed the *in vivo* observation of fluorescent signal by cSLO imaging but also enabled the histological identification of GFP-positive donor cones in an area of TUNEL-positive host cells, thereby accurately localising the region of laser injury. Selection of younger donor retinas would have compromised the number of GFP-expressing cones available for quantification at the stage of laser-induced photoreceptor apoptosis, the latter having been shown to be an event that occurs early following laser exposure.

CHAPTER 6

INTEGRATION OF CONE PHOTORECEPTORS POST TRANSPLANTATION

6.1 Introduction

6.1.1 Aim

To investigate the feasibility of integration following cone transplantation and the functional response that would result from successful integration.

6.1.2 Overview

In order to successfully repair a foveal laser injury involving the loss of cone photoreceptors, the only possible means of maintaining or restoring visual acuity is by replacing cones. The results of the last chapter showed that donor cones survive following transplantation. However, unless these cells integrate with host structures, they will not be able to confer a functional response. Whilst different cell types have been investigated for their beneficial effects following transplantation post retinal laser injury,[405-407] the option of cone transplantation remains unexplored.

On this note, although the published literature shows much evidence of rod integration following transplantation, there is limited data on the results of cone transplantation. Following the intravitreal transplantation of human ES-derived photoreceptors into neonatal mice, S-opsin was detected in donor cones.[408] In another study, the subretinal transplantation of retinal progenitor cells in rhodopsin knockout mice resulted in the expression of S-opsin in presumptive donor cone photoreceptors.[409] The most recent study of cone transplantation showed that transplantation of FAC-sorted photoreceptors derived from the CrxGFP transgenic mouse resulted in successful integration of donor cones with expression of arrestin and Rxrλ cone markers.[300] Importantly, and of relevance to the findings discussed in

this chapter, in all previously described examples, the transplanted cones had an identical morphology to host cones and were aligned in the correct orientation with appropriate spatial distribution.

Further to this, an under-recognised or under-reported phenomenon in the field of retinal cell transplantation is the concept of cell (specifically cell-cell) fusion. Cell fusion is a fundamental biological event characterised by the fusion of intercellular membranes and occurs in processes ranging from fertilisation to tumorigenesis. Although the underlying mechanisms are not fully understood, it is recognised that intercellular fusion is likely a distinct entity to the type of fusion events occurring on an intracellular level, the latter involving fusion between membrane-bound organelles.[410] In the area of tissue regeneration using stem cells, the process of cell fusion has emerged as an unforeseen and confounding factor. For instance, circulating haematopoeitic stem cells (HSCs) have been shown to fuse with a number of target cells including hepatocytes, cardiac myocytes, and oligodendrocytes.[189,411,412] Furthermore, in studies of liver regeneration, macrophages derived from HSCs, rather than the HSCs themselves, have been shown to fuse with hepatocytes.[413] Applying these concepts to the retinal transplantation model, it remains to be understood whether transplanted cells fuse rather than integrate with the host and whether fusion involves an intermediate cell rather than the donor cell itself.

6.1.3 Summary of results

The findings in these studies can be summarised as follows:

1) Cones integrated successfully following transplantation.
2) Cell fusion occurred between transplant and host photoreceptors.
3) Transplanted cones showed evidence of functional response with changes in intracellular calcium.
4) Treated mice exhibited behavioural light aversion.

6.2 Experimental design

Experiments were conducted as follows:

Subretinal transplantation

For integration studies, donor retinas were derived from the following strains:

1. OPN1-EGFP containing GFP-positive cones on a wild type background.
2. OPN1-EGFP-dsRed mice containing GFP-positive cones and a ubiquitous dsRed reporter on an *rd1* background.

Following papain dissociation of P1 retinas, resultant donor cells ($2x10^5$ cells in 1µl) of either of the aforementioned strains were transplanted into the subretinal space of neonatal P1 wild type or TKO mice (Figure 6.1). For fusion studies, donor retinas were derived from dsRed P1 neonates and transplanted into the subretinal space of Nrl.GFP P1 neonates.

Host mice were sacrificed at three weeks by either cervical dislocation (for wild types) or perfusion fixation (for *rd1* strains). Eyes were processed for sectioning, immunohistochemistry, and imaged using the confocal microscope as previously described.

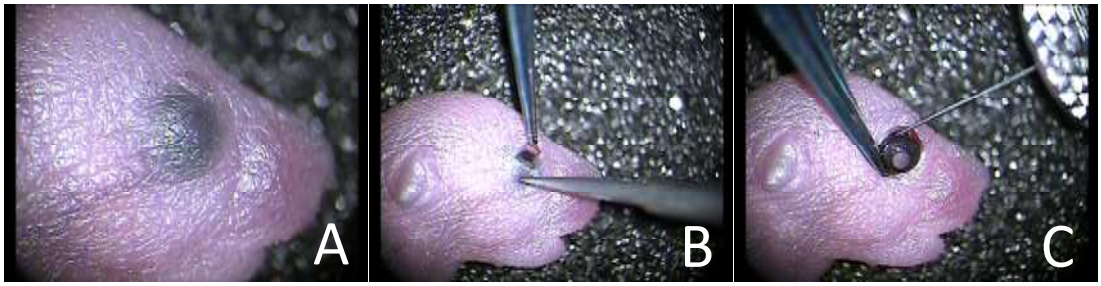

Figure 6.1. Images showing the method of delivering a subretinal injection into an early postnatal mouse. An anaesthetised P1 pup is shown with lids fused at this stage of development (**A**). Following an incision made along the surface marking that will eventually give rise to the palpebral fissure, the lids are separated with further blunt dissection through the conjunctiva to expose the eye (**B**). By proptosing and rotating the eye, a subretinal injection can be delivered by tangentially entering the globe, thereby minimising reflux of injected contents (**C**).

qPCR analysis

At three weeks following transplantation into P1 pups, eyecups from treated and uninjected TKO mice were processed for RNA extraction and subsequent qPCR analysis in order to observe the expression of the *CNGA3* gene.

Calcium imaging

At three weeks following transplantation into P1 pups, retinal explants from TKO mice and controls were assessed with respect to changes in intracellular calcium concentration following the application of an mGluR8 agonist (S-3,4-DCPG) and antagonist (CPPG).

Pupillometry

Pupillometry was conducted at three weeks of age, following bilateral transplantation into P1 TKO mice versus untreated age-matched TKO and wild type

controls.

Behavioural light aversion (BLA)

BLA was tested at three weeks of age, following bilateral transplantation into P1 TKO versus controls using a light-dark box system (Figure 6.2). The movement of each mouse was digitally recorded for 30 minutes, following which treated TKO mice were immediately sacrificed for histological assessment. Analysis was conducted offline using tracking software (Figure 6.3).

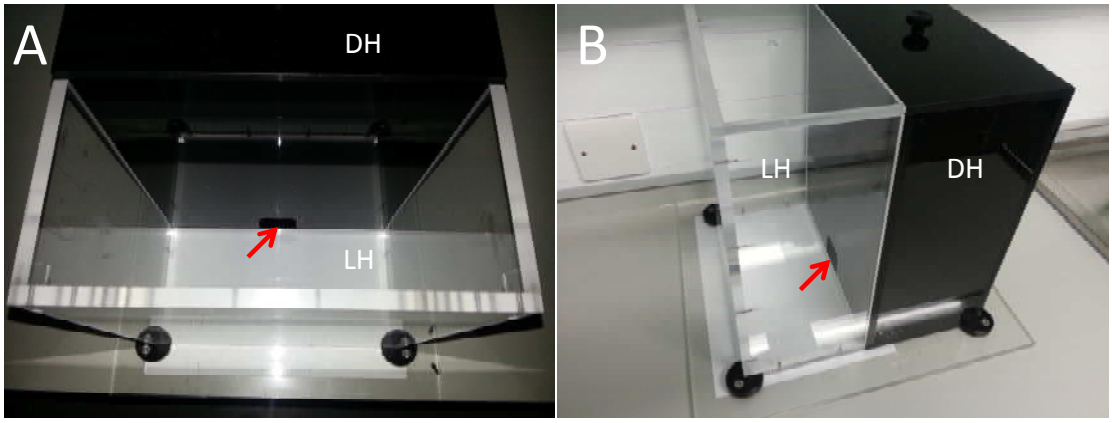

Figure 6.2. Images showing the apparatus used for testing of behavioural light aversion. A light-dark box is shown from above (**A**) and the side (**B**). A red arrow indicates the aperture via which the mouse transfers between the front light half (LH) and back dark half (DH).

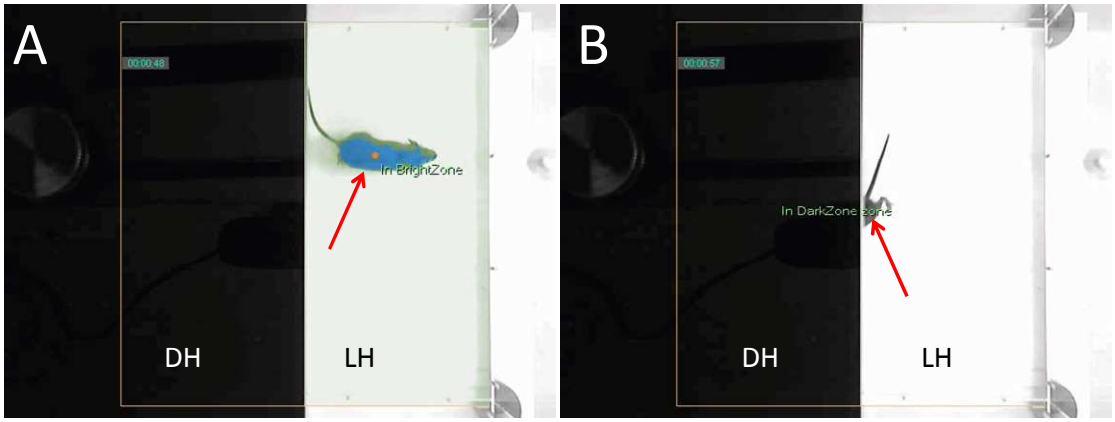

Figure 6.3. Video-stills demonstrating the automated tracking of movements. A light-dark box is shown from above with the mouse (arrow) in the front light half tracked as "In BrightZone" (**A**). On crossing to the back dark half the mouse (arrow) is tracked as "In DarkZone" (**B**). LH, light half; DH, dark half.

6.3 Results

6.3.1 Cone integration

As explained in the previous chapter, transplantation into adult hosts showed the survival of donor cones but did not yield any integrated cones. However, transplantation into neonatal eyes resulted in successful integration. This was characterised by the survival of cones in the subretinal space with expression of the GFP and dsRed reporter and extension of processes towards and into the host ONL (Figure 6.4). The remainder of the dsRed-positive donor cells that did not express GFP were all other retinal cells aside from M cones and rods, the former that would necessarily have shown GFP expression and the latter having degenerated due to the underlying *rd1* mutation.

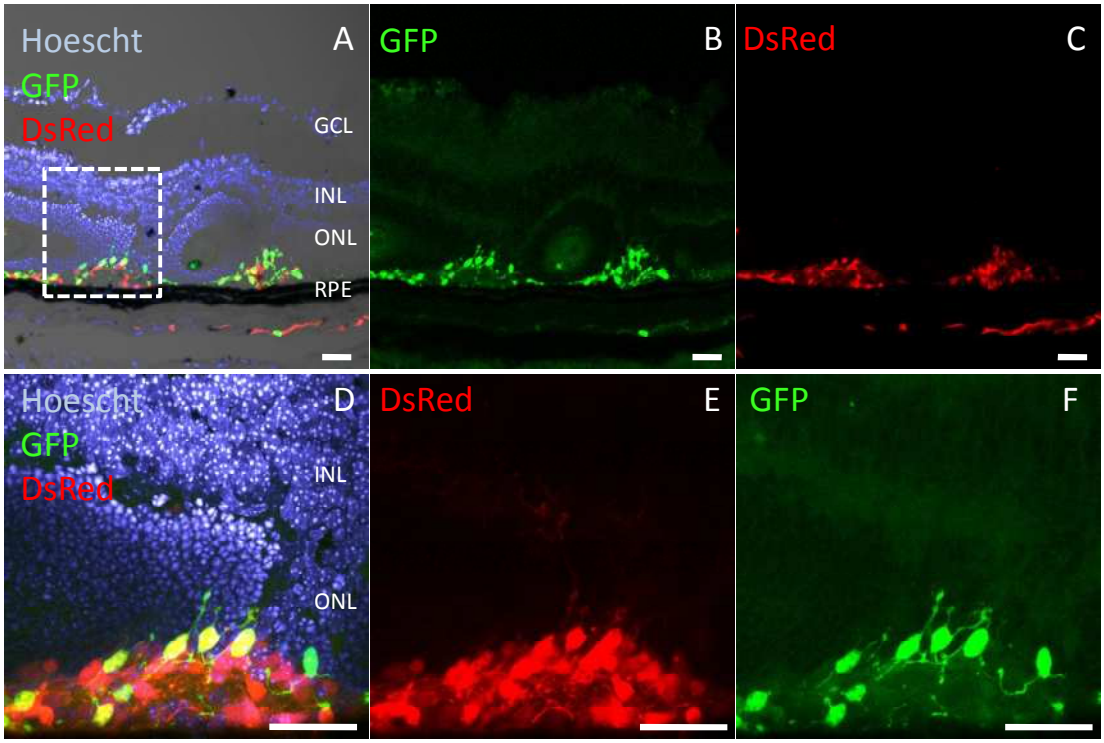

Figure 6.4. Retinal sections showing the survival of transplanted subretinal GFP-dsRed cones. The panel demonstrates the results following transplantation of Opn1-

EGFP-dsRed retinal cells into the wild type subretinal space. As per the results seen following injection into adult hosts, although donor cones do not express GFP at the time of transplantation, at the stage of sectioning, GFP expression is obvious within the donor cells, as is the expression of dsRed (**A-C**). A difference seen between adult and postnatal hosts was the greater disruption of the host ONL occurring in the latter, with the ONL often folded into whorls at the site of injection (an example of this is seen to the right of the dashed box in **A**). The findings within the area of the dashed box have been enlarged showing the extension of processes from cones towards and into the host ONL (**D-F**). Scale bar: 20μm.

Analysis of integration

Integration values for transplanted GFP-positive cones (median = 17.5 cells, range of number of cones observed per retina = 5-32) were lower than for other dsRed cells (median = 92.0 cells, range of number of cells observed per retina = 52-165). This difference (P = 0.0002, Mann-Whitney U test) was expected since GFP-positive cones constituted a small proportion of the total number of transplanted cells (Figure 6.5). For the same reason, a difference was observed (*P* = 0.0002, Mann-Whitney U test) in the number of subretinal donor GFP-positive cones (median = 210.5 cells, range of number of cones observed per retina = 103-566) compared to the number of other dsRed cells (median = 1584 cells, range of number of cells observed per retina = 640-2670). Taking into account these findings, no difference was observed in the ratio of GFP cones to dsRed cells within the integrated or subretinal population (P =0.854, Mann-Whitney test).

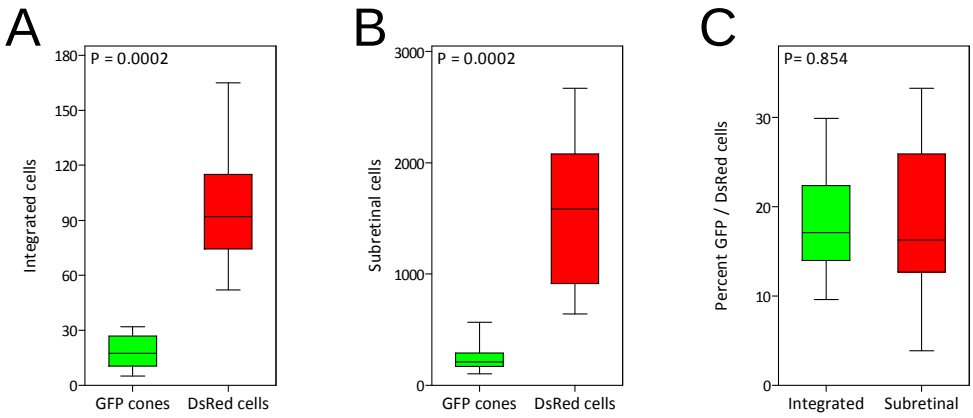

Figure 6.5. Analysis of integrated and subretinal cells following transplantation of GFP-dsRed cones. Fewer GFP cones integrated (A) or were present in the subretinal space (B) compared to accompanying dsRed cells. However, the proportion of GFP to dsRed cells was no different between the integrated and subretinal group (C). Horizontal bars indicate the median value. N = 8 per group, Mann-Whitney test.

Morphology

Evidence of transplanted cones was apparent from a number of morphological features (Figure 6.6). In addition to the presence of the GFP and dsRed fluorophore that was absent from the surrounding host retina, donor cones were arranged in an atypical location. In some instances, the cell body was located in the subretinal space and in other cases, it was seen in the inner part of the ONL, both being irregular for cone position. From donor cell bodies located within the host ONL, an extension was orientated towards either the RPE or OPL, representing the inner and outer cone process (Figure 6.7 A-D). From subretinal cells, an extension was seen to pass through the host ONL towards the OPL (Figure 6.7 E-H). This extension appeared to represent an inner process as it terminated in a configuration similar to a broad cone pedicle. However, where the latter was not apparent, the extension may have represented an outer segment orientated in the opposite direction to a

regular cone. Anti-recoverin staining confirmed the identity of the transplanted cells as photoreceptors with localisation of the antibody to the cell membrane (Figure 6.11).

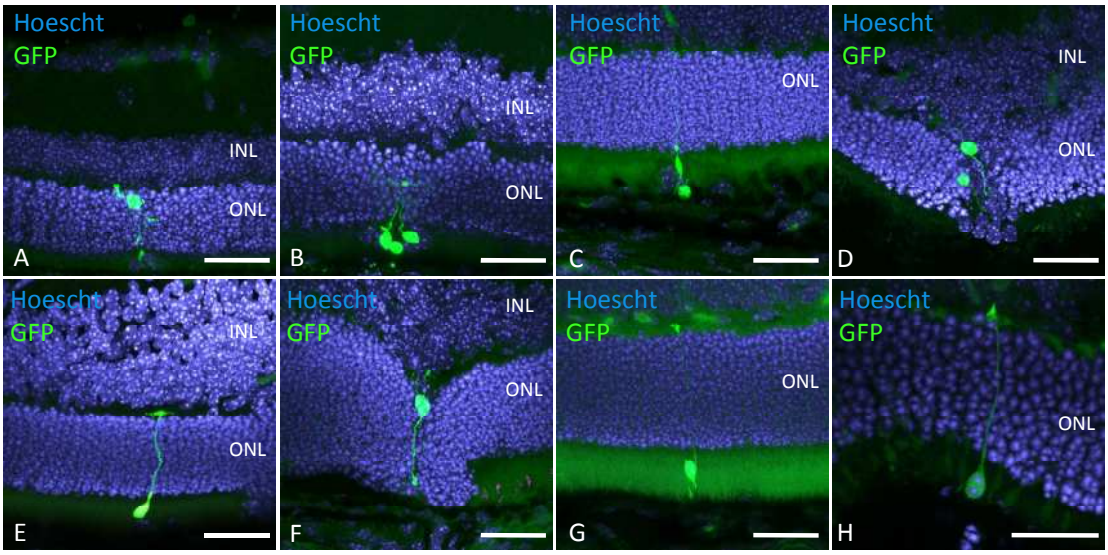

Figure 6.6. Successful integration of cone photoreceptors. This panel summarises the representative examples of GFP-positive cones that have integrated into the host retina. The dsRed component has been omitted for clarity. All cones demonstrate normal morphology albeit in an abnormal location. Each example is explained in more detail with corresponding IHC in later sections. Scale bar: 40µm.

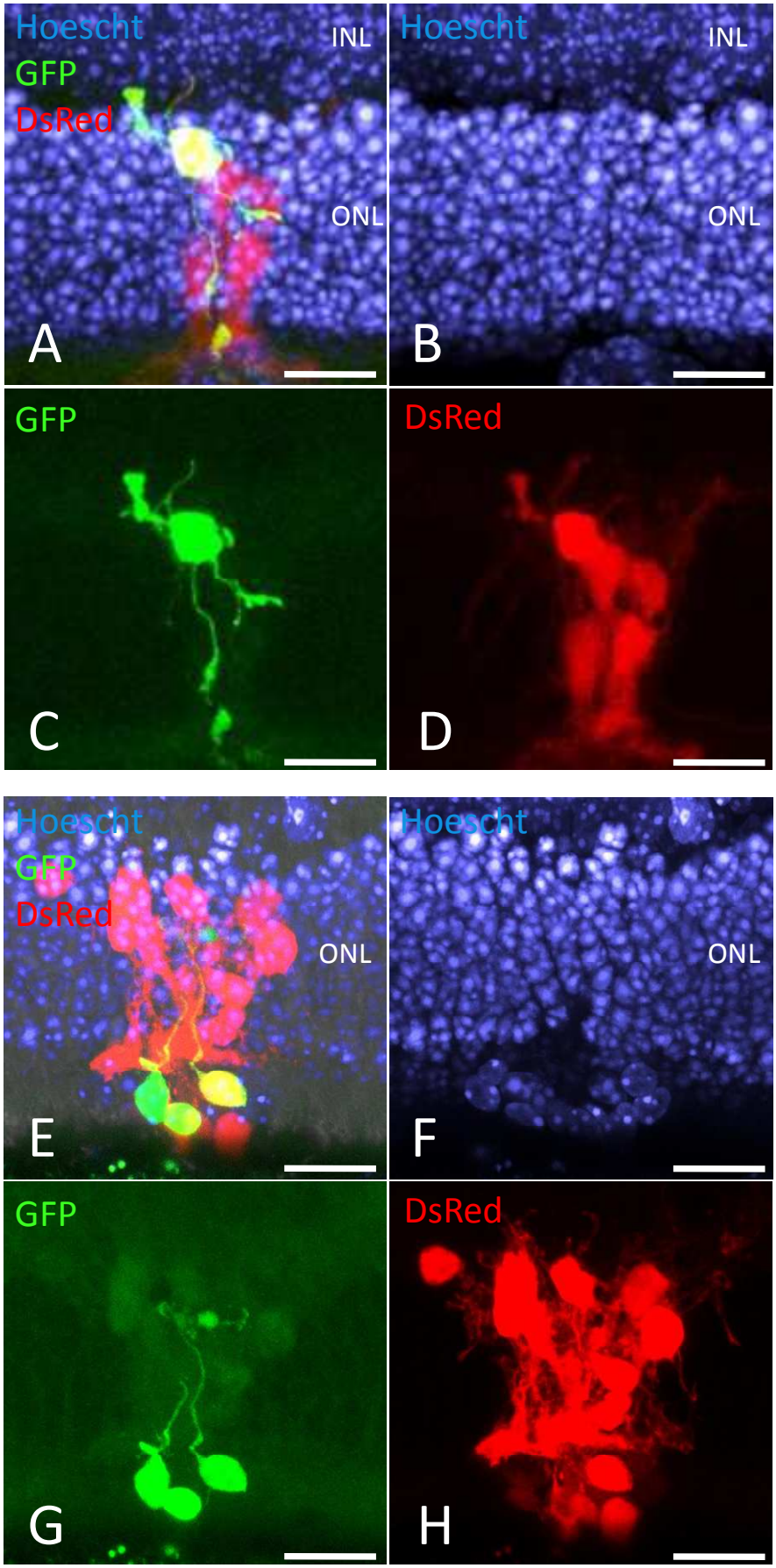
Hoescht
GFP
DsRed
INL
ONL
A
Hoescht
INL
ONL
B
GFP
C
DsRed
D
Hoescht
GFP
DsRed
ONL
E
Hoescht
ONL
F
GFP
G
DsRed
H

Figure 6.7. High power confocal micrographs of integrated cones. An integrated GFP-dsRed cone is shown in the host ONL with surrounding accompanying dsRed donor cells (**A-D**). Under normal circumstances, cone nuclei are distributed towards the outer part of the ONL. However, in this example, the donor cone nucleus is situated at the inner part of ONL, with a process extending in both directions towards the RPE and outer plexiform layer. A second example demonstrates a cluster of integrated GFP-dsRed cones with correct orientation of processes towards the host outer plexiform layer (**E-H**). Of note, the nuclei of these donor cones lie in the subretinal space (**F**) confirming that these cells are exogenously derived. Again, numerous donor dsRed cells are associated with this cluster. Scale bar: 15µm.

Cone markers

As expected, anti-arrestin antibody colocalised to the entirety of the integrated GFP-positive cone. The example in Figure 6.8 shows a subretinal cell body with a presumed inner process extending through the ONL towards a terminal bulb representing a cone pedicle.

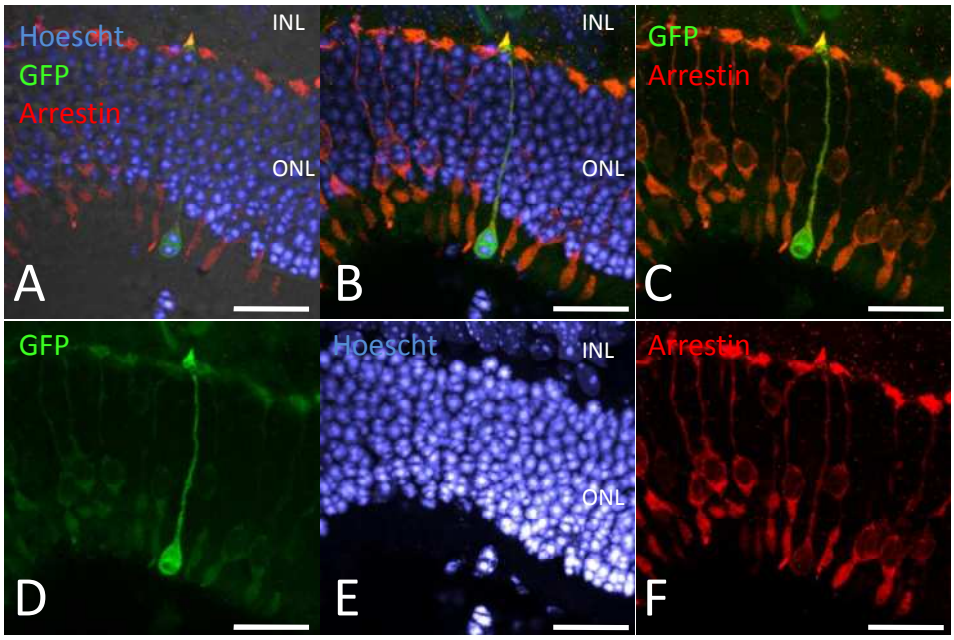

Figure 6.8. Arrestin staining of an integrated GFP-positive cone. This panel of images shows an example of an integrated cone derived from an Opn1-EGFP donor with its cell body and nucleus located within the subretinal space (**A**, **B**, **E**). A process extends through the entire ONL towards a cone pedicle at the outer plexiform (**D**). The entirety of the donor cone stains positive for anti-arrestin antibody in a similar pattern to surrounding host cones (**C**, **F**). Scale bar: 20µm.

Integrated cones formed outer segments as evidenced by the presence of anti-RG opsin staining. In Figure 6.9, the antibody is shown to colocalise to the outer segment which is upside down in terms of its location towards the host OPL. Figure 6.10 shows scattered antibody staining within the subretinal donor mass containing GFP-positive cones.

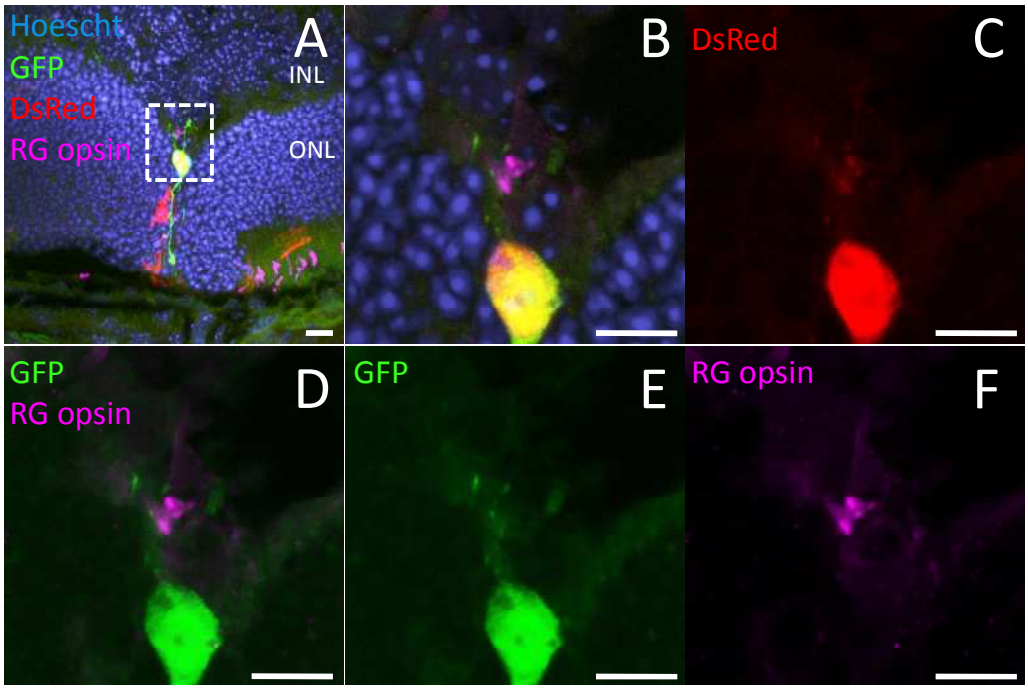

Figure 6.9. RG opsin staining of an integrated GFP-dsRed cone. A single GFP-dsRed-positive cone is shown here with the cell body at the inner part of the host ONL and a process extending through the entire ONL orientated towards the RPE rather than the outer plexiform layer (**A**). The features seen within the dashed box (**A**) have been enlarged (**B**-**F**) to enable closer inspection of RG opsin staining. The abnormal location of RG opsin staining towards the outer plexiform layer (**B**, **D**, **F**) rather than in the layer of host cone outer segments confirms the exogenous derivation of this cone, as does its being dsRed-positive (**C**). Scale bar: 10µm.

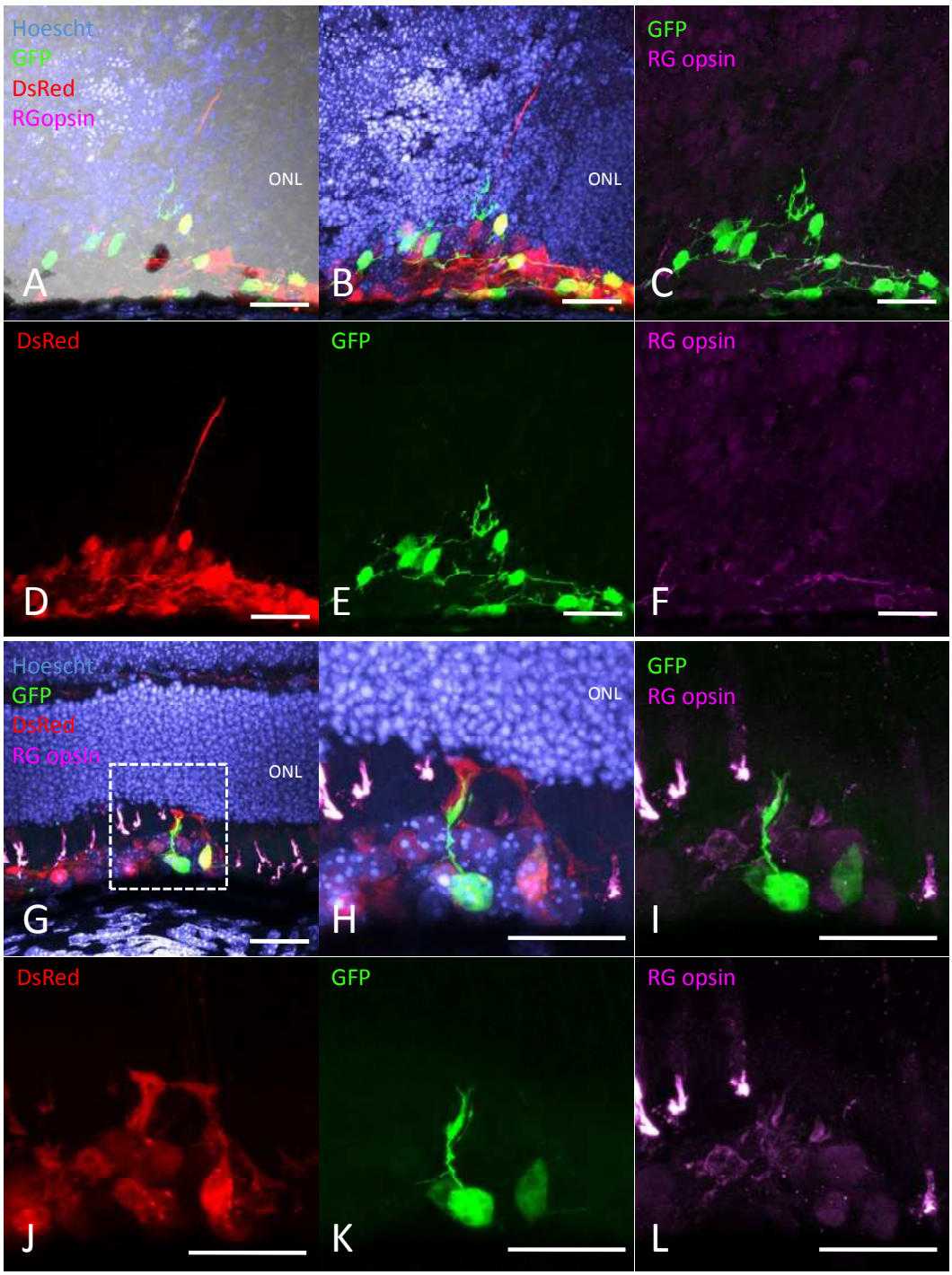

Figure 6.10. RG opsin staining following transplantation of GFP-dsRed cones. Two examples are shown in separate panels (**A**-**F** and **G**-**L** respectively), both of which show RG opsin staining within the subretinal mass of transplanted cells. The antibody colocalises to the outer segments of GFP-positive cones. The area within the dashed rectangle (**G**) has been enlarged in images **H**-**L**. Scale bar: 20µm.

Anti-recoverin antibody colocalised to the membrane of the integrated cone cell body (Figure 6.11). Likewise, positive staining was observed in subretinal GFP-positive cones with minimal staining of other dsRed donor cells (Figure 6.12). This was expected given the absence of rods from the transplanted mass, in contrast to the observation of abundant staining in transplanted Opn1-EGFP cells as described previously.

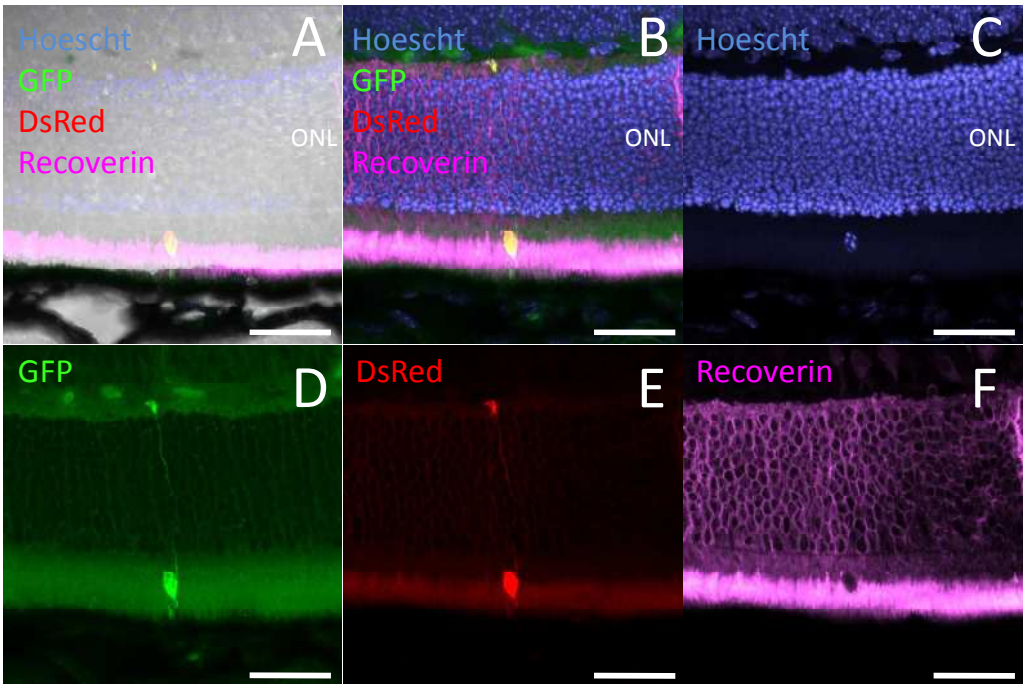

Figure 6.11. Recoverin staining of an integrated GFP-dsRed cone. A single GFP-dsRed-positive cone is seen with its cell body in the subretinal space abutting the RPE (**A**). An extension representing either an inner process or outer segment passes through the entire ONL to reach the outer plexiform layer (**B, D**). The exogenous derivation of this cell is confirmed by the subretinal position of the cell nucleus (**C**). This cell is also dsRed-positive, not only acting as a further reporter but also confirming that rods will be absent from the donor cell mass due to the underlying *rd1* mutation (**E**). Anti-recoverin antibody is localised to the cell membrane and therefore the cytoplasm shows no staining (**F**). Scale bar: 20µm.

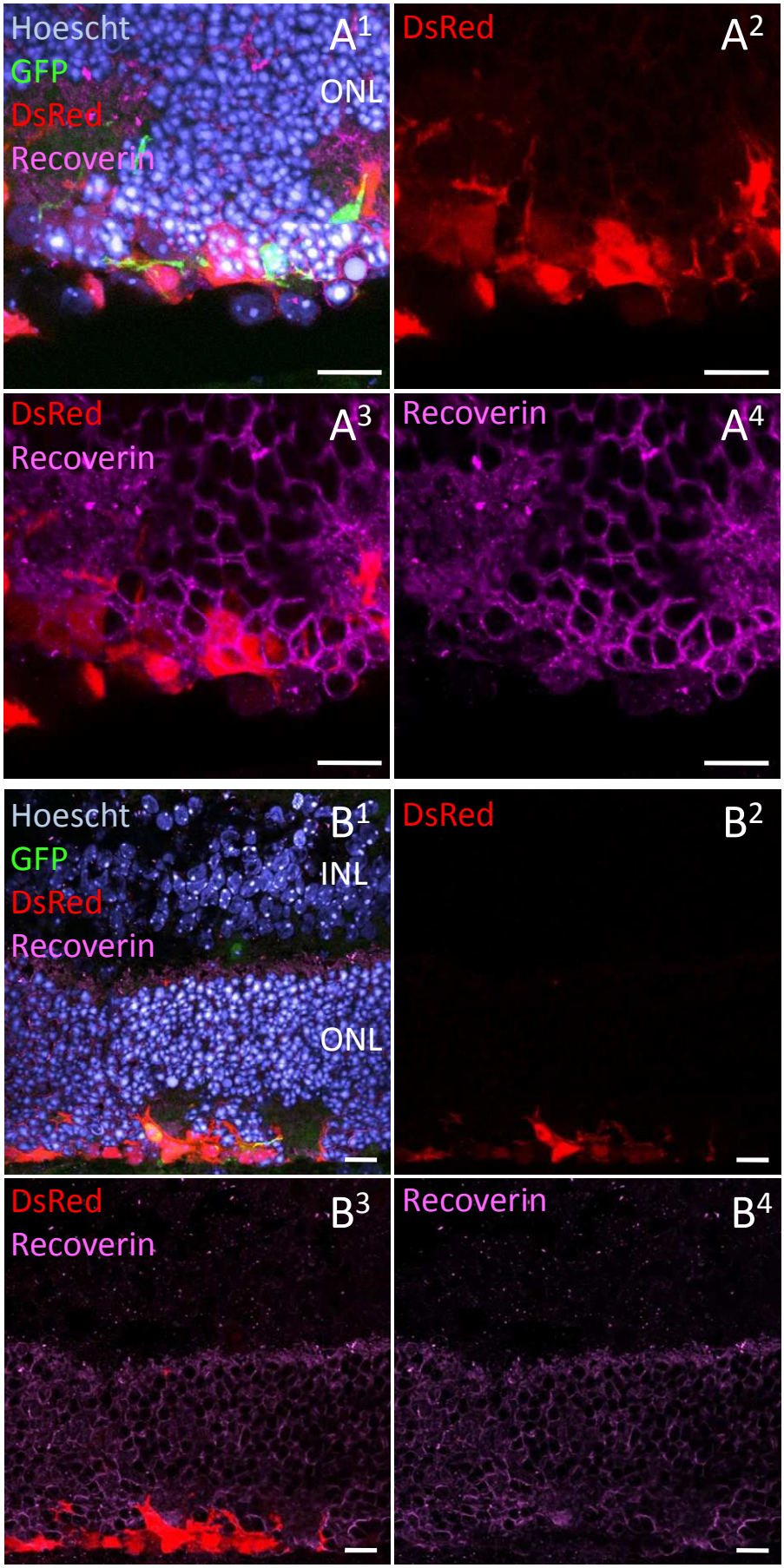
Hoescht
GFP
DsRed
Recoverin
A1
ONL
DsRed
A2
DsRed
Recoverin
A3
Recoverin
A4
Hoescht
GFP
DsRed
Recoverin
B1
INL
ONL
DsRed
B2
DsRed
Recoverin
B3
Recoverin
B4

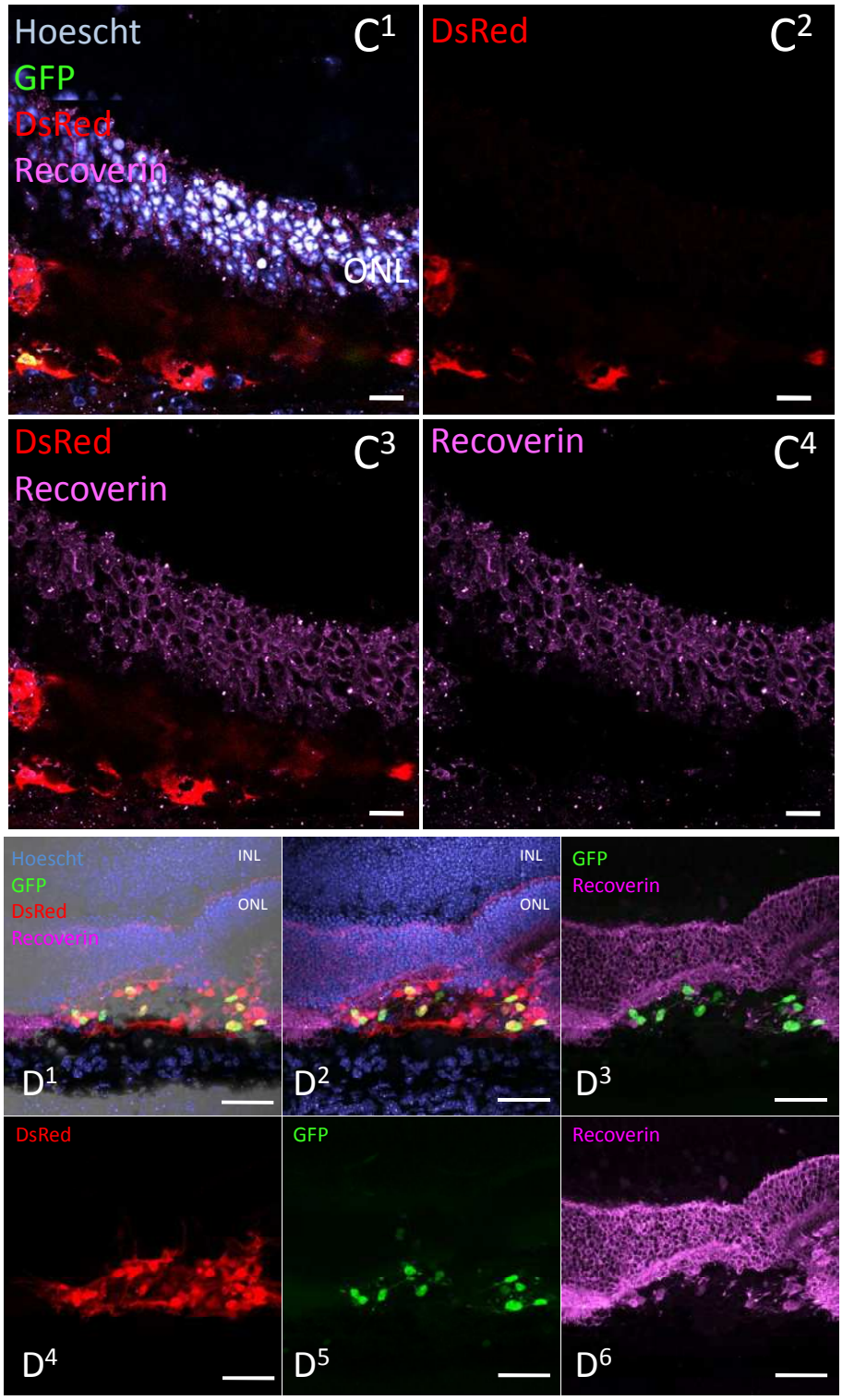

Figure 6.12. Recoverin staining following transplantation of GFP-dsRed cones. Four examples are shown in separate panels, all of which show minimal recoverin staining within the subretinal mass of transplanted cells. In this area, anti-recoverin antibody colocalises to GFP-dsRed cones (as seen) and S-cones. Rods are absent from the donor mass due to the *rd1* mutation. Positive staining is apparent within the host ONL. Scale bar: 20µm.

Glial cells

Anti-GFAP antibody was used to determine the presence of glial cells or activated Müller cells within the donor mass. Integrated GFP-positive cones did not show positive staining (Figure 6.13). However, staining was seen within and associated with the transplanted dsRed cells indicating the presence of glial cells (Figure 6.14). Other dsRed-positive areas showed no staining indicating that these cells were of non-glial origin and likely represented the remainder of donor inner retinal cells (Figure 6.15).

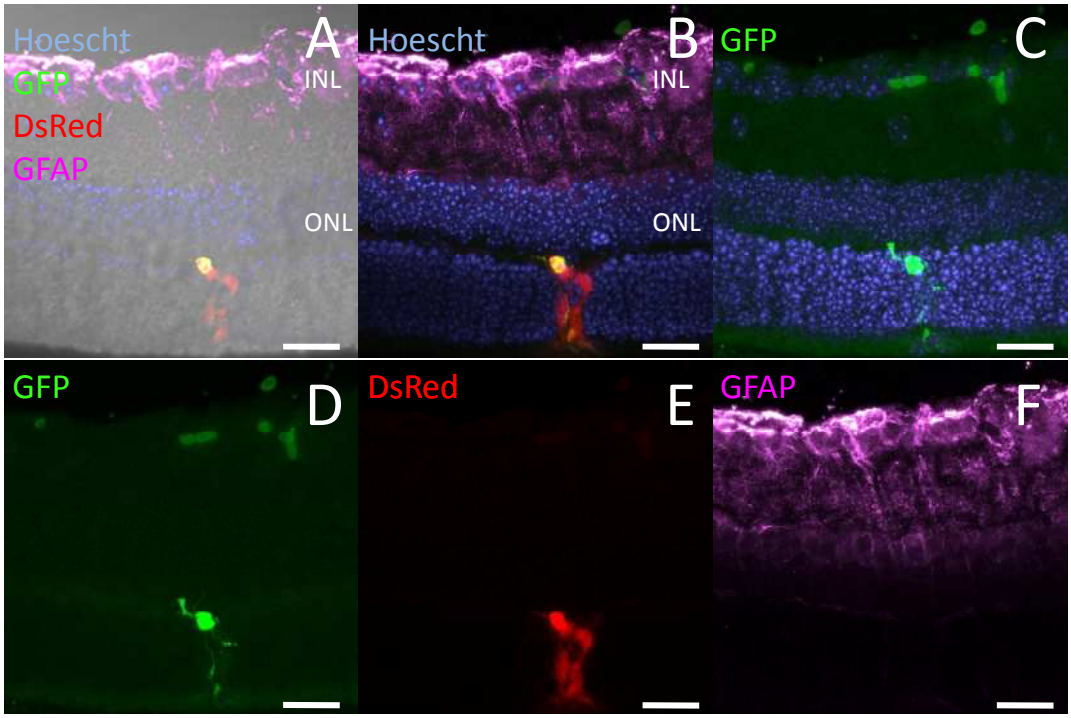

Figure 6.13. GFAP staining in the presence of an integrated GFP-dsRed cone. A single GFP-dsRed-positive cone is shown here with the cell body at the inner part of the host ONL and a process extending through the entire ONL orientated towards the RPE rather than the outer plexiform layer (**A**-**D**). Anti-GFAP antibody colocalises to glial cells towards the inner retina but not to the GFP-dsRed cone. Scale bar: 20µm.

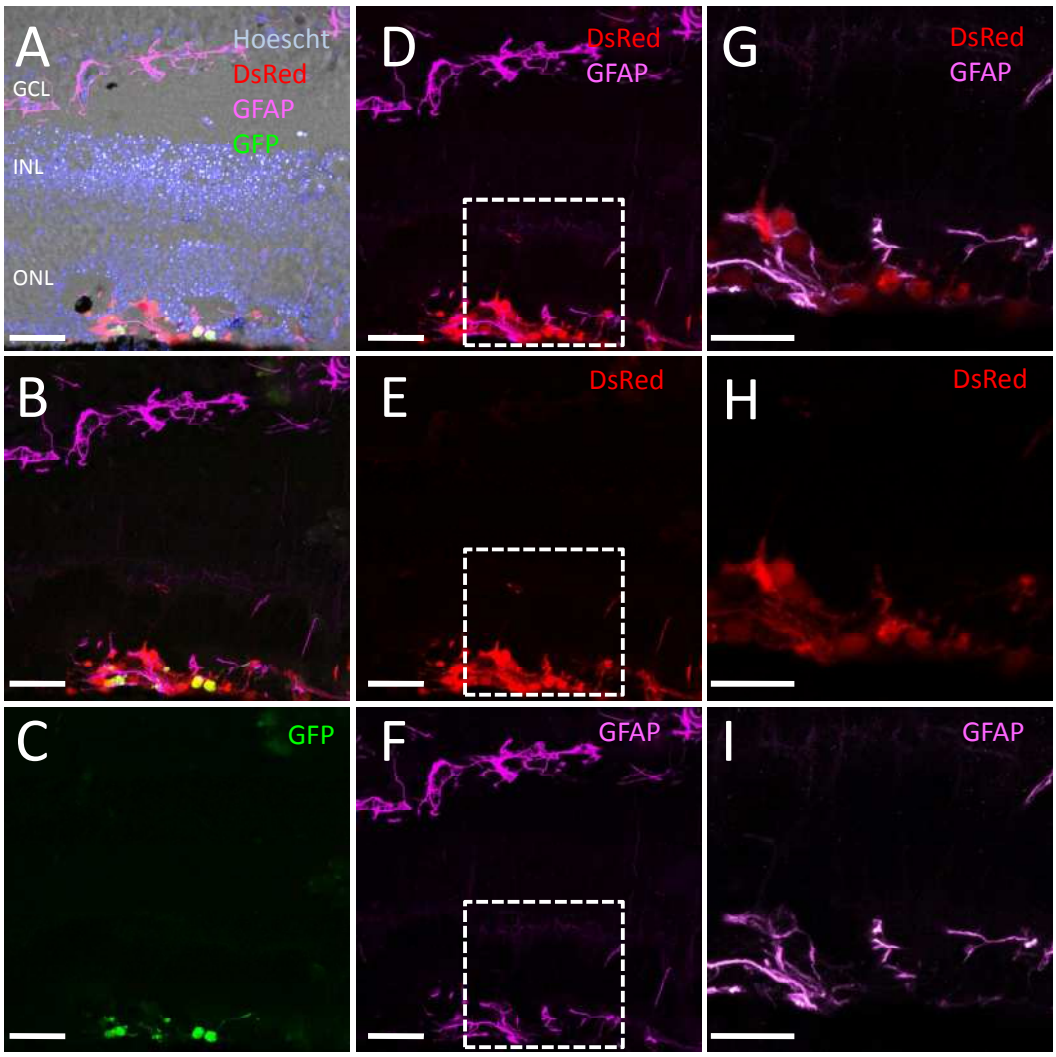

Figure 6.14. GFAP staining following transplantation of GFP-dsRed cones (i).A subretinal mass of transplanted Opn1-EGFP-dsRed cells is seen containing GFP-dsRed cones (**A**-**C**). Anti-GFAP antibody colocalises to the inner retina and to the subretinal space (**D**-**F**). The features within the white dashed rectangles have been enlarged with their corresponding images shown adjacent (**G**-**I**). With regards staining of the subretinal transplant, the antibody colocalises to some dsRed cells but no GFP cones. Scale bar: 20µm.

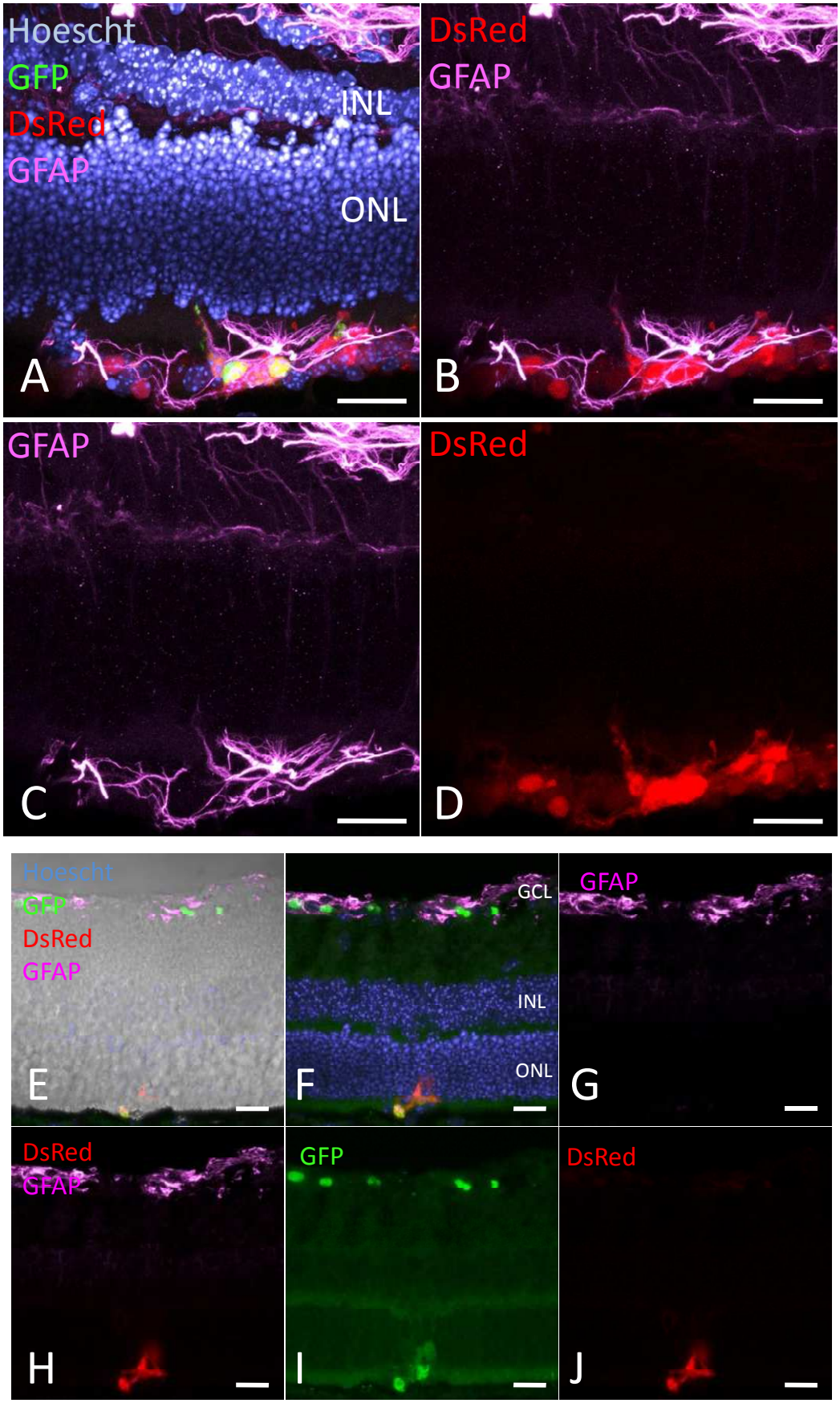
Hoescht
GFP
DsRed
GFAP
INL
ONL
A
DsRed
GFAP
B
GFAP
C
DsRed
D
Hoescht
GFP
DsRed
GFAP
E
GCL
INL
ONL
F
GFAP
G
DsRed
GFAP
H
GFP
I
DsRed
J

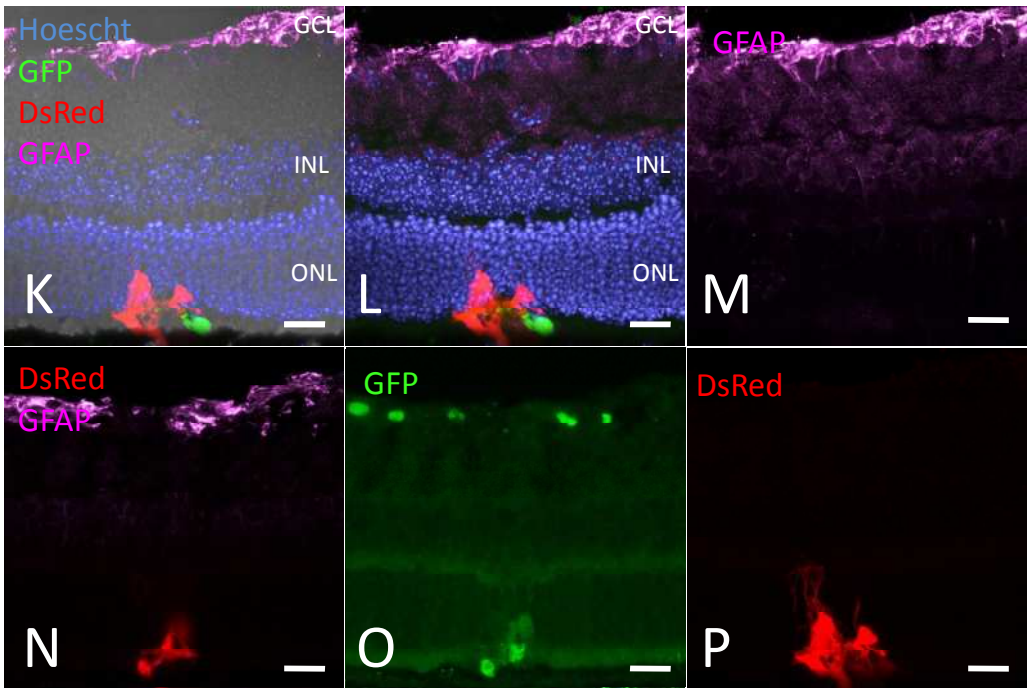

Figure 6.15. GFAP staining following transplantation of GFP-dsRed cones (ii). Three further examples are shown of GFAP staining (**A**-**D**, **E**-**J**, and **K**-**P** respectively). In the first panel, anti-GFAP antibody again colocalises to the inner retina and subretinal space, in the latter staining certain dsRed cells but sparing the GFP cones. In the second and third panel, GFAP staining is limited to the inner retina with no evidence of colocalisation to the subretinal space.

Integrated cones were often associated with a cluster of dsRed-positive donor cells. Anti-glutamine synthetase antibody did not uniformly colocalise to these cells, thereby indicating the scattered location of Müller cells within the donor mass (Figure 6.16-6.18). Importantly, the antibody did not stain donor GFP-positive cells, thereby excluding the possibility of these being Müller cells.

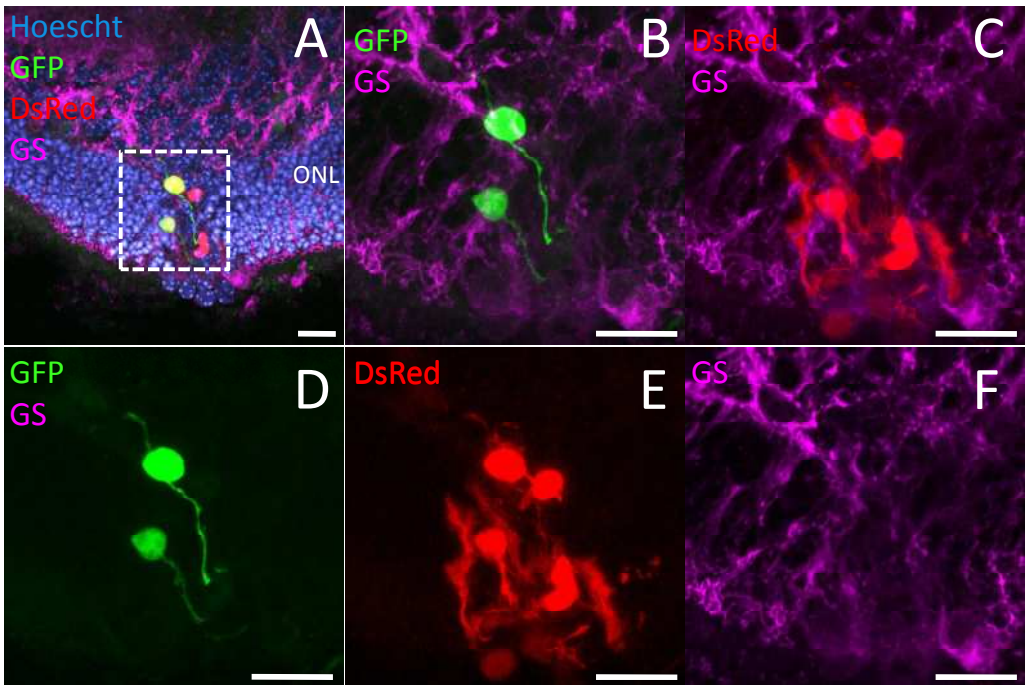

Figure 6.16. Glutamine synthetase staining in the presence of an integrated GFP-dsRed cone (i). A single GFP-dsRed-positive cone is seen with its cell body at the inner part of the host ONL (**A**). A process extends through the entire ONL orientated towards the RPE with a smaller extension directed towards the outer plexiform layer (**B, D**). The abnormal location of this cell confirms its exogenous derivation as does it being dsRed-positive (**C, E**). Anti-glutamine synthetase antibody colocalises to surrounding Müller cells but not to the GFP-dsRed cone (**B, F**). Scale bar: 20µm. GS, Glutamine synthetase.

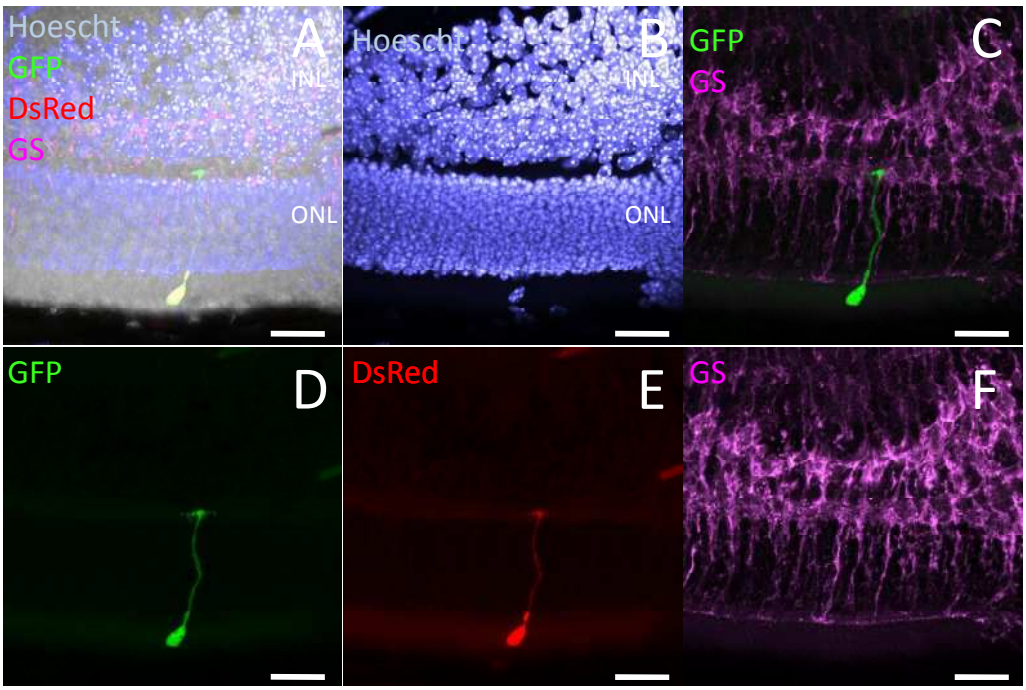

Figure 6.17. Glutamine synthetase staining in the presence of an integrated GFP-dsRed cone (ii). A further example of a single GFP-dsRed-positive cone is provided here showing the cell body and nucleus within the subretinal space (**A**, **B**). A process extends through the entire ONL orientated towards the outer plexiform layer (**C**, **D**). The abnormal location of the cell nucleus confirms its exogenous derivation as does it being dsRed-positive (**E**). Anti-glutamine synthetase antibody colocalises to surrounding Müller cells but not to the GFP-dsRed cone (**C**, **F**). Scale bar: 20µm. GS, Glutamine synthetase.

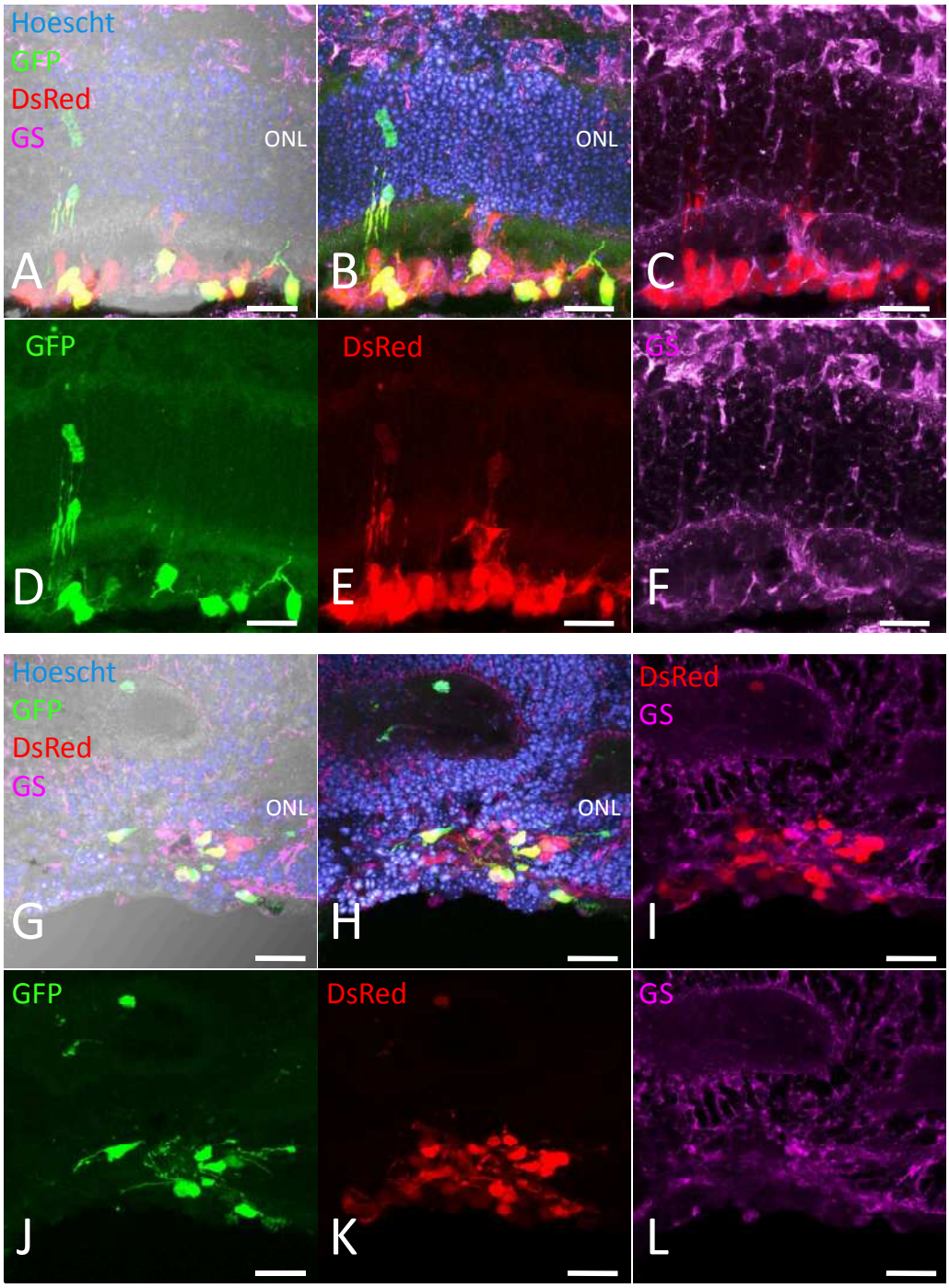
Hoescht
GFP
DsRed
GS
ONL
A
B
C
GFP
DsRed
GS
D
E
F
Hoescht
GFP
DsRed
GS
ONL
G
H
DsRed
GS
I
GFP
DsRed
GS
J
K
L

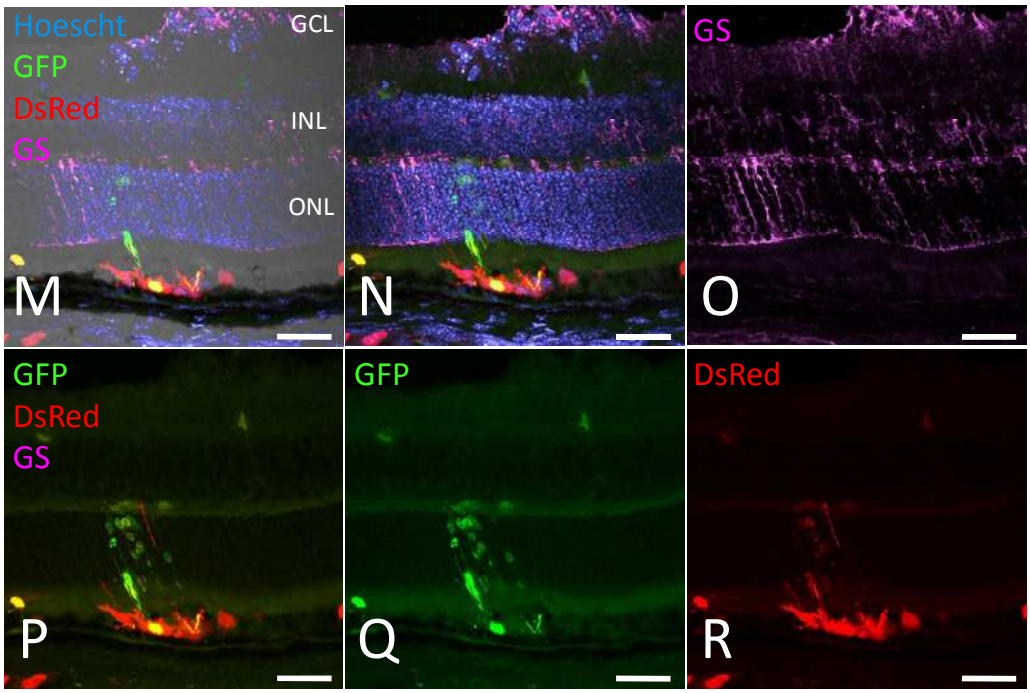

Figure 6.18. Glutamine synthetase (GS) staining following transplantation of GFP-dsRed cones. Three examples are shown in separate panels (**A**-**F**, **G**-**L**, and **M**-**R** respectively), all of which show scattered and minimal GS staining within the subretinal mass of transplanted cells. The antibody identifies Müller cells that extend from their footplates at the inner retina to the external limiting membrane. Scale bar: 20µm.

6.3.2 Fusion

Incidental findings

The experiments involving Opn1-EGFP-dsRed transplants into wild type hosts was accompanied by the observation of possible fusion events in addition to integration. Although more definitive results to confirm this process are described later, the incidental findings at this initial stage were characterised by the presence of well-organised GFP- and dsRed-positive cells within the host ONL (Figure 6.19). These cells were aligned in the same orientation as the host cells with a cell body located towards the inner zone of the host ONL and an appearance similar to host rods with a spherular synapse. The GFP and dsRed fluorescence of these cells was of lower

intensity compared to that of subretinal donor cells, evidenced by the background autofluorescence from surrounding tissue.

Aside from the purported fused cells often being associated with a clump of donor dsRed cells in the near vicinity, they stained positive for the pan-photoreceptor marker, recoverin (Figure 6.20). However, no arrestin staining was noted in these cells, thereby excluding the likelihood of their being cones (Figure 6.21).

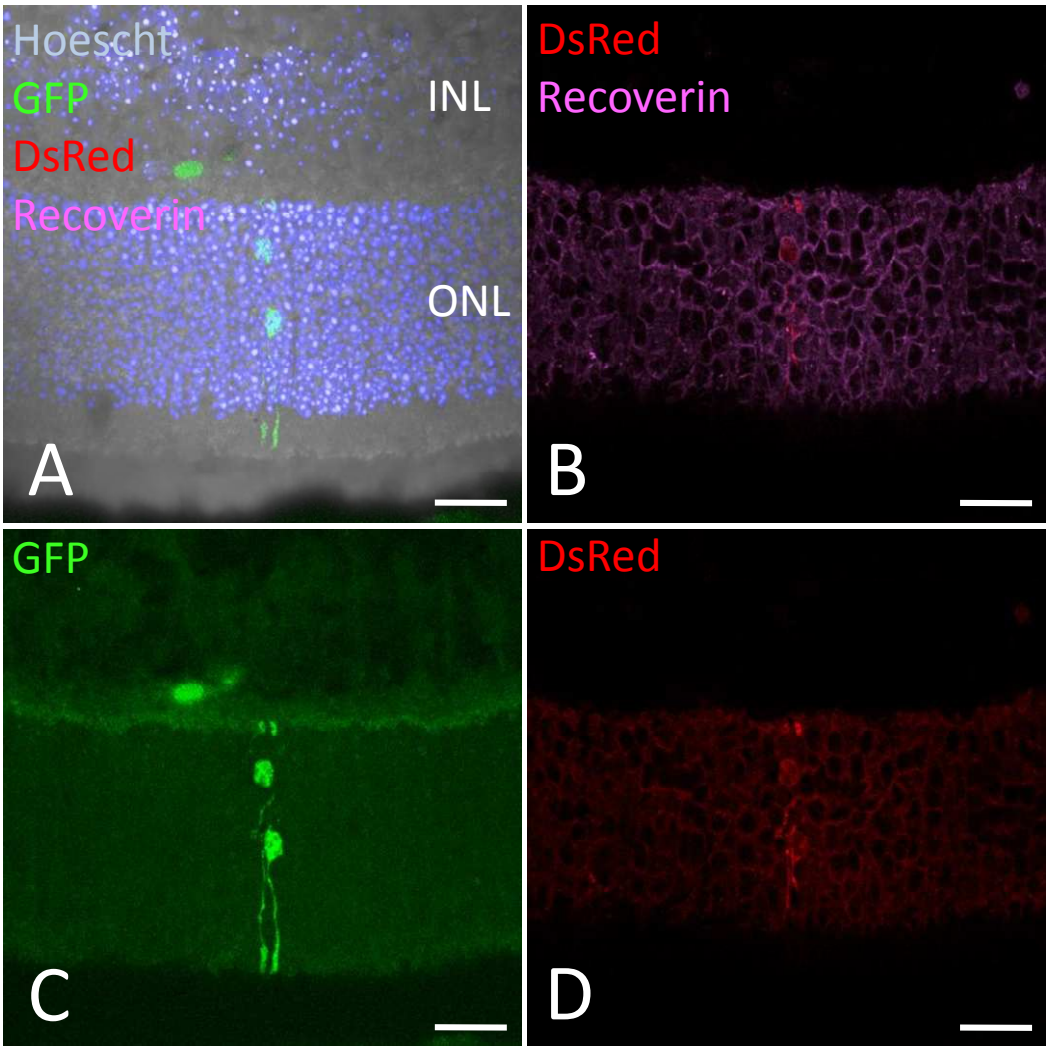

Figure 6.19. GFP and dsRed expression by host photoreceptors post transplantation with recoverin staining (i). Following transplantation of GFP-dsRed cones into a wild type retina, a number of host photoreceptors showed expression of GFP and dsRed protein. This figure shows two vertically orientated GFP-dsRed-positive photoreceptors (**A**) that stain positive for anti-recoverin antibody (**B**) and have rod-

like morphology due to the position of their cell bodies towards the inner part of the ONL and due to their having spherules (**C**). Additionally, there is no disruption of the ONL. The dsRed expression is of lower intensity than that seen in donor cells as determined by the surrounding signal that has been increased in order to show positivity within the ectopically-expressing cells (**D**). Scale bar: 20µm.

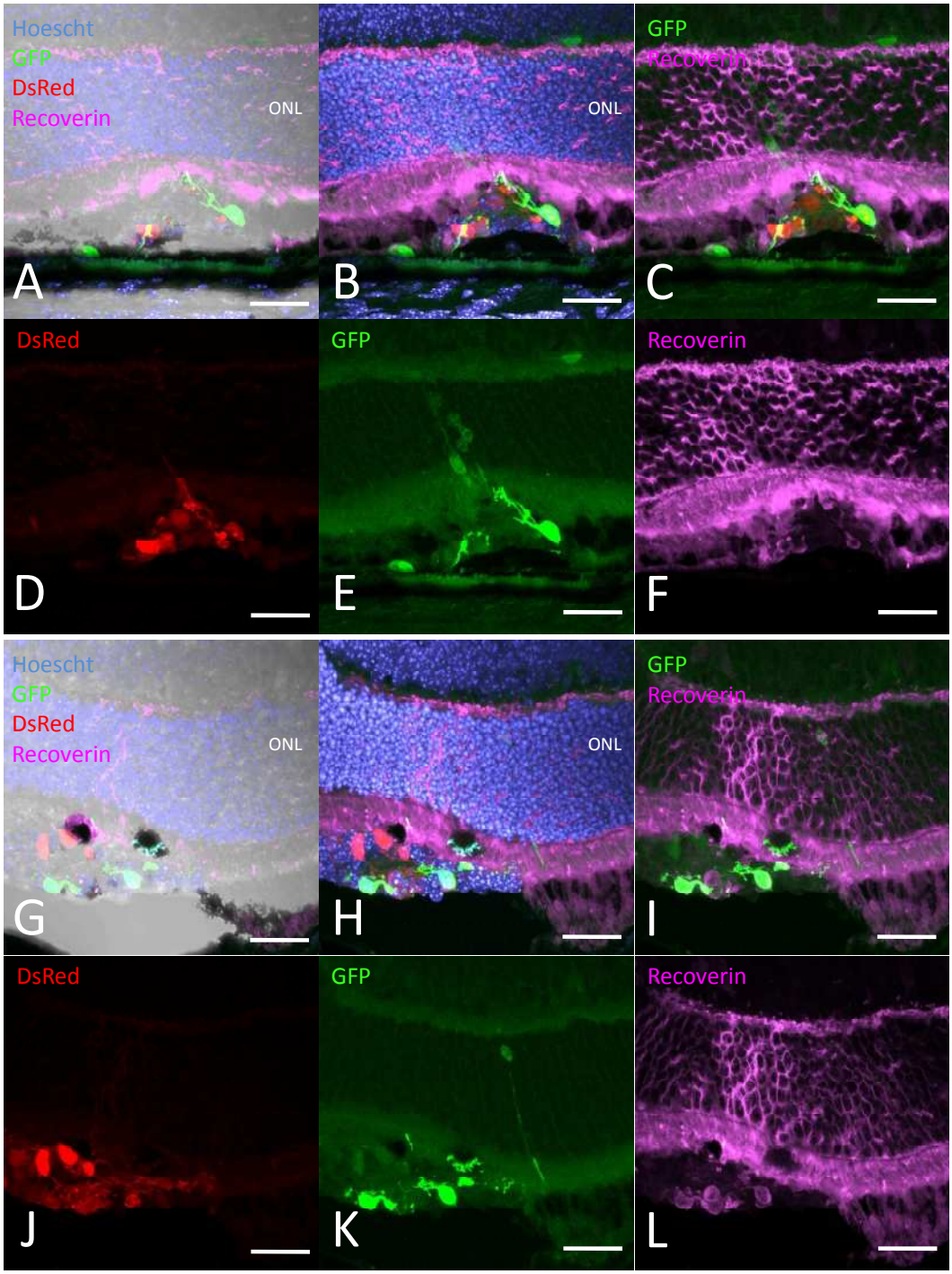

Figure 6.20. GFP and dsRed expression by host photoreceptors post transplantation with recoverin staining (ii). Two further examples are shown of host photoreceptors that express GFP and dsRed protein (**A**-**F** and **G**-**L** respectively). The first panel shows a cluster of cells within the host ONL that weakly express dsRed (**D**) and GFP (**E**). The

second panel shows a single photoreceptor with a cell body at the innermost part of the host ONL that also shows weak expression of dsRed (**J**) and GFP (**K**). Both examples show a subretinal cluster of transplanted donor GFP-dsRed cells. However, the fluorescent intensity of these cells is higher than that of cells within the ONL, which also stain positive for recoverin. Scale bar: 20µm.

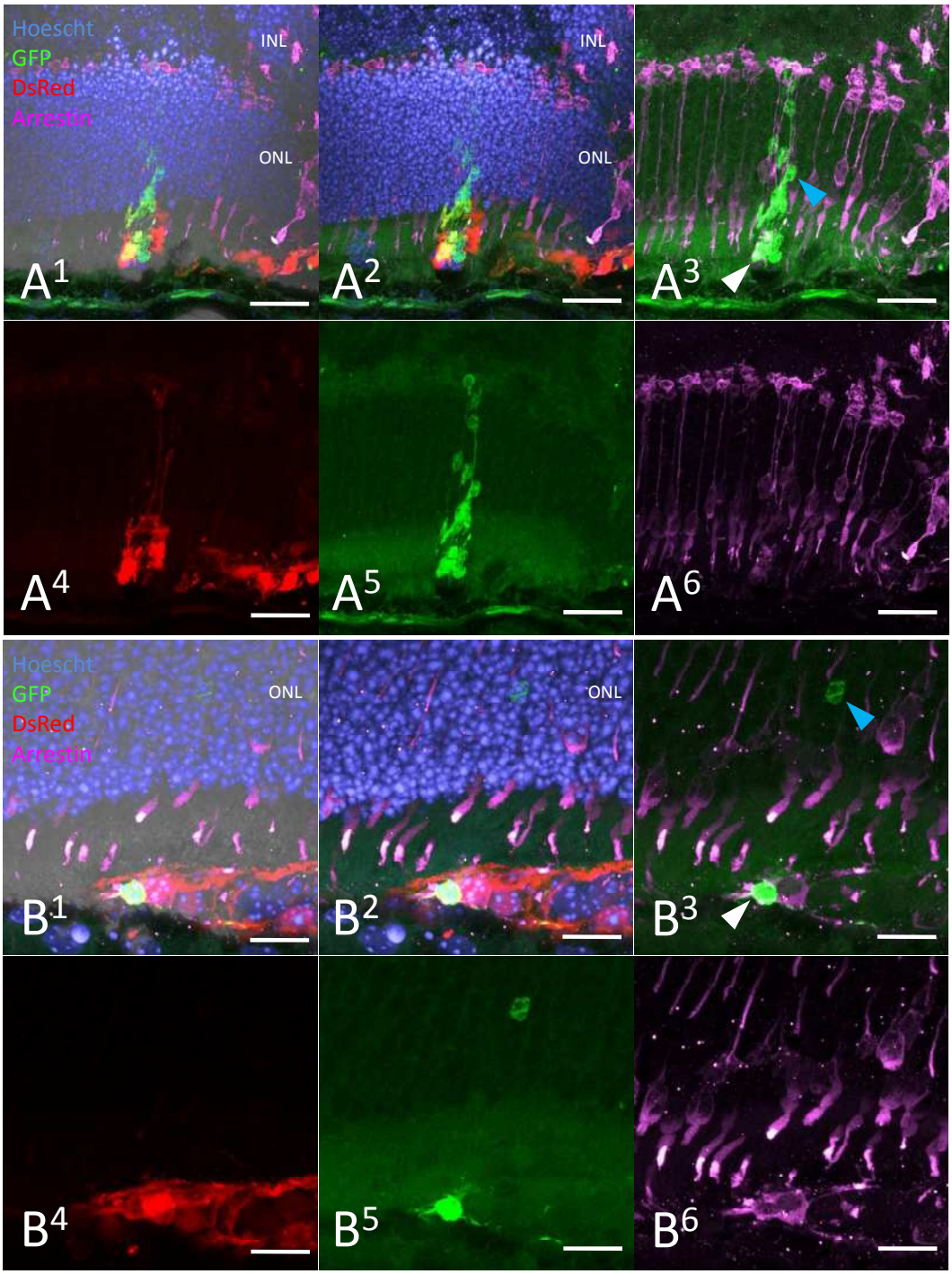

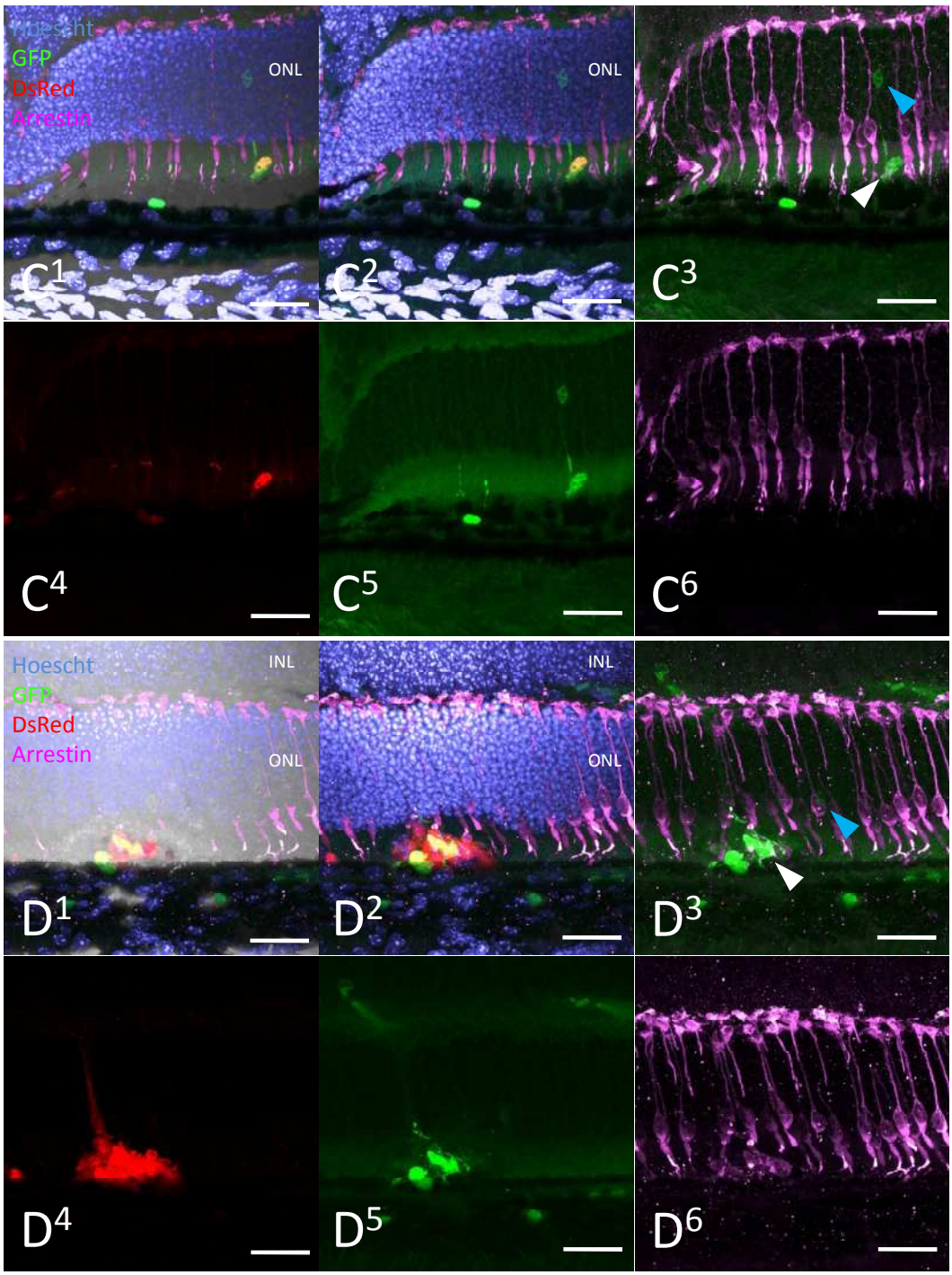

Figure 6.21. GFP and dsRed expression by host photoreceptors post transplantation with arrestin staining. Four examples are shown of host photoreceptors that express GFP and dsRed protein with arrestin staining (**A**-**D**). Each panel shows a subretinal donor cell (or cluster; white arrowhead) that is both GFP-dsRed- and arrestin-positive. Within the host ONL are cells that weakly express dsRed and GFP (blue arrowhead). The latter cells do not stain positive for arrestin, unlike the subretinal GFP-dsRed cones that are arrestin-positive. Scale bar: 20µm.

Observations following the causation of fusion

As described previously, experiments were conducted to potentially cause cell fusion. To do this, dissociated retinas from P1 dsRed (non-GFP) mice carrying the *rd1* mutation were injected into the subretinal space of P1 Nrl-GFP mice. As the two fluorophores were mutually exclusive in their tissue expression, any cells expressing both reporters could only have arisen by the process of cell fusion. Since all Nrl-GFP cells were rod photoreceptors, an additional hypothesis was that any GFP-positive cells within the ONL that also expressed dsRed were fused host rods since donor rods were absent owing to the *rd1* mutation.

At three weeks following transplantation, a clear distinction was seen between the host GFP-positive ONL and the transplanted dsRed-positive cells within the subretinal space (Figure 6.22). Overlying the transplanted area were examples of fused cells that were characterised by co-expression of the GFP and dsRed reporter (Figure 6.23). These cells were often associated with adjacent subretinal dsRed-positive donor cells. Although a positive internal control of arrestin staining was seen within the host ONL, no staining was observed in cells that co-expressed the GFP and dsRed reporter, thereby confirming that these were not cones and could only be rods (Figure 6.24). Conversely, positive arrestin staining was seen in transplanted dsRed-positive cells that did not show GFP-expression, thereby confirming that these were cones and not rods (Figure 6.25).

Integration of dsRed cells was observed in the neonatal Nrl-GFP host (median = 80.5 cells; range of total number of integrated dsRed cells per retina = 62-152) but not in the adult host (Figure 6.26). In comparison, the number of fused cells was similar in

the neonatal (median = 37 cells; range of total number of fused dsRed cells per retina = 15-69) and adult host (median = 54 cells, range of total number of fused dsRed cells per retina = 24-90, *P* = 0.0002, Mann-Whitney test). Therefore, in the neonatal host, integrated cells were approximately treble the number of fused cells.

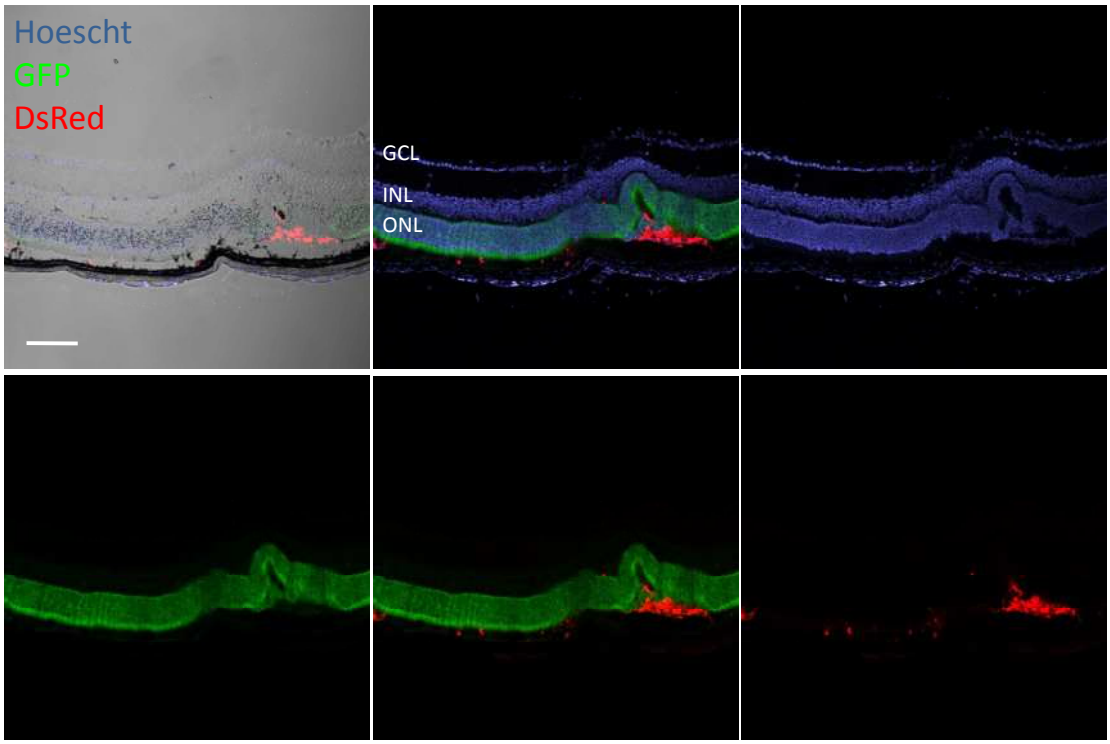

Figure 6.22. Subretinal transplantation of dsRed retinal cells into Nrl-GFP hosts. A clear demarcation is seen between donor dsRed cells within the subretinal space and the host Nrl-GFP ONL. Each fluorophore is restricted to its cell of origin. Scale bar: 50µm.

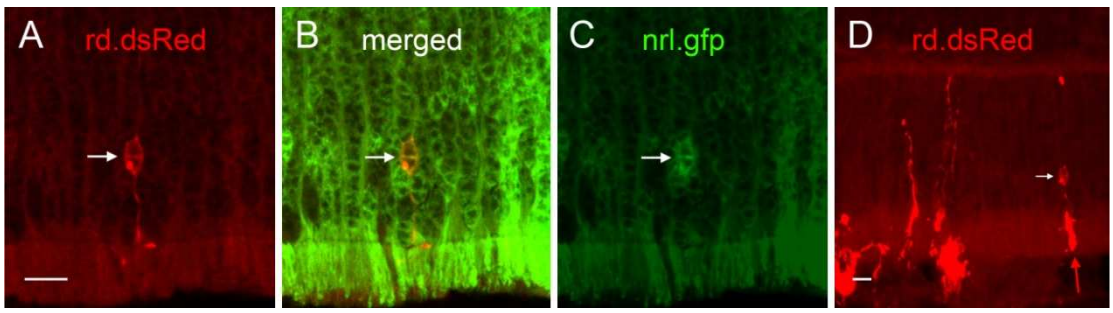

Figure 6.23. Example of cell fusion. A cell (white arrow) with a profile similar to that of host cells in terms of cell body location, alignment of processes, and a spherular

synapse, is seen within the host ONL. This cell shows both dsRed and GFP expression (**A**-**C**) and is intimately associated with a subretinal cluster of dsRed-positive cells (red arrow – **D**). Scale bar: 10µm.

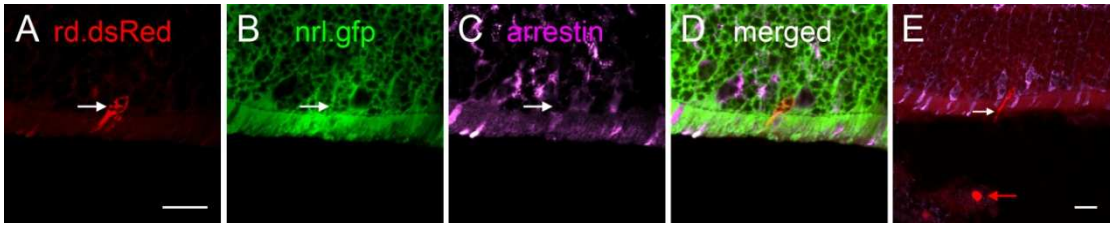

Figure 6.24. Negative arrestin staining following cell fusion. A GFP-positive host cell (white arrow) within the ONL also shows dsRed expression (**A**, **B**). This cell does not stain positive for arrestin (**C**-**D**). However, the window defects within the host ONL that are GFP-negative show arrestin staining thereby providing an internal control to identify the location of cone photoreceptors. A subretinal clump of dsRed donor cells is present in close proximity (red arrow - **E**). Scale bar: 10µm.

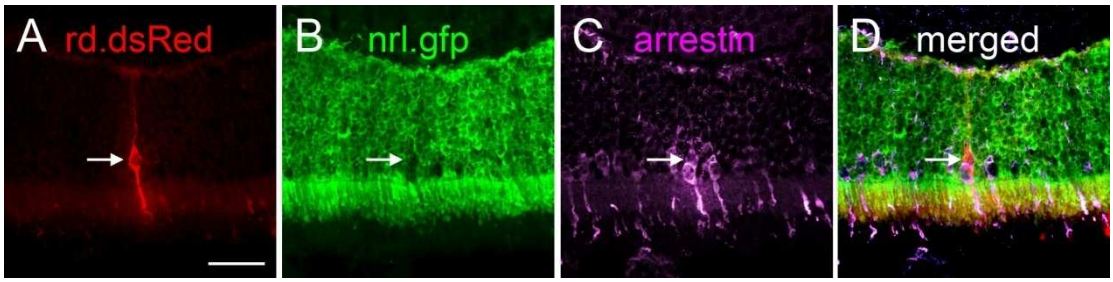

Figure 6.25. Transplanted cone in cell fusion experiment. A dsRed-positive cell (white arrow - **A**) is seen within the host ONL that is located within a window area that is GFP-negative (**B**). This cell stains positive for cone arrestin (**C**, **D**). Scale bar: 20µm.

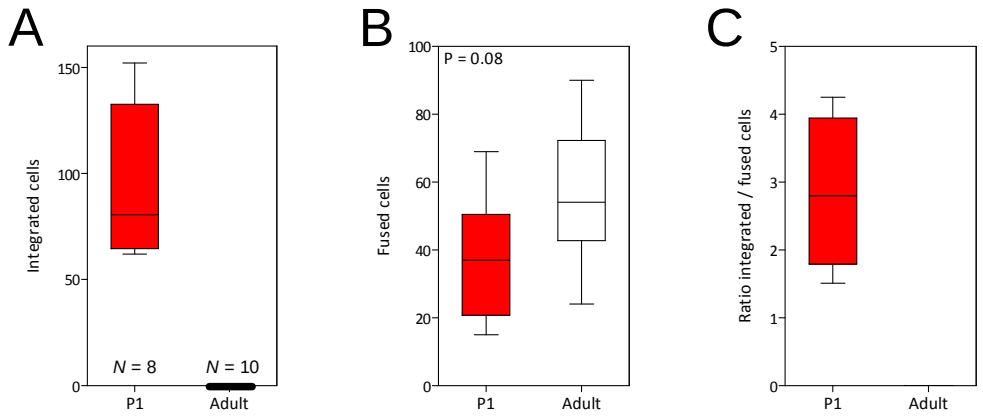

Figure 6.26. Analysis of integrated and fused cells following transplantation of dsRed cells. Although dsRed cells integrated in the neonatal retina, no integration occurred in the adult host (**A**). A similar number of fusion events was observed in the neonatal and adult host (*P* = 0.08, Mann-Whitney test, **B**). In the neonatal host, the number of integrated cells per eye was approximately treble that of fused cells (**C**).

6.3.3 Functional effects following cone transplantation

In order to study the effect of cone transplantation on visual function, P1 Opn1-EGFP-dsRed retinal cells were transplanted into the subretinal space of P1 TKO mice.

Morphology

Anti-CNGA3 antibody colocalised to the putative outer segment of transplanted cones (Figures 6.27 and 6.28). As a positive internal control, staining was absent from the outer segment of host cones as expected in the TKO (*OPN4*$^{-/-}$ *GNAT1*$^{-/-}$ *CNGA3*$^{-/-}$) retina.

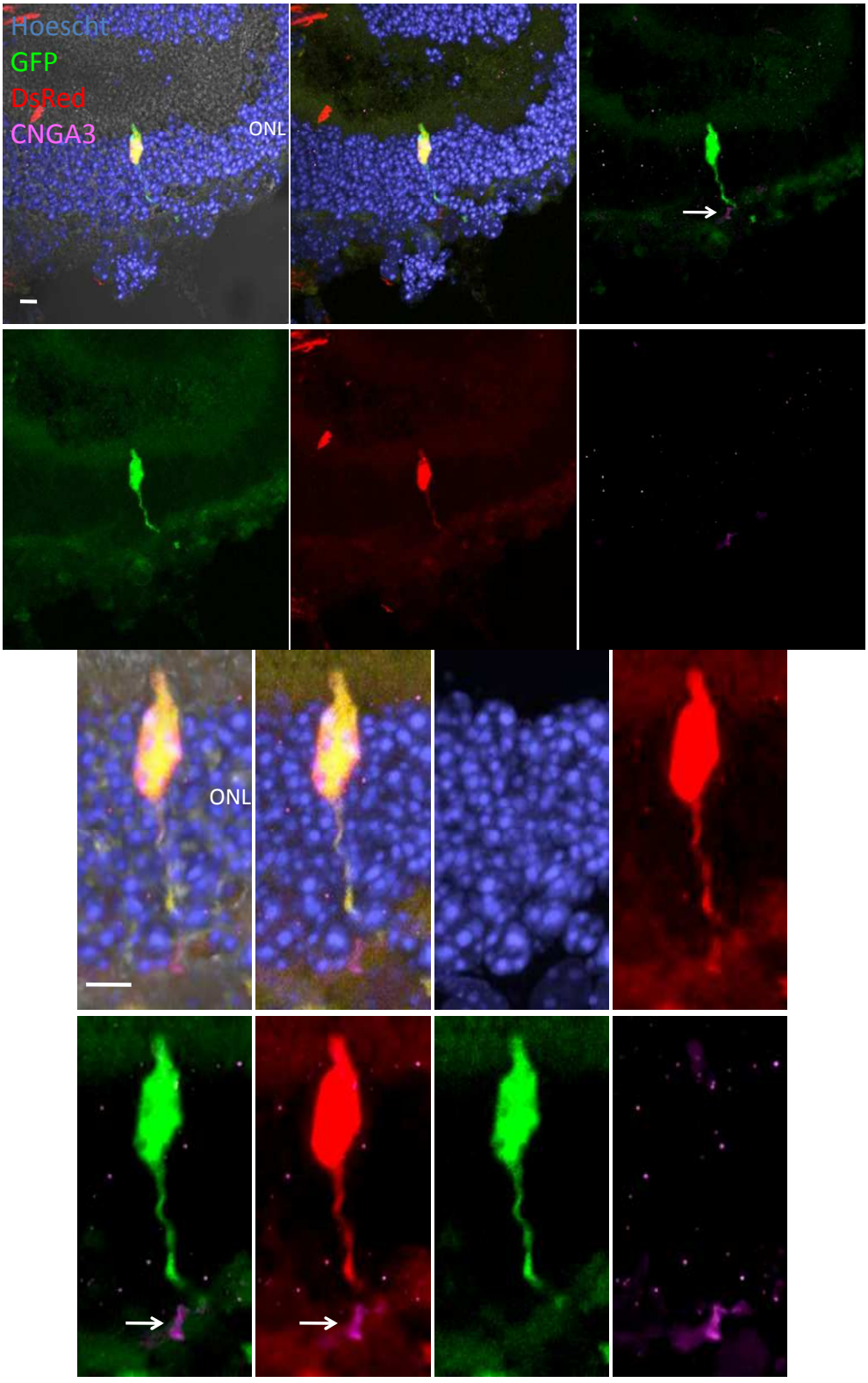

Figure 6.27. CNGA3 staining of an integrated GFP-dsRed cones in a TKO host. The upper panel shows the absence of CNGA3 staining in the host retina as expected in the TKO model. However, the integrated donor cone shows positive staining suggestive of the formation of an outer segment (white arrow). This is seen more clearly in the enlarged images in the lower panel. Scale bar: 10 µm.

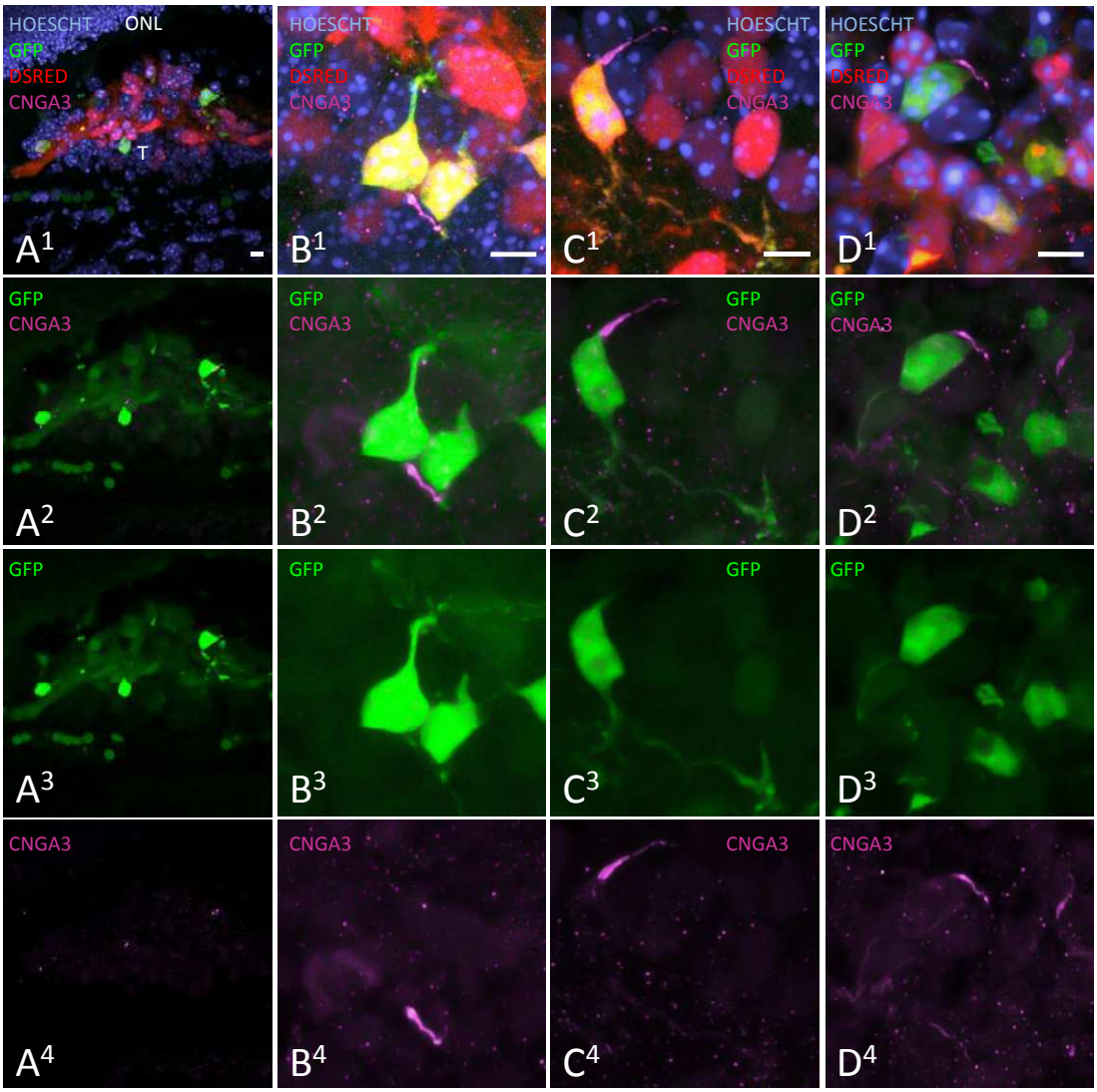

Figure 6.28. CNGA3 staining of GFP-dsRed cones post transplantation into TKO hosts. Four examples are shown in columns of CNGA3 staining of donor cone outer segments (COS). No staining is seen of host COS due to the knockout of the *CNGA3* gene in TKO hosts (**A**) whereas the high power micrographs show definitive staining of GFP-dsRed-positive donor COS. Scale bar: 5µm. ONL, outer nuclear layer; T, transplanted cells.

qPCR analysis

In correlation with the histological findings, *CNGA3* gene expression was restored to the TKO retina at three weeks following cone transplantation compared to no observable effect in uninjected control TKO retinas ($P = 0.005$, $N = 8$ eyes per group, paired t-test, Figure 6.29).

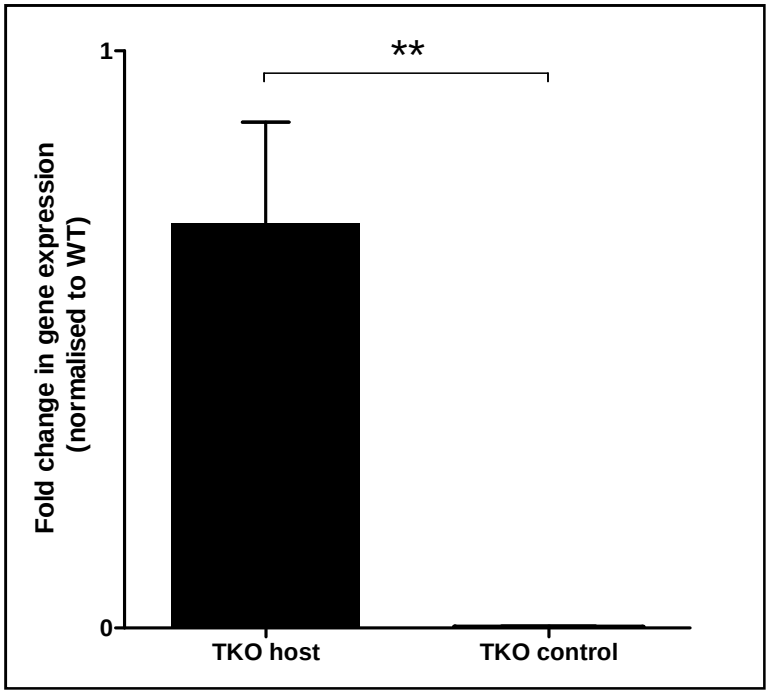

Figure 6.29. The expression of the *CNGA3* gene following cone transplantation in TKO hosts. qPCR analysis in TKO eyecups comparing injected with uninjected eyes (normalised to wild type). *CNGA3* gene expression was elevated in injected hosts and no expression was detected in knockout controls. Error bar ± SEM, $N = 16$. $P = 0.005$, paired t-test.

Calcium Imaging

The functional response of transplanted cones was confirmed *ex vivo* by calcium imaging. Initial confirmation of tissue viability in order to optimise the experimental method was provided by the application of KCl (100µM) to the retinal explant. A sustained and reproducible increase in fluorescence intensity was observed

immediately following application suggesting an increase in intracellular calcium (Figure 6.30). Since the latter was an expected effect of KCl application, this confirmed the validity of the model for further work.

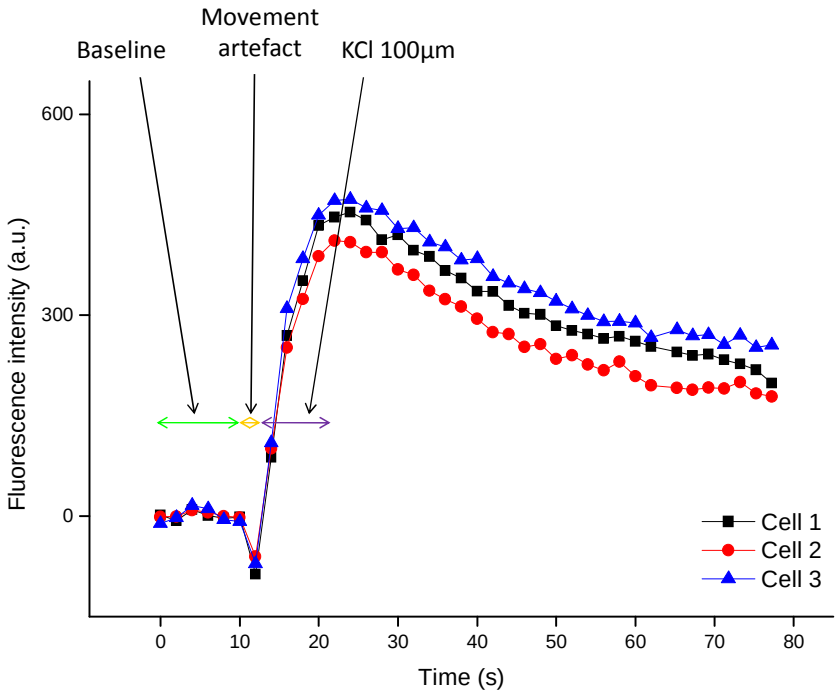

Figure 6.30. Calcium imaging results following application of KCl (100µM). Traces of three representative control cells are shown demonstrating changes in fluorescence intensity following drug application relative to baseline. An increase in fluorescence indicates an increase in intracellular calcium $[Ca^{2+}]_i$. Although movement artefact caused a small and short-lived spike of the trace, a prolonged increase in fluorescence equating to an increase in $[Ca^{2+}]_i$ was seen following application of KCl that reached a peak before returning to baseline.

Transplanted cones were identified by the presence of GFP as detected by stimulation at 488nm. Similarly, positive staining of photoreceptors with the ratiometric FURA-2 dye was detected by stimulation at 340nm and 380nm to enable selection of GFP-positive and -negative areas (Figure 6.31). The application of the specific mGluR8 agonist, (S)-3,4-dicarboxyphenylglycine (DCPG), resulted in an

expected decrease in intracellular calcium concentration in 70.6 ± 1.4% of GFP-positive (donor) cells vs. 70.2 ± 0.9% of controls (**t_{12} = 0.67, *P* = 0.52, *N* = 4, Figure 6.32). The addition of the specific mGluR8 antagonist, (RS)-a-cyclopropyl-4-phosphonophenylglycine (CPPG), blocked this change in intracellular calcium in both transplanted and host cells (Figures 6.32 and 6.33).

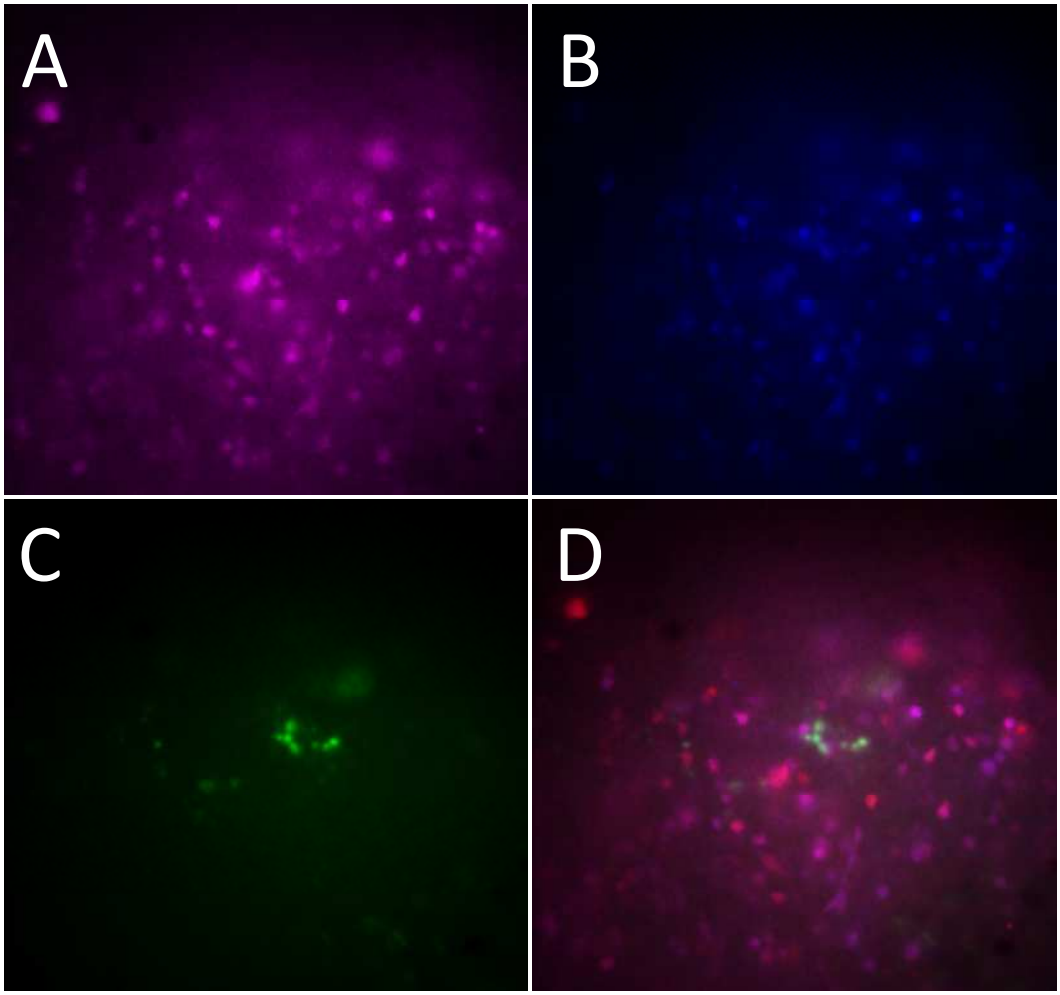

Figure 6.31. Representative fluorescence images during calcium imaging. Images were obtained with stimulation at 340 nm (A), 380 nm (B), and 488 nm (C), enabling the selection of GFP-positive and -negative cells for analysis (F).

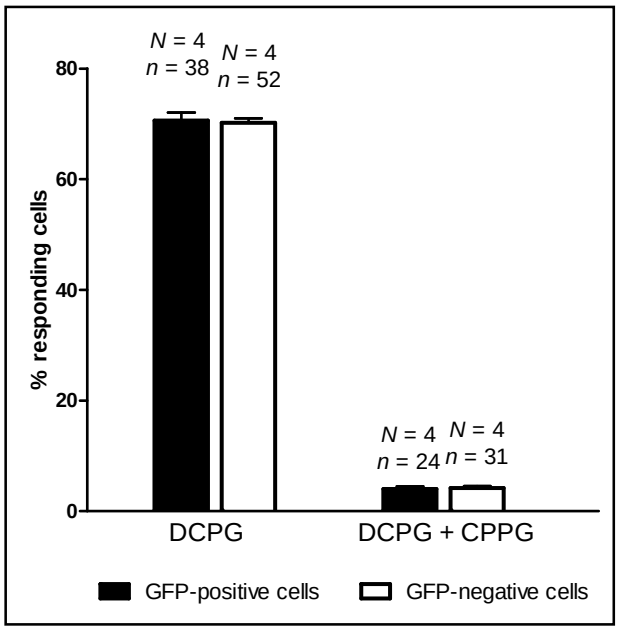

Figure 6.32. Analysis of response following the application of DCPG and CPPG. Addition of the specific mGluR8 agonist, DCPG, resulted in a decrease in intracellular calcium in GFP-positive cells that was almost identical to GFP-negative cells. This effect was blocked by the mGluR8 antagonist, CPPG, in a similar manner between GFP-positive and -negative cells. Error bar ± SEM.

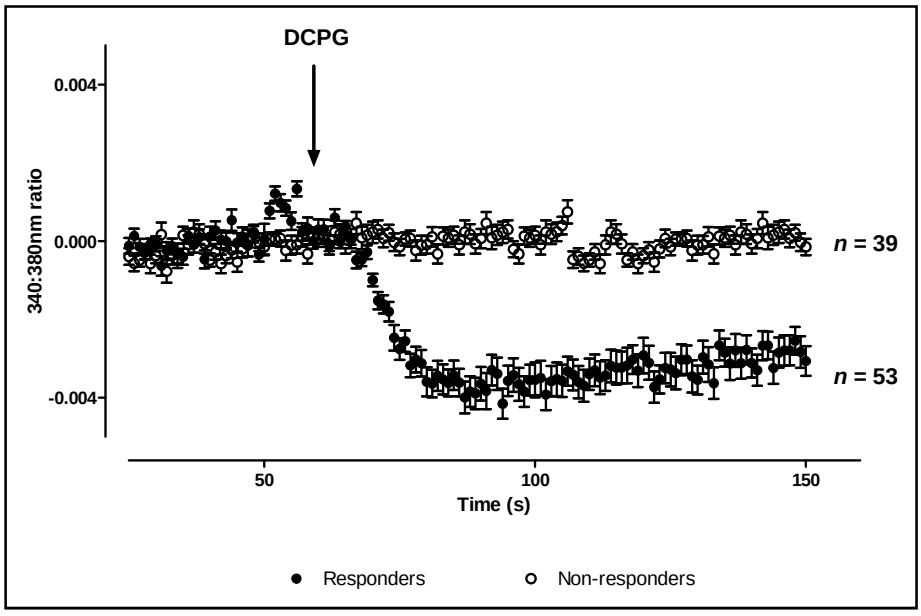

Figure 6.33. Averaged traces of GFP-positive cells in response to DCPG application. The changes in fluorescence in 92 GFP-positive cells are shown in response to DCPG stimulation, demonstrating a clear difference between responding and non-responding cells.

Pupillometry

No pupil response was observed in treated or untreated TKO mice compared to the expected response seen in wild type controls (Figure 6.34).

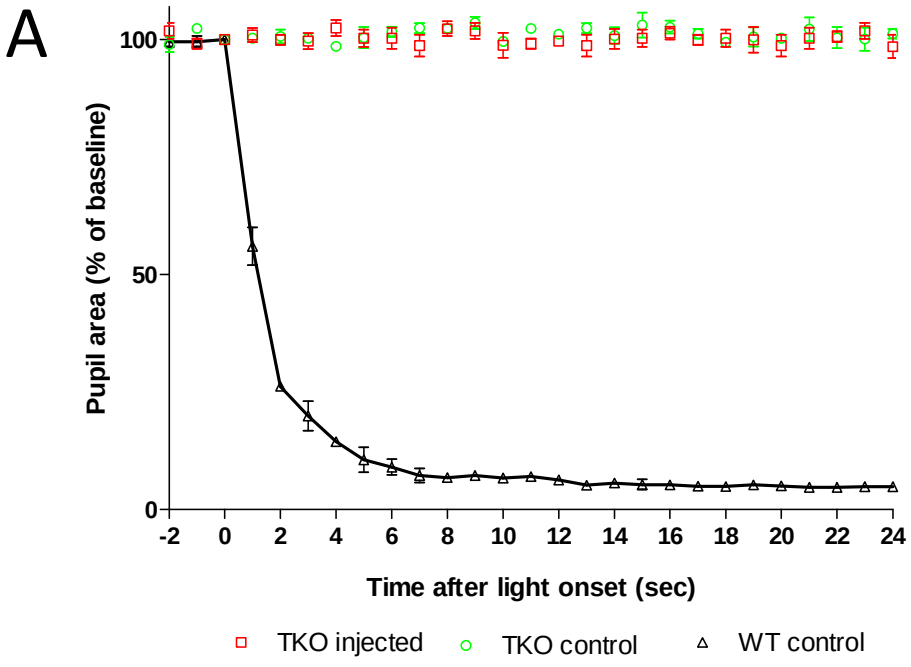

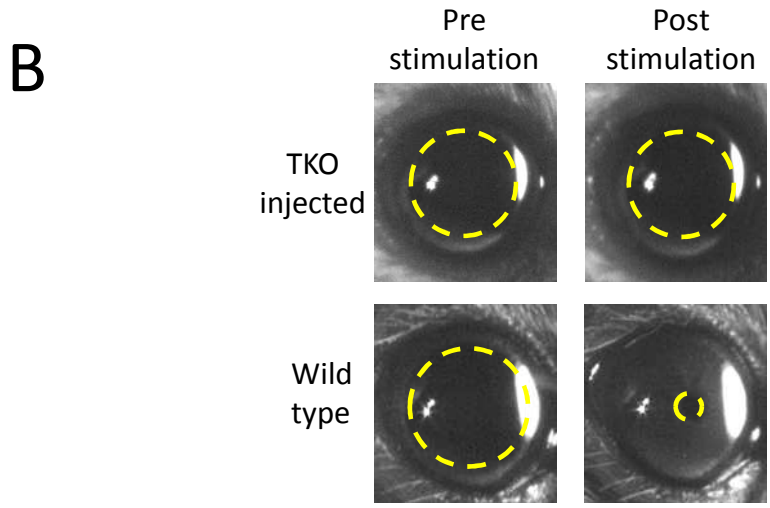

Figure 6.34. Changes in pupil size following cone transplantation in TKO hosts. Analysis of pupillometry results comparing injected TKO hosts with uninjected TKO and wild type (WT) controls (**A**). No change in pupil size was observed in injected or uninjected TKO eyes. The wild type response showed an early constriction as expected. *N* = 6 mice per group. Representative pupil images are shown (**B**).

Behavioural testing

Each 30-minute trial was conducted under bright light illumination of the front half (FH) of the light-dark box. In terms of duration, treated TKO and wild type mice spent more time (66.3 ± 5.0% and 79.0 ± 3.5% respectively) in the dark back half (BH) compared to sham-injected mice (53.7 ± 2.3%, $F_{3,34}$ = 10.5, P = 0.031 and 0.0002 respectively, one-way ANOVA with Dunnett's post-hoc test, Figure 6.35). No difference was observed between the sham-injected and uninjected group (51.7 ± 1.9%, P = 0.95). As a proxy measure of anxiety-related behaviour that would have potentially confounded the result of time spent in each half of the light-dark box, the number of transitions between compartments was measured and was found to be no different across groups (P = 0.960, one-way ANOVA, Figure 6.36).

Following transplantation, five out of eleven TKO mice receiving cone donor cells spent more than 66.0% (representing the upper 95% confidence interval) of the time in the dark BH of the light-dark box (Figure 6.37). Compared to this, no sham- or non-injected mice spent more than this duration in the dark. Of the cone-transplanted group, there was a significant correlation between the time spent in the dark BH and integrated cone number (F-test P = 0.017; Figure 6.38).

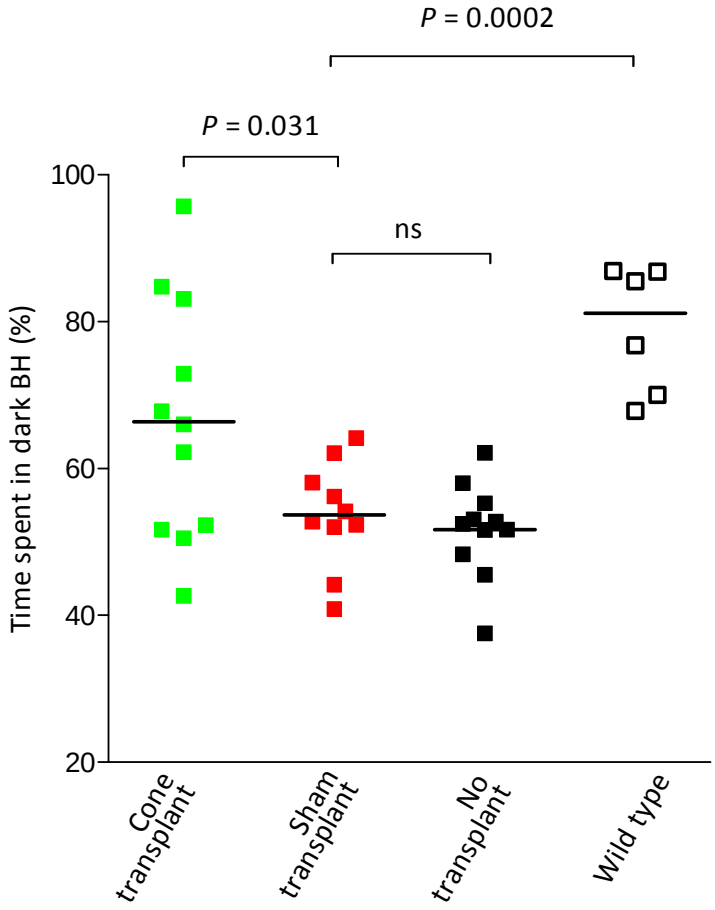

Figure 6.35. Analysis of behavioural light aversion following cone transplantation in TKO hosts. This scatter plot shows the time spent in the dark back half (BH) of the light-dark box in four separate groups. From left to right, the coloured boxes indicate TKO mice receiving GFP-dsRed cone transplants, sham transplants of TKO retinal cells, and no transplant respectively. The clear boxes represent wild type mice. TKO mice injected with GFP-dsRed cones and wild type controls spent more time in the dark than sham-injected (P = 0.031 and P = 0.0002 respectively). No difference was observed between the sham-injected and uninjected control groups. Horizontal bars indicate the median value. One-way ANOVA with Dunnett's post-hoc test.

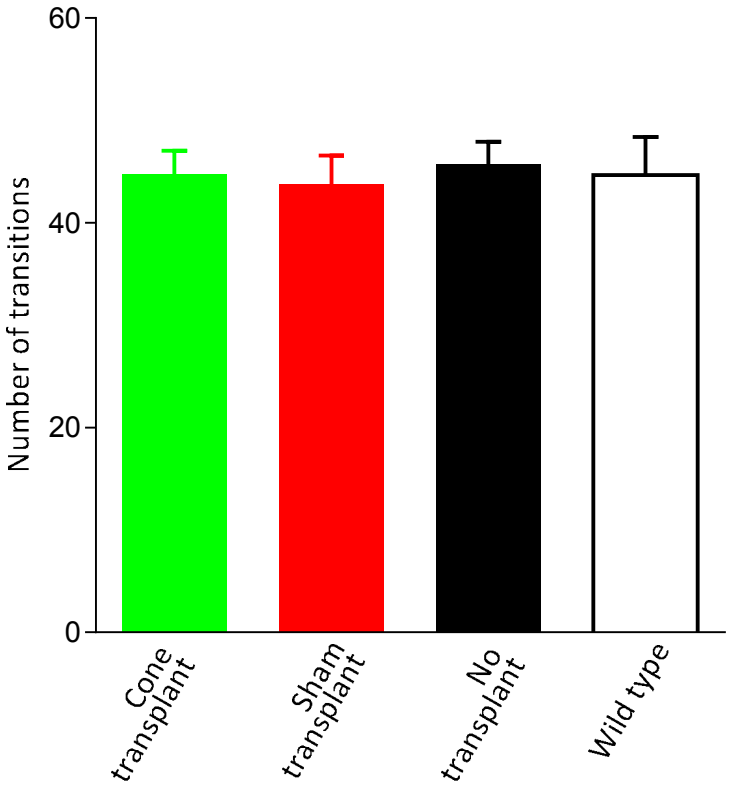

Figure 6.36. The number of transitions between compartments of the light-dark box. Anxiety-related behaviour (transitions between compartments) was similar across groups (P = 0.960, one-way ANOVA).

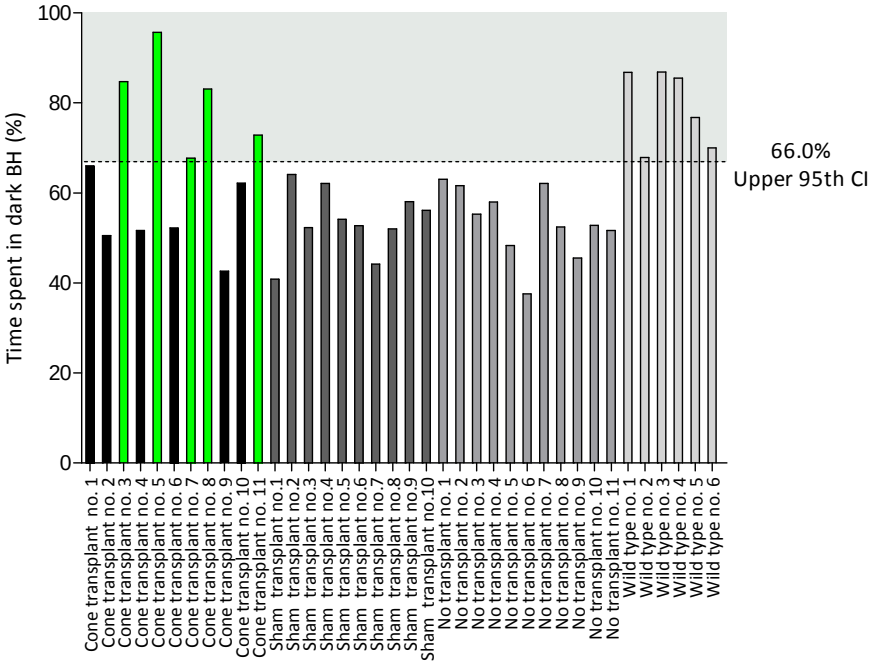

Figure 6.37. Results of behavioural light aversion testing for all mice. This chart shows the performance of GFP-dsRed cone-injected (black), sham-injected (dark grey) and non-injected (mid grey) TKO and wild-type (light grey) mice. Treated animals with a rate of at least 66.0% (that represents the upper 95% confidence interval) are shown in green throughout.

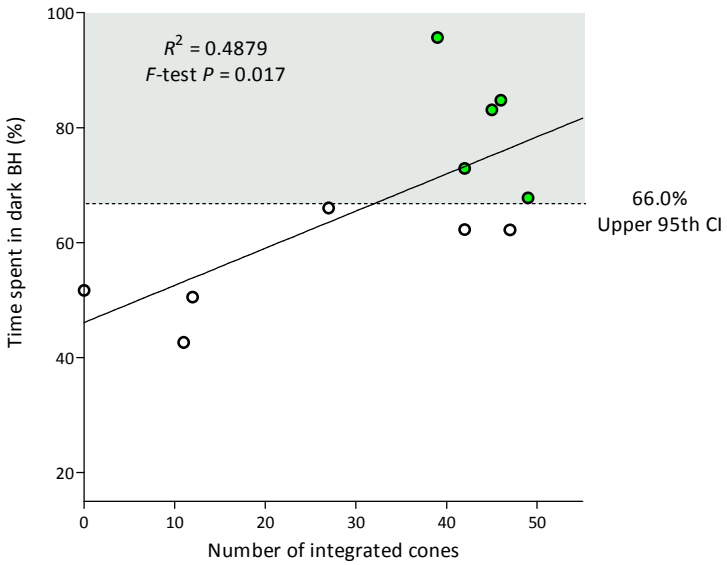

Figure 6.38. Correlation of behavioural light aversion results according to integrated cones. Results are shown of the GFP-dsRed cone-injected TKO mice with time spent in the dark plotted against integrated GFP-dsRed cone number. A positive correlation is seen between time spent in the dark and integrated cone number (*F*-test, $P = 0.017$).

6.4 Discussion

Compared to previous photoreceptor transplantation studies that have shown a regular morphology of integrated cells, the results described in this chapter contradict some of these findings. Although our observations have focused on cone photoreceptors, they can be extrapolated in order to draw conclusions of what should be expected following rod transplantation. Initial reports of cone transplantation identified the presence of S cones as detected by opsin staining.[408,409] As per other transplantation studies, the purported integrated photoreceptors were regularly aligned with and of the same morphology as host photoreceptors. Similarly, in a study involving transplantation of FAC-sorted photoreceptors, integrated cones showed the identical features to host cells with no displacement of cell structure. Of note, the integrated cones in these reports were often accompanied by a subretinal donor clump in the near vicinity. Contrary to these findings, we noted that transplanted cones showed an abnormal morphology compared to their host counterparts. Donor cones showed an ectopic location of the cell body, either in the subretinal space or at the inner part of the outer nuclear layer, both representing an atypical position for the cone cell body, thereby confirming their exogenous derivation. Although it could be argued that these were abnormal cones in an abnormal position, they nevertheless showed expression of the markers for cone arrestin, opsin, Cnga3, and recoverin.

Additionally, the integrated cones showed normal function in an *ex vivo* environment as confirmed by calcium imaging. This result is in agreement with previous studies that have investigated the effect of DCPG on transplanted rods,

including the finding that transplanted rods showed a similar response to that of host rods.[301,397] Of note, the mGluR8 autoreceptor has been identified in the presynaptic terminals of both types of photoreceptor, with diffuse distribution having been shown in the rod spherules and in the cone pedicles.[414] Application of the selective agonist for group III mGluRs (that include mGluR8), L-2-amino-4-phosphonobutyrate (L-AP4), has been shown to reduce spontaneous excitatory postsynaptic currents in the carp retina, thereby confirming the presynaptic action on cone synaptic terminals to reduce glutamate transmitter release.[415]

As further evidence of the functional response of transplanted cones, treated animals showed positive light aversion behaviour in comparison to untreated and sham-injected controls. The latter group controlled for the inflammatory effect of the intraocular injection that could potentially have a bearing on visual function. Since BLA experiments were conducted in bright light, this negated the effect of the anomalous *Gnat2* pathway that has been shown to support rod-like visual responses in *Gnat1* knockout animals.[416]

With regards to cell fusion experiments, no previous photoreceptor transplant work has reported this phenomenon as a possible cause of cell integration. However, our findings proved that photoreceptor fusion was possible and may explain some of the observations that have been shown in previous work. Although the precise mechanism is outside the scope of this thesis, we hypothesise that fusion with transplanted retinal cells was responsible for the expression of the same markers in host photoreceptors that did not otherwise express these.

CHAPTER 7

GENERAL DISCUSSION

The purpose of the work reported in this thesis has been to investigate treatment options for retinal laser injury. This was assessed in various mouse models by administering intravitreal CNTF immediately following injury and by exploring the feasibility of cone transplantation.

An initial model was developed that showed the *in vivo* loss of cone photoreceptors, as detected by autofluorescence imaging. This was confirmed by histological techniques that showed attenuation of the ONL in the area of laser exposure. Additionally, the detection of TUNEL-positive photoreceptors proved that apoptosis was the cause of cell death in affected cells. On the basis of this, intravitreal CNTF was delivered immediately post injury in order to reduce the loss of photoreceptors. A protective effect was shown with less attenuation of the ONL in the area of laser injury compared to sham-injected controls. Specifically, less attenuation of cone photoreceptors was detected by AF imaging in a longitudinal study using cone fluorescent mice. The mode of action of CNTF post laser injury as detected by qPCR analysis, involved inhibition of the pro-apoptotic *Bax* and induction of the anti-apoptotic *Bcl-2* pathways.

Cone transplantation was shown to be a viable method of restoring visual function. Following transplantation into adult hosts, cones survived in the subretinal space but did not integrate. Transplantation into neonatal hosts however, showed successful integration. Cell fusion was shown to occur In both age groups of hosts with co-expression of otherwise mutually exclusive fluorescent reporters. In an *ex vivo* model of cone transplantation, donor cones showed a normal physiological response following the application of the mGluR8 agonist, DCPG. Transplanted mice

also showed light aversion behaviour compared to controls. The logical follow on from this work would be to further investigate the effect of cone transplantation following retinal laser injury.

Adapting the observations to the clinical setting, the results of this thesis show that an effective neuroprotective treatment is possible following a foveal laser injury. Currently there is no battlefield treatment available to military personnel who might be exposed to an acute retinal laser injury. The development of a simple injection neuroprotection treatment would therefore be timely and might have a positive effect on the morale of troops if risks of laser exposure ever became significant in future combat deployments. Additionally, although much work is required to enable effective translation, the results of the transplantation experiments provide preliminary data to support this technique as a method of restoring visual function following the loss of cones. This would be of paramount importance in the setting of a foveal laser injury, which would primarily damage cone photoreceptors.

7.1 Non–invasive imaging in retinal laser application

A novel finding in this thesis is that the cSLO presents a unique method of visualising the *in vivo* effects of laser injury on cone photoreceptors. The model as described, enables cone loss to be followed longitudinally, which may simulate the effects of a human foveal laser injury that primarily affects cone photoreceptors. Due to its *in vivo* application, this technique provides a unique method of assessing laser-induced

photoreceptor damage, and specifically cone injury, as it directly monitors the temporal effects on cones following laser.

Beck et al. first reported the *in vivo* cSLO imaging of fluorescent cones in the Opn1-EGFP mouse.[417] The authors showed a stable GFP expression, as detected by 488nm AF, that did not affect retinal function for up to three months of age. This allowed quantification of cone number in retinal degeneration models by crossbreeding the Opn1-EGFP model with *cpfl1* and *Rpe65*$^{-/-}$ mutant mice.

Fundus autofluorescence (FAF) is used clinically to assess retinal disease, most commonly employing laser excitation wavelengths of 488nm and 790nm respectively. Lipofuscin, a byproduct of the visual cycle, constitutes the main fluorophore that exhibits AF using a 488nm laser source with changes in AF intensity or distribution having been shown to correlate with disease profile. [418] With 790nm excitation, AF signal is thought to originate from oxidised melanin within the choroid and RPE.[419,420] Although retinal diseases showing similar changes in AF signal at both 488nm and 790nm wavelength, certain differences are present that may relate to changes in the melanosome compartment.[421] This concurs with our finding of paradoxical increased 790nm AF versus decreased 488nm AF in areas of laser application.

AF imaging has been used to detect retinal changes in response to laser application. In a report of laser application for macular diseases, 488nm excitation detected initially hypoautofluorescent areas that later developed increased AF signal in otherwise subclinical lesions.[379] This appearance was also seen at different laser doses in Brown-Norway rats although lower laser power correlated with less

hyperautofluorescence.[422] We noted a similar pattern of AF when using small diameter, short duration burns with initial hypoautoflourescence followed by later hyperautofluorescence. Changing the settings to deliver large diameter, longer duration burns did not result in later hyperautofluorescence. This enabled the detection of changes in fluorescent cones that were otherwise obscured by increased AF. The observation of the increasing loss of GFP fluorescence over 6 weeks with the expansion of lesion area indicated that cones were progressively lost following an initial injury in this model. This result concurs with published reports of enlargement of retinal laser lesions in humans over time, where lesion enlargement by 42% at 32 months and 103% at 1 year[381] was determined by measuring the macular laser lesion diameter following treatment for choroidal neovascularization.

An additional observation that supports the temporal loss of cones following laser is the detection of TUNEL assay in injured photoreceptors. This technique has been used to indentify photoreceptor apoptosis in previous models of laser injury.[382,405] These findings are in accordance with our results demonstrating that photoreceptor apoptosis occurs early following laser injury.

We have further shown that the *in vivo* findings concur with histological observations showing an increased loss of photoreceptors, both rods and cones, with time. The histological results are in agreement with previous studies demonstrating this temporal correlation.[423] Various techniques have been used to study the effects of laser injury in different animal models, including fluorescein angiography, near infrared reflectance, white light fundoscopy, and electroretinography.[374-377,424] However, the conclusions from previous investigations

have primarily relied on histological data which have a number of limitations. There are several drawbacks to this method of evaluating the effect of injury. Firstly, histological techniques are necessarily cross-sectional and, therefore, subject to errors arising from biological variability between animals at different time points.[378] Secondly, there are potential errors that may arise from tissue sectioning and resultant selection bias. Due to asymmetry of the injured area, variability of laser exposure and selection bias, quantification of photoreceptor nuclei or ONL thickness in a lasered area may be potentially inaccurate. However, coupled with a longitudinal imaging method, as per the technique described in this thesis, this provides for a more robust method of analysis. That said, a limitation of this *in vivo* study is that media clarity needs to be maintained in the presence of the intravitreal agent, which, therefore, excludes certain opaque compounds (e.g., triamcinolone acetonide) from investigation that may otherwise be used in routine clinical practice via this route. Thirdly, there are material considerations since this method uses more animals than a longitudinal *in vivo* study. This is of particular importance in the setting of large animal studies that are limited by availability, such as primates, or in human studies, wherein tissue samples may be difficult to obtain. Lastly, histological methods provide only a limited area of selection rather than an overview acquired by *in vivo* imaging. Overall, although the mainstay of retinal research techniques has been provided by histology, the *in vivo* imaging method that we have described provides a straightforward and consistent mode of retinal analysis.

7.2 Cone neuroprotection by CNTF following laser injury

Another major finding in the current work is that CNTF protects cones against laser-induced photoreceptor injury. Previous studies have demonstrated the neuroprotective properties of CNTF on photoreceptors, including the application of this agent in human clinical trials.[162,425] The neuroprotective effect of CNTF has been demonstrated in previous rodent models of retinal injury,[387] and more recently, in a retinal explant model of cone degeneration.[388] Therefore, we chose to assess CNTF as a potential therapeutic agent in our model of cone loss induced by laser exposure. By using a multimodal approach consisting of both *in vivo* imaging and *in vitro* histological and molecular techniques, we were able to confirm the protective effect of CNTF in our model of laser injury.

Many different agents have been investigated for their effect on photoreceptor survival following laser application. These have shown varied results with regards their neuroprotective effects. For instance, corticosteroids, which have an immunomodulatory function, have been shown to have a protective effect when administered as an intravenous dose of methylprednisolone in laser injuries of nonhuman primate retina.[382,426] However, conflicting reports have shown that steroids inhibit regeneration of the outer blood-retina barrier following laser injury[427] whilst others have shown only a short-term effect on the prognosis of argon-induced retinal laser injuries in pigmented rats.[428]

Additional agents that have been reported to show beneficial effects following retinal laser injury include the NMDA receptor antagonists,[429] the neurotrophic factors BDNF and FGF,[430] and certain T-cell immunomodulators.[431] However, these

studies were based in histological observations and any findings on photoreceptor survival would have reflected the survival response of rod photoreceptors in the main, given their proportion relative to cones. A human foveal injury that causes immediate blindness primarily involves cones, whereas a peripheral retinal laser injury that mainly affects rods, does not cause such a profound loss of vision as it spares the central vision. Due to these anatomical variations, our study is more specific to demonstrating a protective effect on cones, relevant to the human fovea.

The results also demonstrate that the timing of treatment is critical to cone survival. Since the TUNEL assay showed a temporal correlation with maximal apoptosis occurring within the first day following injury, early treatment was targeted accordingly. The localisation of TUNEL staining at different depths of the ONL indicated that apoptotic cell death occurred in both rods and cones, whereas the greater ONL loss occurring at six weeks, which again indicated the occurrence of both rod and cone death, correlated with the *in vivo* findings of progressive cone loss during this period. The onset of apoptosis following retinal laser has been shown in previous studies with TUNEL-positive cells having been identified from as early as 8 to 24 hours following injury.[405,432,433] Translating this to the clinical scenario, for maximal efficacy in terms of protecting foveal cone photoreceptors, treatment would need to be delivered at the earliest possible juncture following injury.

The precise mechanism of cone death was not identified in this thesis beyond demonstrating the alteration of certain genes involved in apoptosis. In particular, the role of the RPE in photoreceptor cell death was not established. The question

remains about whether injured RPE has a role in the demise of photoreceptors. Certainly, in a number of disease conditions, RPE death leads to secondary photoreceptor attrition. Dry ARMD is a disease that leads to geographic atrophy with loss of RPE and death of the overlying photoreceptors.[434] Another specific example of the relationship between this group of cells is that of Stargardt's disease. This inherited form of juvenile macular degeneration, primarily caused by mutations in the *ABCA4* gene, results in a defective ATP-binding cassette transporter, leading to a build up of the toxic metabolite, lipofuscin, in the RPE.[435]

Photoreceptor cell death is a secondary consequence of this injury to the RPE. By observing the pathophysiology of the aforementioned diseases, we hypothesise that in addition to the direct photothermal effect on cones and the occurrence of secondary cell death due to apoptosis, laser-induced RPE injury may have a causal relationship with cone photoreceptor cell death. Certainly, the area of RPE loss has been shown to expand following laser application.[380] On the basis of this, it is possible that continuing RPE loss after the initial insult may result in further photoreceptor, and specifically, cone loss with time, as reported in our study. Since CNTF has been shown to improve RPE survival *in vitro*,[185] it is possible that the protective effect on the RPE may have a role in improving photoreceptor survival. This is in addition to the role of the Müller cell that, as has been discussed in previous chapters, is proposed to have a role in CNTF-mediated photoreceptor neuroprotection via the Jak-STAT pathway.[108,132,133]

Bcl-2, *Bax*, and *c-Fos* are fundamental components in the intrinsic or mitochondrial apoptotic pathway. Bax protein is a potent proapoptotic initiator in the cell death

cascade. Following homodimerization, the resulting configuration forms a channel across the mitochondrial membrane. This allows cytochrome-C to exit the mitochondria and enter the cytosolic space, where it is involved in conversion of pro-Caspase-9 to Caspase-9 and subsequent initiation of apoptosis.[390] CNTF has previously been shown to inhibit Bax in studies of axotomized motor neurons following sciatic nerve transection.[391] The antiapoptotic molecule, Bcl-2, which is an integral membrane protein localized to mitochondria, inhibits the activation of Bax following initiation of a death signal.43 As such, the ratio between these two proteins reflects the susceptibility of cells to a death signal, with positive correlations having been shown between higher Bcl-2/Bax ratios and injury.[392,393] Additionally, the *c-Fos* gene, which encodes a nuclear phosphoprotein that constitutes the transcription factor activator protein 1 (AP-1), has been implicated as having a role in light-induced photoreceptor degeneration.[394] Upregulation of *c-Fos* gene expression has been demonstrated in rodent models of retinal cell apoptosis following photic injury.[383] Our results are consistent with the aforementioned findings, showing a reduction of Bax mRNA, an increase in the Bcl-2/Bax ratio, and a trend toward reduction of c-Fos mRNA following CNTF administration post-laser trauma, thus suggesting that CNTF affects Bax, Bcl-2, and c-Fos at both the transcriptional and post-translational levels.Nonetheless, the precise mechanism by which CNTF improves photoreceptor survival is unknown. CNTF has been shown to act on the alpha CNTR receptor (CNTFRα), the beta leukemia inhibitory factor receptor (LIFRβ), and the glycoprotein 130 receptor (gp130R).[395] Photoreceptors lack a CNTF receptor, which is found on inner retinal neurons and Müller cells. Based on this, the postulated mechanism underlying CNTF-dependent photoreceptor

protection is thought to be related to Müller cell activation and antiapoptotic Janus kinase/signal transducer and activator of transcription (JAK/STAT) and MAPK signaling pathways.[108]

Given the interspecies differences in anatomy, genomes, and response to injury, in certain disease processes it may be difficult to make a direct correlation between the results observed in rodents and humans.[436] However, in both the rodent and human eye, photoreceptor cell death following laser injury has been shown in previous work, as has the protective effect on photoreceptors with the use of CNTF. Therefore, the study as presented in this thesis combines the use of these established facts and thus allows the extrapolation of results specific to cone injury.

In conclusion, although this research has a military focus with regard to developing a potential treatment for offensive laser weapons on the battlefield, the model as described might be relevant to assessing any treatment relevant to cone neuroprotection and diseases of the human fovea.

7.3 Cone transplantation

The thesis reports the results of cone transplantation demonstrating that this type of photoreceptor is capable of maturation, survival, integration, and restoration of function in the host retina. Almost exclusively, previous studies have reported the role of rod transplantation which is in part due to the high proportion of rods relative to cones in the murine retina. In our study, as a result of the intercross between the rd.Dsred and Opn1-EGFP mouse, rods were absent from the

transplanted cells due to the underlying retinal degeneration. Therefore, any morphological or functional result would not be rod-derived.

FACS and MACS techniques have been used to derive a purified population of photoreceptors. FACS-derived photoreceptors[300] or rods alone[301] have shown integration following transplantation into wild type and appropriate functional knockout hosts. However, no study to date has reported the results following transplantation of an isolated population of cones. Our methods to derive this cell type were hampered by a low yield following FACS and contamination by a high proportion of rods during MACS. Even in our biological sorting method to eliminate rods from the donor population, other retinal cells were present within the cell mass and this needs to be considered in the interpretation of behavioural results.

Our results show that cones survive but do not integrate into the adult host. This is contradictory to the findings of rod-transplantation experiments to date. Although there are many cues to guide integration, the presence of the outer limiting membrane may present a particular barrier to transplanted cells. Disruption of this layer has been shown to improve the integration efficiency of donor rods[283,437] in adult hosts and could potentially have this effect on isolated cones. We show successful integration of cones in neonatal hosts. This age offers a more suitable subretinal niche with absence of an outer limiting membrane which may explain the report of S-opsin labelling cells, probable immature cones, following the intravitreal transplantation of human ESC-derived retinal cells into neonatal mice.[408]

We show the occurrence of cell fusion that may explain some of the findings observed following photoreceptor transplantation. Although the regular anatomy

and morphology of reported donor cells is not in itself a reason to question the validity of integration, the acquisition of an exogenous fluorophore marker following transplantation is certainly evidence of fusion rather than integration. Cell fusion has not been reported in retinal transplantation studies but is a recognised phenomenon in liver studies. Following transplantation into the liver, hematopoietic stem cells (HSCs) can give rise to nonhematopoietic cells, i.e. hepatocytes, a property that has been termed stem cell "plasticity".[438,439] However, more recent studies have shown that the process of cell fusion may be a contributory factor to the generation of new hepatocytes following HSC transplantation. In mice lacking the liver-specific enzyme, fumarylacetoacetate hydrolase (FAH), the majority of new hepatocytes formed after HSC transplantation contained genomes from both the donor and host.[440] Several *in vitro* studies have also shown the occurrence of cell fusion, simulating what would occur in the *in vivo* environment. In the presence of IL-4 and IL-13, monocyte-macrophage fusion has been shown to generate multinucleated cells.[441] On the basis of these facts, we hypothesise that fusion events occur following the transplantation of donor photoreceptors with the host outer retina. The implication of this is that aside from actual integration, cell fusion may enable the genomic transfer between donor and host in order to address a mutation within host cells.

7.4 Future work

Different therapeutic options have been investigated for their effect on photoreceptors following laser injury, however, no treatment has specifically shown the preservation of cones, relevant to foveal damage. The experiments described

here have provided a robust model for the *in vivo* study on the longitudinal response of laser injury on cone survival, providing evidence of the neuroprotective effect of CNTF. Additionally, cone transplantation has been shown to be a viable method to restore function via the integration of this cell type in the host retina. In future, it may be helpful to combine these therapies in order to investigate the efficacy of CNTF on cone survival post transplantation.

Although CNTF shows a protective effect on cone survival, further work would help explore a number of issues. It would be interesting to determine the *in vivo* effect of CNTF on rod photoreceptors. Certainly, the histology results in this thesis support the overall survival of photoreceptors but in order to more accurately identify the response of rods, the *in vivo* injury model could be repeated using the Nrl-GFP transgenic mouse, in which all rods express GFP. Additionally, the continued expression of CNTF may have a more beneficial effect on cone survival post laser and therefore, the use of appropriate delivery systems requires investigation. This may take the form of encapsulated cell technology for which CNTF has been shown to improve cone survival in a human clinical trial to treat dry ARMD.[162] A biological means of delivering prolonged dose of and agent would be via the use of viral gene therapy. Delivery of CNTF by recombinant adeno-associated virus (rAAV) has been shown to delay photoreceptor degeneration in the rhodopsin knockout mouse.[442] Although in the laser injury setting this would require a subretinal injection of the viral transgene, the transduction of photoreceptors beyond the area of injection would potentially support injured cells without further trauma due to the treatment site.

With regards cone transplantation work, there are many outstanding questions that need investigation in future studies. The main methodological issue that requires optimisation is the adequate separation of cones from the remainder of donor retinal cells. Clearly, the method of FAC-sorting is not ideal given the low yield of cones due to their relatively low proportion in the murine retina but also due to the length of time required per sort which may compromise the viability of donor cells. The identification of a suitable cell surface marker to detect immature cones would enable the possibility of MACS to purify this population. Although the thyroid hormone receptor, TRβ2, and the photoreceptor cell–specific nuclear receptor (PNR), are involved in cone differentiation and thus represent early cone markers, both are transcription factors and therefore localise to the nucleus,[443] rather than the cell membrane which is a requirement in order to make MACS possible.

Due to the RPE loss that would occur following a foveal laser injury, it is likely that any restoration of cones via transplantation would need to be done using supraphysiological numbers in order to allow for any attrition due to the absence of an underlying RPE scaffold. Currently, the standard number of cells in transplantation experiments is 2×10^5 per eye. This is partly due to the optimal cell titre that can delivered per unit volume. Such techniques as anterior chamber paracentesis can be used to increase the volume of subretinal injection.[444] Further studies could be directed to see if the number of cells could be increased in order to increase cone integration, although this would not be necessary if a purified population were to be identified by cell sorting.

Lastly, although this thesis has introduced the concept of cell fusion in photoreceptor transplantation, this area requires much exploration. In order to show that some of the observations made in previous rod transplantation work were due to fusion, the fusion experiments that we have described would need to be conducted using fluorescent rod donors rather than a transplant that eliminates this cell type.

CHAPTER 8

REFERENCES

References

1. Kolb H. The architecture of functional neural circuits in the vertebrate retina. The Proctor Lecture. *Invest Ophthalmol Vis Sci* 1994 Apr;35(5):2385-404.
2. Bloomfield SA, Dacheux RF. Rod vision: pathways and processing in the mammalian retina. *Prog Retin Eye Res* 2001 May;20(3):351-84.
3. Masland RH. The fundamental plan of the retina. *Nat Neurosci* 2001 Sep;4(9):877-86.
4. Nicholls JG. From neuron to brain. 5th ed. 2012. Sunderland, Mass.: Sinauer Associates.
5. Kolb H, Linberg KA, Fisher SK. Neurons of the human retina: a Golgi study. *J Comp Neurol* 1992 Apr 8;318(2):147-87.
6. Bernardos RL, Barthel LK, Meyers JR, Raymond PA. Late-stage neuronal progenitors in the retina are radial Muller glia that function as retinal stem cells. *J Neurosci* 2007 Jun 27;27(26):7028-40.
7. Newman E, Reichenbach A. The Muller cell: a functional element of the retina. *Trends Neurosci* 1996 Aug;19(8):307-12.
8. Hollander H, Makarov F, Dreher Z, van Driel D, Chan-Ling TL, Stone J. Structure of the macroglia of the retina: sharing and division of labour between astrocytes and Muller cells. *J Comp Neurol* 1991 Nov 22;313(4):587-603.
9. Kim JH, Yu YS, Kim DH, Kim KW. Recruitment of pericytes and astrocytes is closely related to the formation of tight junction in developing retinal vessels. *J Neurosci Res* 2009 Feb 15;87(3):653-9.
10. Chen L, Yang P, Kijlstra A. Distribution, markers, and functions of retinal microglia. *Ocul Immunol Inflamm* 2002 Mar;10(1):27-39.
11. Jin M, Li S, Moghrabi WN, Sun H, Travis GH. Rpe65 is the retinoid isomerase in bovine retinal pigment epithelium. *Cell* 2005 Aug 12;122(3):449-59.
12. Young RW, Bok D. Participation of the retinal pigment epithelium in the rod outer segment renewal process. *J Cell Biol* 1969 Aug;42(2):392-403.
13. Adijanto J, Banzon T, Jalickee S, Wang NS, Miller SS. CO2-induced ion and fluid transport in human retinal pigment epithelium. *J Gen Physiol* 2009 Jun;133(6):603-22.
14. Shi G, Maminishkis A, Banzon T, Jalickee S, Li R, Hammer J, Miller SS. Control of chemokine gradients by the retinal pigment epithelium. *Invest Ophthalmol Vis Sci* 2008 Oct;49(10):4620-30.
15. Besharse JC, Dana R, Dartt DA. Encyclopedia of the eye. 2010. Oxford: Academic Press. pp 89–100
16. Taylor HR, West S, Munoz B, Rosenthal FS, Bressler SB, Bressler NM. The long-term effects of visible light on the eye. *Arch Ophthalmol* 1992 Jan;110(1):99-104.

17. Lawrence JC. In vitro studies of skin after irradiation by a ruby laser. *Br J Plast Surg* 1967 Jul;20(3):257-62.

18. Borland RG, Nicholson AN. Laser safety codes. *Proc R Soc Med* 1973 Sep;66(9):845-6.

19. Barkana Y, Belkin M. Laser eye injuries. *Surv Ophthalmol* 2000 May-Jun;44(6):459-78.

20. Krauss JM, Puliafito CA, Steinert RF. Laser interactions with the cornea. *Surv Ophthalmol* 1986 Jul-Aug;31(1):37-53.

21. Maiman TH. Stimulated Optical Radiation in Ruby. *Nature* 1960;187:493-4.

22. Javan A, Bennett, W.R. and Herriott, D.R. Population Inversion and Continuous Optical Maser Oscillation in a Gas Discharge Containing a He-Ne Mixture. *Phys Rev Lett* 1961;63:106–10.

23. Turbe G. Laser weapons at sea. *Int Defence Rev* 1990;8:853-5.

24. Mainster MA, Stuck BE, Brown J, Jr. Assessment of alleged retinal laser injuries. *Arch Ophthalmol* 2004 Aug;122(8):1210-7.

25. Geeraets WJ, Berry ER. Ocular spectral characteristics as related to hazards from lasers and other light sources. *Am J Ophthalmol* 1968 Jul;66(1):15-20.

26. Marshall J. Thermal and mechanical mechanisms in laser damage to the retina. *Invest Ophthalmol* 1970 Feb;9(2):97-115.

27. Frisch GD, Shawaluk PD, Adams DO. Remote nerve fibre bundle alterations in the retina as caused by argon laser photocoagulation. *Nature* 1974 Mar 29;248(447):433-5.

28. Marshall J, Mellerio J. Disappearance of retino-epithelial scar tissue from ruby laser photocoagulations. *Exp Eye Res* 1971 Sep;12(2):173-4.

29. Wald G. Human Vision and the Spectrum. *Science* 1945 Jun 29;101(2635):653-8.

30. Gursky O, Atkinson D. High- and low-temperature unfolding of human high-density apolipoprotein A-2. *Protein Sci* 1996 Sep;5(9):1874-82.

31. Krasowska A, Rosiak D, Szkapiak K, Lukaszewicz M. Chemiluminescence detection of peroxyl radicals and comparison of antioxidant activity of phenolic compounds. *Curr Top Biophys* 2000;24:89-95.

32. Monk PN, Shaw PJ. ALS: life and death in a bad neighborhood. *Nat Med* 2006 Aug;12(8):885-7.

33. Block ML, Zecca L, Hong JS. Microglia-mediated neurotoxicity: uncovering the molecular mechanisms. *Nat Rev Neurosci* 2007 Jan;8(1):57-69.

34. Joly S, Francke M, Ulbricht E, Beck S, Seeliger M, Hirrlinger P, Hirrlinger J, Lang KS, Zinkernagel M, Odermatt B, Samardzija M, Reichenbach A, Grimm C, Reme CE. Cooperative phagocytes: resident microglia and bone marrow immigrants remove dead photoreceptors in retinal lesions. *Am J Pathol* 2009 Jun;174(6):2310-23.

35. Langmann T. Microglia activation in retinal degeneration. *J Leukoc Biol* 2007 Jun;81(6):1345-51.

36. Gerstman BS, Glickman RD. Activated rate processes and a specific biochemical mechanism for explaining delayed laser induced thermal damage to the retina. *J Biomed Opt* 1999 Jul;4(3):345-51.

37. Glickman RD, Jacques SL, Schwartz JA, Rodriguez T, Lam KW, Buhr G. Photodisruption increases the free radical reactivity of melanosomes isolated from retinal pigment epithelium. *SPIE* 1996;2681:460-7.

38. Zhu K, Jutila A, Kinnunen PK. Steady state and time resolved effects of guanidine hydrochloride on the structure of Humicola lanuginosa lipase revealed by fluorescence spectroscopy. *Protein Sci* 2000 Mar;9(3):598-609.

39. Boulton M, Dontsov A, Jarvis-Evans J, Ostrovsky M, Svistunenko D. Lipofuscin is a photoinducible free radical generator. *J Photochem Photobiol B* 1993 Aug;19(3):201-4.

40. Guzman MG, Kouri G, Valdes L, Bravo J, Alvarez M, Vazques S, Delgado I, Halstead SB. Epidemiologic studies on Dengue in Santiago de Cuba, 1997. *Am J Epidemiol* 2000 Nov 1;152(9):793-9; discussion 804.

41. Armstrong D. Free radicals in molecular biology, aging, and disease. 1984. New York: Raven Press.

42. Gan EV, Haberman HF, Menon IA. Oxidation of NADH by melanin and melanoproteins. *Biochim Biophys Acta* 1974 Nov 25;370(1):62-9.

43. Matylevitch NP, Schuschereba ST, Mata JR, Gilligan GR, Lawlor DF, Goodwin CW, Bowman PD. Apoptosis and accidental cell death in cultured human keratinocytes after thermal injury. *Am J Pathol* 1998 Aug;153(2):567-77.

44. Thomsen S. Pathologic analysis of photothermal and photomechanical effects of laser-tissue interactions. *Photochem Photobiol* 1991 Jun;53(6):825-35.

45. Sliney DH, Trokel SL. Medical lasers and their safe use. 1993. New York: Springer-Verlag.

46. Leszczynski D, Pitsillides CM, Pastila RK, Rox Anderson R, Lin CP. Laser-beam-triggered microcavitation: a novel method for selective cell destruction. *Radiat Res* 2001 Oct;156(4):399-407.

47. Raymond LA. Neodymium:YAG laser treatment for hemorrhages under the internal limiting membrane and posterior hyaloid face in the macula. *Ophthalmology* 1995 Mar;102(3):406-11.

48. Boldrey EE, Little HL, Flocks M, Vassiliadis A. Retinal injury due to industrial laser burns. *Ophthalmology* 1981 Feb;88(2):101-7.

49. Barbanel CS, Ducatman AM, Garston MJ, Fuller T. Laser hazards in research laboratories. *J Occup Med* 1993 Apr;35(4):369-74.

50. Boulton M, Rozanowska M, Rozanowski B. Retinal photodamage. *J Photochem Photobiol B* 2001 Nov 15;64(2-3):144-61.

51. Hope-Ross MW, Mahon GJ, Gardiner TA, Archer DB. Ultrastructural findings in solar retinopathy. *Eye (Lond)* 1993;7 (Pt 1):29-33.

52. Li ZY, Tso MO, Wang HM, Organisciak DT. Amelioration of photic injury in rat retina by ascorbic acid: a histopathologic study. *Invest Ophthalmol Vis Sci* 1985 Nov;26(11):1589-98.

53. Festjens N, Vanden Berghe T, Vandenabeele P. Necrosis, a well-orchestrated form of cell demise: signalling cascades, important mediators and concomitant immune response. *Biochim Biophys Acta* 2006 Sep-Oct;1757(9-10):1371-87.

54. Scaffidi P, Misteli T, Bianchi ME. Release of chromatin protein HMGB1 by necrotic cells triggers inflammation. *Nature* 2002 Jul 11;418(6894):191-5.

55. Zhou Z, Yamamoto Y, Sugai F, Yoshida K, Kishima Y, Sumi H, Nakamura H, Sakoda S. Hepatoma-derived growth factor is a neurotrophic factor harbored in the nucleus. *J Biol Chem* 2004 Jun 25;279(26):27320-6.

56. Bowen ID, Lockshin RA. Cell death in biology and pathology. 1981. London ; New York: Chapman and Hall.

57. Arends MJ, Morris RG, Wyllie AH. Apoptosis. The role of the endonuclease. *Am J Pathol* 1990 Mar;136(3):593-608.

58. Savill J, Dransfield I, Hogg N, Haslett C. Vitronectin receptor-mediated phagocytosis of cells undergoing apoptosis. *Nature* 1990 Jan 11;343(6254):170-3.

59. Morris RG, Hargreaves AD, Duvall E, Wyllie AH. Hormone-induced cell death. 2. Surface changes in thymocytes undergoing apoptosis. *Am J Pathol* 1984 Jun;115(3):426-36.

60. Lauber K, Bohn E, Krober SM, Xiao YJ, Blumenthal SG, Lindemann RK, Marini P, Wiedig C, Zobywalski A, Baksh S, Xu Y, Autenrieth IB, Schulze-Osthoff K, Belka C, Stuhler G, Wesselborg S. Apoptotic cells induce migration of phagocytes via caspase-3-mediated release of a lipid attraction signal. *Cell* 2003 Jun 13;113(6):717-30.

61. Fadok VA, Voelker DR, Campbell PA, Cohen JJ, Bratton DL, Henson PM. Exposure of phosphatidylserine on the surface of apoptotic lymphocytes triggers specific recognition and removal by macrophages. *J Immunol* 1992 Apr 1;148(7):2207-16.

62. Vaux DL, Cory S, Adams JM. Bcl-2 gene promotes haemopoietic cell survival and cooperates with c-myc to immortalize pre-B cells. *Nature* 1988 Sep 29;335(6189):440-2.

63. Muzio M, Stockwell BR, Stennicke HR, Salvesen GS, Dixit VM. An induced proximity model for caspase-8 activation. *J Biol Chem* 1998 Jan 30;273(5):2926-30.

64. Huang B, Eberstadt M, Olejniczak ET, Meadows RP, Fesik SW. NMR structure and mutagenesis of the Fas (APO-1/CD95) death domain. *Nature* 1996 Dec 19-26;384(6610):638-41.

65. Irmler M, Thome M, Hahne M, Schneider P, Hofmann K, Steiner V, Bodmer JL, Schroter M, Burns K, Mattmann C, Rimoldi D, French LE, Tschopp J. Inhibition of death receptor signals by cellular FLIP. *Nature* 1997 Jul 10;388(6638):190-5.

66. Li P, Nijhawan D, Budihardjo I, Srinivasula SM, Ahmad M, Alnemri ES, Wang X. Cytochrome c and dATP-dependent formation of Apaf-1/caspase-9 complex initiates an apoptotic protease cascade. *Cell* 1997 Nov 14;91(4):479-89.

67. Rodriguez J, Lazebnik Y. Caspase-9 and APAF-1 form an active holoenzyme. *Genes Dev* 1999 Dec 15;13(24):3179-84.

68. Du C, Fang M, Li Y, Li L, Wang X. Smac, a mitochondrial protein that promotes cytochrome c-dependent caspase activation by eliminating IAP inhibition. *Cell* 2000 Jul 7;102(1):33-42.

69. Klionsky DJ, Emr SD. Autophagy as a regulated pathway of cellular degradation. *Science* 2000 Dec 1;290(5497):1717-21.

70. Rubinsztein DC, Gestwicki JE, Murphy LO, Klionsky DJ. Potential therapeutic applications of autophagy. *Nat Rev Drug Discov* 2007 Apr;6(4):304-12.

71. Holler N, Zaru R, Micheau O, Thome M, Attinger A, Valitutti S, Bodmer JL, Schneider P, Seed B, Tschopp J. Fas triggers an alternative, caspase-8-independent cell death pathway using the kinase RIP as effector molecule. *Nat Immunol* 2000 Dec;1(6):489-95.

72. Zhang DW, Shao J, Lin J, Zhang N, Lu BJ, Lin SC, Dong MQ, Han J. RIP3, an energy metabolism regulator that switches TNF-induced cell death from apoptosis to necrosis. *Science* 2009 Jul 17;325(5938):332-6.

73. Degterev A, Huang Z, Boyce M, Li Y, Jagtap P, Mizushima N, Cuny GD, Mitchison TJ, Moskowitz MA, Yuan J. Chemical inhibitor of nonapoptotic cell death with therapeutic potential for ischemic brain injury. *Nat Chem Biol* 2005 Jul;1(2):112-9.

74. Degterev A, Hitomi J, Germscheid M, Ch'en IL, Korkina O, Teng X, Abbott D, Cuny GD, Yuan C, Wagner G, Hedrick SM, Gerber SA, Lugovskoy A, Yuan J. Identification of RIP1 kinase as a specific cellular target of necrostatins. *Nat Chem Biol* 2008 May;4(5):313-21.

75. Lynch DR, Dawson TM. Secondary mechanisms in neuronal trauma. *Curr Opin Neurol* 1994 Dec;7(6):510-6.

76. Blennow K, de Leon MJ, Zetterberg H. Alzheimer's disease. *Lancet* 2006 Jul 29;368(9533):387-403.

77. Ebadi M, Bashir RM, Heidrick ML, Hamada FM, Refaey HE, Hamed A, Helal G, Baxi MD, Cerutis DR, Lassi NK. Neurotrophins and their receptors in nerve injury and repair. *Neurochem Int* 1997 Apr-May;30(4-5):347-74.

78. Kishimoto T, Akira S, Taga T. Interleukin-6 and its receptor: a paradigm for cytokines. *Science* 1992 Oct 23;258(5082):593-7.

79. Korsching S. The neurotrophic factor concept: a reexamination. *J Neurosci* 1993 Jul;13(7):2739-48.

80. Ip NY, Yancopoulos GD. Neurotrophic factors and their receptors. *Ann Neurol* 1994;35 Suppl:S13-6.

81. Tessarollo L. Pleiotropic functions of neurotrophins in development. *Cytokine Growth Factor Rev* 1998 Jun;9(2):125-37.

82. Levi-Montalcini R, Hamburger V. Selective growth stimulating effects of mouse sarcoma on the sensory and sympathetic nervous system of the chick embryo. *J Exp Zool* 1951 Mar;116(2):321-61.

83. Halban PA, Irminger JC. Sorting and processing of secretory proteins. *Biochem J* 1994 Apr 1;299 (Pt 1):1-18.

84. Zhou XF, Rush RA. Endogenous brain-derived neurotrophic factor is anterogradely transported in primary sensory neurons. *Neuroscience* 1996 Oct;74(4):945-53.

85. Hofer M, Pagliusi SR, Hohn A, Leibrock J, Barde YA. Regional distribution of brain-derived neurotrophic factor mRNA in the adult mouse brain. *EMBO J* 1990 Aug;9(8):2459-64.

86. Huang EJ, Reichardt LF. Neurotrophins: roles in neuronal development and function. *Annu Rev Neurosci* 2001;24:677-736.

87. Hilton DJ, Gough NM. Leukemia inhibitory factor: a biological perspective. *J Cell Biochem* 1991 May;46(1):21-6.

88. Curtis R, Scherer SS, Somogyi R, Adryan KM, Ip NY, Zhu Y, Lindsay RM, DiStefano PS. Retrograde axonal transport of LIF is increased by peripheral nerve injury: correlation with increased LIF expression in distal nerve. *Neuron* 1994 Jan;12(1):191-204.

89. Taupin JL, Pitard V, Dechanet J, Miossec V, Gualde N, Moreau JF. Leukemia inhibitory factor: part of a large ingathering family. *Int Rev Immunol* 1998;16(3-4):397-426.

90. Pennica D, Arce V, Swanson TA, Vejsada R, Pollock RA, Armanini M, Dudley K, Phillips HS, Rosenthal A, Kato AC, Henderson CE. Cardiotrophin-1, a cytokine present in embryonic muscle, supports long-term survival of spinal motoneurons. *Neuron* 1996 Jul;17(1):63-74.

91. Pennica D, Swanson TA, Shaw KJ, Kuang WJ, Gray CL, Beatty BG, Wood WI. Human cardiotrophin-1: protein and gene structure, biological and binding activities, and chromosomal localization. *Cytokine* 1996 Mar;8(3):183-9.

92. Sanchez MP, Silos-Santiago I, Frisen J, He B, Lira SA, Barbacid M. Renal agenesis and the absence of enteric neurons in mice lacking GDNF. *Nature* 1996 Jul 4;382(6586):70-3.

93. Yan Q, Matheson C, Lopez OT. In vivo neurotrophic effects of GDNF on neonatal and adult facial motor neurons. *Nature* 1995 Jan 26;373(6512):341-4.

94. Milbrandt J, de Sauvage FJ, Fahrner TJ, Baloh RH, Leitner ML, Tansey MG, Lampe PA, Heuckeroth RO, Kotzbauer PT, Simburger KS, Golden JP, Davies JA, Vejsada R, Kato AC, Hynes M, Sherman D, Nishimura M, Wang LC, Vandlen R, Moffat B, Klein RD, Poulsen K, Gray C, Garces A, Johnson EM, Jr., et al. Persephin, a novel neurotrophic factor related to GDNF and neurturin. *Neuron* 1998 Feb;20(2):245-53.

95. Heuckeroth RO, Lampe PA, Johnson EM, Milbrandt J. Neurturin and GDNF promote proliferation and survival of enteric neuron and glial progenitors in vitro. *Dev Biol* 1998 Aug 1;200(1):116-29.

96. Treanor JJ, Goodman L, de Sauvage F, Stone DM, Poulsen KT, Beck CD, Gray C, Armanini MP, Pollock RA, Hefti F, Phillips HS, Goddard A, Moore MW, Buj-Bello A, Davies AM, Asai N, Takahashi M, Vandlen R, Henderson CE, Rosenthal A. Characterization of a multicomponent receptor for GDNF. *Nature* 1996 Jul 4;382(6586):80-3.

97. LeRoith D, Clemmons D, Nissley P, Rechler MM. NIH conference. Insulin-like growth factors in health and disease. *Ann Intern Med* 1992 May 15;116(10):854-62.

98. Fernyhough P, Willars GB, Lindsay RM, Tomlinson DR. Insulin and insulin-like growth factor I enhance regeneration in cultured adult rat sensory neurones. *Brain Res* 1993 Apr 2;607(1-2):117-24.

99. Withers DJ, White M. Perspective: The insulin signaling system--a common link in the pathogenesis of type 2 diabetes. *Endocrinology* 2000 Jun;141(6):1917-21.

100. Jain KK. The handbook of neuroprotection. 2011. New York: Humana Press.

101. Itoh N, Ornitz DM. Evolution of the Fgf and Fgfr gene families. *Trends Genet* 2004 Nov;20(11):563-9.

102. Goldfarb M, Schoorlemmer J, Williams A, Diwakar S, Wang Q, Huang X, Giza J, Tchetchik D, Kelley K, Vega A, Matthews G, Rossi P, Ornitz DM, D'Angelo E.

Fibroblast growth factor homologous factors control neuronal excitability through modulation of voltage-gated sodium channels. *Neuron* 2007 Aug 2;55(3):449-63.

103. Maina F, Hilton MC, Ponzetto C, Davies AM, Klein R. Met receptor signaling is required for sensory nerve development and HGF promotes axonal growth and survival of sensory neurons. *Genes Dev* 1997 Dec 15;11(24):3341-50.

104. Adler R, Landa KB, Manthorpe M, Varon S. Cholinergic neuronotrophic factors: intraocular distribution of trophic activity for ciliary neurons. *Science* 1979 Jun 29;204(4400):1434-6.

105. Lin LF, Mismer D, Lile JD, Armes LG, Butler ET, 3rd, Vannice JL, Collins F. Purification, cloning, and expression of ciliary neurotrophic factor (CNTF). *Science* 1989 Nov 24;246(4933):1023-5.

106. Takahashi R, Yokoji H, Misawa H, Hayashi M, Hu J, Deguchi T. A null mutation in the human CNTF gene is not causally related to neurological diseases. *Nat Genet* 1994 May;7(1):79-84.

107. Stockli KA, Lillien LE, Naher-Noe M, Breitfeld G, Hughes RA, Raff MC, Thoenen H, Sendtner M. Regional distribution, developmental changes, and cellular localization of CNTF-mRNA and protein in the rat brain. *J Cell Biol* 1991 Oct;115(2):447-59.

108. Peterson WM, Wang Q, Tzekova R, Wiegand SJ. Ciliary neurotrophic factor and stress stimuli activate the Jak-STAT pathway in retinal neurons and glia. *J Neurosci* 2000 Jun 1;20(11):4081-90.

109. Ip NY, Li YP, van de Stadt I, Panayotatos N, Alderson RF, Lindsay RM. Ciliary neurotrophic factor enhances neuronal survival in embryonic rat hippocampal cultures. *J Neurosci* 1991 Oct;11(10):3124-34.

110. de Almeida LP, Zala D, Aebischer P, Deglon N. Neuroprotective effect of a CNTF-expressing lentiviral vector in the quinolinic acid rat model of Huntington's disease. *Neurobiol Dis* 2001 Jun;8(3):433-46.

111. Masu Y, Wolf E, Holtmann B, Sendtner M, Brem G, Thoenen H. Disruption of the CNTF gene results in motor neuron degeneration. *Nature* 1993 Sep 2;365(6441):27-32.

112. DeChiara TM, Vejsada R, Poueymirou WT, Acheson A, Suri C, Conover JC, Friedman B, McClain J, Pan L, Stahl N, Ip NY, Yancopoulos GD. Mice lacking the CNTF receptor, unlike mice lacking CNTF, exhibit profound motor neuron deficits at birth. *Cell* 1995 Oct 20;83(2):313-22.

113. Bazan JF. Structural design and molecular evolution of a cytokine receptor superfamily. *Proc Natl Acad Sci U S A* 1990 Sep;87(18):6934-8.

114. Boulanger MJ, Garcia KC. Shared cytokine signaling receptors: structural insights from the gp130 system. *Adv Protein Chem* 2004;68:107-46.

115. Auernhammer CJ, Melmed S. Leukemia-inhibitory factor-neuroimmune modulator of endocrine function. *Endocr Rev* 2000 Jun;21(3):313-45.

116. Segal RA, Greenberg ME. Intracellular signaling pathways activated by neurotrophic factors. *Annu Rev Neurosci* 1996;19:463-89.

117. Stahl N, Boulton TG, Farruggella T, Ip NY, Davis S, Witthuhn BA, Quelle FW, Silvennoinen O, Barbieri G, Pellegrini S, et al. Association and activation of Jak-Tyk

kinases by CNTF-LIF-OSM-IL-6 beta receptor components. *Science* 1994 Jan 7;263(5143):92-5.

118. Stahl N, Farruggella TJ, Boulton TG, Zhong Z, Darnell JE, Jr., Yancopoulos GD. Choice of STATs and other substrates specified by modular tyrosine-based motifs in cytokine receptors. *Science* 1995 Mar 3;267(5202):1349-53.

119. Davis S, Aldrich TH, Ip NY, Stahl N, Scherer S, Farruggella T, DiStefano PS, Curtis R, Panayotatos N, Gascan H, et al. Released form of CNTF receptor alpha component as a soluble mediator of CNTF responses. *Science* 1993 Mar 19;259(5102):1736-9.

120. De Serio A, Graziani R, Laufer R, Ciliberto G, Paonessa G. In vitro binding of ciliary neurotrophic factor to its receptors: evidence for the formation of an IL-6-type hexameric complex. *J Mol Biol* 1995 Dec 15;254(5):795-800.

121. Davis S, Yancopoulos GD. The molecular biology of the CNTF receptor. *Curr Opin Neurobiol* 1993 Feb;3(1):20-4.

122. Helgren ME, Squinto SP, Davis HL, Parry DJ, Boulton TG, Heck CS, Zhu Y, Yancopoulos GD, Lindsay RM, DiStefano PS. Trophic effect of ciliary neurotrophic factor on denervated skeletal muscle. *Cell* 1994 Feb 11;76(3):493-504.

123. Davis S, Aldrich TH, Valenzuela DM, Wong VV, Furth ME, Squinto SP, Yancopoulos GD. The receptor for ciliary neurotrophic factor. *Science* 1991 Jul 5;253(5015):59-63.

124. Ip NY, Nye SH, Boulton TG, Davis S, Taga T, Li Y, Birren SJ, Yasukawa K, Kishimoto T, Anderson DJ, et al. CNTF and LIF act on neuronal cells via shared signaling pathways that involve the IL-6 signal transducing receptor component gp130. *Cell* 1992 Jun 26;69(7):1121-32.

125. Nesbitt JE, Fuentes NL, Fuller GM. Ciliary neurotrophic factor regulates fibrinogen gene expression in hepatocytes by binding to the interleukin-6 receptor. *Biochem Biophys Res Commun* 1993 Jan 29;190(2):544-50.

126. Bellido T, Stahl N, Farruggella TJ, Borba V, Yancopoulos GD, Manolagas SC. Detection of receptors for interleukin-6, interleukin-11, leukemia inhibitory factor, oncostatin M, and ciliary neurotrophic factor in bone marrow stromal/osteoblastic cells. *J Clin Invest* 1996 Jan 15;97(2):431-7.

127. MacLennan AJ, Gaskin AA, Lado DC. CNTF receptor alpha mRNA expression in rodent cell lines and developing rat. *Brain Res Mol Brain Res* 1994 Sep;25(3-4):251-6.

128. Ip NY, McClain J, Barrezueta NX, Aldrich TH, Pan L, Li Y, Wiegand SJ, Friedman B, Davis S, Yancopoulos GD. The alpha component of the CNTF receptor is required for signaling and defines potential CNTF targets in the adult and during development. *Neuron* 1993 Jan;10(1):89-102.

129. Chun MH, Ju WK, Kim KY, Lee MY, Hofmann HD, Kirsch M, Oh SJ. Upregulation of ciliary neurotrophic factor in reactive Muller cells in the rat retina following optic nerve transection. *Brain Res* 2000 Jun 23;868(2):358-62.

130. Cao W, Wen R, Li F, Lavail MM, Steinberg RH. Mechanical injury increases bFGF and CNTF mRNA expression in the mouse retina. *Exp Eye Res* 1997 Aug;65(2):241-8.

131. Liu C, Peng M, Laties AM, Wen R. Preconditioning with bright light evokes a protective response against light damage in the rat retina. *J Neurosci* 1998 Feb 15;18(4):1337-44.

132. Honjo M, Tanihara H, Kido N, Inatani M, Okazaki K, Honda Y. Expression of ciliary neurotrophic factor activated by retinal Muller cells in eyes with NMDA- and kainic acid-induced neuronal death. *Invest Ophthalmol Vis Sci* 2000 Feb;41(2):552-60.

133. Wahlin KJ, Campochiaro PA, Zack DJ, Adler R. Neurotrophic factors cause activation of intracellular signaling pathways in Muller cells and other cells of the inner retina, but not photoreceptors. *Invest Ophthalmol Vis Sci* 2000 Mar;41(3):927-36.

134. Xie HQ, Adler R. Green cone opsin and rhodopsin regulation by CNTF and staurosporine in cultured chick photoreceptors. *Invest Ophthalmol Vis Sci* 2000 Dec;41(13):4317-23.

135. Ozawa Y, Nakao K, Shimazaki T, Takeda J, Akira S, Ishihara K, Hirano T, Oguchi Y, Okano H. Downregulation of STAT3 activation is required for presumptive rod photoreceptor cells to differentiate in the postnatal retina. *Mol Cell Neurosci* 2004 Jun;26(2):258-70.

136. Rhee KD, Goureau O, Chen S, Yang XJ. Cytokine-induced activation of signal transducer and activator of transcription in photoreceptor precursors regulates rod differentiation in the developing mouse retina. *J Neurosci* 2004 Nov 3;24(44):9779-88.

137. Zhang SS, Wei J, Qin H, Zhang L, Xie B, Hui P, Deisseroth A, Barnstable CJ, Fu XY. STAT3-mediated signaling in the determination of rod photoreceptor cell fate in mouse retina. *Invest Ophthalmol Vis Sci* 2004 Jul;45(7):2407-12.

138. Zhang SS, Liu MG, Kano A, Zhang C, Fu XY, Barnstable CJ. STAT3 activation in response to growth factors or cytokines participates in retina precursor proliferation. *Exp Eye Res* 2005 Jul;81(1):103-15.

139. Zack DJ. Neurotrophic rescue of photoreceptors: are Muller cells the mediators of survival? *Neuron* 2000 May;26(2):285-6.

140. Mey J, Thanos S. Intravitreal injections of neurotrophic factors support the survival of axotomized retinal ganglion cells in adult rats in vivo. *Brain Res* 1993 Feb 5;602(2):304-17.

141. Cui Q, Harvey AR. CNTF promotes the regrowth of retinal ganglion cell axons into murine peripheral nerve grafts. *Neuroreport* 2000 Dec 18;11(18):3999-4002.

142. Leaver SG, Cui Q, Plant GW, Arulpragasam A, Hisheh S, Verhaagen J, Harvey AR. AAV-mediated expression of CNTF promotes long-term survival and regeneration of adult rat retinal ganglion cells. *Gene Ther* 2006 Sep;13(18):1328-41.

143. Pease ME, Zack DJ, Berlinicke C, Bloom K, Cone F, Wang Y, Klein RL, Hauswirth WW, Quigley HA. Effect of CNTF on retinal ganglion cell survival in experimental glaucoma. *Invest Ophthalmol Vis Sci* 2009 May;50(5):2194-200.

144. Leibinger M, Muller A, Andreadaki A, Hauk TG, Kirsch M, Fischer D. Neuroprotective and axon growth-promoting effects following inflammatory stimulation on mature retinal ganglion cells in mice depend on ciliary neurotrophic factor and leukemia inhibitory factor. *J Neurosci* 2009 Nov 11;29(45):14334-41.

145. Ooto S, Akagi T, Kageyama R, Akita J, Mandai M, Honda Y, Takahashi M. Potential for neural regeneration after neurotoxic injury in the adult mammalian retina. *Proc Natl Acad Sci U S A* 2004 Sep 14;101(37):13654-9.

146. Bonni A, Sun Y, Nadal-Vicens M, Bhatt A, Frank DA, Rozovsky I, Stahl N, Yancopoulos GD, Greenberg ME. Regulation of gliogenesis in the central nervous system by the JAK-STAT signaling pathway. *Science* 1997 Oct 17;278(5337):477-83.

147. Zhou WT, Ni YQ, Jin ZB, Zhang M, Wu JH, Zhu Y, Xu GZ, Gan DK. Electrical stimulation ameliorates light-induced photoreceptor degeneration in vitro via suppressing the proinflammatory effect of microglia and enhancing the neurotrophic potential of Muller cells. *Exp Neurol* 2012 Sep 10;238(2):192-208.

148. Valter K, Bisti S, Stone J. Location of CNTFRalpha on outer segments: evidence of the site of action of CNTF in rat retina. *Brain Res* 2003 Sep 26;985(2):169-75.

149. Escartin C, Brouillet E, Gubellini P, Trioulier Y, Jacquard C, Smadja C, Knott GW, Kerkerian-Le Goff L, Deglon N, Hantraye P, Bonvento G. Ciliary neurotrophic factor activates astrocytes, redistributes their glutamate transporters GLAST and GLT-1 to raft microdomains, and improves glutamate handling in vivo. *J Neurosci* 2006 May 31;26(22):5978-89.

150. Escartin C, Pierre K, Colin A, Brouillet E, Delzescaux T, Guillermier M, Dhenain M, Deglon N, Hantraye P, Pellerin L, Bonvento G. Activation of astrocytes by CNTF induces metabolic plasticity and increases resistance to metabolic insults. *J Neurosci* 2007 Jul 4;27(27):7094-104.

151. Ueki Y, Le YZ, Chollangi S, Muller W, Ash JD. Preconditioning-induced protection of photoreceptors requires activation of the signal-transducing receptor gp130 in photoreceptors. *Proc Natl Acad Sci U S A* 2009 Dec 15;106(50):21389-94.

152. Ikeda K, Tatsuno T, Noguchi H, Nakayama C. Ciliary neurotrophic factor protects rat retina cells in vitro and in vivo via PI3 kinase. *Curr Eye Res* 2004 Oct-Nov;29(4-5):349-55.

153. Beltran WA, Allore HG, Johnson E, Towle V, Tao W, Acland GM, Aguirre GD, Zeiss CJ. CREB1/ATF1 activation in photoreceptor degeneration and protection. *Invest Ophthalmol Vis Sci* 2009 Nov;50(11):5355-63.

154. LaVail MM, Unoki K, Yasumura D, Matthes MT, Yancopoulos GD, Steinberg RH. Multiple growth factors, cytokines, and neurotrophins rescue photoreceptors from the damaging effects of constant light. *Proc Natl Acad Sci U S A* 1992 Dec 1;89(23):11249-53.

155. LaVail MM, Yasumura D, Matthes MT, Lau-Villacorta C, Unoki K, Sung CH, Steinberg RH. Protection of mouse photoreceptors by survival factors in retinal degenerations. *Invest Ophthalmol Vis Sci* 1998 Mar;39(3):592-602.

156. Chong NH, Alexander RA, Waters L, Barnett KC, Bird AC, Luthert PJ. Repeated injections of a ciliary neurotrophic factor analogue leading to long-term photoreceptor survival in hereditary retinal degeneration. *Invest Ophthalmol Vis Sci* 1999 May;40(6):1298-305.

157. Beltran WA, Wen R, Acland GM, Aguirre GD. Intravitreal injection of ciliary neurotrophic factor (CNTF) causes peripheral remodeling and does not prevent photoreceptor loss in canine RPGR mutant retina. *Exp Eye Res* 2007 Apr;84(4):753-71.

158. Cayouette M, Behn D, Sendtner M, Lachapelle P, Gravel C. Intraocular gene transfer of ciliary neurotrophic factor prevents death and increases responsiveness of rod

photoreceptors in the retinal degeneration slow mouse. *J Neurosci* 1998 Nov 15;18(22):9282-93.

159. Liang FQ, Aleman TS, Dejneka NS, Dudus L, Fisher KJ, Maguire AM, Jacobson SG, Bennett J. Long-term protection of retinal structure but not function using RAAV.CNTF in animal models of retinitis pigmentosa. *Mol Ther* 2001 Nov;4(5):461-72.

160. Tao W, Wen R, Goddard MB, Sherman SD, O'Rourke PJ, Stabila PF, Bell WJ, Dean BJ, Kauper KA, Budz VA, Tsiaras WG, Acland GM, Pearce-Kelling S, Laties AM, Aguirre GD. Encapsulated cell-based delivery of CNTF reduces photoreceptor degeneration in animal models of retinitis pigmentosa. *Invest Ophthalmol Vis Sci* 2002 Oct;43(10):3292-8.

161. Sieving PA, Caruso RC, Tao W, Coleman HR, Thompson DJ, Fullmer KR, Bush RA. Ciliary neurotrophic factor (CNTF) for human retinal degeneration: phase I trial of CNTF delivered by encapsulated cell intraocular implants. *Proc Natl Acad Sci U S A* 2006 Mar 7;103(10):3896-901.

162. Zhang K, Hopkins JJ, Heier JS, Birch DG, Halperin LS, Albini TA, Brown DM, Jaffe GJ, Tao W, Williams GA. Ciliary neurotrophic factor delivered by encapsulated cell intraocular implants for treatment of geographic atrophy in age-related macular degeneration. *Proc Natl Acad Sci U S A* 2011 Apr 12;108(15):6241-5.

163. Bok D, Yasumura D, Matthes MT, Ruiz A, Duncan JL, Chappelow AV, Zolutukhin S, Hauswirth W, LaVail MM. Effects of adeno-associated virus-vectored ciliary neurotrophic factor on retinal structure and function in mice with a P216L rds/peripherin mutation. *Exp Eye Res* 2002 Jun;74(6):719-35.

164. Schlichtenbrede FC, MacNeil A, Bainbridge JW, Tschernutter M, Thrasher AJ, Smith AJ, Ali RR. Intraocular gene delivery of ciliary neurotrophic factor results in significant loss of retinal function in normal mice and in the Prph2Rd2/Rd2 model of retinal degeneration. *Gene Ther* 2003 Mar;10(6):523-7.

165. Bush RA, Lei B, Tao W, Raz D, Chan CC, Cox TA, Santos-Muffley M, Sieving PA. Encapsulated cell-based intraocular delivery of ciliary neurotrophic factor in normal rabbit: dose-dependent effects on ERG and retinal histology. *Invest Ophthalmol Vis Sci* 2004 Jul;45(7):2420-30.

166. Wen R, Song Y, Kjellstrom S, Tanikawa A, Liu Y, Li Y, Zhao L, Bush RA, Laties AM, Sieving PA. Regulation of rod phototransduction machinery by ciliary neurotrophic factor. *J Neurosci* 2006 Dec 27;26(52):13523-30.

167. Cibis GW, Fitzgerald KM, Harris DJ, Rothberg PG, Rupani M. The effects of dystrophin gene mutations on the ERG in mice and humans. *Invest Ophthalmol Vis Sci* 1993 Dec;34(13):3646-52.

168. Cibis GW, Fitzgerald KM. The negative ERG is not synonymous with nightblindness. *Trans Am Ophthalmol Soc* 2001;99:171-5; discussion 5-6.

169. McGill TJ, Prusky GT, Douglas RM, Yasumura D, Matthes MT, Nune G, Donohue-Rolfe K, Yang H, Niculescu D, Hauswirth WW, Girman SV, Lund RD, Duncan JL, LaVail MM. Intraocular CNTF reduces vision in normal rats in a dose-dependent manner. *Invest Ophthalmol Vis Sci* 2007 Dec;48(12):5756-66.

170. Li Y, Tao W, Luo L, Huang D, Kauper K, Stabila P, Lavail MM, Laties AM, Wen R. CNTF induces regeneration of cone outer segments in a rat model of retinal degeneration. *PLoS One* 2010;5(3):e9495.

171. Delyfer MN, Leveillard T, Mohand-Said S, Hicks D, Picaud S, Sahel JA. Inherited retinal degenerations: therapeutic prospects. *Biol Cell* 2004 May;96(4):261-9.

172. Leveillard T, Mohand-Said S, Lorentz O, Hicks D, Fintz AC, Clerin E, Simonutti M, Forster V, Cavusoglu N, Chalmel F, Dolle P, Poch O, Lambrou G, Sahel JA. Identification and characterization of rod-derived cone viability factor. *Nat Genet* 2004 Jul;36(7):755-9.

173. Mattson MP, Scheff SW. Endogenous neuroprotection factors and traumatic brain injury: mechanisms of action and implications for therapy. *J Neurotrauma* 1994 Feb;11(1):3-33.

174. Kirsch M, Lee MY, Meyer V, Wiese A, Hofmann HD. Evidence for multiple, local functions of ciliary neurotrophic factor (CNTF) in retinal development: expression of CNTF and its receptors and in vitro effects on target cells. *J Neurochem* 1997 Mar;68(3):979-90.

175. Carri NG, Richardson P, Ebendal T. Choroid coat extract and ciliary neurotrophic factor strongly promote neurite outgrowth in the embryonic chick retina. *Int J Dev Neurosci* 1994 Oct;12(6):567-78.

176. Cui Q, Lu Q, So KF, Yip HK. CNTF, not other trophic factors, promotes axonal regeneration of axotomized retinal ganglion cells in adult hamsters. *Invest Ophthalmol Vis Sci* 1999 Mar;40(3):760-6.

177. Muller A, Hauk TG, Fischer D. Astrocyte-derived CNTF switches mature RGCs to a regenerative state following inflammatory stimulation. *Brain* 2007 Dec;130(Pt 12):3308-20.

178. Fischer D, Pavlidis M, Thanos S. Cataractogenic lens injury prevents traumatic ganglion cell death and promotes axonal regeneration both in vivo and in culture. *Invest Ophthalmol Vis Sci* 2000 Nov;41(12):3943-54.

179. Lorber B, Berry M, Logan A. Different factors promote axonal regeneration of adult rat retinal ganglion cells after lens injury and intravitreal peripheral nerve grafting. *J Neurosci Res* 2008 Mar;86(4):894-903.

180. Boyd ZS, Kriatchko A, Yang J, Agarwal N, Wax MB, Patil RV. Interleukin-10 receptor signaling through STAT-3 regulates the apoptosis of retinal ganglion cells in response to stress. *Invest Ophthalmol Vis Sci* 2003 Dec;44(12):5206-11.

181. Kretz A, Happold CJ, Marticke JK, Isenmann S. Erythropoietin promotes regeneration of adult CNS neurons via Jak2/Stat3 and PI3K/AKT pathway activation. *Mol Cell Neurosci* 2005 Aug;29(4):569-79.

182. Zhang C, Li H, Liu MG, Kawasaki A, Fu XY, Barnstable CJ, Shao-Min Zhang S. STAT3 activation protects retinal ganglion cell layer neurons in response to stress. *Exp Eye Res* 2008 Jun;86(6):991-7.

183. Muller A, Hauk TG, Leibinger M, Marienfeld R, Fischer D. Exogenous CNTF stimulates axon regeneration of retinal ganglion cells partially via endogenous CNTF. *Mol Cell Neurosci* 2009 Jun;41(2):233-46.

184. Walsh N, Valter K, Stone J. Cellular and subcellular patterns of expression of bFGF and CNTF in the normal and light stressed adult rat retina. *Exp Eye Res* 2001 May;72(5):495-501.

185. Li R, Wen R, Banzon T, Maminishkis A, Miller SS. CNTF mediates neurotrophic factor secretion and fluid absorption in human retinal pigment epithelium. *PLoS One* 2011;6(9):e23148.

186. Fisher SK, Erickson PA, Lewis GP, Anderson DH. Intraretinal proliferation induced by retinal detachment. *Invest Ophthalmol Vis Sci* 1991 May;32(6):1739-48.

187. Zrenner E, Bartz-Schmidt KU, Benav H, Besch D, Bruckmann A, Gabel VP, Gekeler F, Greppmaier U, Harscher A, Kibbel S, Koch J, Kusnyerik A, Peters T, Stingl K, Sachs H, Stett A, Szurman P, Wilhelm B, Wilke R. Subretinal electronic chips allow blind patients to read letters and combine them to words. *Proc Biol Sci* 2011 May 22;278(1711):1489-97.

188. Humayun MS, Weiland JD, Fujii GY, Greenberg R, Williamson R, Little J, Mech B, Cimmarusti V, Van Boemel G, Dagnelie G, de Juan E. Visual perception in a blind subject with a chronic microelectronic retinal prosthesis. *Vision Res* 2003 Nov;43(24):2573-81.

189. Wagers AJ, Weissman IL. Plasticity of adult stem cells. *Cell* 2004 Mar 5;116(5):639-48.

190. Eiraku M, Takata N, Ishibashi H, Kawada M, Sakakura E, Okuda S, Sekiguchi K, Adachi T, Sasai Y. Self-organizing optic-cup morphogenesis in three-dimensional culture. *Nature* 2011 Apr 7;472(7341):51-6.

191. Ying QL, Nichols J, Chambers I, Smith A. BMP induction of Id proteins suppresses differentiation and sustains embryonic stem cell self-renewal in collaboration with STAT3. *Cell* 2003 Oct 31;115(3):281-92.

192. Sato N, Meijer L, Skaltsounis L, Greengard P, Brivanlou AH. Maintenance of pluripotency in human and mouse embryonic stem cells through activation of Wnt signaling by a pharmacological GSK-3-specific inhibitor. *Nat Med* 2004 Jan;10(1):55-63.

193. Sumi T, Fujimoto Y, Nakatsuji N, Suemori H. STAT3 is dispensable for maintenance of self-renewal in nonhuman primate embryonic stem cells. *Stem Cells* 2004;22(5):861-72.

194. Daheron L, Opitz SL, Zaehres H, Lensch MW, Andrews PW, Itskovitz-Eldor J, Daley GQ. LIF/STAT3 signaling fails to maintain self-renewal of human embryonic stem cells. *Stem Cells* 2004;22(5):770-8.

195. Pera MF, Andrade J, Houssami S, Reubinoff B, Trounson A, Stanley EG, Ward-van Oostwaard D, Mummery C. Regulation of human embryonic stem cell differentiation by BMP-2 and its antagonist noggin. *J Cell Sci* 2004 Mar 1;117(Pt 7):1269-80.

196. Hori J, Ng TF, Shatos M, Klassen H, Streilein JW, Young MJ. Neural progenitor cells lack immunogenicity and resist destruction as allografts. *Stem Cells* 2003;21(4):405-16.

197. Svendsen CN, Skepper J, Rosser AE, ter Borg MG, Tyres P, Ryken T. Restricted growth potential of rat neural precursors as compared to mouse. *Brain Res Dev Brain Res* 1997 Apr 18;99(2):253-8.

198. Kalyani AJ, Piper D, Mujtaba T, Lucero MT, Rao MS. Spinal cord neuronal precursors generate multiple neuronal phenotypes in culture. *J Neurosci* 1998 Oct 1;18(19):7856-68.

199. He W, Ingraham C, Rising L, Goderie S, Temple S. Multipotent stem cells from the mouse basal forebrain contribute GABAergic neurons and oligodendrocytes to the cerebral cortex during embryogenesis. *J Neurosci* 2001 Nov 15;21(22):8854-62.

200. Hitoshi S, Tropepe V, Ekker M, van der Kooy D. Neural stem cell lineages are regionally specified, but not committed, within distinct compartments of the developing brain. *Development* 2002 Jan;129(1):233-44.

201. Smith R, Bagga V, Fricker-Gates RA. Embryonic neural progenitor cells: the effects of species, region, and culture conditions on long-term proliferation and neuronal differentiation. *J Hematother Stem Cell Res* 2003 Dec;12(6):713-25.

202. Suhonen JO, Peterson DA, Ray J, Gage FH. Differentiation of adult hippocampus-derived progenitors into olfactory neurons in vivo. *Nature* 1996 Oct 17;383(6601):624-7.

203. Temple S. The development of neural stem cells. *Nature* 2001 Nov 1;414(6859):112-7.

204. Chow RL, Lang RA. Early eye development in vertebrates. *Annu Rev Cell Dev Biol* 2001;17:255-96.

205. Nguyen M, Arnheiter H. Signaling and transcriptional regulation in early mammalian eye development: a link between FGF and MITF. *Development* 2000 Aug;127(16):3581-91.

206. Mikami Y. Reciprocal transformation of the parts in the developing eye-vesicle, with special reference to the inductive influence of the lens-ectoderm on the retinal determination. *Zool Mag* 1939;51:253–56.

207. Liu IS, Chen JD, Ploder L, Vidgen D, van der Kooy D, Kalnins VI, McInnes RR. Developmental expression of a novel murine homeobox gene (Chx10): evidence for roles in determination of the neuroretina and inner nuclear layer. *Neuron* 1994 Aug;13(2):377-93.

208. Burmeister M, Novak J, Liang MY, Basu S, Ploder L, Hawes NL, Vidgen D, Hoover F, Goldman D, Kalnins VI, Roderick TH, Taylor BA, Hankin MH, McInnes RR. Ocular retardation mouse caused by Chx10 homeobox null allele: impaired retinal progenitor proliferation and bipolar cell differentiation. *Nat Genet* 1996 Apr;12(4):376-84.

209. Ferda Percin E, Ploder LA, Yu JJ, Arici K, Horsford DJ, Rutherford A, Bapat B, Cox DW, Duncan AM, Kalnins VI, Kocak-Altintas A, Sowden JC, Traboulsi E, Sarfarazi M, McInnes RR. Human microphthalmia associated with mutations in the retinal homeobox gene CHX10. *Nat Genet* 2000 Aug;25(4):397-401.

210. Amirpour N, Karamali F, Rabiee F, Rezaei L, Esfandiari E, Razavi S, Dehghani A, Razmju H, Nasr-Esfahani MH, Baharvand H. Differentiation of human embryonic stem cell-derived retinal progenitors into retinal cells by Sonic hedgehog and/or retinal pigmented epithelium and transplantation into the subretinal space of sodium iodate-injected rabbits. *Stem Cells Dev* 2012 Jan;21(1):42-53.

211. Vogel-Hopker A, Momose T, Rohrer H, Yasuda K, Ishihara L, Rapaport DH. Multiple functions of fibroblast growth factor-8 (FGF-8) in chick eye development. *Mech Dev* 2000 Jun;94(1-2):25-36.

212. Pittack C, Grunwald GB, Reh TA. Fibroblast growth factors are necessary for neural retina but not pigmented epithelium differentiation in chick embryos. *Development* 1997 Feb;124(4):805-16.

213. Lamba DA, Karl MO, Ware CB, Reh TA. Efficient generation of retinal progenitor cells from human embryonic stem cells. *Proc Natl Acad Sci U S A* 2006 Aug 22;103(34):12769-74.

214. Ikeda H, Osakada F, Watanabe K, Mizuseki K, Haraguchi T, Miyoshi H, Kamiya D, Honda Y, Sasai N, Yoshimura N, Takahashi M, Sasai Y. Generation of Rx+/Pax6+ neural retinal precursors from embryonic stem cells. *Proc Natl Acad Sci U S A* 2005 Aug 9;102(32):11331-6.

215. Turner DL, Snyder EY, Cepko CL. Lineage-independent determination of cell type in the embryonic mouse retina. *Neuron* 1990 Jun;4(6):833-45.

216. Engelhardt M, Wachs FP, Couillard-Despres S, Aigner L. The neurogenic competence of progenitors from the postnatal rat retina in vitro. *Exp Eye Res* 2004 May;78(5):1025-36.

217. James J, Das AV, Bhattacharya S, Chacko DM, Zhao X, Ahmad I. In vitro generation of early-born neurons from late retinal progenitors. *J Neurosci* 2003 Sep 10;23(23):8193-203.

218. Franklin RJ, Ffrench-Constant C. Remyelination in the CNS: from biology to therapy. *Nat Rev Neurosci* 2008 Nov;9(11):839-55.

219. Cameron HA, McKay R. Stem cells and neurogenesis in the adult brain. *Curr Opin Neurobiol* 1998 Oct;8(5):677-80.

220. Alvarez-Buylla A, Garcia-Verdugo JM, Tramontin AD. A unified hypothesis on the lineage of neural stem cells. *Nat Rev Neurosci* 2001 Apr;2(4):287-93.

221. Clarke DL, Johansson CB, Wilbertz J, Veress B, Nilsson E, Karlstrom H, Lendahl U, Frisen J. Generalized potential of adult neural stem cells. *Science* 2000 Jun 2;288(5471):1660-3.

222. Bjornson CR, Rietze RL, Reynolds BA, Magli MC, Vescovi AL. Turning brain into blood: a hematopoietic fate adopted by adult neural stem cells in vivo. *Science* 1999 Jan 22;283(5401):534-7.

223. Rietze RL, Valcanis H, Brooker GF, Thomas T, Voss AK, Bartlett PF. Purification of a pluripotent neural stem cell from the adult mouse brain. *Nature* 2001 Aug 16;412(6848):736-9.

224. Nishida A, Takahashi M, Tanihara H, Nakano I, Takahashi JB, Mizoguchi A, Ide C, Honda Y. Incorporation and differentiation of hippocampus-derived neural stem cells transplanted in injured adult rat retina. *Invest Ophthalmol Vis Sci* 2000 Dec;41(13):4268-74.

225. Sanchez-Ramos J, Song S, Cardozo-Pelaez F, Hazzi C, Stedeford T, Willing A, Freeman TB, Saporta S, Janssen W, Patel N, Cooper DR, Sanberg PR. Adult bone marrow stromal cells differentiate into neural cells in vitro. *Exp Neurol* 2000 Aug;164(2):247-56.

226. Tomita M, Adachi Y, Yamada H, Takahashi K, Kiuchi K, Oyaizu H, Ikebukuro K, Kaneda H, Matsumura M, Ikehara S. Bone marrow-derived stem cells can differentiate into retinal cells in injured rat retina. *Stem Cells* 2002;20(4):279-83.

227. Kicic A, Shen WY, Wilson AS, Constable IJ, Robertson T, Rakoczy PE. Differentiation of marrow stromal cells into photoreceptors in the rat eye. *J Neurosci* 2003 Aug 27;23(21):7742-9.

228. Gong L, Wu Q, Song B, Lu B, Zhang Y. Differentiation of rat mesenchymal stem cells transplanted into the subretinal space of sodium iodate-injected rats. *Clin Experiment Ophthalmol* 2008 Oct;36(7):666-71.

229. Zhang ZQ, Dong FT. [In vitro differentiation of rat mesenchymal stem cells into photoreceptors]. *Zhonghua Yan Ke Za Zhi* 2008 Jun;44(6):540-4.

230. Yu S, Tanabe T, Dezawa M, Ishikawa H, Yoshimura N. Effects of bone marrow stromal cell injection in an experimental glaucoma model. *Biochem Biophys Res Commun* 2006 Jun 16;344(4):1071-9.

231. Li N, Li XR, Yuan JQ. Effects of bone-marrow mesenchymal stem cells transplanted into vitreous cavity of rat injured by ischemia/reperfusion. *Graefes Arch Clin Exp Ophthalmol* 2009 Apr;247(4):503-14.

232. Wang S, Lu B, Girman S, Duan J, McFarland T, Zhang QS, Grompe M, Adamus G, Appukuttan B, Lund R. Non-invasive stem cell therapy in a rat model for retinal degeneration and vascular pathology. *PLoS One* 2010;5(2):e9200.

233. Inoue Y, Iriyama A, Ueno S, Takahashi H, Kondo M, Tamaki Y, Araie M, Yanagi Y. Subretinal transplantation of bone marrow mesenchymal stem cells delays retinal degeneration in the RCS rat model of retinal degeneration. *Exp Eye Res* 2007 Aug;85(2):234-41.

234. Takahashi K, Yamanaka S. Induction of pluripotent stem cells from mouse embryonic and adult fibroblast cultures by defined factors. *Cell* 2006 Aug 25;126(4):663-76.

235. Takahashi K, Tanabe K, Ohnuki M, Narita M, Ichisaka T, Tomoda K, Yamanaka S. Induction of pluripotent stem cells from adult human fibroblasts by defined factors. *Cell* 2007 Nov 30;131(5):861-72.

236. Weismann A, Poulton EB, Schönland S, Shipley AE. Essays upon heredity and kindred biological problems. 2d ed. 1891. Oxford,: Clarendon press.

237. Hussein SM, Batada NN, Vuoristo S, Ching RW, Autio R, Narva E, Ng S, Sourour M, Hamalainen R, Olsson C, Lundin K, Mikkola M, Trokovic R, Peitz M, Brustle O, Bazett-Jones DP, Alitalo K, Lahesmaa R, Nagy A, Otonkoski T. Copy number variation and selection during reprogramming to pluripotency. *Nature* 2011 Mar 3;471(7336):58-62.

238. Laurent LC, Ulitsky I, Slavin I, Tran H, Schork A, Morey R, Lynch C, Harness JV, Lee S, Barrero MJ, Ku S, Martynova M, Semechkin R, Galat V, Gottesfeld J, Izpisua Belmonte JC, Murry C, Keirstead HS, Park HS, Schmidt U, Laslett AL, Muller FJ, Nievergelt CM, Shamir R, Loring JF. Dynamic changes in the copy number of pluripotency and cell proliferation genes in human ESCs and iPSCs during reprogramming and time in culture. *Cell Stem Cell* 2011 Jan 7;8(1):106-18.

239. Mayshar Y, Ben-David U, Lavon N, Biancotti JC, Yakir B, Clark AT, Plath K, Lowry WE, Benvenisty N. Identification and classification of chromosomal aberrations in human induced pluripotent stem cells. *Cell Stem Cell* 2010 Oct 8;7(4):521-31.

240. Kokkinaki M, Sahibzada N, Golestaneh N. Human induced pluripotent stem-derived retinal pigment epithelium (RPE) cells exhibit ion transport, membrane potential, polarized vascular endothelial growth factor secretion, and gene expression pattern similar to native RPE. *Stem Cells* 2011 May;29(5):825-35.

241. Hirami Y, Osakada F, Takahashi K, Okita K, Yamanaka S, Ikeda H, Yoshimura N, Takahashi M. Generation of retinal cells from mouse and human induced pluripotent stem cells. *Neurosci Lett* 2009 Jul 24;458(3):126-31.

242. Meyer JS, Howden SE, Wallace KA, Verhoeven AD, Wright LS, Capowski EE, Pinilla I, Martin JM, Tian S, Stewart R, Pattnaik B, Thomson JA, Gamm DM. Optic vesicle-like structures derived from human pluripotent stem cells facilitate a customized approach to retinal disease treatment. *Stem Cells* 2011 Aug;29(8):1206-18.

243. Phillips MJ, Wallace KA, Dickerson SJ, Miller MJ, Verhoeven AD, Martin JM, Wright LS, Shen W, Capowski EE, Percin EF, Perez ET, Zhong X, Canto-Soler MV, Gamm DM. Blood-derived human iPS cells generate optic vesicle-like structures with the capacity to form retinal laminae and develop synapses. *Invest Ophthalmol Vis Sci* 2012 Apr;53(4):2007-19.

244. Nakano T, Ando S, Takata N, Kawada M, Muguruma K, Sekiguchi K, Saito K, Yonemura S, Eiraku M, Sasai Y. Self-formation of optic cups and storable stratified neural retina from human ESCs. *Cell Stem Cell* 2012 Jun 14;10(6):771-85.

245. Reh TA, Levine EM. Multipotential stem cells and progenitors in the vertebrate retina. *J Neurobiol* 1998 Aug;36(2):206-20.

246. Nishiguchi KM, Kaneko H, Nakamura M, Kachi S, Terasaki H. Identification of photoreceptor precursors in the pars plana during ocular development and after retinal injury. *Invest Ophthalmol Vis Sci* 2008 Jan;49(1):422-8.

247. Tropepe V, Coles BL, Chiasson BJ, Horsford DJ, Elia AJ, McInnes RR, van der Kooy D. Retinal stem cells in the adult mammalian eye. *Science* 2000 Mar 17;287(5460):2032-6.

248. Cicero SA, Johnson D, Reyntjens S, Frase S, Connell S, Chow LM, Baker SJ, Sorrentino BP, Dyer MA. Cells previously identified as retinal stem cells are pigmented ciliary epithelial cells. *Proc Natl Acad Sci U S A* 2009 Apr 21;106(16):6685-90.

249. Kiyama T, Li H, Gupta M, Lin YP, Chuang AZ, Otteson DC, Wang SW. Distinct neurogenic potential in the retinal margin and the pars plana of mammalian eye. *J Neurosci* 2012 Sep 12;32(37):12797-807.

250. Jadhav AP, Roesch K, Cepko CL. Development and neurogenic potential of Muller glial cells in the vertebrate retina. *Prog Retin Eye Res* 2009 Jul;28(4):249-62.

251. Bringmann A, Iandiev I, Pannicke T, Wurm A, Hollborn M, Wiedemann P, Osborne NN, Reichenbach A. Cellular signaling and factors involved in Muller cell gliosis: neuroprotective and detrimental effects. *Prog Retin Eye Res* 2009 Nov;28(6):423-51.

252. Yurco P, Cameron DA. Responses of Muller glia to retinal injury in adult zebrafish. *Vision Res* 2005 Apr;45(8):991-1002.

253. Raymond PA, Barthel LK, Bernardos RL, Perkowski JJ. Molecular characterization of retinal stem cells and their niches in adult zebrafish. *BMC Dev Biol* 2006;6:36.

254. Fimbel SM, Montgomery JE, Burket CT, Hyde DR. Regeneration of inner retinal neurons after intravitreal injection of ouabain in zebrafish. *J Neurosci* 2007 Feb 14;27(7):1712-24.

255. Osakada F, Ooto S, Akagi T, Mandai M, Akaike A, Takahashi M. Wnt signaling promotes regeneration in the retina of adult mammals. *J Neurosci* 2007 Apr 11;27(15):4210-9.

256. Das AV, Mallya KB, Zhao X, Ahmad F, Bhattacharya S, Thoreson WB, Hegde GV, Ahmad I. Neural stem cell properties of Muller glia in the mammalian retina: regulation by Notch and Wnt signaling. *Dev Biol* 2006 Nov 1;299(1):283-302.

257. Fischer AJ, Reh TA. Muller glia are a potential source of neural regeneration in the postnatal chicken retina. *Nat Neurosci* 2001 Mar;4(3):247-52.

258. Giannelli SG, Demontis GC, Pertile G, Rama P, Broccoli V. Adult human Muller glia cells are a highly efficient source of rod photoreceptors. *Stem Cells* 2011 Feb;29(2):344-56.

259. Joly S, Pernet V, Samardzija M, Grimm C. Pax6-positive Muller glia cells express cell cycle markers but do not proliferate after photoreceptor injury in the mouse retina. *Glia* 2011 Jul;59(7):1033-46.

260. Koppányi T. Die Replantation von Augen. *Archiv für mikroskopische Anatomie und Entwicklungsmechanik* 1923;99(1):43-57.

261. Royo PE, Quay WB. Retinal transplantation from fetal to maternal mammalian eye. *Growth* 1959 Dec;23:313-36.

262. McLoon SC, Lund RD. Specific projections of retina transplanted to rat brain. *Exp Brain Res* 1980;40(3):273-82.

263. McLoon SC, Lund RD. Development of fetal retina, tectum, and cortex transplanted to the superior colliculus of adult rats. *J Comp Neurol* 1983 Jul 10;217(4):376-89.

264. Harvey AR, Lund RD. Transplantation of tectal tissue in rats. IV. Maturation of transplants and development of host retinal projection. *Brain Res* 1984 Jan;314(1):27-37.

265. Simons DJ, Lund RD. Fetal retinae transplanted over tecta of neonatal rats respond to light and evoke patterned neuronal discharges in the host superior colliculus. *Brain Res* 1985 Jul;353(1):156-9.

266. Horsburgh GM, Lund RD, Hankin MH. Retinal transplants in congenitally blind mice: patterns of projection and synaptic connectivity. *J Comp Neurol* 1993 Jan 15;327(3):323-40.

267. Sauve Y, Girman SV, Wang S, Keegan DJ, Lund RD. Preservation of visual responsiveness in the superior colliculus of RCS rats after retinal pigment epithelium cell transplantation. *Neuroscience* 2002;114(2):389-401.

268. Sauve Y, Pinilla I, Lund RD. Partial preservation of rod and cone ERG function following subretinal injection of ARPE-19 cells in RCS rats. *Vision Res* 2006 Apr;46(8-9):1459-72.

269. Gamm DM, Wang S, Lu B, Girman S, Holmes T, Bischoff N, Shearer RL, Sauve Y, Capowski E, Svendsen CN, Lund RD. Protection of visual functions by human neural progenitors in a rat model of retinal disease. *PLoS One* 2007;2(3):e338.

270. Francis PJ, Wang S, Zhang Y, Brown A, Hwang T, McFarland TJ, Jeffrey BG, Lu B, Wright L, Appukuttan B, Wilson DJ, Stout JT, Neuringer M, Gamm DM, Lund RD. Subretinal transplantation of forebrain progenitor cells in nonhuman primates:

survival and intact retinal function. *Invest Ophthalmol Vis Sci* 2009 Jul;50(7):3425-31.

271. Rothermel A, Willbold E, Degrip WJ, Layer PG. Pigmented epithelium induces complete retinal reconstitution from dispersed embryonic chick retinae in reaggregation culture. *Proc Biol Sci* 1997 Sep 22;264(1386):1293-302.

272. Rothermel A, Layer PG. Photoreceptor plasticity in reaggregates of embryonic chick retina: rods depend on proximal cones and on tissue organization. *Eur J Neurosci* 2001 Mar;13(5):949-58.

273. Wolburg H, Willbold E, Layer PG. Muller glia endfeet, a basal lamina and the polarity of retinal layers form properly in vitro only in the presence of marginal pigmented epithelium. *Cell Tissue Res* 1991 Jun;264(3):437-51.

274. Hering H, Kroger S. Synapse formation and agrin expression in stratospheroid cultures from embryonic chick retina. *Dev Biol* 1999 Oct 15;214(2):412-28.

275. Sharma RK, Bergstrom A, Ehinger B. Influence of technique and transplantation site on rosette formation in rabbit retinal transplants. *Acta Ophthalmol Scand* 1997 Feb;75(1):3-10.

276. Seiler MJ, Aramant RB, Bergstrom A. Co-transplantation of embryonic retina and retinal pigment epithelial cells to rabbit retina. *Curr Eye Res* 1995 Mar;14(3):199-207.

277. Khodair MA, Zarbin MA, Townes-Anderson E. Synaptic plasticity in mammalian photoreceptors prepared as sheets for retinal transplantation. *Invest Ophthalmol Vis Sci* 2003 Nov;44(11):4976-88.

278. Akagawa K, Hicks D, Barnstable CJ. Histiotypic organization and cell differentiation in rat retinal reaggregate cultures. *Brain Res* 1987 Dec 29;437(2):298-308.

279. Watanabe T, Raff MC. Rod photoreceptor development in vitro: intrinsic properties of proliferating neuroepithelial cells change as development proceeds in the rat retina. *Neuron* 1990 Mar;4(3):461-7.

280. Layer PG, Willbold E. Embryonic chicken retinal cells can regenerate all cell layers in vitro, but ciliary pigmented cells induce their correct polarity. *Cell Tissue Res* 1989 Nov;258(2):233-42.

281. Sheffield JB. Studies on aggregation of embryonic cells: initial cell adhesions and the formation of intercellular junctions. *J Morphol* 1970 Nov;132(3):245-63.

282. Kinouchi R, Takeda M, Yang L, Wilhelmsson U, Lundkvist A, Pekny M, Chen DF. Robust neural integration from retinal transplants in mice deficient in GFAP and vimentin. *Nat Neurosci* 2003 Aug;6(8):863-8.

283. West EL, Pearson RA, Tschernutter M, Sowden JC, MacLaren RE, Ali RR. Pharmacological disruption of the outer limiting membrane leads to increased retinal integration of transplanted photoreceptor precursors. *Exp Eye Res* 2008 Apr;86(4):601-11.

284. Ghosh F, Neeley WL, Arner K, Langer R. Selective removal of photoreceptor cells in vivo using the biodegradable elastomer poly(glycerol sebacate). *Tissue Eng Part A* 2011 Jul;17(13-14):1675-82.

285. Baker PS, Brown GC. Stem-cell therapy in retinal disease. *Curr Opin Ophthalmol* 2009 May;20(3):175-81.

286. del Cerro M, Gash DM, Rao GN, Notter MF, Wiegand SJ, Gupta M. Intraocular retinal transplants. *Invest Ophthalmol Vis Sci* 1985 Aug;26(8):1182-5.

287. Turner JE, Blair JR. Newborn rat retinal cells transplanted into a retinal lesion site in adult host eyes. *Brain Res* 1986 Apr;391(1):91-104.

288. Gouras P, Flood MT, Kjedbye H, Bilek MK, Eggers H. Transplantation of cultured human retinal epithelium to Bruch's membrane of the owl monkey's eye. *Curr Eye Res* 1985 Mar;4(3):253-65.

289. Gouras P, Algvere P. Retinal cell transplantation in the macula: new techniques. *Vision Res* 1996 Dec;36(24):4121-5.

290. Wasselius J, Ghosh F. Adult rabbit retinal transplants. *Invest Ophthalmol Vis Sci* 2001 Oct;42(11):2632-8.

291. Seiler M, Aramant RB, Ehinger B, Adolph AR. Transplantation of embryonic retina to adult retina in rabbits. *Exp Eye Res* 1990 Aug;51(2):225-8.

292. Radtke ND, Seiler MJ, Aramant RB, Petry HM, Pidwell DJ. Transplantation of intact sheets of fetal neural retina with its retinal pigment epithelium in retinitis pigmentosa patients. *Am J Ophthalmol* 2002 Apr;133(4):544-50.

293. Algvere PV, Berglin L, Gouras P, Sheng Y. Transplantation of fetal retinal pigment epithelium in age-related macular degeneration with subfoveal neovascularization. *Graefes Arch Clin Exp Ophthalmol* 1994 Dec;232(12):707-16.

294. Weisz JM, Humayun MS, De Juan E, Jr., Del Cerro M, Sunness JS, Dagnelie G, Soylu M, Rizzo L, Nussenblatt RB. Allogenic fetal retinal pigment epithelial cell transplant in a patient with geographic atrophy. *Retina* 1999;19(6):540-5.

295. Kaplan HJ, Tezel TH, Berger AS, Wolf ML, Del Priore LV. Human photoreceptor transplantation in retinitis pigmentosa. A safety study. *Arch Ophthalmol* 1997 Sep;115(9):1168-72.

296. Aramant R, Seiler M, Turner JE. Donor age influences on the success of retinal grafts to adult rat retina. *Invest Ophthalmol Vis Sci* 1988 Mar;29(3):498-503.

297. del Cerro M, Ison JR, Bowen GP, Lazar E, del Cerro C. Intraretinal grafting restores visual function in light-blinded rats. *Neuroreport* 1991 Sep;2(9):529-32.

298. Silverman MS, Hughes SE, Valentino TL, Liu Y. Photoreceptor transplantation: anatomic, electrophysiologic, and behavioral evidence for the functional reconstruction of retinas lacking photoreceptors. *Exp Neurol* 1992 Jan;115(1):87-94.

299. Gust J, Reh TA. Adult donor rod photoreceptors integrate into the mature mouse retina. *Invest Ophthalmol Vis Sci* 2011 Jul;52(8):5266-72.

300. Lakowski J, Baron M, Bainbridge J, Barber AC, Pearson RA, Ali RR, Sowden JC. Cone and rod photoreceptor transplantation in models of the childhood retinopathy Leber congenital amaurosis using flow-sorted Crx-positive donor cells. *Hum Mol Genet* 2010 Dec 1;19(23):4545-59.

301. MacLaren RE, Pearson RA, MacNeil A, Douglas RH, Salt TE, Akimoto M, Swaroop A, Sowden JC, Ali RR. Retinal repair by transplantation of photoreceptor precursors. *Nature* 2006 Nov 9;444(7116):203-7.

302. Pearson RA, Barber AC, Rizzi M, Hippert C, Xue T, West EL, Duran Y, Smith AJ, Chuang JZ, Azam SA, Luhmann UF, Benucci A, Sung CH, Bainbridge JW, Carandini M,

Yau KW, Sowden JC, Ali RR. Restoration of vision after transplantation of photoreceptors. *Nature* 2012 May 3;485(7396):99-103.

303. Aramant RB, Seiler MJ. Transplanted sheets of human retina and retinal pigment epithelium develop normally in nude rats. *Exp Eye Res* 2002 Aug;75(2):115-25.

304. Aramant RB, Seiler MJ. Progress in retinal sheet transplantation. *Prog Retin Eye Res* 2004 Sep;23(5):475-94.

305. Seiler MJ, Aramant RB. Photoreceptor and glial markers in human embryonic retina and in human embryonic retinal transplants to rat retina. *Brain Res Dev Brain Res* 1994 Jul 15;80(1-2):81-95.

306. Aramant RB, Seiler MJ, Ball SL. Successful cotransplantation of intact sheets of fetal retina with retinal pigment epithelium. *Invest Ophthalmol Vis Sci* 1999 Jun;40(7):1557-64.

307. Seiler MJ, Aramant RB. Transplantation of neuroblastic progenitor cells as a sheet preserves and restores retinal function. *Semin Ophthalmol* 2005 Jan-Mar;20(1):31-42.

308. Radtke ND, Aramant RB, Petry HM, Green PT, Pidwell DJ, Seiler MJ. Vision improvement in retinal degeneration patients by implantation of retina together with retinal pigment epithelium. *Am J Ophthalmol* 2008 Aug;146(2):172-82.

309. Seiler MJ, Thomas BB, Chen Z, Wu R, Sadda SR, Aramant RB. Retinal transplants restore visual responses: trans-synaptic tracing from visually responsive sites labels transplant neurons. *Eur J Neurosci* 2008 Jul;28(1):208-20.

310. Seiler MJ, Aramant RB, Seeliger MW, Bragadottir R, Mahoney M, Narfstrom K. Functional and structural assessment of retinal sheet allograft transplantation in feline hereditary retinal degeneration. *Vet Ophthalmol* 2009 May-Jun;12(3):158-69.

311. Yang Y, Mohand-Said S, Leveillard T, Fontaine V, Simonutti M, Sahel JA. Transplantation of photoreceptor and total neural retina preserves cone function in P23H rhodopsin transgenic rat. *PLoS One* 2010;5(10):e13469.

312. Mohand-Said S, Hicks D, Simonutti M, Tran-Minh D, Deudon-Combe A, Dreyfus H, Silverman MS, Ogilvie JM, Tenkova T, Sahel J. Photoreceptor transplants increase host cone survival in the retinal degeneration (rd) mouse. *Ophthalmic Res* 1997;29(5):290-7.

313. Mohand-Said S, Hicks D, Dreyfus H, Sahel JA. Selective transplantation of rods delays cone loss in a retinitis pigmentosa model. *Arch Ophthalmol* 2000 Jun;118(6):807-11.

314. Arai S, Thomas BB, Seiler MJ, Aramant RB, Qiu G, Mui C, de Juan E, Sadda SR. Restoration of visual responses following transplantation of intact retinal sheets in rd mice. *Exp Eye Res* 2004 Sep;79(3):331-41.

315. Woch G, Aramant RB, Seiler MJ, Sagdullaev BT, McCall MA. Retinal transplants restore visually evoked responses in rats with photoreceptor degeneration. *Invest Ophthalmol Vis Sci* 2001 Jun;42(7):1669-76.

316. Sagdullaev BT, Aramant RB, Seiler MJ, Woch G, McCall MA. Retinal transplantation-induced recovery of retinotectal visual function in a rodent model of retinitis pigmentosa. *Invest Ophthalmol Vis Sci* 2003 Apr;44(4):1686-95.

317. Thomas BB, Seiler MJ, Sadda SR, Aramant RB. Superior colliculus responses to light - preserved by transplantation in a slow degeneration rat model. *Exp Eye Res* 2004 Jul;79(1):29-39.

318. Seiler MJ, Aramant RB, Thomas BB, Peng Q, Sadda SR, Keirstead HS. Visual restoration and transplant connectivity in degenerate rats implanted with retinal progenitor sheets. *Eur J Neurosci* 2010 Feb;31(3):508-20.

319. del Cerro M, Notter MF, Grover DA, Olchowka J, Jiang LQ, Wiegand SJ, Lazar E, del Cerro C. Retinal transplants for cell replacement in phototoxic retinal degeneration. *Prog Clin Biol Res* 1989;314:673-86.

320. Seiler MJ, Aramant RB. Intact sheets of fetal retina transplanted to restore damaged rat retinas. *Invest Ophthalmol Vis Sci* 1998 Oct;39(11):2121-31.

321. Silverman MS, Hughes SE. Photoreceptor transplantation in inherited and environmentally induced retinal degeneration: anatomy, immunohistochemistry and function. *Prog Clin Biol Res* 1989;314:687-704.

322. Gouras P, Du J, Gelanze M, Lopez R, Kwun R, Kjeldbye H, Krebs W. Survival and synapse formation of transplanted rat rods. *J Neural Transplant Plast* 1991;2(2):91-100.

323. Gouras P, Tanabe T. Survival and integration of neural retinal transplants in rd mice. *Graefes Arch Clin Exp Ophthalmol* 2003 May;241(5):403-9.

324. del Cerro M, Notter MF, del Cerro C, Wiegand SJ, Grover DA, Lazar E. Intraretinal transplantation for rod-cell replacement in light-damaged retinas. *J Neural Transplant* 1989;1(1):1-10.

325. Zucker CL, Ehinger B, Seiler M, Aramant RB, Adolph AR. Ultrastructural circuitry in retinal cell transplants to rat retina. *J Neural Transplant Plast* 1994 Jan-Mar;5(1):17-29.

326. Jiang LQ, del Cerro M. Reciprocal retinal transplantation: a tool for the study of an inherited retinal degeneration. *Exp Neurol* 1992 Mar;115(3):325-34.

327. Gouras P, Du J, Kjeldbye H, Yamamoto S, Zack DJ. Reconstruction of degenerate rd mouse retina by transplantation of transgenic photoreceptors. *Invest Ophthalmol Vis Sci* 1992 Aug;33(9):2579-86.

328. Kwan AS, Wang S, Lund RD. Photoreceptor layer reconstruction in a rodent model of retinal degeneration. *Exp Neurol* 1999 Sep;159(1):21-33.

329. Radner W, Sadda SR, Humayun MS, Suzuki S, Melia M, Weiland J, de Juan E, Jr. Light-driven retinal ganglion cell responses in blind rd mice after neural retinal transplantation. *Invest Ophthalmol Vis Sci* 2001 Apr;42(5):1057-65.

330. del Cerro M, Lazar ES, Diloreto D, Jr. The first decade of continuous progress in retinal transplantation. *Microsc Res Tech* 1997 Jan 15;36(2):130-41.

331. del Cerro M, Humayun MS, Sadda SR, Cao J, Hayashi N, Green WR, del Cerro C, de Juan E, Jr. Histologic correlation of human neural retinal transplantation. *Invest Ophthalmol Vis Sci* 2000 Sep;41(10):3142-8.

332. Radtke ND, Aramant RB, Seiler MJ, Petry HM, Pidwell D. Vision change after sheet transplant of fetal retina with retinal pigment epithelium to a patient with retinitis pigmentosa. *Arch Ophthalmol* 2004 Aug;122(8):1159-65.

333. Chow AY, Chow VY, Packo KH, Pollack JS, Peyman GA, Schuchard R. The artificial silicon retina microchip for the treatment of vision loss from retinitis pigmentosa. *Arch Ophthalmol* 2004 Apr;122(4):460-9.

334. Bjorklund LM, Sanchez-Pernaute R, Chung S, Andersson T, Chen IY, McNaught KS, Brownell AL, Jenkins BG, Wahlestedt C, Kim KS, Isacson O. Embryonic stem cells develop into functional dopaminergic neurons after transplantation in a Parkinson rat model. *Proc Natl Acad Sci U S A* 2002 Feb 19;99(4):2344-9.

335. Kim JH, Auerbach JM, Rodriguez-Gomez JA, Velasco I, Gavin D, Lumelsky N, Lee SH, Nguyen J, Sanchez-Pernaute R, Bankiewicz K, McKay R. Dopamine neurons derived from embryonic stem cells function in an animal model of Parkinson's disease. *Nature* 2002 Jul 4;418(6893):50-6.

336. McDonald JW, Liu XZ, Qu Y, Liu S, Mickey SK, Turetsky D, Gottlieb DI, Choi DW. Transplanted embryonic stem cells survive, differentiate and promote recovery in injured rat spinal cord. *Nat Med* 1999 Dec;5(12):1410-2.

337. Nistor GI, Totoiu MO, Haque N, Carpenter MK, Keirstead HS. Human embryonic stem cells differentiate into oligodendrocytes in high purity and myelinate after spinal cord transplantation. *Glia* 2005 Feb;49(3):385-96.

338. Ying QL, Nichols J, Evans EP, Smith AG. Changing potency by spontaneous fusion. *Nature* 2002 Apr 4;416(6880):545-8.

339. Hara A, Niwa M, Kunisada T, Yoshimura N, Katayama M, Kozawa O, Mori H. Embryonic stem cells are capable of generating a neuronal network in the adult mouse retina. *Brain Res* 2004 Mar 5;999(2):216-21.

340. Meyer JS, Katz ML, Maruniak JA, Kirk MD. Neural differentiation of mouse embryonic stem cells in vitro and after transplantation into eyes of mutant mice with rapid retinal degeneration. *Brain Res* 2004 Jul 16;1014(1-2):131-44.

341. Dong X, Pulido JS, Qu T, Sugaya K. Differentiation of human neural stem cells into retinal cells. *Neuroreport* 2003 Jan 20;14(1):143-6.

342. Enzmann V, Howard RM, Yamauchi Y, Whittemore SR, Kaplan HJ. Enhanced induction of RPE lineage markers in pluripotent neural stem cells engrafted into the adult rat subretinal space. *Invest Ophthalmol Vis Sci* 2003 Dec;44(12):5417-22.

343. Mizumoto H, Mizumoto K, Shatos MA, Klassen H, Young MJ. Retinal transplantation of neural progenitor cells derived from the brain of GFP transgenic mice. *Vision Res* 2003 Jul;43(16):1699-708.

344. Takahashi M, Palmer TD, Takahashi J, Gage FH. Widespread integration and survival of adult-derived neural progenitor cells in the developing optic retina. *Mol Cell Neurosci* 1998 Dec;12(6):340-8.

345. Sanai N, Tramontin AD, Quinones-Hinojosa A, Barbaro NM, Gupta N, Kunwar S, Lawton MT, McDermott MW, Parsa AT, Manuel-Garcia Verdugo J, Berger MS, Alvarez-Buylla A. Unique astrocyte ribbon in adult human brain contains neural stem cells but lacks chain migration. *Nature* 2004 Feb 19;427(6976):740-4.

346. Kurimoto Y, Shibuki H, Kaneko Y, Ichikawa M, Kurokawa T, Takahashi M, Yoshimura N. Transplantation of adult rat hippocampus-derived neural stem cells into retina injured by transient ischemia. *Neurosci Lett* 2001 Jun 22;306(1-2):57-60.

347. Young MJ, Ray J, Whiteley SJ, Klassen H, Gage FH. Neuronal differentiation and morphological integration of hippocampal progenitor cells transplanted to the

retina of immature and mature dystrophic rats. *Mol Cell Neurosci* 2000 Sep;16(3):197-205.

348. Maclaren RE, Taylor JS. Regeneration in the developing optic nerve: correlating observations in the opossum to other mammalian systems. *Prog Neurobiol* 1997 Oct;53(3):381-98.

349. Van Hoffelen SJ, Young MJ, Shatos MA, Sakaguchi DS. Incorporation of murine brain progenitor cells into the developing mammalian retina. *Invest Ophthalmol Vis Sci* 2003 Jan;44(1):426-34.

350. Tucker BA, Park IH, Qi SD, Klassen HJ, Jiang C, Yao J, Redenti S, Daley GQ, Young MJ. Transplantation of adult mouse iPS cell-derived photoreceptor precursors restores retinal structure and function in degenerative mice. *PLoS One* 2011;6(4):e18992.

351. Klassen H, Sakaguchi DS, Young MJ. Stem cells and retinal repair. *Prog Retin Eye Res* 2004 Mar;23(2):149-81.

352. Chacko DM, Rogers JA, Turner JE, Ahmad I. Survival and differentiation of cultured retinal progenitors transplanted in the subretinal space of the rat. *Biochem Biophys Res Commun* 2000 Feb 24;268(3):842-6.

353. Chacko DM, Das AV, Zhao X, James J, Bhattacharya S, Ahmad I. Transplantation of ocular stem cells: the role of injury in incorporation and differentiation of grafted cells in the retina. *Vision Res* 2003 Apr;43(8):937-46.

354. Lu B, Wang S, Francis PJ, Li T, Gamm DM, Capowski EE, Lund RD. Cell transplantation to arrest early changes in an ush2a animal model. *Invest Ophthalmol Vis Sci* 2010 Apr;51(4):2269-76.

355. Li LX, Turner JE. Transplantation of retinal pigment epithelial cells to immature and adult rat hosts: short- and long-term survival characteristics. *Exp Eye Res* 1988 Nov;47(5):771-85.

356. Lopez R, Gouras P, Kjeldbye H, Sullivan B, Reppucci V, Brittis M, Wapner F, Goluboff E. Transplanted retinal pigment epithelium modifies the retinal degeneration in the RCS rat. *Invest Ophthalmol Vis Sci* 1989 Mar;30(3):586-8.

357. Sheedlo HJ, Li L, Turner JE. Photoreceptor cell rescue at early and late RPE-cell transplantation periods during retinal disease in RCS dystrophic rats. *J Neural Transplant Plast* 1991;2(1):55-63.

358. Lavail MM, Li L, Turner JE, Yasumura D. Retinal pigment epithelial cell transplantation in RCS rats: normal metabolism in rescued photoreceptors. *Exp Eye Res* 1992 Oct;55(4):555-62.

359. Gias C, Jones M, Keegan D, Adamson P, Greenwood J, Lund R, Martindale J, Johnston D, Berwick J, Mayhew J, Coffey P. Preservation of visual cortical function following retinal pigment epithelium transplantation in the RCS rat using optical imaging techniques. *Eur J Neurosci* 2007 Apr;25(7):1940-8.

360. Li SY, Yin ZQ, Chen SJ, Chen LF, Liu Y. Rescue from light-induced retinal degeneration by human fetal retinal transplantation in minipigs. *Curr Eye Res* 2009 Jul;34(7):523-35.

361. Algvere PV, Berglin L, Gouras P, Sheng Y, Kopp ED. Transplantation of RPE in age-related macular degeneration: observations in disciform lesions and dry RPE atrophy. *Graefes Arch Clin Exp Ophthalmol* 1997 Mar;235(3):149-58.

362. Lee E, MacLaren RE. Sources of retinal pigment epithelium (RPE) for replacement therapy. *Br J Ophthalmol* 2011 Apr;95(4):445-9.

363. Binder S, Stanzel BV, Krebs I, Glittenberg C. Transplantation of the RPE in AMD. *Prog Retin Eye Res* 2007 Sep;26(5):516-54.

364. Krebs I, Binder S, Stolba U, Kellner L, Glittenberg C, Goll A. Subretinal surgery and transplantation of autologous pigment epithelial cells in retinal angiomatous proliferation. *Acta Ophthalmol* 2008 Aug;86(5):504-9.

365. Ma Z, Han L, Wang C, Dou H, Hu Y, Feng X, Xu Y, Wang Z, Yin Z, Liu Y. Autologous transplantation of retinal pigment epithelium-Bruch's membrane complex for hemorrhagic age-related macular degeneration. *Invest Ophthalmol Vis Sci* 2009 Jun;50(6):2975-81.

366. Abe T, Yoshida M, Yoshioka Y, Wakusawa R, Tokita-Ishikawa Y, Seto H, Tamai M, Nishida K. Iris pigment epithelial cell transplantation for degenerative retinal diseases. *Prog Retin Eye Res* 2007 May;26(3):302-21.

367. van Zeeburg EJ, Maaijwee KJ, Missotten TO, Heimann H, van Meurs JC. A free retinal pigment epithelium-choroid graft in patients with exudative age-related macular degeneration: results up to 7 years. *Am J Ophthalmol* 2012 Jan;153(1):120-7 e2.

368. Haruta M, Sasai Y, Kawasaki H, Amemiya K, Ooto S, Kitada M, Suemori H, Nakatsuji N, Ide C, Honda Y, Takahashi M. In vitro and in vivo characterization of pigment epithelial cells differentiated from primate embryonic stem cells. *Invest Ophthalmol Vis Sci* 2004 Mar;45(3):1020-5.

369. Klimanskaya I, Hipp J, Rezai KA, West M, Atala A, Lanza R. Derivation and comparative assessment of retinal pigment epithelium from human embryonic stem cells using transcriptomics. *Cloning Stem Cells* 2004;6(3):217-45.

370. Lund RD, Wang S, Klimanskaya I, Holmes T, Ramos-Kelsey R, Lu B, Girman S, Bischoff N, Sauve Y, Lanza R. Human embryonic stem cell-derived cells rescue visual function in dystrophic RCS rats. *Cloning Stem Cells* 2006 Fall;8(3):189-99.

371. Carr AJ, Vugler AA, Hikita ST, Lawrence JM, Gias C, Chen LL, Buchholz DE, Ahmado A, Semo M, Smart MJ, Hasan S, da Cruz L, Johnson LV, Clegg DO, Coffey PJ. Protective effects of human iPS-derived retinal pigment epithelium cell transplantation in the retinal dystrophic rat. *PLoS One* 2009;4(12):e8152.

372. Wang NK, Tosi J, Kasanuki JM, Chou CL, Kong J, Parmalee N, Wert KJ, Allikmets R, Lai CC, Chien CL, Nagasaki T, Lin CS, Tsang SH. Transplantation of reprogrammed embryonic stem cells improves visual function in a mouse model for retinitis pigmentosa. *Transplantation* 2010 Apr 27;89(8):911-9.

373. Schwartz SD, Hubschman JP, Heilwell G, Franco-Cardenas V, Pan CK, Ostrick RM, Mickunas E, Gay R, Klimanskaya I, Lanza R. Embryonic stem cell trials for macular degeneration: a preliminary report. *Lancet* 2012 Feb 25;379(9817):713-20.

374. Schmitz-Valckenberg S, Guo L, Maass A, Cheung W, Vugler A, Moss SE, Munro PM, Fitzke FW, Cordeiro MF. Real-time in vivo imaging of retinal cell apoptosis after laser exposure. *Invest Ophthalmol Vis Sci* 2008 Jun;49(6):2773-80.

375. Gorgels TG, van Norren D. Ultraviolet and green light cause different types of damage in rat retina. *Invest Ophthalmol Vis Sci* 1995 Apr;36(5):851-63.

376. Dunsky IL, Lappin PW. Evaluation of retinal thresholds for C.W. laser radiation. *Vision Res* 1971 Jul;11(7):733-8.

377. Baurmann H, Sasaki K, Chioralia G. Investigations on laser coagulated rat eyes by fluorescence angiography and microscopy. *Albrecht Von Graefes Arch Klin Exp Ophthalmol* 1975;193(4):245-52.

378. Blanch RJ, Ahmed Z, Berry M, Scott RA, Logan A. Animal models of retinal injury. *Invest Ophthalmol Vis Sci* 2012;53(6):2913-20.

379. Framme C, Brinkmann R, Birngruber R, Roider J. Autofluorescence imaging after selective RPE laser treatment in macular diseases and clinical outcome: a pilot study. *Br J Ophthalmol* 2002 Oct;86(10):1099-106.

380. Dastgheib K, Bressler SB, Green WR. Clinicopathologic correlation of laser lesion expansion after treatment of choroidal neovascularization. *Retina* 1993;13(4):345-52.

381. Brancato R, Pece A, Avanza P, Radrizzani E. Photocoagulation scar expansion after laser therapy for choroidal neovascularization in degenerative myopia. *Retina* 1990;10(4):239-43.

382. Brown J, Jr., Hacker H, Schuschereba ST, Zwick H, Lund DJ, Stuck BE. Steroidal and nonsteroidal antiinflammatory medications can improve photoreceptor survival after laser retinal photocoagulation. *Ophthalmology* 2007 Oct;114(10):1876-83.

383. Grimm C, Wenzel A, Hafezi F, Reme CE. Gene expression in the mouse retina: the effect of damaging light. *Mol Vis* 2000 Dec 13;6:252-60.

384. Oltvai ZN, Milliman CL, Korsmeyer SJ. Bcl-2 heterodimerizes in vivo with a conserved homolog, Bax, that accelerates programmed cell death. *Cell* 1993 Aug 27;74(4):609-19.

385. Wilson AS, Hobbs BG, Shen WY, Speed TP, Schmidt U, Begley CG, Rakoczy PE. Argon laser photocoagulation-induced modification of gene expression in the retina. *Invest Ophthalmol Vis Sci* 2003 Apr;44(4):1426-34.

386. Lu Y, Fukuyama S, Yoshida R, Kobayashi T, Saeki K, Shiraishi H, Yoshimura A, Takaesu G. Loss of SOCS3 gene expression converts STAT3 function from anti-apoptotic to pro-apoptotic. *J Biol Chem* 2006 Dec 1;281(48):36683-90.

387. MacLaren RE, Buch PK, Smith AJ, Balaggan KS, MacNeil A, Taylor JS, Osborne NN, Ali RR. CNTF gene transfer protects ganglion cells in rat retinae undergoing focal injury and branch vessel occlusion. *Exp Eye Res* 2006 Nov;83(5):1118-27.

388. Lipinski DM, Singh MS, MacLaren RE. Assessment of cone survival in response to CNTF, GDNF, and VEGF165b in a novel ex vivo model of end-stage retinitis pigmentosa. *Invest Ophthalmol Vis Sci* 2011 Sep;52(10):7340-6.

389. Lipinski DM, Yusuf M, Barnard AR, Damant C, Charbel Issa P, Singh MS, Lee E, Davies WL, Volpi EV, MacLaren RE. Characterization of a dominant cone degeneration in a green fluorescent protein-reporter mouse with disruption of Loci associated with human dominant retinal dystrophy. *Invest Ophthalmol Vis Sci* 2011 Aug;52(9):6617-23.

390. Kuwana T, Mackey MR, Perkins G, Ellisman MH, Latterich M, Schneiter R, Green DR, Newmeyer DD. Bid, Bax, and lipids cooperate to form supramolecular openings in the outer mitochondrial membrane. *Cell* 2002 Nov 1;111(3):331-42.

391. Rezende AC, Vieira AS, Rogerio F, Rezende LF, Boschero AC, Negro A, Langone F. Effects of systemic administration of ciliary neurotrophic factor on Bax and Bcl-2

proteins in the lumbar spinal cord of neonatal rats after sciatic nerve transection. *Braz J Med Biol Res* 2008 Nov;41(11):1024-8.

392. Raghupathi R, Strauss KI, Zhang C, Krajewski S, Reed JC, McIntosh TK. Temporal alterations in cellular Bax:Bcl-2 ratio following traumatic brain injury in the rat. *J Neurotrauma* 2003 May;20(5):421-35.

393. Goldenberg-Cohen N, Dratviman-Storobinsky O, Dadon Bar El S, Cheporko Y, Hochhauser E. Protective effect of Bax ablation against cell loss in the retinal ganglion layer induced by optic nerve crush in transgenic mice. *J Neuroophthalmol* 2011 Dec;31(4):331-8.

394. Hafezi F, Steinbach JP, Marti A, Munz K, Wang ZQ, Wagner EF, Aguzzi A, Reme CE. The absence of c-fos prevents light-induced apoptotic cell death of photoreceptors in retinal degeneration in vivo. *Nat Med* 1997 Mar;3(3):346-9.

395. Kassen SC, Thummel R, Campochiaro LA, Harding MJ, Bennett NA, Hyde DR. CNTF induces photoreceptor neuroprotection and Muller glial cell proliferation through two different signaling pathways in the adult zebrafish retina. *Exp Eye Res* 2009 Jun;88(6):1051-64.

396. Barak A, Goldkorn T, Morse LS. Laser induces apoptosis and ceramide production in human retinal pigment epithelial cells. *Invest Ophthalmol Vis Sci* 2005 Jul;46(7):2587-91.

397. Singh MS, Charbel Issa P, Butler R, Martin C, Lipinski DM, Sekaran S, Barnard AR, Maclaren RE. Reversal of end-stage retinal degeneration and restoration of visual function by photoreceptor transplantation. *Proc Natl Acad Sci U S A* 2013 Jan 15;110(3):1101-6.

398. Bowes C, Li T, Danciger M, Baxter LC, Applebury ML, Farber DB. Retinal degeneration in the rd mouse is caused by a defect in the beta subunit of rod cGMP-phosphodiesterase. *Nature* 1990 Oct 18;347(6294):677-80.

399. Eberle D, Schubert S, Postel K, Corbeil D, Ader M. Increased integration of transplanted CD73-positive photoreceptor precursors into adult mouse retina. *Invest Ophthalmol Vis Sci* 2011 Aug;52(9):6462-71.

400. Swaroop A, Kim D, Forrest D. Transcriptional regulation of photoreceptor development and homeostasis in the mammalian retina. *Nat Rev Neurosci* 2010 Aug;11(8):563-76.

401. Fei Y, Hughes TE. Transgenic expression of the jellyfish green fluorescent protein in the cone photoreceptors of the mouse. *Vis Neurosci* 2001 Jul-Aug;18(4):615-23.

402. Yang Y, Mohand-Said S, Danan A, Simonutti M, Fontaine V, Clerin E, Picaud S, Leveillard T, Sahel JA. Functional cone rescue by RdCVF protein in a dominant model of retinitis pigmentosa. *Mol Ther* 2009 May;17(5):787-95.

403. Morrow EM, Furukawa T, Cepko CL. Vertebrate photoreceptor cell development and disease. *Trends Cell Biol* 1998 Sep;8(9):353-8.

404. Eter N, Engel DR, Meyer L, Helb HM, Roth F, Maurer J, Holz FG, Kurts C. In vivo visualization of dendritic cells, macrophages, and microglial cells responding to laser-induced damage in the fundus of the eye. *Invest Ophthalmol Vis Sci* 2008 Aug;49(8):3649-58.

405. Wang HC, Brown J, Alayon H, Stuck BE. Transplantation of quantum dot-labelled bone marrow-derived stem cells into the vitreous of mice with laser-induced retinal

injury: survival, integration and differentiation. *Vision Res* 2010 Mar 31;50(7):665-73.

406. Pak NV, Podgornyi OV, Aleksandrova MA, Chentsova EV, Ivanov AN, Golubeva ON, Poltavtseva RA, Marey MV, Sukhikh GT. Transplantation of cultured human neural stem cells in rabbits with experimental laser-induced damage to the retina. *Bull Exp Biol Med* 2004 Nov;138(5):525-8.

407. Singh T, Prabhakar S, Gupta A, Anand A. Recruitment of stem cells into the injured retina after laser injury. *Stem Cells Dev* 2012 Feb 10;21(3):448-54.

408. Lamba DA, Gust J, Reh TA. Transplantation of human embryonic stem cell-derived photoreceptors restores some visual function in Crx-deficient mice. *Cell Stem Cell* 2009 Jan 9;4(1):73-9.

409. Klassen HJ, Ng TF, Kurimoto Y, Kirov I, Shatos M, Coffey P, Young MJ. Multipotent retinal progenitors express developmental markers, differentiate into retinal neurons, and preserve light-mediated behavior. *Invest Ophthalmol Vis Sci* 2004 Nov;45(11):4167-73.

410. Chen EH, Olson EN. Unveiling the mechanisms of cell-cell fusion. *Science* 2005 Apr 15;308(5720):369-73.

411. Camargo FD, Chambers SM, Goodell MA. Stem cell plasticity: from transdifferentiation to macrophage fusion. *Cell Prolif* 2004 Feb;37(1):55-65.

412. O'Malley K, Scott EW. Stem cell fusion confusion. *Exp Hematol* 2004 Feb;32(2):131-4.

413. Daley GQ. Alchemy in the liver: fact or fusion? *Nat Med* 2004 Jul;10(7):671-2.

414. Koulen P, Kuhn R, Wassle H, Brandstatter JH. Modulation of the intracellular calcium concentration in photoreceptor terminals by a presynaptic metabotropic glutamate receptor. *Proc Natl Acad Sci U S A* 1999 Aug 17;96(17):9909-14.

415. Hirasawa H, Shiells R, Yamada M. A metabotropic glutamate receptor regulates transmitter release from cone presynaptic terminals in carp retinal slices. *J Gen Physiol* 2002 Jan;119(1):55-68.

416. Allen AE, Cameron MA, Brown TM, Vugler AA, Lucas RJ. Visual responses in mice lacking critical components of all known retinal phototransduction cascades. *PLoS One* 2010;5(11):e15063.

417. Beck SC, Schaeferhoff K, Michalakis S, Fischer MD, Huber G, Rieger N, Riess O, Wissinger B, Biel M, Bonin M, Seeliger MW, Tanimoto N. In vivo analysis of cone survival in mice. *Invest Ophthalmol Vis Sci* 2010 Jan;51(1):493-7.

418. Delori FC, Dorey CK, Staurenghi G, Arend O, Goger DG, Weiter JJ. In vivo fluorescence of the ocular fundus exhibits retinal pigment epithelium lipofuscin characteristics. *Invest Ophthalmol Vis Sci* 1995 Mar;36(3):718-29.

419. Keilhauer CN, Delori FC. Near-infrared autofluorescence imaging of the fundus: visualization of ocular melanin. *Invest Ophthalmol Vis Sci* 2006 Aug;47(8):3556-64.

420. Schmitz-Valckenberg S, Lara D, Nizari S, Normando EM, Guo L, Wegener AR, Tufail A, Fitzke FW, Holz FG, Cordeiro MF. Localisation and significance of in vivo near-infrared autofluorescent signal in retinal imaging. *Br J Ophthalmol* 2011 Aug;95(8):1134-9.

421. Kellner S, Kellner U, Weber BH, Fiebig B, Weinitz S, Ruether K. Lipofuscin- and melanin-related fundus autofluorescence in patients with ABCA4-associated retinal dystrophies. *Am J Ophthalmol* 2009 May;147(5):895-902, e1.

422. Boretsky A, Motamedi M, Bell B, van Kuijk F. Quantitative evaluation of retinal response to laser photocoagulation using dual-wavelength fundus autofluorescence imaging in a small animal model. *Invest Ophthalmol Vis Sci* 2011 Aug;52(9):6300-7.

423. Solberg Y, Dubinski G, Tchirkov M, Belkin M, Rosner M. Methylprednisolone therapy for retinal laser injury. *Surv Ophthalmol* 1999 Oct;44 Suppl 1:S85-92.

424. Ben-Shlomo G, Belokopytov M, Rosner M, Dubinsky G, Belkin M, Epstein Y, Ofri R. Functional deficits resulting from laser-induced damage in the rat retina. *Lasers Surg Med* 2006 Aug;38(7):689-94.

425. Talcott KE, Ratnam K, Sundquist SM, Lucero AS, Lujan BJ, Tao W, Porco TC, Roorda A, Duncan JL. Longitudinal study of cone photoreceptors during retinal degeneration and in response to ciliary neurotrophic factor treatment. *Invest Ophthalmol Vis Sci* 2011 Apr;52(5):2219-26.

426. Lam TT, Takahashi K, Fu J, Tso MO. Methylprednisolone therapy in laser injury of the retina. *Graefes Arch Clin Exp Ophthalmol* 1993 Dec;231(12):729-36.

427. Marshall J. Structural aspects of laser-induced damage and their functional implications. *Health Phys* 1989 May;56(5):617-24.

428. Rosner M, Solberg Y, Turetz J, Belkin M. Neuroprotective therapy for argon-laser induced retinal injury. *Exp Eye Res* 1997 Oct;65(4):485-95.

429. Solberg Y, Rosner M, Turetz J, Belkin M. MK-801 has neuroprotective and antiproliferative effects in retinal laser injury. *Invest Ophthalmol Vis Sci* 1997 Jun;38(7):1380-9.

430. Schuschereba ST, Bowman PD, Ferrando RE, Lund DJ, Quong JA, Vargas JA. Accelerated healing of laser-injured rabbit retina by basic fibroblast growth factor. *Invest Ophthalmol Vis Sci* 1994 Mar;35(3):945-54.

431. Shulman S, Belokopytov M, Dubinsky G, Belkin M, Rosner M. Ameliorative effect of PN-277 on laser-induced retinal damage. *Graefes Arch Clin Exp Ophthalmol* 2009 Mar;247(3):343-8.

432. Kasaoka M, Ma J, Lashkari K. c-Met modulates RPE migratory response to laser-induced retinal injury. *PLoS One* 2012;7(7):e40771.

433. Wood JP, Shibeeb O, Plunkett M, Casson RJ, Chidlow G. Retinal damage profiles and neuronal effects of laser treatment: comparison of a conventional photocoagulator and a novel 3-nanosecond pulse laser. *Invest Ophthalmol Vis Sci* 2013;54(3):2305-18.

434. Bird AC, Bressler NM, Bressler SB, Chisholm IH, Coscas G, Davis MD, de Jong PT, Klaver CC, Klein BE, Klein R, et al. An international classification and grading system for age-related maculopathy and age-related macular degeneration. The International ARM Epidemiological Study Group. *Surv Ophthalmol* 1995 Mar-Apr;39(5):367-74.

435. Cremers FP, van de Pol DJ, van Driel M, den Hollander AI, van Haren FJ, Knoers NV, Tijmes N, Bergen AA, Rohrschneider K, Blankenagel A, Pinckers AJ, Deutman AF, Hoyng CB. Autosomal recessive retinitis pigmentosa and cone-rod dystrophy caused

by splice site mutations in the Stargardt's disease gene ABCR. *Hum Mol Genet* 1998 Mar;7(3):355-62.

436. Shanks N, Greek R, Greek J. Are animal models predictive for humans? *Philos Ethics Humanit Med* 2009;4:2.

437. Pearson RA, Barber AC, West EL, MacLaren RE, Duran Y, Bainbridge JW, Sowden JC, Ali RR. Targeted disruption of outer limiting membrane junctional proteins (Crb1 and ZO-1) increases integration of transplanted photoreceptor precursors into the adult wild-type and degenerating retina. *Cell Transplant* 2010;19(4):487-503.

438. Lagasse E, Connors H, Al-Dhalimy M, Reitsma M, Dohse M, Osborne L, Wang X, Finegold M, Weissman IL, Grompe M. Purified hematopoietic stem cells can differentiate into hepatocytes in vivo. *Nat Med* 2000 Nov;6(11):1229-34.

439. Petersen BE, Bowen WC, Patrene KD, Mars WM, Sullivan AK, Murase N, Boggs SS, Greenberger JS, Goff JP. Bone marrow as a potential source of hepatic oval cells. *Science* 1999 May 14;284(5417):1168-70.

440. Vassilopoulos G, Wang PR, Russell DW. Transplanted bone marrow regenerates liver by cell fusion. *Nature* 2003 Apr 24;422(6934):901-4.

441. Anderson JM. Multinucleated giant cells. *Curr Opin Hematol* 2000 Jan;7(1):40-7.

442. Liang FQ, Dejneka NS, Cohen DR, Krasnoperova NV, Lem J, Maguire AM, Dudus L, Fisher KJ, Bennett J. AAV-mediated delivery of ciliary neurotrophic factor prolongs photoreceptor survival in the rhodopsin knockout mouse. *Mol Ther* 2001 Feb;3(2):241-8.

443. Yanagi Y, Takezawa S, Kato S. Distinct functions of photoreceptor cell-specific nuclear receptor, thyroid hormone receptor beta2 and CRX in one photoreceptor development. *Invest Ophthalmol Vis Sci* 2002 Nov;43(11):3489-94.

444. Guo Y, Saloupis P, Shaw SJ, Rickman DW. Engraftment of adult neural progenitor cells transplanted to rat retina injured by transient ischemia. *Invest Ophthalmol Vis Sci* 2003 Jul;44(7):3194-201.

APPENDIX

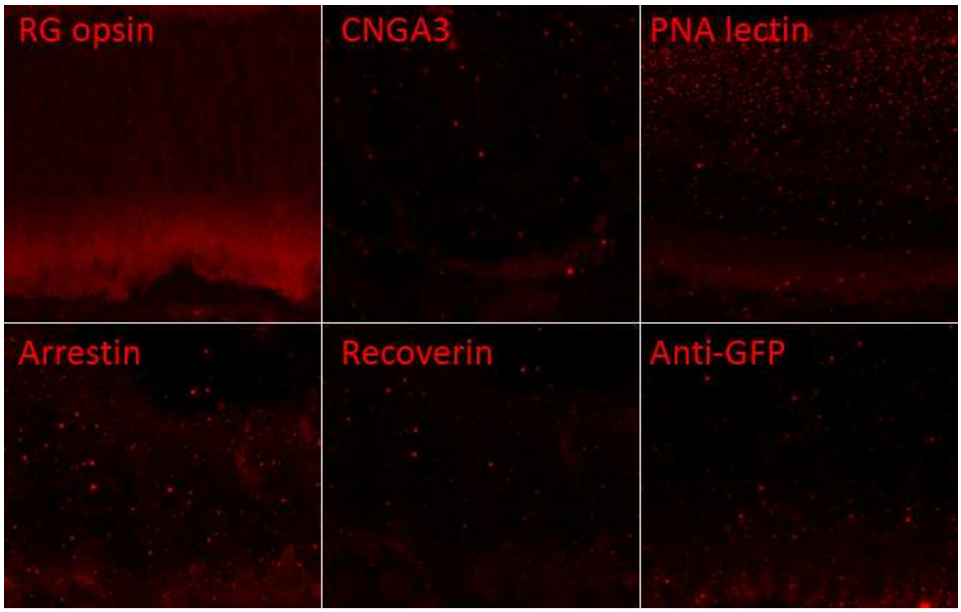

Figure 1. Control samples for immunohistochemistry (IHC). The primary antibody was omitted during the IHC steps. The panels do not show non-specific binding of each antibody.

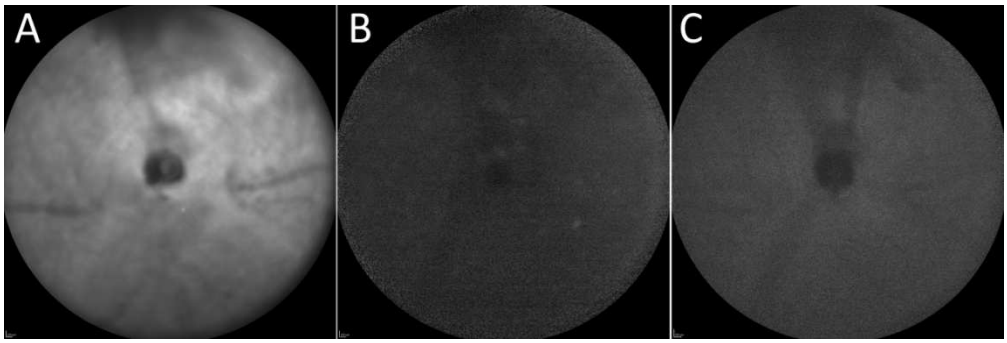

Figure 2. cSLO images of a wild type retina. Reflectance (**A**), 488nm (**B**) and 790nm (**C**) autofluorescence images of the same eye are shown.

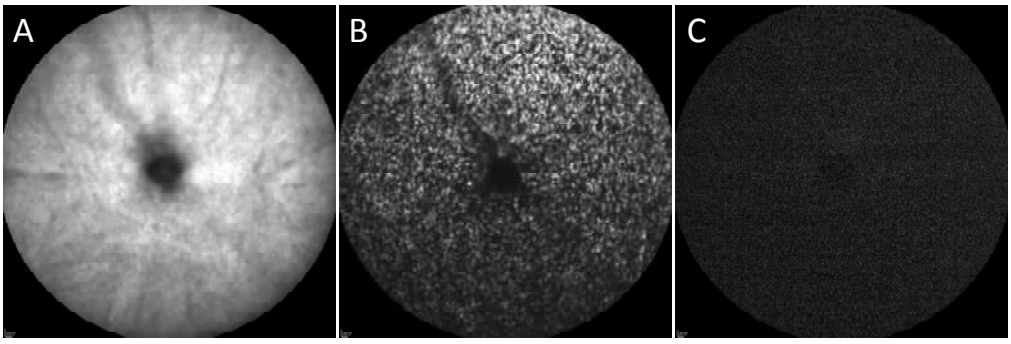

Figure 3. cSLO images of an Opn1-EGFP retina. Reflectance (**A**), 488nm (**B**) and 790nm (**C**) autofluorescence images of the same eye are shown.